NASA CR 159447

GE Document No. 78SDS4252

1878-1978

FINAL REPORT

MINI-BRAYTON HEAT SOURCE ASSEMBLY DEVELOPMENT

27 JUNE 1974 TO 1 OCTOBER 1978

1 NOVEMBER 1978

space division

GENERAL ELECTRIC

1 Report No	2 Government Accession No	3 Recipient's Catalog No
NASA CR 159447		

4 Title and Subtitle	5 Report Date
Mini-Brayton Heat Source Assembly Development - Final Report	1 November, 1978
	6 Performing Organization Code

7 Author(s)	8 Performing Organization Report No
D. Wein and W. F. Zimmerman	78SD4252
	10 Work Unit No

9 Performing Organization Name and Address	11 Contract or Grant No
General Electric Company Space Division P. O. Box 8661 Philadelphia, Pennsylvania 19101	NAS 3 - 18541

12 Sponsoring Agency Name and Address	13 Type of Report and Period Covered
National Aeronautics and Space Administration Lewis Research Center Cleveland, Ohio 44135	Contract Report 27 June, 1974 to 1 Oct., 1978
	14 Sponsoring Agency Code

15 Supplementary Notes

Project Manager: R. H. Titran
Materials and Structures Division
NASA - Lewis Research Center

16 Abstract

This report summarizes the work accomplished on the Mini-Brayton Heat Source Assembly program, which was performed by the General Electric Company for the NASA-Lewis Research Center under Contract NAS3-18541.

The objectives of the program were to develop the required technologies to design, fabricate and assemble components for a high temperature Heat Source Assembly (HSA) which would generate and transfer the thermal energy for a space borne Brayton Isotope Power System (BIPS).

The HSA contract effort encompassed, 1) technology development associated with the fabrication of the columbium alloy (C-103) Heat Source Heat Exchanger (HSHX) with the major thrust of this being on a diffusion welding (autoclaving) process for the core of the HSHX, 2) technology development on a high temperature multifoil insulation system that also functions as an emergency cooling system for the isotope heat source, 3) design of the HSA and all its components, 4) fabrication of the HSA and its components with a major effort being on the HSHX, and 5) acceptance testing of the HSHX and the HSA.

17 Key Words (Suggested by Author(s))	18 Distribution Statement
Nuclear Heat Source; Isotope Power System; Spaceborne Dynamic Power System, Brayton Cycle	

19 Security Classif (of this report)	20 Security Classif (of this page)	21 No of Pages	22 Price*
Unclassified	Unclassified	295	

* For sale by the National Technical Information Service, Springfield Virginia 22161

NASA CR 159447

GE Document No. 78SDS4252

FINAL REPORT

(Contract NAS3-18541)

MINI-BRAYTON HEAT SOURCE ASSEMBLY DEVELOPMENT

27 JUNE 1974 TO 1 OCTOBER 1978

D. Wein
W. F. Zimmerman

1 NOVEMBER 1978

TECHNICAL MANAGEMENT:

R. H. Titran

NATIONAL AERONAUTICS AND SPACE ADMINISTRATION
LEWIS RESEARCH CENTER
21000 BROOKPARK ROAD
CLEVELAND, OHIO 44135

ADVANCED ENERGY PROGRAMS

SPACE DIVISION

Valley Forge Space Center
P.O. Box 8661, Philadelphia, Penna. 19101

GENERAL ELECTRIC

ACKNOWLEDGEMENTS

The following members of the General Electric Company - Space Division technical staff made significant contributions to this report.

P. Aller

E. C. Duderstadt

D. Fox

E. H. Sayell

W. Saylor

In addition to those listed above, numberous individuals contributed to the successful completion of this contract. A brief, but not necessarily, inclusive list follows:

GE-VALLEY FORGE

O. R. Bitzer

J. K. Callender

L. E. Douglas

V. F. Haley

C. E. Kelly

H. A. Nordeen

E. P. Sardaro

G. V. Schmidt

E. M. Sheehan

L. L. Tyahla

E. J. Urbanik

C. W. Whitmore

GE-EVENDALE

G. Anderson

P. Blanz

E. L. Burns

L. N. Clements

J. R. Galley

L. C. Hockstahl

J. Hopkins

J. R. Monday

C. E. North

D. R. Pence

BATTELLE COLUMBUS LABORATORIES

D. Woessner and his Staff

TABLE OF CONTENTS

Section		Page
1	INTRODUCTION	1-1
	1.1 Objectives	1-1
	1.2 Scope	1-1
	1.3 Brayton Isotope Power System Description	1-2
	1.4 HSA Description and Components	1-6
2	SUMMARY	2-1
	2.1 HSA Configuration	2-1
	2.2 C-103 HSHX Fabrication Development	2-3
	2.3 Insulation/Emergency Cooling Verification	2-6
	2.4 Fabrication and Acceptance Testing	2-10
3	HEAT SOURCE HEAT EXCHANGER FABRICATION DEVELOPMENT	3-1
	3.1 Diffusion Welding	3-3
	3.2 Machining	3-25
	3.3 GTA Welding	3-38
	3.4 Forming	3-43
	3.5 Leaching	3-45
	3.6 Cyclic Pressure Tests	3-47
	3.7 Non Destructive Test Inspection	3-60
4	INSULATION/EMERGENCY COOLING/AUXILIARY COOLING VERIFICATION	4-1
	4.1 Insulation Life Stability Tests	4-2
	4.2 Insulation Thermal Conductivity Tests	4-17
	4.3 Insulation Vibration Tests	4-22
	4.4 Material Compatibility Tests	4-34
	4.5 Insulation Meltdown Tests	4-67
5	HSA DESIGN	5-1
	5.1 Design Requirements	5-1
	5.2 HSA Configuration	5-7
	5.3 Structural Analyses and Design	5-20
	5.4 Hydraulic Analysis	5-34
	5.5 Thermal Analyses	5-39
	5.6 System Interfaces	5-52
6	HARDWARE FABRICATION	6-1
	6.1 Cleanliness Requirements	6-1
	6.2 Heat Source Heat Exchanger Fabrication	6-2
	6.3 Support and Miscellaneous Hardware	6-32
	6.4 Insulation	6-41
	6.5 Weight	6-41

TABLE OF CONTENTS (continued)

Section		Page
7	ACCEPTANCE TESTS	7-1
	7.1 Requirements	7-1
	7.2 Test Flow Plan	7-2
	7.3 HSHX Proof Pressure Test	7-2
	7.4 HSHX Pressure Drop Test	7-7
	7.5 HSHX Leak Tests	7-12
	7.6 HSA Proof Pressure Test	7-12
	7.7 HSA Pressure Decay Test	7-12
8	CONCLUSIONS AND RECOMMENDATIONS	8-1
9	REFERENCES	9-1
APPENDIX A	ACRONYMS	A-1

LIST OF ILLUSTRATIONS

Figure		Page
1-1	Typical Brayton Isotope Power System.	1-4
1-2	BIPS Module	1-5
2-1	Heat Source Assembly.	2-12
2-2	C-103 Machined Cylinder	2-13
2-3	Photomicrographs Showing Typical Microstructures of Diffusion Welds in HSHX Cylinder Number 1	2-14
2-4	Photograph of HSHX S/N 1 after Completion of Conformance Tests and Re-inspection	2-15
3-1	Finned Specimens without Mo Filler Bars	3-6
3-2	Photomicrographs of Typical C-103 Sheet Specimens Diffusion Welded at 1700K	3-9
3-3	Photomicrographs of C-103 Specimens Diffusion Welded at 1730K.	3-10
3-4	Mini-Bulge Test Specimens after Hydro Tests	3-12
3-5	Holographs of Specimen 121.	3-13/3-14
3-6	Photomicrographs of C-103 Diffusion Welded Specimen 133.	3-16
3-7	Photomicrographs of Specimen 132.	3-20
3-8	Photomicrographs of Specimen 131.	3-21
3-9	Photograph of Load Arrangement in Run 11.	3-24
3-10	Diffusion Welding Trial Parts Awaiting Assembly	3-26
3-11	Typical Trial Part Components for the 5. cm Diffusion Welding Assembly.	3-27
3-12	Trial Assembly of 23. cm Trial Part	3-28
3-13	Photograph of Trial Part No. 1 Diffusion Welding Assembly Prior to Welding	3-29
3-14	Photograph of Trial Part No. 1 Diffusion Welding Assembly after 5 Hour, 1700K and 62. MPa Welding Cycles.	3-30
3-15	Five cm Trial Part #2 Upper End Ring.	3-31
3-16	Upper Portion of 23. cm Trial Part including Short Length Mo Bars and Mo Bar Joints with Surface Dimples	3-32
3-17	Diffusion Welded 5. cm Trial Part No. 1 after Molybdenum Filler Bars and Outer Barrier Cylinders Removed	3-33

LIST OF ILLUSTRATIONS (continued)

Figure		Page
3-18	Photomicrographs Showing Typical Microstructure of Diffusion Welds in the 23. cm Trial Part	3-34
3-19	Climb-Straddle Milling of Fins on Trial Part Inner Cylinders	3-37
3-20	Automatic GTA Welded Curved 0.13 cm Thick C-103 Sheets with Rabbetted Edges for Self Fixturing	3-40
3-21	Photomicrographs of Automatic GTA Weld of Curved 0.13 cm Thick C-103 Sheet at Locations Shown in Figure 3-20.	3-41
3-22	Forming Process for Toroid Halves	3-44
3-23	Cyclic Pressure Test Specimen for Diffusion Weld Joint Strength Evaluation	3-48
3-24	Photograph of Cyclic Pressure Test Specimen before Testing	3-50
3-25	Microstructure of Diffusion Welded Joint of C-103 Fin and Top Plate Cyclic Test Specimen.	3-51
3-26	Schematic of Cyclic Pressure Test	3-52
3-27	Holograph of Cyclic Pressure Test Specimen after Testing Showing Diffusion Weld Integrity.	3-54
3-28	Holographs of Cyclic Pressure Test Specimen Made at Pressures Indicated	3-55/3-56
3-29	Cyclic Pressure Specimen After Destructive Pressurization at Room Temperature.	3-59
3-30	NDT Effect Standard for Mini Brayton HSHX Diffusion Welds	3-61
3-31	"C" Scan Trace of Ultrasonic Calibration Standard with Intentional Defects	3-61
4-1	Life Stability Test	4-5
4-2	Life Stability Test Assembly.	4-6
4-3	Raw and Normalized Life Stability Test Data - 1090K Hot Face.	4-9
4-4	Raw and Normalized Life Stability Test Data - 1145K Hot Face.	4-10
4-5	Raw and Normalized Life Stability Test Data - 1200K Hot Face.	4-11
4-6	Raw and Normalized Life Stability Test Data - 1255K Hot Face.	4-12

LIST OF ILLUSTRATIONS (continued)

Figure		Page
4-7	Raw and Normalized Life Stability Test Data - 1145K Thermal Cycle	4-13
4-8	Raw and Normalized Life Stability Test of Bare Nickel Foil @ 1255K Hot Face	4-14
4-9	External Appearance of 1255K Life Stability Test Sample Prior to Diagnostic Disassembly	4-16
4-10	Internal Appearance of 1255K (1800°F Life Stability) Test Sample during Diagnostic Disassembly	4-16
4-11	Thermal Conductivity of Multi-Foil Thermal Insulation	4-20
4-12	Thermal Conductivity of Multi-Foil Thermal Insulation at 6.9 KPa Contact Pressure	4-21
4-13	Random Vibration Envelope	4-24
4-14	Insulation Vibration Test Set-Up.	4-26
4-15	Vibration Test Fixture.	4-27
4-16	Vibration Test Fixture.	4-28
4-17	Vibration Test Fixture Photos Showing Setup for Vibrating along the Plane of the Sample	4-29
4-18	C-103 Sputtered with 2 μm of Nickel and Vacuum Heat Treated for 63 Hours at 1323K	4-43
4-19	C-103 Sputtered with 2 μm of Nickel Vacuum Heat Treated for 63 Hours at 1323K and Bent over a 3t Radius	4-43
4-20	C-103 Sputtered with 2 μm of Nickel, Vacuum Heat Treated for 63 Hours at 1323K and Bent over a 3t Bend Radius.	4-44
4-21	C-103 Sputtered with 2 μm of Nickel, Vacuum Heat Treated for 63 Hours at 1323K and Bent over a 3t Bend Radius.	4-44
4-22	Ni/Mo/Nb/CaO: ZrO_2 Compatibility Test Capsules.	4-47
4-23	Typical Cross Sections of Ni Foils.	4-48
4-24	Typical Cross Sections of Nickel Foils.	4-49
4-25	Typical Cross Sections of Niobium Foils	4-50
4-26	Typical Cross Sections of Molybdenum Foils.	4-51
4-27	Typical Cross Sections of Foils Exposed to H_2O.	4-52
4-28	Typical Cross Sections of Foils Exposed to H_2O.	4-53
4-29	Reduction of Pure ZrO_2 by Mo and Nb at 950°C.	4-57
4-30	Reduction of ZrO_2 by Ni and by Ni/Nb at 950°C	4-58

LIST OF ILLUSTRATIONS (continued)

Figure		Page
4-31	Reduction of ZrO_2 by Nb and Accelerated Evaporation of Ni	4-59
4-32	Reduction of Pure ZrO_2 by Ni and Ni/Nb at 720°C	4-60
4-33	Observations of Crucible #1 Tested at 1323K	4-61
4-34	Typical Cross Section of Nb Wrapped Nb Foils at 1323K	4-62
4-35	Typical Cross Section of Ni Foils and Unwrapped Nb Foil at 1323K	4-63
4-36	Observations of Crucible #2 Tested at 1323K	4-64
4-37	Typical Cross Sections of Ni Foils from Crucible #2 Tested at 1323K	4-65
4-38	Typical Cross Section of Nb Foil Wrapped in Mo Tested at 1323K.	4-66
4-39	All Nickel Foil Small Scale Meltdown Test Assembly #1	4-69
4-40	Photograph of All Nickel Foil Test Sample after First Meltdown Attempt.	4-70
4-41	Photograph of All Nickel Foil Test Sample after First Meltdown Attempt.	4-70
4-42	Response of Test T/C's during Melt Test #1.	4-72
4-43	Tantalum Foil Outer Cylinder.	4-73
4-44	Planar End Insulation and Heater Assembly	4-73
4-45	Melting/Vaporization of Nickel Screen and Insulation Blanket Cylindrical Section	4-74
4-46	Typical Solidly Fused Area of Multifoil Insulation at 44th Layer	4-74
4-47	Small Scale Meltdown Test Assembly #2	4-77
4-48	Temperature Profile of Meltdown Test #2	4-78
4-49	Insulation Specimen after Meltdown Test #2.	4-79
4-50	End View of Specimen after Meltdown Test #2 - View with One End Cap Removed	4-80
4-51	Photomicrograph of Cross Section of Insulation after Meltdown Test #2.	4-81
5-1	Predicted Creep Strength and Approximate 90% Confidence Limits for 1% Strain in 7 Years for C-103	5-5
5-2	Heat Source Assembly.	5-10
5-3	Housing	5-11

LIST OF ILLUSTRATIONS (continued)

Figure		Page
5-4	Dome.	5-12
5-5	End Enclosures.	5-13
5-6	Heat Source Heat Exchanger.	5-14
5-7	Insulation Cylinder	5-15
5-8	Insulation Ends	5-16
5-9	HSA Bellow.	5-17
5-10	Heat Exchanger.	5-21
5-11	Common Center Line Header Variations.	5-23
5-12	Bending Stress on Cylinder Wall vs. Unwelded Fin Length.	5-27
5-13	HSHX Pressure Profile	5-36
5-14	HSA 2D Thermal Model.	5-41
5-15	HSA Temperature Profile during Normal Operation	5-43
5-16	HSA Insulation Temperature Profile.	5-44
5-17	Two Dimensional ECS Response HSA with LES 8/9 Heat Source.	5-49
5-18	3D HSA Shutdown Transient with Fluid Flow Stopped	5-51
5-19	System Interfaces	5-53
6-1	Highlights of HSHX Manufacturing Process Plan	6-4 thru 6-9
6-2	Machined Inner Cylinder	6-11
6-3	HSHX Production Parts	6-14
6-4	Sealed Production Cylinder No. 1 before Autoclaving . . .	6-17
6-5	Typical Pressure-Temperature Profile during Autoclaving	6-17
6-6	Machining (Scalloping) of Inner and Outer Seal Cylinders of 1st Autoclaved Production Cylinder	6-18
6-7	Recovered Diffusion Welded Assembly after Leaching. . . .	6-19
6-8	Ultrasonic Inspection of Production Cylinder.	6-20
6-9	Ultrasonic Scan of Production Cylinder.	6-21
6-10	Metallography - 1st Production Cylinder	6-22
6-11	Machined Inner Scroll	6-25
6-12	HSHX Weld Assembly in Various Stages of Completion. . . .	6-27
6-13	Port Hole Machining	6-28

LIST OF ILLUSTRATIONS (continued)

Figure		Page
6-14	Bracket Fixturing	6-29
6-15	Final Stud Machining to Interface Dimensions	6-30
6-16	Completed Heat Source Heat Exchanger	6-31
6-17	Stainless Steel Housing	6-33
6-18	Stainless Steel Dome with Gas Management Assembly	6-34
6-19	Preload Screw	6-35
6-20	Titanium End Enclosure	6-36
6-21	Gas Management Assembly	6-38
6-22	Connectors	6-39
6-23	HSA Bellows	6-40
6-24	Insulation Cylinder	6-42
6-25	Insulation End Cap	6-43
7-1	Mini-Brayton HSA Acceptance Test Flow Plan	7-4
7-2	HSHX Proof Pressure Test Set-Up	7-6
7-3	HSHX Pressure Drop Flow Test Set-Up	7-8
7-4	HSHX Pressure Drop Flow Test Results	7-11

LIST OF TABLES

Table		Page
1-1	Heat Source Assembly Subsystems and Components.	1-8
3-1	Interstitial Impurity Contents of Diffusion Welded Specimens at 1700°K	3-18
4-1	Test Specimen Temperature Readings Before and After Vibration Tests	4-31
4-2	Insulation Vibration Test Sample Weight Data.	4-32
4-3	Chronology of All Nickel Test Specimen Diagnostic Disassembly	4-75
5-1	PICS Temperature Limits	5-7
5-2	Summary of HSHX Design Variations	5-24
5-3	HSHX Stress Summary	5-25
5-4	HSHX Maximum Stress Levels for Unwelded Fins.	5-28
5-5	Effect of Partial Welding	5-30
5-6	Normal Operating Temperatures Near The Exit End of The HSA	5-42
5-7	ACS Analysis Summary.	5-47
5-8	Maximum Temperature Excursion Due to Shutdown Transient	5-50
6-1	Loose Particulate Acceptance Criteria for HSHX Fluid Loop.	6-1
6-2	HSA Weight Summary.	6-44
7-1	BIPS System Flow Requirements	7-9
7-2	HSA Scaled Pressure Drop Test Data.	7-10

SECTION 1

INTRODUCTION

This report summarizes the work accomplished on the Mini-Brayton Heat Source Assembly program, which was performed by the General Electric Company for the NASA-Lewis Research Center under Contract NAS3-18541. The contract started June 27, 1974 and technical effort extended through September, 1978.

1.1 OBJECTIVES

The objectives of the program were to develop the required technologies to design, fabricate and assemble components for a high temperature Heat Source Assembly (HSA) which generates and transfers the thermal energy for a space borne Brayton Isotope Power System (BIPS).

1.2 SCOPE

The HSA contract effort encompassed the following major efforts.

1. Technology development associated with the fabrication of the columbium* alloy (C-103) Heat Source Heat Exchanger (HSHX). This included machining, forming, welding, with the major thrust being on a diffusion welding (autoclaving) process for the core of the HSHX.

2. Technology development on a high temperature multifoil insulation system that also functions as an emergency cooling system for the isotope heat source.

* Throughout this report "columbium" (Cb) and its scientific designation "niobium" (Nb) will be both used synonymously.

3. Design of the HSA and all its components.

4. Fabrication of the HSA and its components with a major effort being on the HSHX.

5. Acceptance testing of the HSHX and the HSA.

1.3 BRAYTON ISOTOPE POWER SYSTEM (BIPS) DESCRIPTION

The Brayton Isotope Power System (BIPS)* is a 500 to 2000 watts electrical (We) seven-year life space power system. It utilizes a closed Brayton cycle shown in Figure 1-1, to convert thermal energy from an Isotope Heat Source (IHS) to electrical energy at a net efficiency exceeding 25 percent. The HSA which is one of the major components of the BIPS, contains the Multi-Hundred Watt Isotope Heat Source (for space missions) or the MHW Electric Heat Source (for ground tests) both of which generate 2400 watts of thermal energy. The IHS is a flight qualified heat source presently supplying power on LES 8 and 9 and the Voyager spacecraft. Heat is transferred to the working fluid (an inert gas mixture of Xenon and Helium) as it flows through a heat exchanger within the HSA.

Emerging from the HSA, temperature and pressure are at a maximum and the working fluid is expanded in a turbine, driving a compressor and alternator - all mounted on a common shaft. "Work" in the form of electrical energy is extracted in this Miniature Brayton Rotating Unit (Mini-BRU). The Mini-BRU, an offspring of the NASA BRU which has

---

* In earlier Design Study Reports the Brayton Isotope Power System was referred to as the Mini-Brayton Power System.

accumulated over 31,000 hours of operation, was developed under a separate NASA Contract.

The working fluid then passes through a recuperator where it rejects some of its thermal energy which is used to preheat the gas returning to the HSA. The recuperator, also developed under a separate NASA contract minimizes waste heat rejection from the cycle and results in operation of high cycle efficiency.

After emerging from the recuperator the cycle waste heat is rejected in a radiator. The working fluid then enters the compressor and is discharged into the recuperator at higher temperature and pressure. Passing through the recuperator it is preheated before entering the HSA where the closed cycle resumes.

The Brayton power cycle has several outstanding characteristics which makes it very attractive for space applications. The use of an inert gaseous working fluid allows the cycle to operate over a wide temperature range which provides high Carnot efficiences; by employing a recuperator, high system efficiencies can be realized. The system is adaptable for efficient operation over a wide range of power levels which can be controlled by changing the system operating pressure while the turbomachinery size remains fixed. A gaseous working fluid allows the use of simple, self-acting gas bearings, ensuring long component life of the rotating component.

An illustration of the integrated BIPS Module is shown in Figure 1-2.

Ground tests of the system are to be conducted under an ERDA (DOE) contract during 1978.

FIGURE 1-1

TYPICAL BRAYTON ISOTOPE POWER SYSTEM

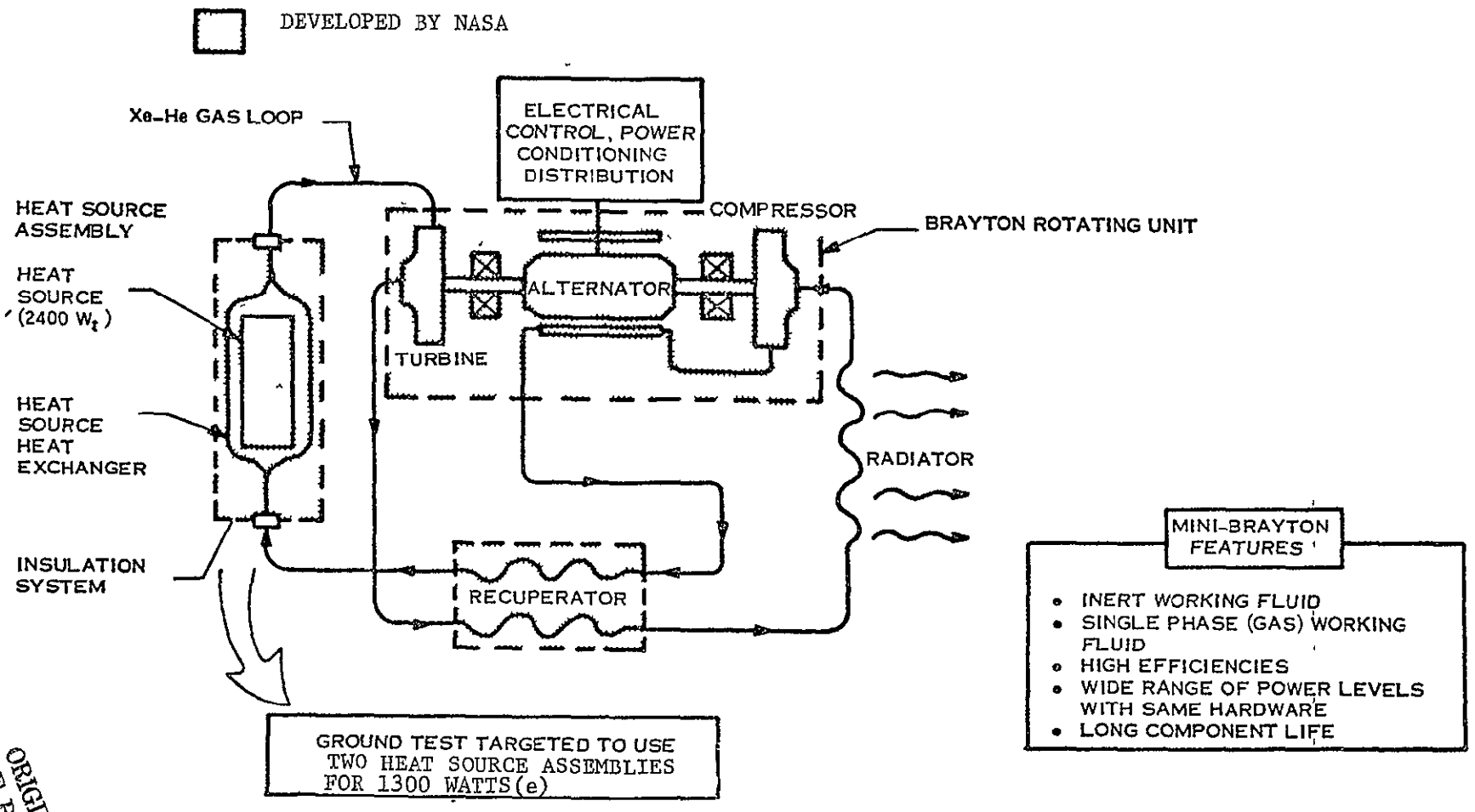

FIGURE 1-2

BIPS MODULE

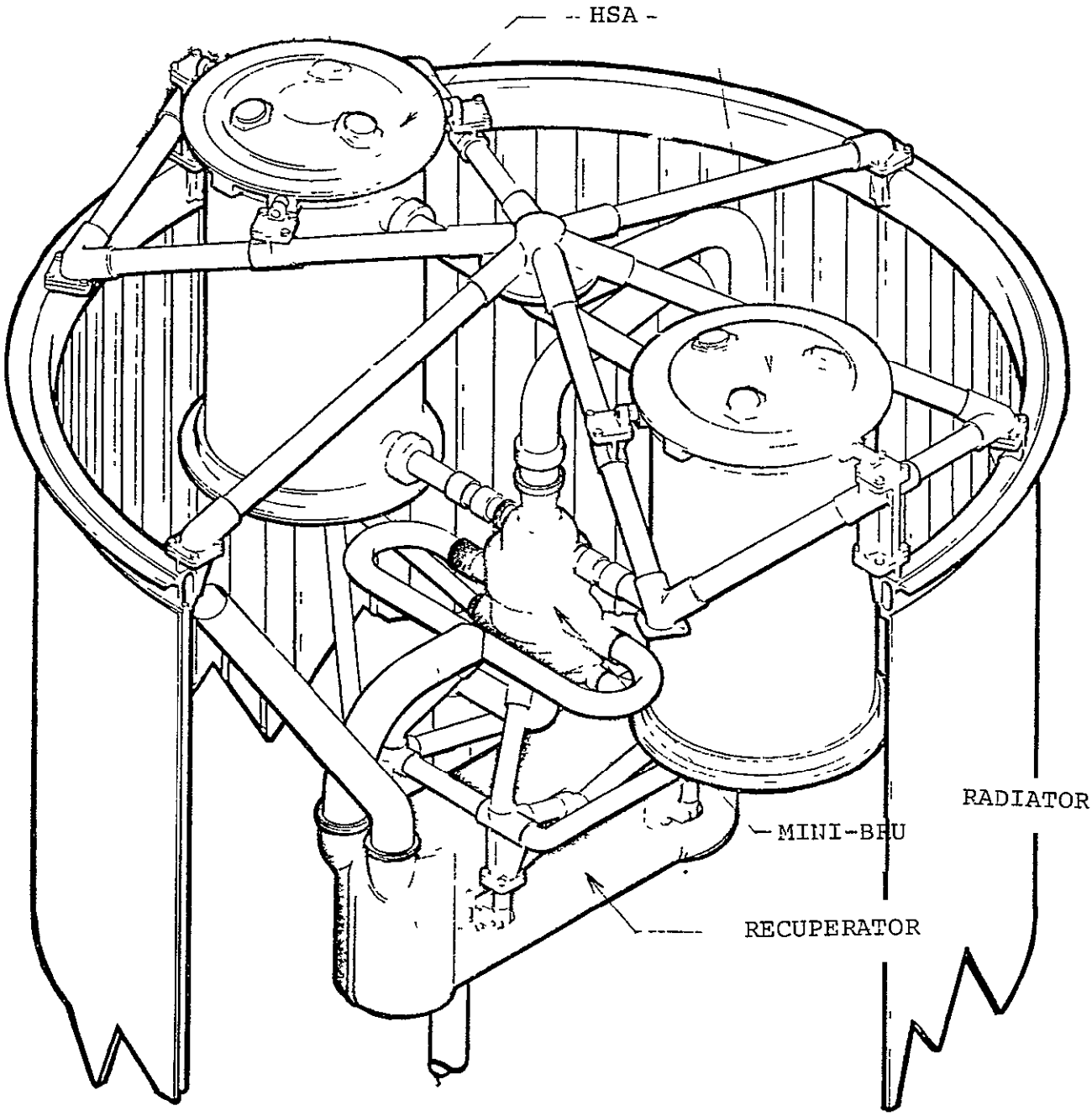

1.4 HSA DEFINITION AND COMPONENTS

The Heat Source Assembly generates the thermal energy required for operation of the Mini-Brayton System and transfers this energy via a heat exchanger fluid loop to the Power Conversion System. The subsystems and respective components which collectively comprise the HSA are listed in Table 1-1.

The Isotope Heat Source is fueled with 2400 watts (thermal) of $^{238}PuO_2$ ceramic fuel of 82 percent theoretical density. The design provides positive safety margins for any re-entry up to 11,000 m/sec (36,000 ft/sec) and for all credible accident modes. This Multi-Hundred Watt Heat Source is flight qualified for the LES 8/9 and Voyager missions. During the BIPS ground demonstration tests, Electric Heat Source(s) (EHS) developed during the Multi-Hundred Watt Radioisotope Thermo-Electric Generator program will be utilized in place of the Isotope Heat Source(s).

The Heat Source Heat Exchanger (HSHX) transfers heat from the Heat Source to the BIPS working fluid by means of a heat exchanger and associated headers and ports.

The Auxiliary Cooling Subsystem (ACS) provides requires cooling of the heat source and refractory HSA materials during non-operational periods of the BIPS on the launch pad or during launch.

The Emergency Cooling Subsystem (ECS) is a passive system that is automatically activated in emergency situations that could result in an overtemperature condition of the heat source. Such emergencies can be

precipitated by unplanned delays in orbit achievement prior to starting up the power system; failure of the power conversion system (e.g., loss of radiator integrity, Mini-BRU failure, leaks in the gas loop, etc.); unplanned shuttle landing in remote areas where auxiliary coolant is unavailable, etc. The ECS is capable of operating during all mission phases included prelaunch. It is unlikely, however, that the ECS would ever activate during the prelaunch phase since auxiliary cooling is provided and the Heat Source is under positive control.

The Heat Source Insulation Subsystem (HSIS) consists of multifoil insulation blankets which surround the HSA structure and minimizes the heat loss from the system. Penetrations through the insulation are provided for the primary cooling system (BIPS working fluid loop) and for heat source supports.

Table 1-1. Heat Source Assembly Subsystems and Components

Subsystem or Component	Symbol	Function	Major Components
Heat Source	HS	Source of Thermal Energy for Power Conversion System (2400 W_t)	• PuO_2 Fuel • Re-entry Protection Systems
Heat Source Heat Exchanger	HSHX	Transfers heat from the HS to the Power Conversion System during Normal Operation	• Heat Exchanger • Headers • Ports • Brackets and Studs
Auxiliary Cooling Subsystem	ACS	Cools HS during Non-Operational Periods on Launch Pad	• Gas Management Valve • Inert Gas
Emergency Cooling Subsystem	ECS	Melting and fusing insulation	• Multifoil Insulation (HSIS)
Heat Source Insulation Subsystem	HSIS	Limits Heat Loss from HS during Operation	• Multifoil Insulation

SECTION 2

SUMMARY

The effort of this contract resulted in the fabrication of components for (and assembly of) three Heat Source Assemblies. A major accomplishment was the assembly of a diffusion welded refractory alloy Heat Source Heat Exchanger which represents an advancement in the state of the art of this technology. Another principal thrust of the program was major progress in the development of a high temperature multifoil insulation system which functions as an emergency cooling system for the isotope heat source in the event of a loss of cooling accident. Acceptance tests on the HSHX's were conducted prior to delivery of the hardware. A brief summary of the design, development, fabrication and testing tasks follow.

2.1 HSA CONFIGURATION

The Heat Source Assembly, which is shown in Figure 2-1, would utilize in a flight configuration, the existing Multi-Hundred Watt (MHW) plutonium fueled Isotope Heat Source developed by the ERDA and the General Electric Company for the LES 8 and 9 and Voyager spacecraft missions. In its ground test configuration (which is the hardware delivered at the end of this contract) it utilizes the MHW Electric Heat Source. Surrounding the heat source and supported from it, is a columbium alloy (C-103) Heat Source Heat Exchanger (HSHX). The HSHX is a finned plate heat exchanger of cylindrical geometry with torroidal headers with inlet and outlet ports at the extremities. The flow channels are formed by machined fins of the inner cylinder. The outer HSHX cylinder is

diffusion welded to the fins at high temperature and pressure in a Hot Isostatic Press (autoclave). The headers are then welded to the cylindrical core and the ports welded to the headers to complete the assembly. Support brackets with studs are welded to each of the headers to provide the mechanical support interface with the Heat Source. Surrounding the HSHX is an insulation blanket which is wound on a 30 mil columbium structural support. The insulation consists of 39 inner layers of .0013 cm (½ mil) molybdenum foil followed by 20 layers of .0013 cm (½ mil) nickel foil. The most outboard layer is 0.008 cm (3 mil) stainless steel (CRES 301) foil to aid in handling. One side of each ½ mil foil is sparcely coated with zirconia particles (ZrO_2) to provide spacing between layers. The ZrO_2 particles are of the order of microns in size and occupy less than 5% of the foil surface area. Stack up thickness of a 60 layer cylindrical blanket is approximately 1. cm ($\sim$0.4 inches); stack up of a flat sample is only 0.4 cm (0.15 inches). This small stack up characteristic is a significant design feature that relates to prelaunch ground cooling of the HSA. Ground cooling is required to maintain the isotope heat source at safe temperatures when the primary cooling loop (Brayton fluid loop) is non operative. It would also be required to maintain refractory alloys at a temperature below which oxidation would occur if exposed to an oxidizing environment. Ground cooling is accomplished by backfilling the HSA with an inert gas (helium or argon), The inert gas thermally shorts the insulation blanket thus providing a low thermal resistance path to the external surface of the HSA. This same passive cooling scheme can also be used during launch and orbit insertion if the BIPS has not been started up. The insulation blanket serves one other important function. It functions in orbit as an

Emergency Cooling System (ECS) in the event of a power system failure which could potentially cause an over-temperature of the isotope heat source. The insulation blanket should melt and fuse at a sufficiently low temperature, permitting a low thermal resistance path for heat flow from the heat source to the space heat sink. This will preclude gross overheating of the heat source which could lead to failure of the isotope containment and a potential radiological hazard in the event of accidental loss of, or circulation of the Brayton working fluid.

An outer housing, external to the insulation, provides the structural load paths for the HSA and the mechanical interface with the power system. The housing is sealed (although not hermetically) to contain an inert gas during ground cooling. It would be provided with a pressure release device to vent the gas in orbit. The ground test hardware is equipped with a gas management valve for loading and venting the inert Auxiliary Cooling Gas. Titanium end enclosures which mechanically lock into the housing, are preloaded at assembly to support the heat source during launch.

2.2 C-103 HSHX FABRICATION DEVELOPMENT

The manufacture of the HSHX from C-103 columbium base alloy requires forming, machining, and joining operations which, in most cases, are conventional and have been performed routinely. However, the machining of thin fins on the inner cylinder, the forming and machining of the header components, the precision fit-up and welding of the thin header scroll components, and the diffusion welding of the heat exchanger finned cylinder section required more intensive development and less conventional tooling and manufacturing process techniques. In addition,

radiographic, holographic and ultrasonic non-destructive techniques to assess the soundness of weld joints and diffusion welded sections were studied.

Fin Machining

The "finned" flow channel heat exchanger design requires the milling of the flow passages on the inner cylinder. After this operation, one hundred forty eight (148) fragile fins, 0.064 cm (0.025 inch) thick and 0.41 cm (0.160 inch) high, project from the inner cylinder. The radially outermost surface of these fins form the interface for diffusion welding to the outer cylinder. Thus, the OD surface finish of the cylinder before milling must be as good as reasonably possible and this surface finish must be maintained during the milling of the flow passages (fins). The fragile nature of the fins requires that care be taken to prevent breakage during milling or handling. Areas investigated included cutter tooth geometry, coolants, feed rates, cutter speeds and feed direction. A photograph of the machined inner cylinder with the integral fins is shown in Figure 2-2.

Diffusion Welding

The gas pressure diffusion welding or Hot Isostatic Pressing (HIP) process is particularly well suited to the production of complex, internally cored components such as the HSHX.

The diffusion welding development had as its goal to establish practical process parameters which result in a monolythic HSHX core as evidenced by grain growth across the joint interface and the absence of any bond line porosity or other discontinuities.

Areas investigated included cleaning techniques, methods of protecting the sample couple from contamination during the autoclaving, process parameters i.e., pressure, temperature and time, and methods to prevent collapsing of fins during the hot gas pressure welding.

The cleaning process selected on the basis of the least likelihood of residual contaminants during diffusion welding, consists of acid etching plus vacuum heat treating the C-103 prior to the hot gas bonding.

In order to protect the elements to be diffusion welded, it was found necessary to double "can" them in columbium alloy foil.

Numerous flat coupons as well as finned samples, were diffusion welded under varying temperature, and pressure conditions. The initial goal during the early autoclave runs was to obtain welding at sufficiently low temperatures and pressures to preclude bending of the unsupported flow channel fins. Otherwise support bars would have to be machined and placed between fins to prevent collapsing during the hot isostatic pressing and removed after diffusion welding. Although this was a desirable objective, it could not be accomplished. High pressure diffusion welding was required. The unsupported flow passages were filled with precisely machined molybdenum. The molybdenum filler bars are leached out after the diffusion welding process by immersing the parts in an acid solution of 25% HNO_3-25% H_2SO_4- 50% H_2O at approximately 347^{o}K (165^{o}F). The acid does not attack the columbium alloy.

The autoclaving temperature investigated covered the range 1365°K - 1810°K (2000°F to 2800°F) with pressures varying between 1.4 MPa (200 psi) and 69 MPa (10,000 psi). The parameters selected to insure diffusion welds which consistently exhibit no evidence of a weld interface line was 1810°K (2800°F), 69 MPa (10,000 psi) for three hours. To obtain the temperature and pressure in a facility large enough for the HSHX, an autoclave at the Battelle Columbus Laboratories was modified under a subcontract to General Electric Co., and various trial parts diffusion welded to verify the process. An example of the quality of a typical diffusion weld resulting from autoclaving at Battelle is shown in the photograph of Figure 2-3.

Inspection of the diffusion weld areas are accomplished by ultrasonic scans using a calibration standard with prescribed defect sizes.

Welding and Forming

GTA welding of thick C-103 plates and thin sheet material have been accomplished without any problems. Welding parameters were established.

Forming of the outer header scrolls requires careful tooling design to avoid wrinkling of the "skin". Inner scrolls were machined from thick plate.

2.3 INSULATION/EMERGENCY COOLING VERIFICATION

The thermal insulation system serves the following functions:

a) It limits heat loss from the HSA during normal operation.

b) It permits conduction when thermally shorted with an inert gas on the pad, to provide auxiliary cooling of the Heat Source when electrical power is not generated by the BRU.

c) It should melt and fuse at a sufficiently low temperature to provide emergency cooling in orbit in the event of loss of the Brayton working fluid.

The zirconia coated multifoil insulation blanket, developed by Thermo-Electron Corp. under an AEC Contract, appeared to meet these BIPS requirements. Preliminary selection of the insulation system to meet these requirements were made after numerous material compatibility tests. As described in 2.1, the insulation consists of 39 layers of molybdenum foil followed by 20 layers of nickel foil coated with zirconia particles that are cold sprayed on the foil and then fired at approximately 1075°K for one to two hours. The system has a eutectic temperature of 1590°K (2400°F) and limits the Mo-Ni interface to 925°K. The zirconia particles act as spacers between the foils to limit solid conduction effects. Because of the small ZrO_2 particle size, the stackup thickness of the insulation is small. When shorted with an inert gas the thermal resistance across the relatively small thickness of insulation is minimal, thus permitting adequate heat transfer to cool the Heat Source on the pad, during launch, and during the first few orbits if the Brayton Rotating Unit is not circulating the working fluid.

A major uncertainty of the insulation system was the ability of the cold sprayed zirconia particles to remain adhered to the nickel foil under anticipated vibration environments. NASA had some early experience with loss of particles during transportation. A second major concern was the capability of the insulation to provide stable thermal performance at the high operational temperatures anticipated. Material interactions and self welding of the foils over long periods of time is considered a possibility. The third area requiring test verification was the meltdown

operation for the emergency cooling function. Small scale meltdown tests indicate that this passive technique can preclude overtemperature of the heat source, by decreasing the number of molybdenum foils to ~18, resulting in a Ni-Mo interface temperature of 1075°K or by correspondingly substituting 33 columbium foils for the molybdenum foil and limiting the Cb-Ni interface to 975°K. Further development effort however is necessary in view of the potential radiological hazard associated with nuclear systems to finalize the insulation ECS system for flight hardware and assure long term operational stability for the 7 year lifetime.

Life Stability Tests

Early in the program life stability tests were conducted on an all nickel insulation system to verify stable performance in vacuum under operational temperatures for reasonably long times. A total of six tests were conducted on five cylindrical test samples simulating the HSA configuration for a minimum of 1000 hours, in vacuum at hot insulation face temperatures of 1090°K, 1145°K, 1200°K and 1255°K (1500°F, 1600°F, 1700°F and 1800°F). One sample was thermally cycled five times between room temperatures and 1145°K (1600°F) over a 1500 hour period after it had already completed 1000 hours of testing at 1090°K (1500°F). The samples consisted of 60 layers of .00127 cm (1/2 mil) nickel foil with a dispersed zirconia coating on one side. One sample for comparison purposes, was pure nickel foil without the zirconia coating. These preliminary test results indicated stable thermal performance for all samples except for the insulation that did not have zirconia coated nickel foil. No self welding of the foils was evident on the zirconia coated samples when disassembled after the tests.

Later during the program, accelerated life tests were conducted in an evacuated oven on different combinations of foil (Nickel, Molybdenum and Columbium) with zirconia (ZrO_2) at elevated temperatures. It was concluded from this study that some self welding of nickel foil and instability of the calcia (CaO) stabilized ZrO_2 could occur over the 7 year life time. It was concluded that the ZrO_2 coated nickel should be limited to 975°K with columbium or molybdenum foil inboard. The columbium foil results in a lower eutectic point (1450°K) with nickel, resulting in earlier meltdown of the system in the ECS mode. However, since more long term tests would be required to optimize the system, it was considered prudent to select a very stable system for the ground test hardware to preclude performance degradation during the BIPS test program. Hence, a molybdenum-nickel foil system was chosen with the nickel restricted to a very safe temperature of 925°K.

Vibration and Thermal Conductivity Tests

The purpose of the vibration tests were to verify the capability of the zirconia particles to adhere to the foil under vibration environments. Four test samples consisting of 60 layers of zirconia coated 0.00127 cm (1/2 mil) nickel foil, stacked in a 10.16 cm (4 inch) diameter flat configuration, were subjected to a series of vibration tests at levels up to 20 g's (well in excess of launch loads). The samples, as received from the vendor, had certified weights which included the weight of zirconia.

The samples were weighed before and after each vibration test to determine weight loss. Thermal conductivity measurements were also mode before the first and after the last vibration test for each sample respectively.

Results of the test indicated negligible zirconia weight loss due to vibration. The maximum accumulated zirconia weight loss for any one sample was 2.5%. Thermal conductivity measurements did not indicate any change in the effective thermal conductivity of the examples.

Meltdown Tests

Small scale meltdown tests were conducted on two cylindrical configurations simulating the HSA configuration. One consisted of an all nickel foil system and the second a combination of 36 layers of columbium followed by 24 layers of nickel. Both tests indicated the start of melting at anticipated temperatures, i.e., the melt temperature of nickel 1730°K (2650°F) for the all nickel system and the Cb-Ni eutectic temperature 1450°K (2145°F) for the Cb-Ni foil system. Fusing and solification of the foil occurred locally indicating a marked and sudden degradation of the insulation. It would appear that this short circuiting of the insulation would preclude overtemperature of the heat source with appropriate optimization of the foil materials. Further demonstration on full scale models are required before a flight system can be selected.

2.4 FABRICATION AND ACCEPTANCE TESTING

Components for three HSA's were fabricated and acceptance tests performed. Final assembly and testing of the HSA's will take place at a later date under a separate contract. A photograph of the HSHX, the major component of the HSA, is shown in Figure 2-4. Section 6 contains photographs of other HSA component hardware.

Proof pressure tests on the HSHX were conducted at 2.5 MPa (360 psi) (using a safety factor of 1.5). Pressure drop tests conducted using air at room temperature and matching Reynolds number indicate ΔP exceeds the contract specification by from approximately 10% to 25%. However, in the BIPS 1.3KW_e configuration the HSHX pressure drop would only be about 60% of the allowed ΔP for the HSHX, hence BIPS system requirements are met. Leak tests conducted on the three HSHX's revealed no detectable leak within the sensitivity ($1x10^{-8}$ to $0.9x10^{-9}$ std cc Helium) of the leak detector.

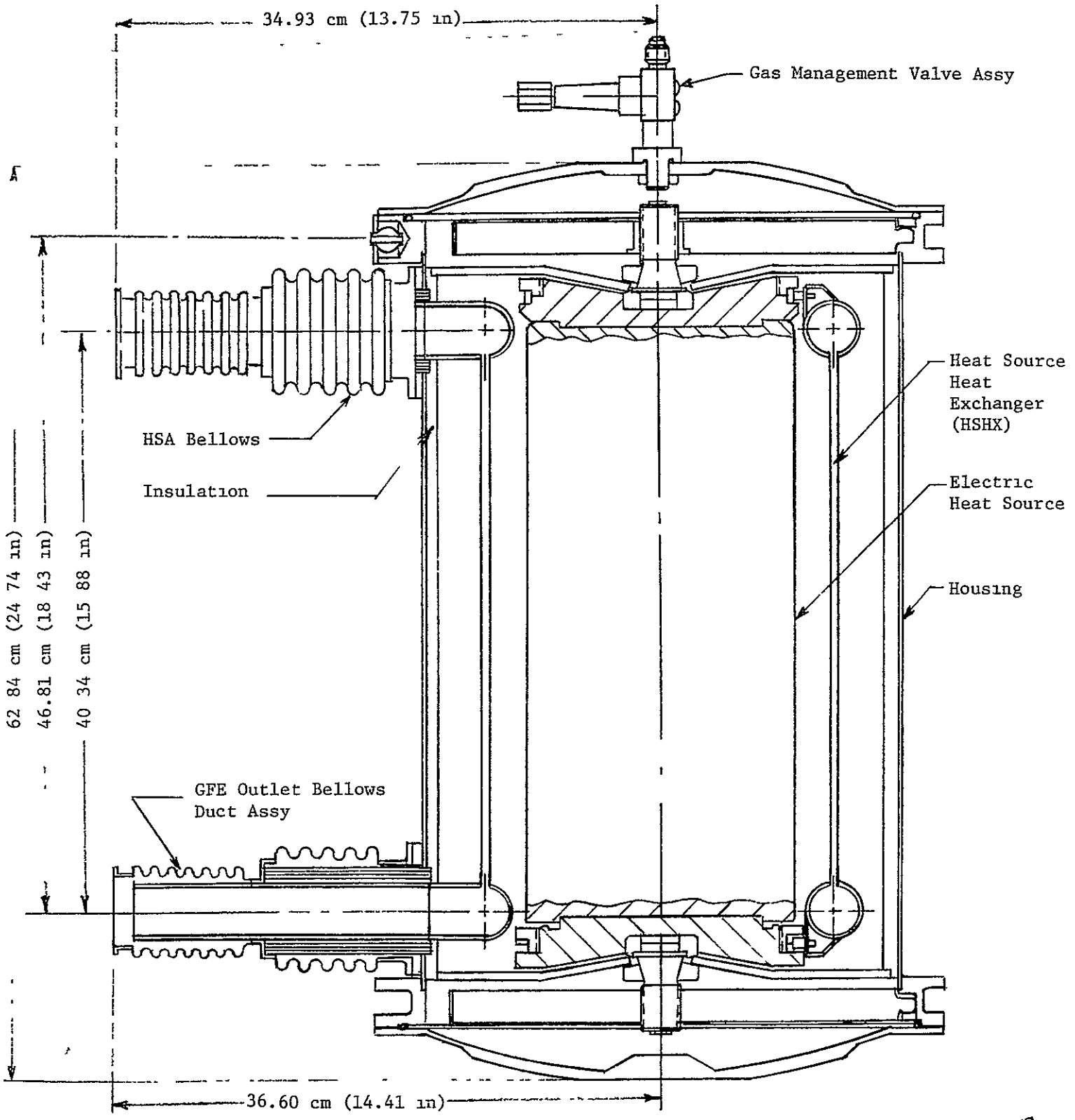

FIGURE 2-1

HEAT SOURCE ASSEMBLY

Figure 2-2
C-103 Machined Inner Cylinder

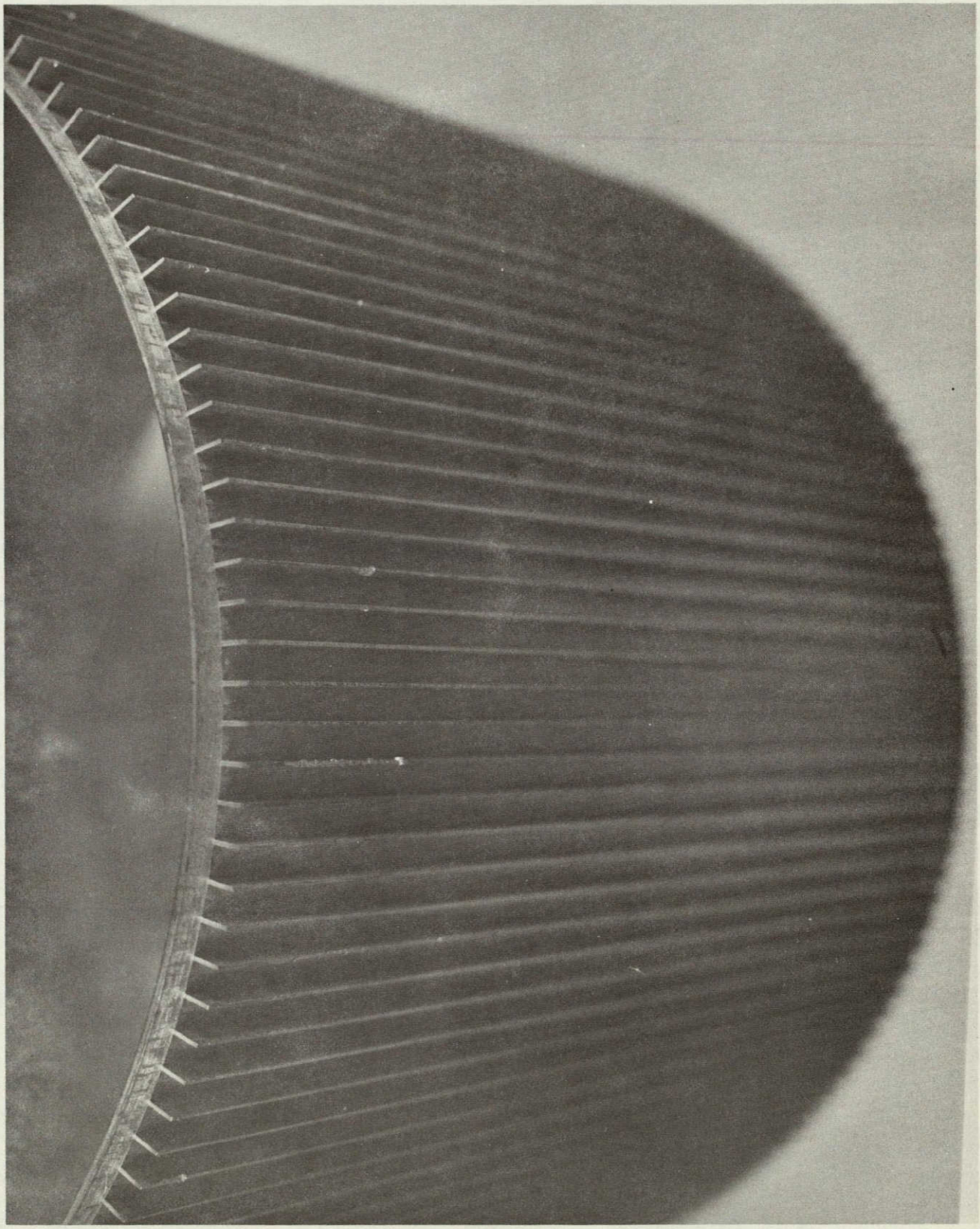

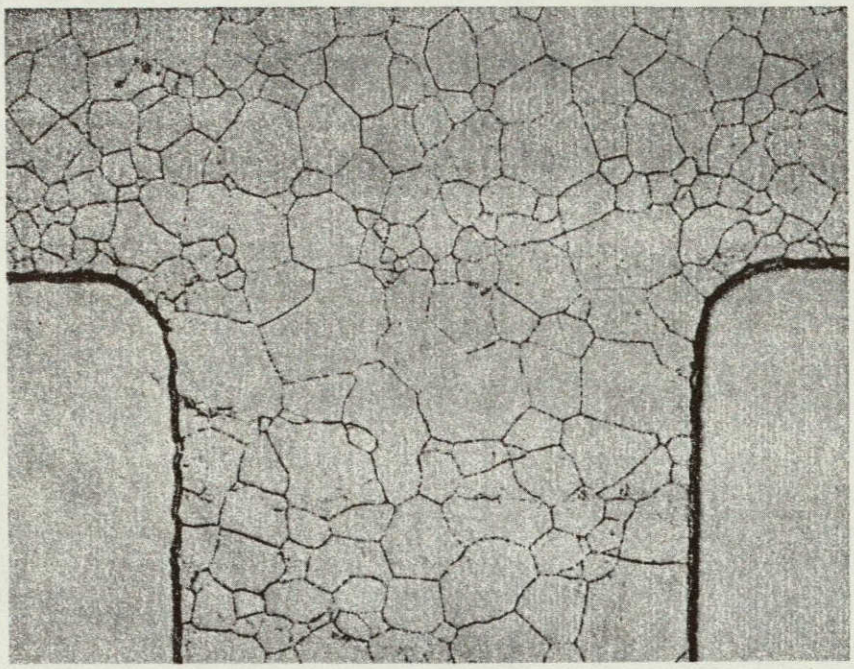

Top Ring, Fin 111 (100X)

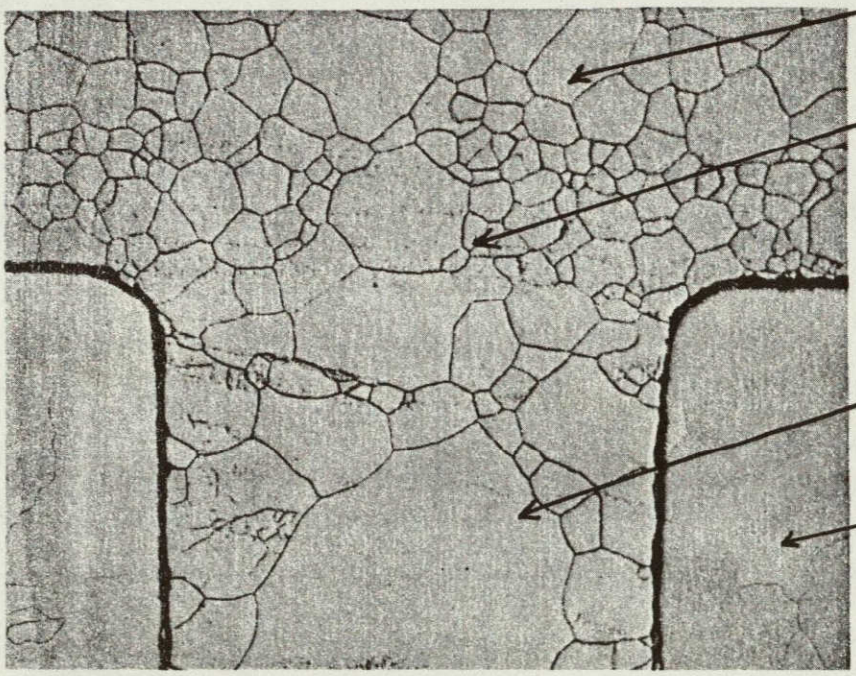

Bottom Ring, Fin 111 (100X)

Figure 2-3. Photomicrographs Showing Typical Microstructures of Diffusion Welds in HSHX Cylinder Number 1.

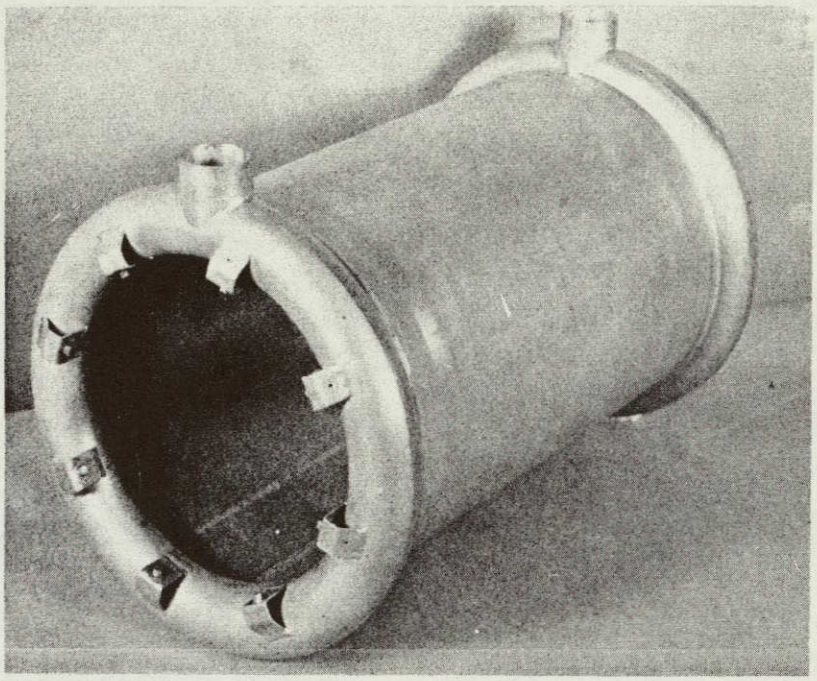

Figure 2-4. Photograph of HSHX S/N 1 After Completion of Conformance Tests and Re-inspection.

SECTION 3

HEAT SOURCE HEAT EXCHANGER FABRICATION DEVELOPMENT

The manufacture of the HSHX from the columbium base alloy C-103 (nominally Cb-10% Hf-1% Ti) includes several non-routine steps and processes. Among these are the machining of nearly 150 fragile fins, 0.0635 cm (0.025 in) thick, 0.4064 cm (0.160 in) high and 38.1 cm (15 in) long in a C-103 cylinder approximately 24.13 cm (9.5 in) in diameter. The outer edges of these fins are later diffusion welded to a thin-walled C-103 cylinder: the diffusion welding process had not been developed for this alloy.

An extensive amount of fabrication development effort was required to establish the procedures for accomplishing these and other non-routine fabrication methods needed to manufacture the HSHX.

The major areas requiring development were as follows:

- Diffusion Welding - Diffusion welding is accomplished in the solid state when components are held together under high pressure at elevated temperature. Factors of extreme importance in achieving joining include the surface finish of the components to be diffusion welded, surface cleanliness, microstructural influences such as cold work, welding atmosphere, temperature, pressure, and time. To achieve sound joints reproducibly, the limits of diffusion welding process parameters had to be established.

- Machining - The machining of many long, thin fins in the C-103 alloy inner cylinder required development because of the fragile nature of the component and the susceptibility to fin breakage. Additionally, the smooth surface finish of the outer edges of the fins must be maintained in order that later diffusion welding to the thin-walled outer cylinder will not be hampered.

- Welding - Although GE had had a considerable amount of experience in the welding of columbium and columbium alloys, it was nevertheless necessary to establish weld parameters and weld shrinkage allowances specifically for C-103 components of the size and thickness utilized in the HSHX. The high cost of refractory metal alloys precludes establishing these parameters on actual parts. It was therefore necessary that they be determined on small trial parts prior to the start of manufacture of the HSHX.

- Forming - The outer halves of the toroids are fabricated from 0.13 cm (0.050 in) thick C-103 sheet. Dimensional tolerances are important as these parts must be welded to mating parts. Again, the high cost of the refractory alloy makes it imperative that the forming process be developed and optimized using less costly materials such as stainless steels prior to forming C-103 parts.

The fabrication development efforts in these various areas are described in the following paragraphs.

3-1 DIFFUSION WELDING

Experimental diffusion welding runs were made using C-103 specimens for the purpose of establishing the limits of the joining process parameters and selecting parameters which produce sound diffusion welded joints reproducibly. Both flat specimens and finned configuration specimens were used in this work. Two autoclaves at the GE-Evendale facility - a 16.5 cm (6.5 in) diameter and 29.2 cm (11.5 in) diameter - were used in this work. The larger autoclave could accommodate a full size HSHX. Initial experiments were conducted in the smaller of the two GE-Evendale autoclaves to take advantage of its availability and lower cost of operation. After considerable development effort, it was determined that a higher temperature capability than the 16.5 cm diameter Evendale autoclave offered was required; a newer and larger autoclave at Battelle Columbus Laboratories was subsequently modified and used for delivered HSHX hardware.

3.1.1 EXPERIMENTS IN 16.5 cm (6.5 in) ID AUTOCLAVE

The first few diffusion welding runs were designed to evaluate several material conditions, surface finishes, and surface cleaning variables. These included three lots of material (two of which were recrystalized and one of which had 70 to 90% cold work), several surface finishes and several surface cleaning methods or combinations thereof (as-rolled by vendor, mechanically polished, acid etched, and vacuum heat treated). Specimens consisted of two pieces of 0.0635 cm (0.025 in) thick C-103 sheet approximately 1.9 cm x 2.54 cm (0.75 in x 1. in) sealed in 0.051 cm (0.020 in) thick tantalum envelopes. It was concluded from these runs that the best diffusion welds were obtained with specimens that had been either

acid etched or acid etched and vacuum heat treated prior to diffusion welding. There did not appear to be a decided advantage of cold working the C-103; polishing and solvent cleaning prior to diffusion welding was less effective than acid pickling. Subsequent diffusion welding was conducted using recrystallized material. Specimen preparation consisted of solvent cleaning followed by acid pickling. The pickling solution for C-103 components was 1 part (by volume) hyrofluric acid (HF), 4 parts nitric acid (HNO_3), 1 part sulfuric acid (H_2SO_4) and 2 parts water (H_2O). When molybdenum filler bars or cover plates were used, they were pickled with 44% (by volume) H_2SO_4, 21% HNO_3, 0.5% hydrochloric acid (HCl), and 34.5% H_2O (30 seconds or less). Pickling was followed by deionized water rinse, alcohol rinse, and a treatment in vacuum for 30 minutes at 1480K (2200°F). Tantalum parts for the pressure envelopes also were acid pickled in the same manner as C-103 alloy and given the vacuum heat treatment. All parts were wrapped in 0.00254 cm (0.001 in) thick tantalum foil prior to the vacuum heat treatment.

Several diffusion welding runs were aimed toward evaluating the feasibility of diffusion welding finned specimens without molybdenum filler bars in the slots. The purpose of this was to avoid, if possible, the cost of the molybdenum, the cost of labor to fabricate the molybdenum filler bars, the added difficulty in handling and assembly, and finally, the necessity of leaching out the molybdenum bars after diffusion welding.

The results of this investigation revealed that unsupported fins would deform at autoclave pressure as low as 4.8 MPa (700 psi) at temperatures of 1700K (2600°F). Figure 3-1 is a dramatic illustration of the effect of a pressure of 6.9 MPa (1000 psi) in the autoclave. Considerably higher pressures were found to be required to obtain excellent diffusion welds. It was concluded consequently that molybdenum filler bars would be required.

Diffusion welding conditions for finned configuration specimens with molybdenum filler bars in the slots were investigated in the next several autoclave runs. Void-free weld interfaces were obtained in three hours at 1700K and 5.5 MPa (2600°F and 8000 psi); however, some voids were present in the joints at pressures of 4.1 MPa (6000 psi) and 4.8 MPa (7000 psi), even though void-free welds had been obtained at pressures as low as 1700K and 3.4 MPa (2600°F at 4900 psi) in earlier runs on flat sheet samples. This suggests that other conditions of the experiments (perhaps metal surface conditions as affected by chemical etching or cleaning) were not identical to those of the earlier runs and that these autoclave parameters could be marginal in obtaining consistently excellent diffusion welds.

3.1.2 EXPERIMENTS IN THE 29.2 cm (11.5 in) ID AUTOCLAVE

Following the demonstration of making successful diffusion welds in 3 hours at 1700K and 5.5 MPa (2600°F and 8000 psi) in the 16.5 cm (6.5 in) ID autoclave in finned specimens, the diffusion welding experimental work was transferred to the 29.2 cm (11.5 in) ID autoclave. This autoclave is large enough to accommodate the full size C-103 cylinder assembly for the HSHX.

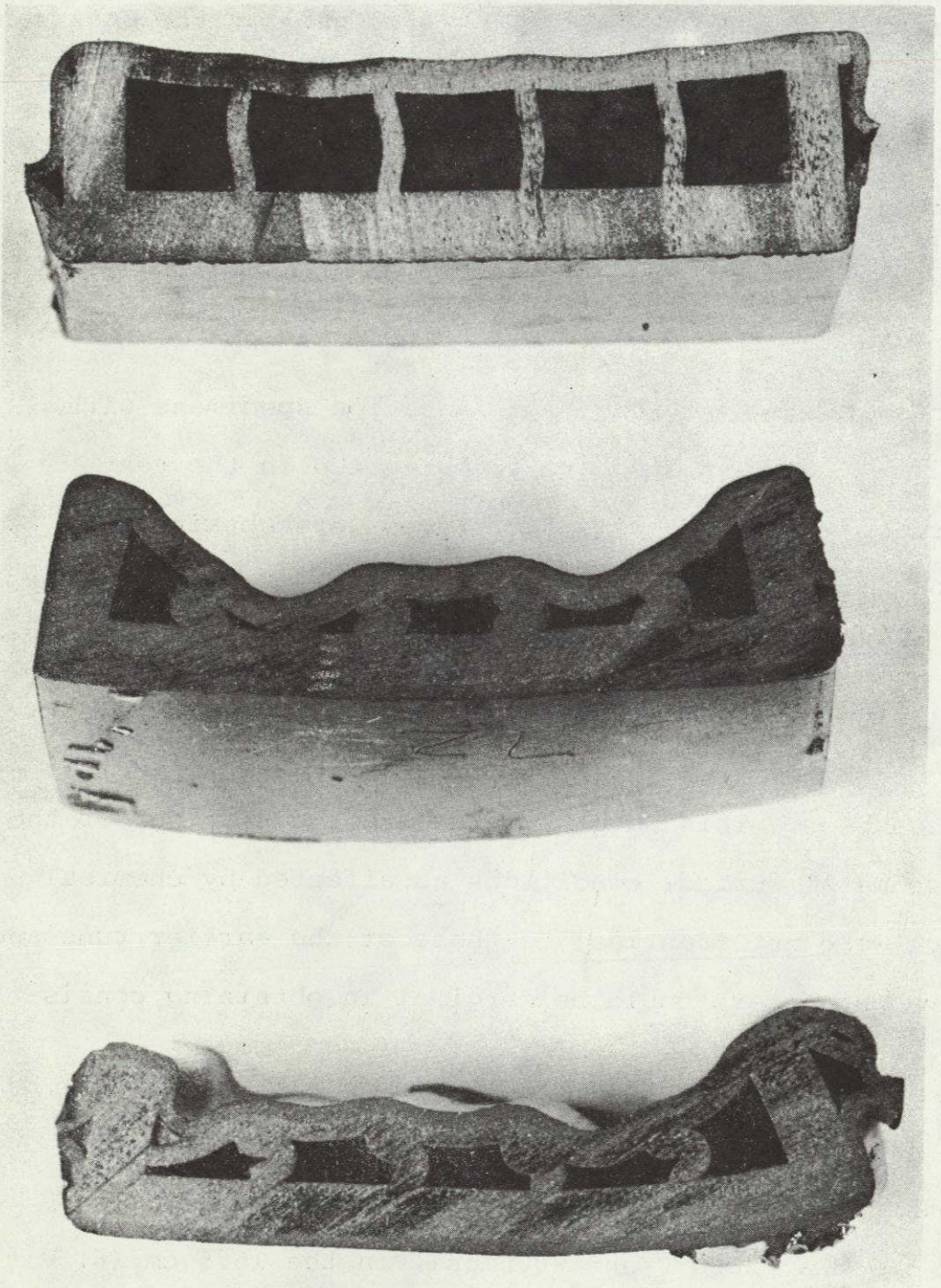

Specimen No. 70
1645K (2500°F)

Specimen No. 72
1700K (2600°F)

Specimen No. 74
1755K (2700°F)

Figure 3-1 Finned Specimens Without Mo Filler Bars
6.9 MPa (1000 psi) Helium Pressure; Equivalent to Approx.
48.3 MPa (7000 psi) Bonding Surface Pressure.

An initial trial run was made to determine temperature gradients in the autoclave. The C-103 cylinder was simulated with a graphite sleeve 25.4 cm (10 in) ID by 29.9 cm (11 in) OD by 45.7 (18 in) in length and the sleeve heated to 1700K (2600°F) at a pressure of 55. MPa (8000 psi) for a period of two hours. Temperature variation along the sleeve was on the order of 5.5K to 11K (10°F to 20°F). This run was an encouraging demonstration that this vessel could be capable of operating uniformly at conditions which appeared suitable for diffusion welding the full sized C-103 cylinder of the HSHX.

In the second run, 0.0635 cm (0.025 in) thick C-103 sheet specimens were positioned at the top and bottom of the graphite sleeve. The conditions of this run were 1700K (2600°F) and 55. MPa (8000 psi) for three hours. Metallographic examination of the specimen revealed well rounded voids or pores at the weld interface in contrast to the excellent welds developed in the small autoclave under supposedly identical conditions.

In the following run, also at 1700K (2600°F), the pressure was increased to 69. MPa (10,000 psi) for the first hour, after which it was lowered to about 55. MPa (8000 psi) to avoid overheating of the pressure vessel. Excellent diffusion welding was achieved at these slightly higher pressure conditions. In this run and all subsequent runs, a graphite-free load support structure made from refractory brick and molybdenum sheet was used. The graphite sleeve used to simulate the C-103 cylinder had been replaced with a molybdenum cylinder, thus removing all graphite from the autoclave vessel.

In the next series of autoclave runs, attempts were made to obtain repeatability of results as well as to re-evaluate the effect of preparation variables of the samples on the quality of the diffusion welds. It was found that on flat sheet samples excellent diffusion welds evidenced by absence of voids at the interface could not always be obtained at 69. MPa (10,000 psi) and 1700K (2600^{o}F), but that increasing the temperature to 1730K (2650^{o}F) improved the quality of the welds. It was also evident that where plastic deformation had occurred, as in a finned configuration (with round molybdenum filler bars) and at the ends of the flat sheet samples, the joint interface was completely obliterated by grain growth. Typical photomicrographs from these runs are shown in figures 3-2 and 3-3. Because of arcing in the autoclave that was experienced at 69 MPa (10,000 psi), pressure was limited to 62. MPa (9000 psi), temperature was limited to 1700K (2600^{o}F), and run duration was extended to 5 hours. Two finned specimens approximately 3.175 cm (1.25 in) square were included in the run. Excellent welding occurred in the finned specimens. Subsequently, both were used in pressure tests to determine weld integrity and strength as described below.

The finned samples were prepared for pressure testing by leaching out the molybdenum bars, vacuum heat treating for 1/2 hour at 1480K (2200^{o}F) to remove hydrogen picked up during diffusion welding, welding plates on each end (one plate having a tube attached), and finally relieving weld induced stresses by annealing at 1480^{o}K (2200^{o}F) for 1/2 hour in vacuum.

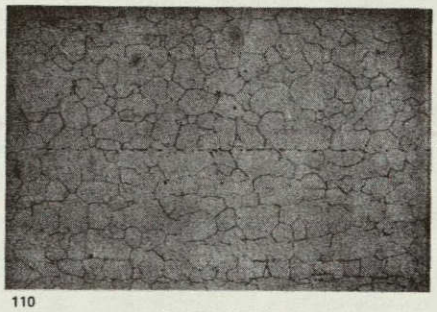

110

SOLVENT CLEAN, PICKLE,
VACUUM HEAT TREAT

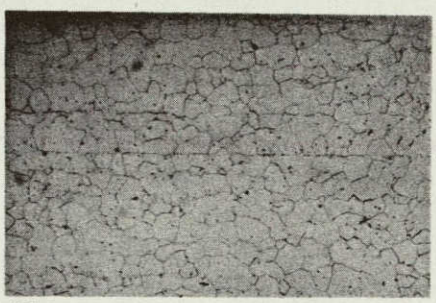

111

SOLVENT CLEAN, PICKLE,
VACUUM HEAT TREAT, EB BAKEOUT

ORIGINAL
INTERFACE

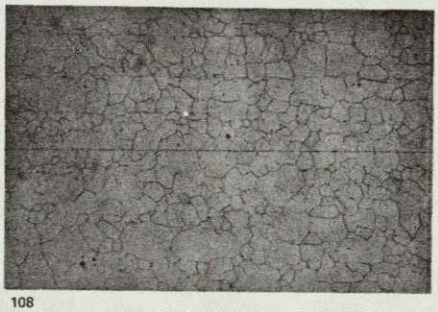

108

600 GRIT POLISH, SOLVENT CLEAN,
EB BAKEOUT

109

SOLVENT CLEAN, PICKLE,
VACUUM HEAT TREAT, EB BAKEOUT

ORIGINAL
INTERFACE

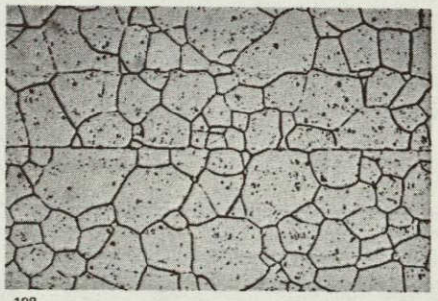

108

AFTER 2 HOURS AT 1920K
IN VACUUM

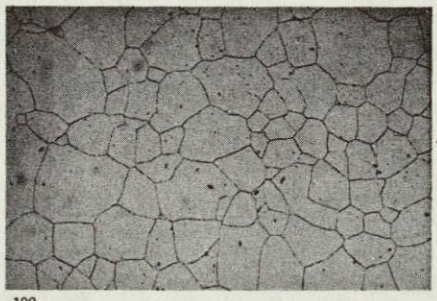

109

AFTER 2 HOURS AT 1920K
IN VACUUM

ORIGINAL
INTERFACE

Figure 3-2 Photomicrographs of Typical C-103 Sheet Specimens Diffusion Welded at 1700K for 1 Hour at 69 MPa Plus 2 Hours at 55 MPa (Run No. 18). (Original Mag 100X; Reduced 50% in Printing).

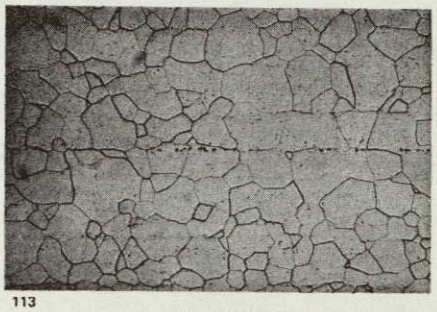

113

SHEET SPECIMEN,
Ta ENVELOPE

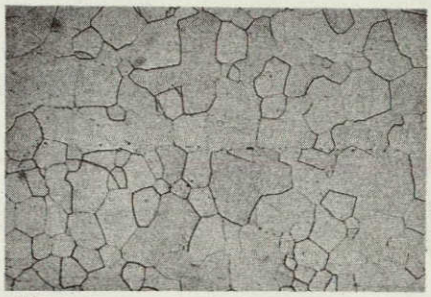

114

SHEET SPECIMEN,
Mo PLATES, Ta ENVELOPE

ORIGINAL
INTERFACE

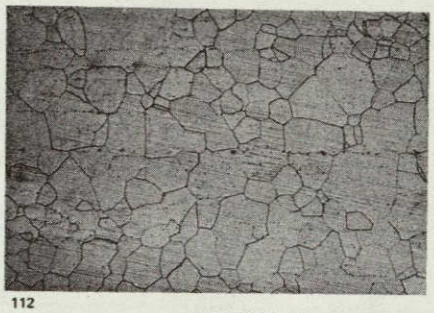

112

SHEET SPECIMEN,
C–103 ENVELOPE

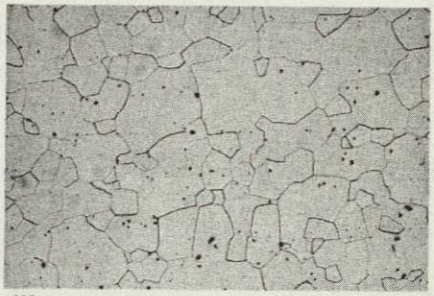

116

SHEET SPECIMEN,
ALTERNATE ACID, Ta ENVELOPE

ORIGINAL
INTERFACE

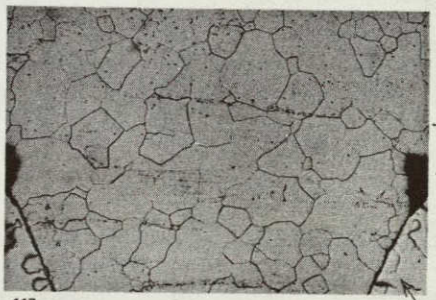

117

FINNED SPECIMEN,
ROUND Mo FILLER BARS

Mo

ORIGINAL AREA
OF INTERFACE

Figure 3-3 Photomicrographs of C-103 Specimens Diffusion Welded at 1730K for 40 Minutes at 69 MPa Plus 2 Hours at 55 MPa (Run No. 19). (Original Mag 100X; Reduced 50% in Printing).

Internal pressure was applied to the specimens to increasingly higher values with a hydraulic pump. Holograms were made periodically to determine whether failure at the fin welds had occurred. Specimen 122 was tested to a pressure of 69 MPa (10,000 psi), where failure occurred by rupture of the C-103 fins at a tensile stress of approximately 483. MPa (70,000 psi). The diffusion welded joints did not fail.

Specimen 121 was given an additional post diffusion welding heat treatment at 1870K (2900°F) for 3 hours. This specimen was not tested to failure, but was subjected to 48. MPa (7000 psi) hydraulic pressure (well into the plastic deformation range). Figure 3-4 shows the specimens after testing. Figure 3-5 shows holograms made during the course of pressure testing Specimen 121 up to 48. MPa (7000 psi). The absence of interference lines crossing the weld line show that cracking did not occur.

The final set of autoclave runs in the "large" GE Evendale autoclave were made to determine the effect of height of the molybdenum filler bars on the quality of diffusion welds made at 1700°K and 62. MPa (2600°F and 9000 psi) for five (5) hours, near the upper temperature and pressure limits of the autoclave. Height of the molybdenum filler bars was varied such that the fins were 0.00254 to 0.00762 cm (0.001 to 0.003 in) higher than the filler bars in one specimen, 0.00762 to 0.0127 cm (0.003 to 0.005 in) higher in another, and 0.0127 to 0.01778 cm (0.005 to 0.007 in) higher in the third specimen. Based on metallographic

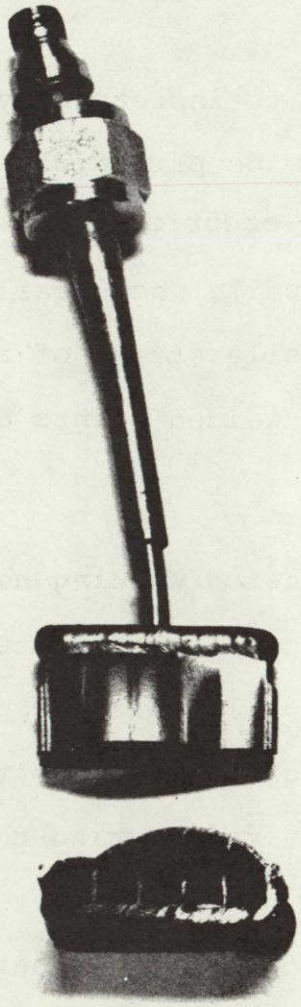

SPECIMEN 122. DIFFUSION WELDED AND PRESSURE TESTED AT 69 MPa (10,000 PSI)

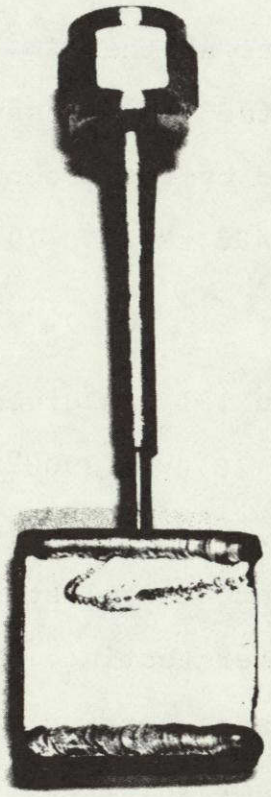

SPECIMEN 121. DIFFUSION WELDED AND VACUUM HEAT TREATED AT 1870°K (2900°F) - 3 HOURS IN VACUUM AND PRESSURE TESTED AT 48 MPa (7000 PSI)

Figure 3-4 Mini-Bulge Test Specimens After Hydro Tests. Both Specimens were Diffusion Welded at 1700°K - 62. MPa (2600°F - 9000 psi) - 5 Hours and Stress Relieved at 1480°K (2200°F) - 1/2 Hour in Vacuum Before and After Weld Assembly of End Plates and Tubing

Neg. 22. 0/1. MPa
(0/150 psi)

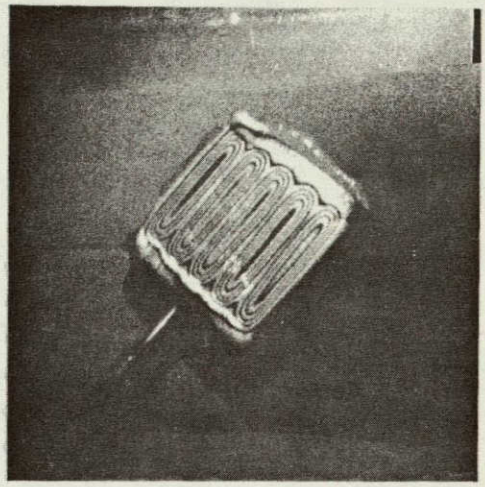

Neg. 23. 0/3.4 MPa
(0/500 psi)

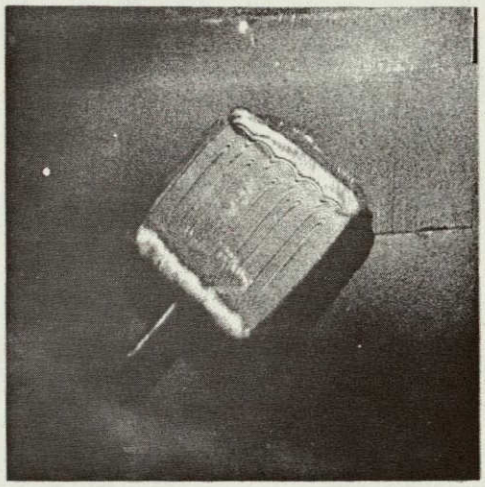

Neg. 24. 0/6.9 MPa
(0/1000 psi)

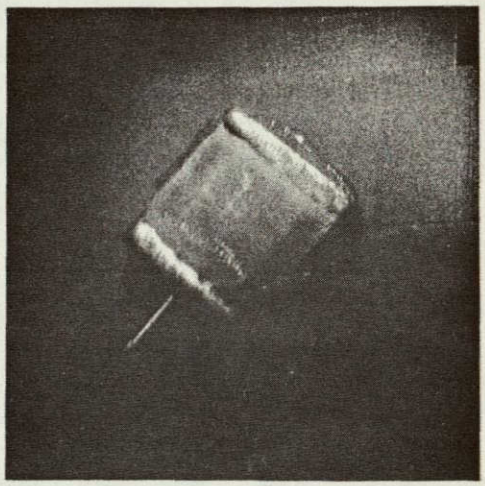

Neg. 25. 0/0 MPa
After 13.8 MPa
(2000 psi)

Figure 3-5 Holographs of Specimen 121 Made at Pressures Indicated.

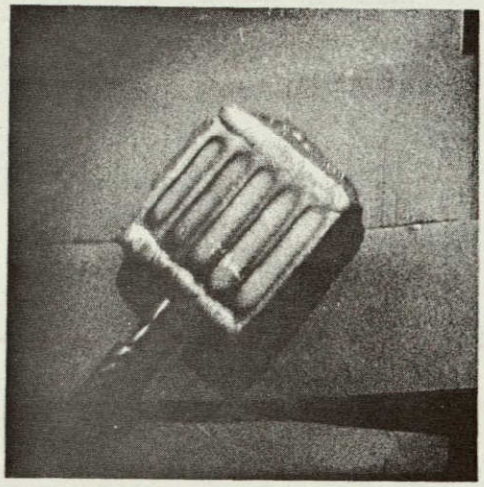

Neg. 26. 0/0 MPa
After 21. MPa (3000 psi)

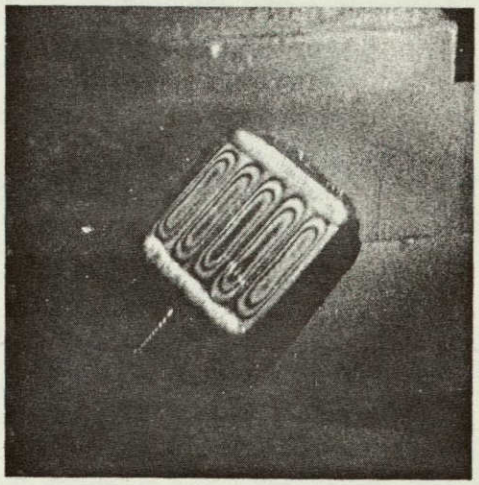

Neg. 27. 0/0 MPa
After 28. MPa (4000 psi)

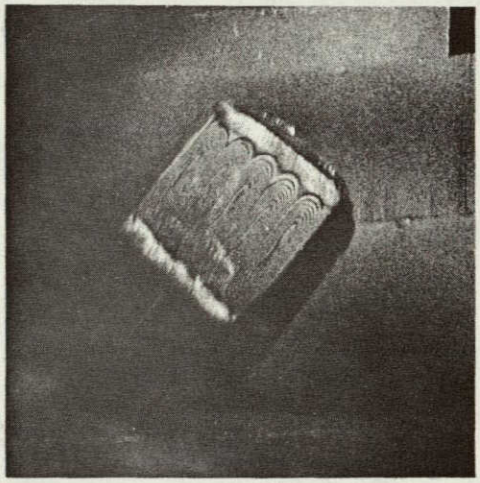

Neg. 28. 0/0 MPa
After 34. MPa (5000 psi)

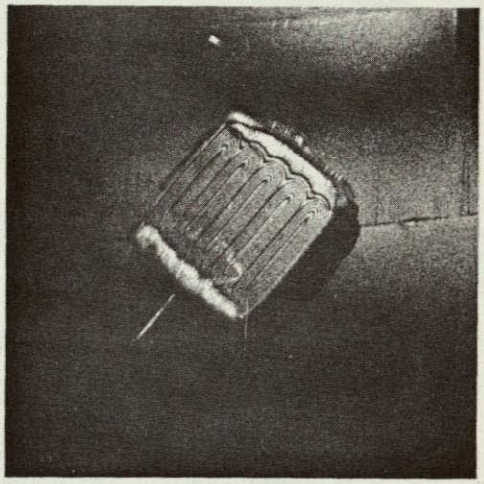

Neg. 31. 0/5516 KPa (800 psi)
After 48. MPa (7000 psi)

Figure 3-5 Holographs of Specimen 121 Made at Pressures Indicated. (Continued)

examination of the microstructures, the best diffusion welding occurred in the specimen in which fins were 0.00762 to 0.0127 cm (0.003 to 0.005 in) higher than the filler bars. The diffusion weld line was free of porosity and grain boundaries were quite random in this specimen, as shown in Figure 3-6. This was one of the best appearing diffusion welds yet obtained. Another segment of this specimen was examined with an electron microprobe analyzer to determine the extent of molybdenum diffusion into the C-103 fins and plates from the filler bars during the high temperature, high pressure diffusion welding process. Prior to the examination, the filler bars and barrier sheets were leached from this segment; after the visible leaching reaction ceased, the segment was exposed to fresh leachant for two additional hours to ensure that all molybdenum was removed from the surfaces. Molybdenum was detected only very near the surfaces. In most instances, it was less than 0.000254 cm (0.0001 in) from the surface, but in one instance it was found 0.000762 cm (0.0003 in) in from the surface. The highest concentration detected was about 10 percent, but concentrations were generally considerably less than that amount. The variability of the concentration profiles, the small amounts detected, and the limited penetration suggests that diffusion of molybdenum into the C-103 under the conditions utilized to diffusion weld the HSHX is not a serious problem. The bulk properties of the C-103 are not affected; temperature bend tests of C-103 sheet specimens autoclaved in contact with molybdenum confirmed this conclusion.

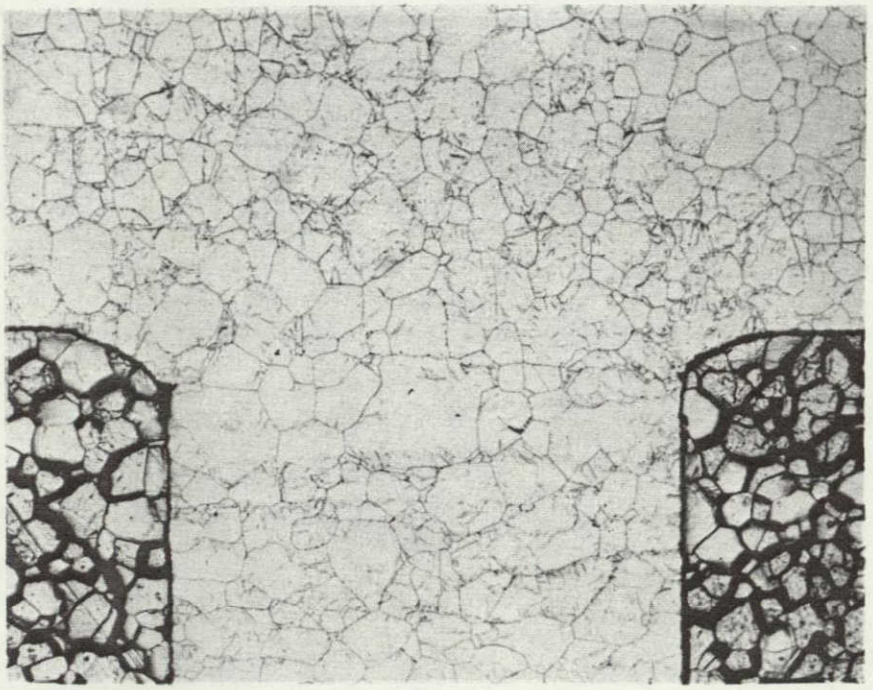

Figure 3-6 Photomicrograph of C-103 Diffusion Welded Specimen 133, fins 0.00762 to 0.0127 cm (0.003 to 0.005 inches) higher than filler bars). 100X

Autoclaved at 1700°K and 62. MPa (2600°F and 9000 psi) for 5 hours

Analyses were made of interstitial impurities of several samples taken from the specimens autoclaved at 1700°K and 62. MPa (2600°F and 9000 psi). The results of these analyses are given in Table 3-1. These data show that nitrogen and oxygen contents are about the same after diffusion welding and leaching of the molybdenum filler bars as they are in the starting material, but that hydrogen content after these processes is about 350-400 parts per million higher than that of the starting C-103. All of the added hydrogen is readily removed by a 1/2 hour anneal in vacuum at 1480K (2200°F). After vacuum annealing the C-103 was completely ductile, no permanent embrittlement results from the hydrogen temporarily picked up in the diffusion welding operation. The data also indicate that oxygen content of the C-103 is increased approximately by a factor of two during a 3 hour heat treatment in vacuum at 1870K (2900°F).

Interstitial impurity analyses summarized below, were also made on C-103 specimens which had been exposed to the leaching acid (25% HNO_3, 25% H_2SO_4, 50% H_2O) used to remove the molybdenum filler bars. No significant increase in impurities occurred as the result of exposures of 24 and 48 hour durations.

Exposure time, hours	Nitrogen ppm	Oxygen ppm	Hydrogen ppm
0	55	222	3
24	56	203	2
48	58	225	10

No significant C-103 weight loss occurs as a result of exposure to the leaching acid and there is no apparent detrimental effect of the leachant on C-103. The slight hydrogen pick-up was removed by a 1/2 hour vacuum anneal at 1480K (2200°F) after leaching.

TABLE 3-1

INTERSTITIAL IMPURITY CONTENTS OF DIFFUSION WELDED C-103 SPECIMENS AT 1700°K AND 62. MPa (2600°F AND 9000 PSI) FOR 5 HOURS

Specimen Number	Condition	Nitrogen	Oxygen	Hydrogen
123	Leached[a]	84	224	351
123	1/2 hr @ 2200°F[b]	59	287	7
133	Leached[a]	35	257	396
133	1/2 hr @ 2200°F[b]	23	255	2
131	3 hrs @ 2900°F[c]	43	441	3
132	3 hrs @ 2900°F[c]	43	565	6

(a) Analysis after molybdenum filled bars leached out.

(b) Analysis after 1/2 hour heat treatment in vacuum subsequent to leaching.

(c) Analysis after 3 hour heat treatment in vacuum subsequent to leaching.

The other specimens with the fins ranging between 0.00254 cm and 0.00762 cm (0.001 to 0.003 in) and (0.005 to 0.007 in) higher than the molybdenum filler bars exhibited porosity along the diffusion weld line.

Segments were heated to 1870K (2900°F) for 3 hours in vacuum after the filler bars were leached out to determine if the diffusion welds could be improved. Insofar as improvement of the diffusion weld is concerned, mixed results were obtained, similar to previous observations. Diffusion welds in these specimens are shown both after autoclaving and after the 3 hours at 1870K (2900°F) in Figures 3-7 and 3-8. The joint interface of Specimen 132 (Figure 3-7) was not improved noticeable by the 1860K (2900°F) treatment, whereas some improvement in weld interface appearance (less porosity and more random grain boundaries) was observed for Specimen 131 (Figure 3-8). Grain size in the cover plates increased during the 3 hours, 1870K (2900°F) heat treatment from 50 micrometers (μm) (ASTM 6) to about 200 micrometers (μm) (ASTM 2). Grain size in the fins, which was about 140 to 200μm (ASTM 2-3) after diffusion welding increased only slightly during the subsequent heat treatment.

At this point in the diffusion welding development effort it was concluded that the maximum temperature - 1700K (2600°F) - attainable in the "large" GE-Evendale autoclave was somewhat marginal in assuring a high probability of attaining repeatable perfect diffusion welds even through it had been demonstrated by the cyclic pressure tests (described in 3.2) that imperfect diffusion welds demonstrated high strength. (Perfect diffusion welds, without evidence of an interface line, were established as a requirement because of the lack of long time - 7 year - creep

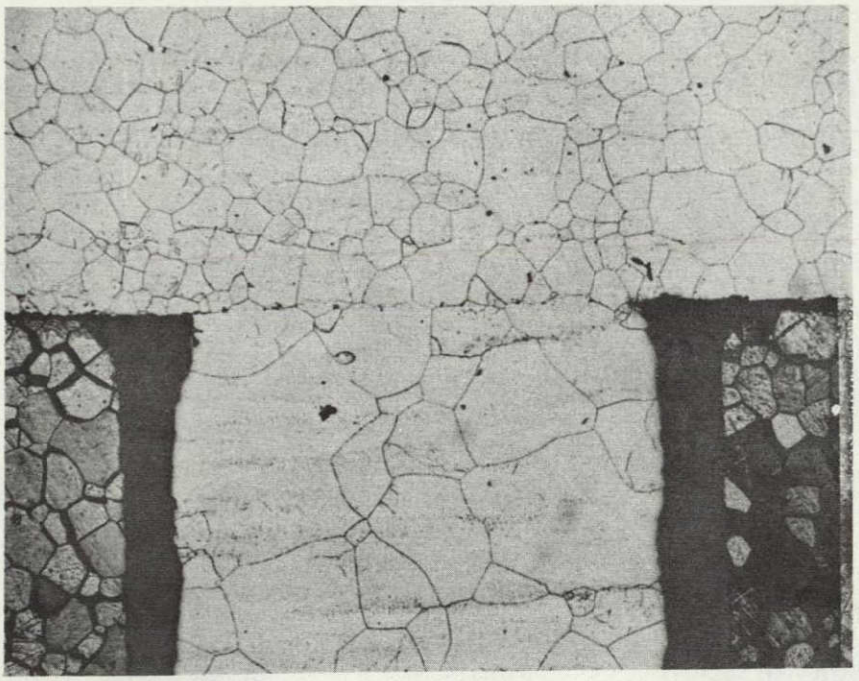

After Diffusion Welding

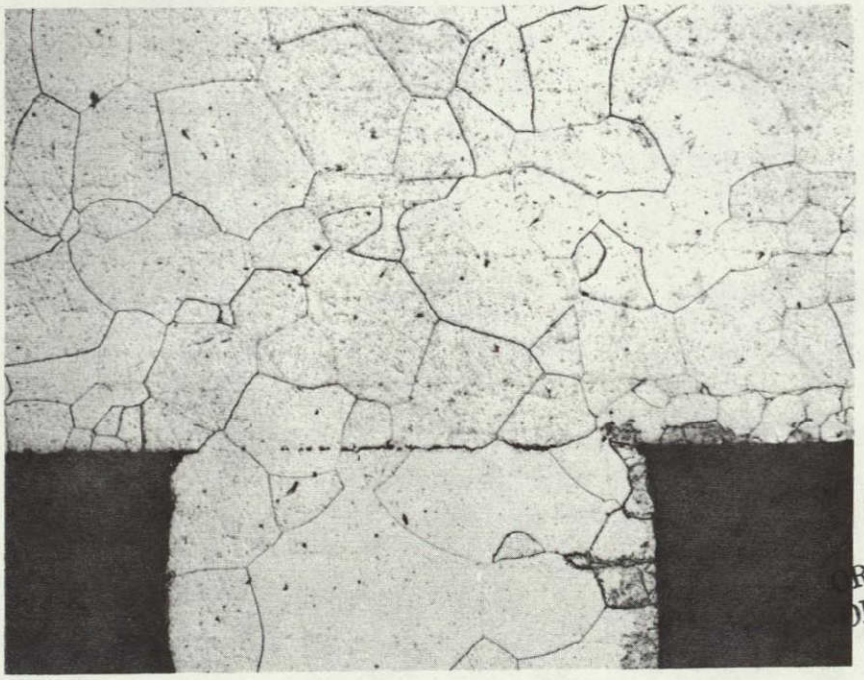

After 3 Hour, 1870°K (2900°F) Heat Treatment

Figure 3-7 Photomicrographs of Specimen 132 (fins 0.00254 to 0.0076 cm (0.001 to 0.003 inches) higher than filler bars). 100X
Autoclaved at 1700°K and 62. MPa (2600°F and 9000 psi for 5 Hours.

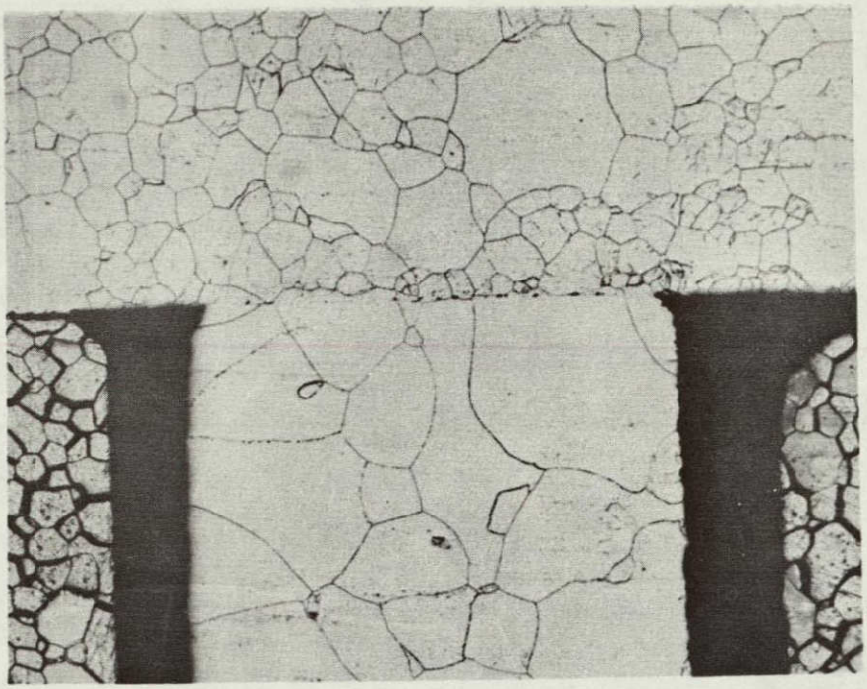

After Diffusion Welding

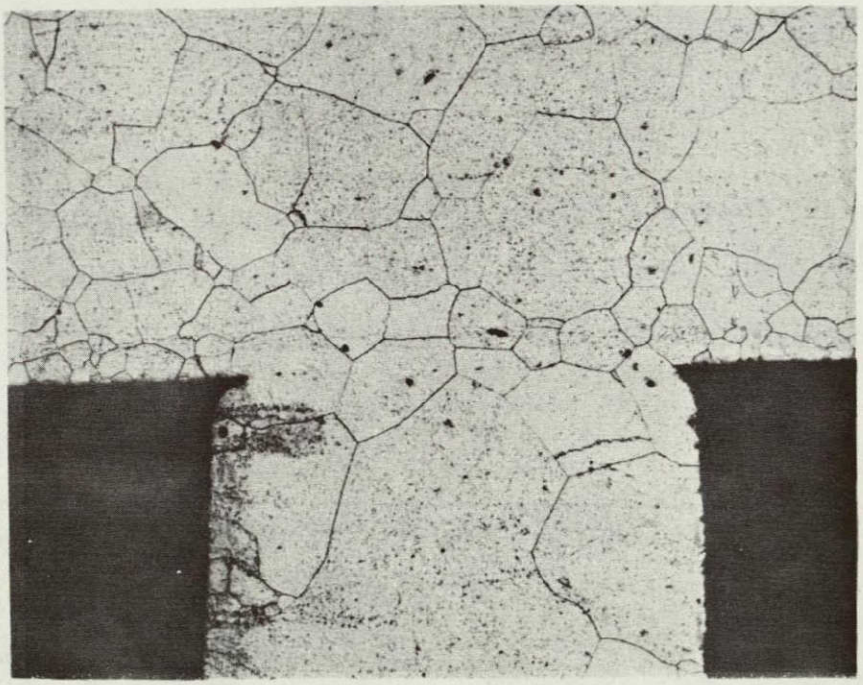

After 3 Hour, 1870°K (2900°F) Heat Treatment

Figure 3-8 Photomicrographs of Specimen 131 (fins 0.0127 to 0.01778 cm (0.005 to 0.007 inches) higher than filler bars). 100X
Autoclaved at 1700°K and 62. MPa (2600°F and 9000 psi) for 5 Hours.

strength data on diffusion welds.) That perfect diffusion welds could not be consistently achieved at 1700K and 62. MPa (2600°F and 9000 psi) even with the ratio of fin to molybdenum filler bars height optimized, was indeed verified at a later date by autoclaving a 5.08 cm (2 in) high full diameter ring sample. Some of the diffusion welds in this specimen were perfect with no micropores and having random grain boundaries across the interface while other diffusion welds contained significant numbers of pores and less random grain growth. Consequently a programmatic decision was made to modify a relatively new, large autoclave at Battelle Columbus Laboratories to attain a capability of 1810K and 69. MPa (2800°F and 10,000 psi) and to use this facility for diffusion welding of deliverable hardware.

3.1.3 BATTELLE AUTOCLAVE AND EXPERIMENTS

Prior to modification for HSHX applications, the Battelle[1] Autoclave No. 8 had a demonstrated capability of processing at temperatures up to 1645K (2500°F) and 103. MPa (15,000 psi). The inside dimensions of the pressure vessel are 66. cm (27 in) diameter and 274. cm (108 in) between heads. In order to extend the temperature capability the furnace was modified by replacing heating elements with molybdenum heater wire supported on alumina spools on the inside of the pressure vessel. A multilayer thermal barrier package is used between the furnace and vessel walls to minimize heat loss to the vessel. The working dimensions of the modified furnace are 51. cm (20 in) diameter by 170. cm (67 in) long. The top portion of the furnace - 51. cm (20 in) long-is used as the working volume for diffusion welding the HSHX.

---

(1) The abbreviation BMI (Battelle Memorial Institute) or BCL (Battelle Columbus Laboratoreis) will be used synonymously in referring to Battelle.

Pressurizing is accomplished by pumping liquid argon through a vaporizer.

A six zone power supply is used to power the furnace.

The temperature within the furnace is monitored by 12 Type "B" thermocouples (Pt30%Rh vs. Pt6%Rh). Eight additional Type "B" thermocouples are used to monitor the work load temperatures.

The loading stand upon which the diffusion welded specimens or HSHX is supported, consists of two molybdenum cylinders 25. cm (10 in) in diameter by 61. cm (24 in) high and one cylinder 25. cm (10 in) in diameter by 30. cm (12 in) high. The cylinders are separated by 0.13 cm (0.05 in) thick molybdenum sheet. In addition, molybdenum foil radiation shields are located in cylinder at its base. An additional heat shield is located in the uppermost cylinder, approximately 2.5 cm (1 in) below its top. These shields are made up from at least three layers of foil and serve to minimize convection currents within the furnace. Temperature uniformity within the working volume is within the specification limit of 1810K $\pm$ 14K ($2800^{o}F \pm 25^{o}F$). A photograph of the load arrangement in the autoclave is shown in Figure 3-9.

Numerous autoclave runs with both flat sheet and finned specimens were made during the checkout and qualification of the Battelle autoclave. It was determined that when the conditions of 1810K ($2800^{o}F$) and 69. MPa (10,000 psi) were met the diffusion welds were consistently excellent, with extensive grain growth across the interface and with no evidence of porosity. After qualification of the autoclave and verification of a

BATTELLE AUTOCLAVE

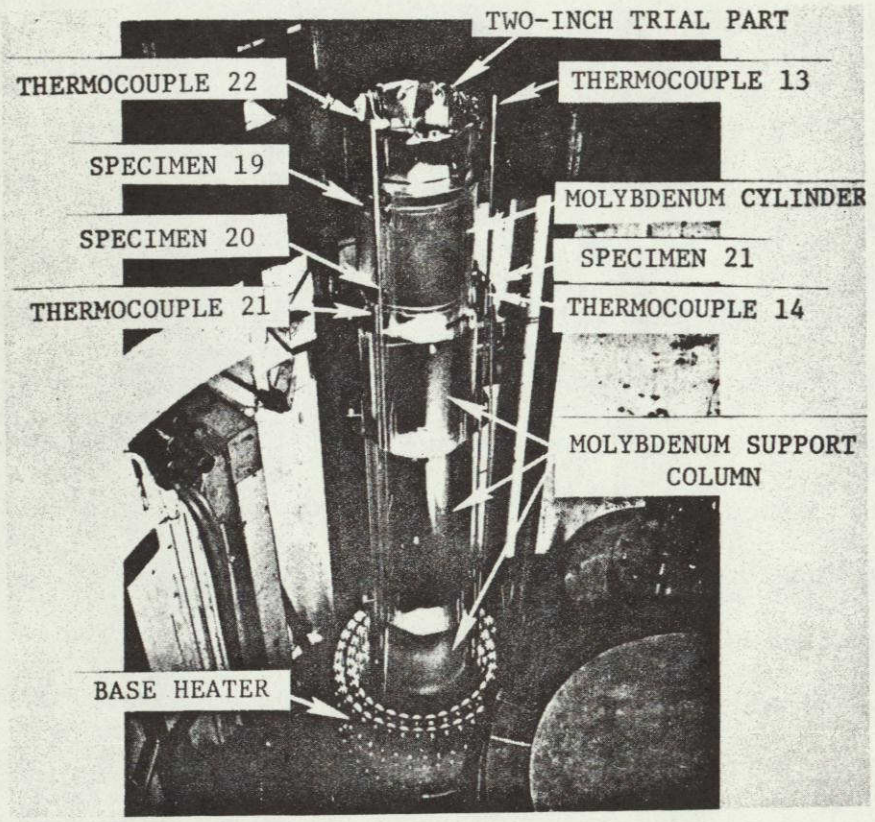

Figure 3-9

Photograph of Load Arrangement in Run 11.
(Taken After the Welding Cycle)

modified design of the clad seal for diffusion welded assemblies, two full ring samples essentially identical to the full scaled HSHX except for length were autoclaved in separate runs. The first of these was a 5. cm (2 in) long ring which had been modified after a leak developed in an earlier run before the clad seal design was changed. The second specimen was 23. cm (9 in) long. Photographs of these specimens in various stages of assembly and post diffusion welding are shown in Figures 3-10 through 3-17. A total of sixty fin diffusion welds were examined metallographically and in each instance the diffusion welds were excellent, that is there was no microporosity at the interface, grain boundaries were random, there was no evidence of the original interface and fillets had formed at the sides of the fins and outer cylinder. Typical microstructure is shown in Figure 3-18.

Demonstration of repeated successful diffusion welds in the Battelle autoclave at 1810^{o}K and 69. MPa (2800^{o}F and 10,000 psi) for three hours completed the diffusion welding development effort and established the parameters for the fabrication of the HSHX's for deliverable hardware.

3.2 MACHINING

The finned heat exchanger design requires the milling of flow passages in the inner cylinder. After this operation, nearly one hundred fifty fragile fins, .064 cm (0.025 in) thick and .41 cm (0.160 in) high, projects from the inner cylinder. C-103 alloy may be compared to AISI 316 stainless steel in machinability with reference to tool wear, and in that it is quite ductile and tends to gall and tear. Because of the extensive machining required to form the many long, narrow fins, preliminary fin machining trials were made.

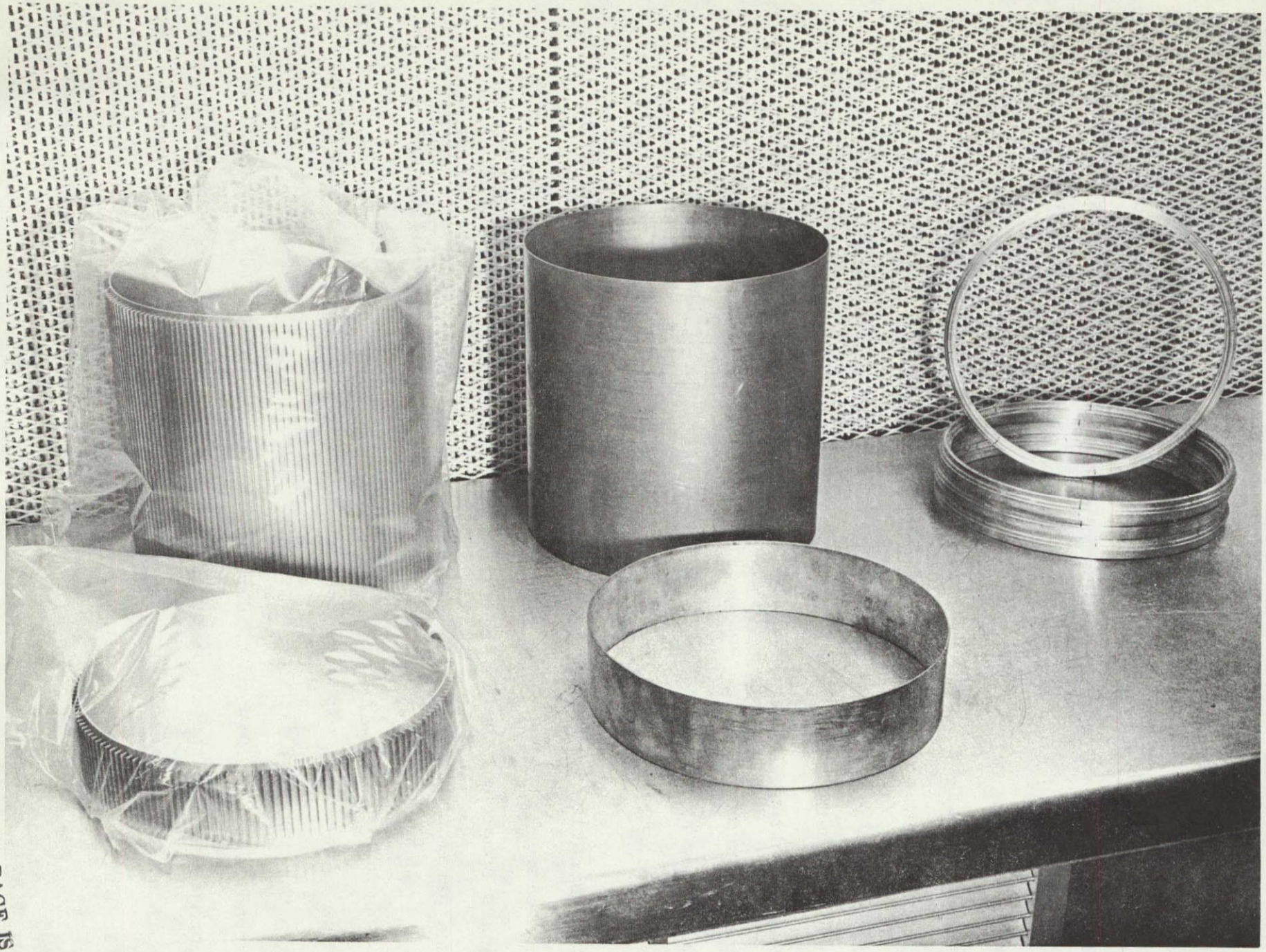

Figure 3-10 Diffusion Welding trial parts awaiting assembly.

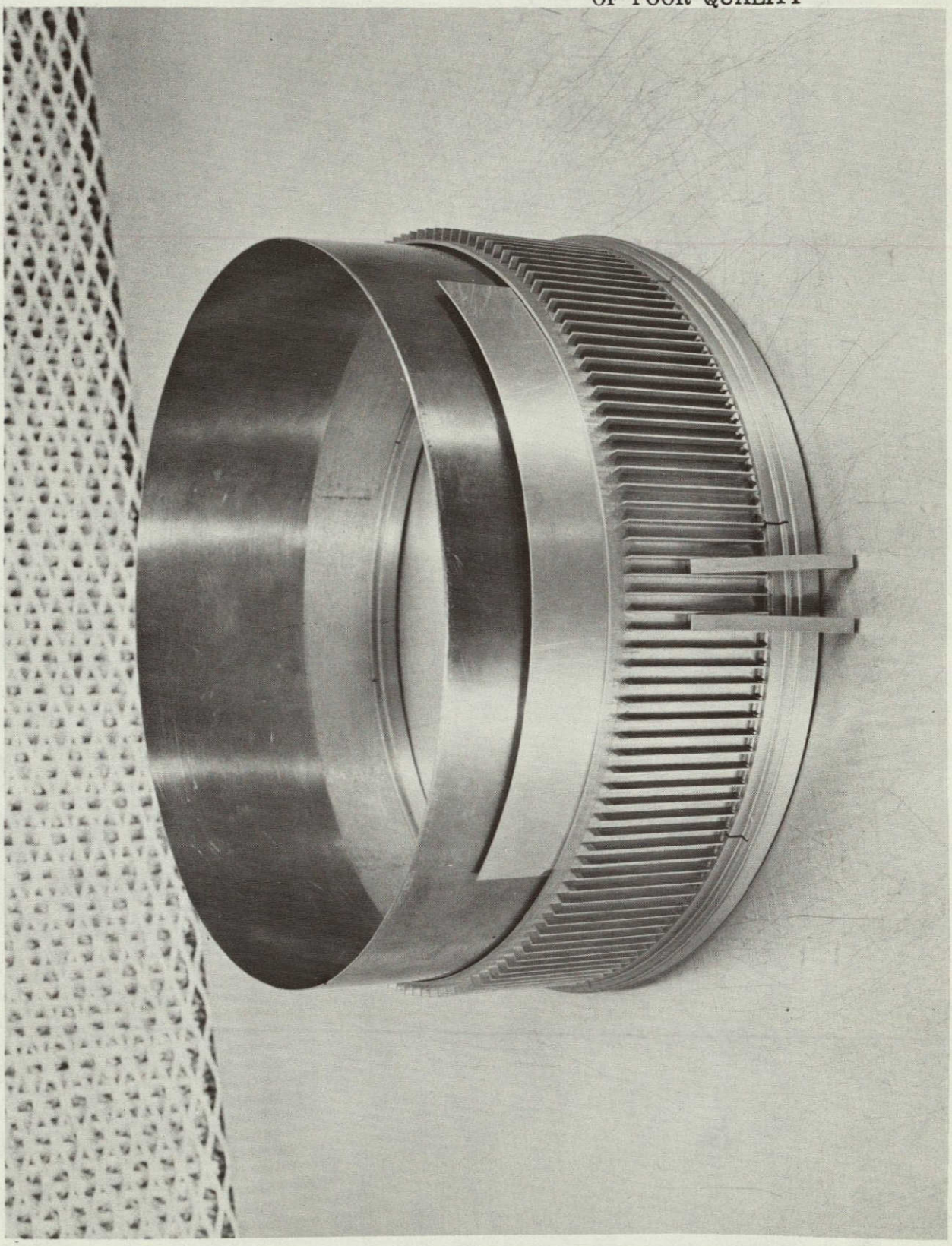

Figure 3-11

Typical Trial Part Components for the 5. cm (2-Inch) Diffusion Welding Assembly. (Parts are ready for trial assembly before final cleaning and pickling.)

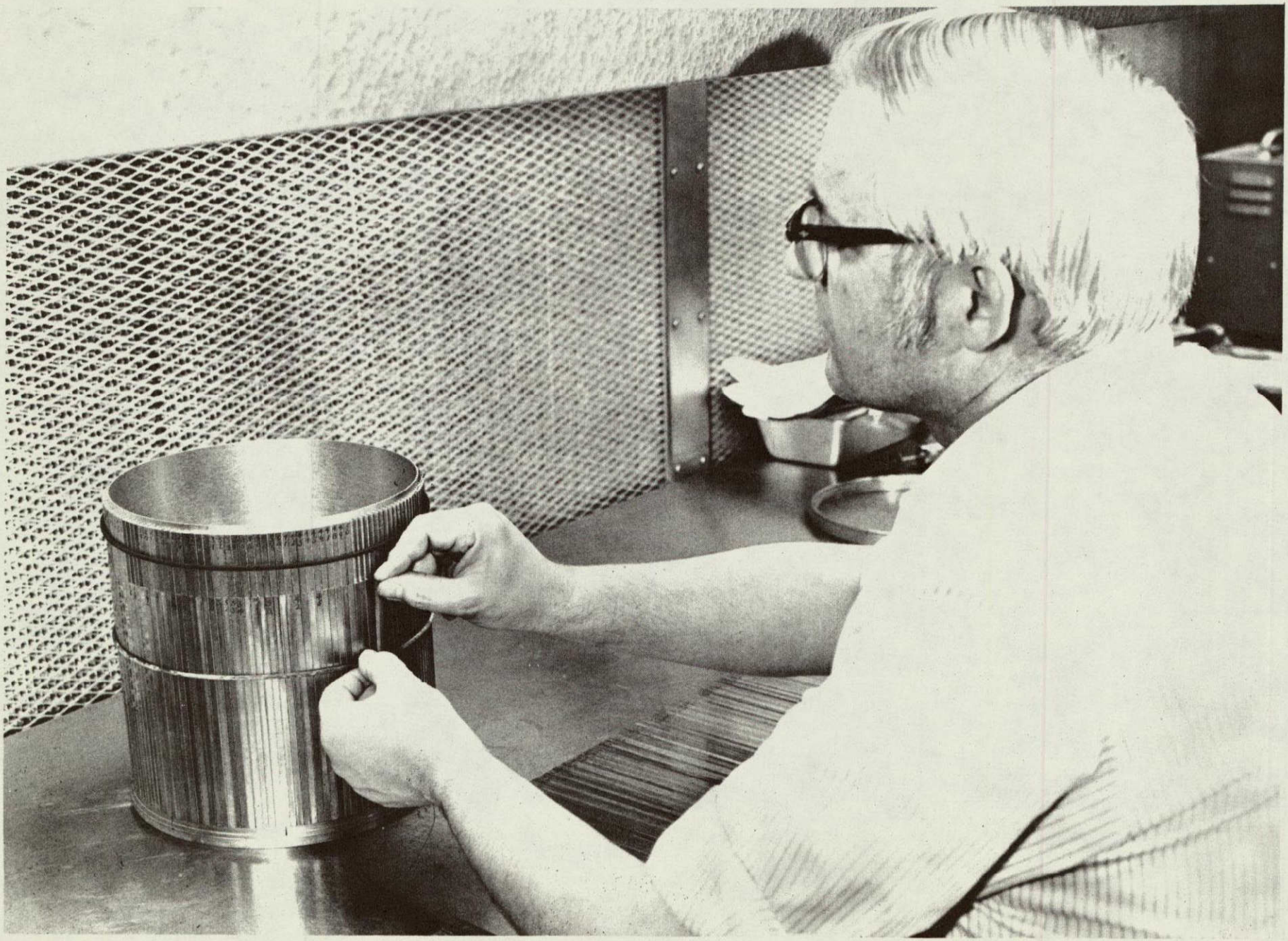

Figure 3-12

Trial assembly of 23. cm (9 inch) trial part.

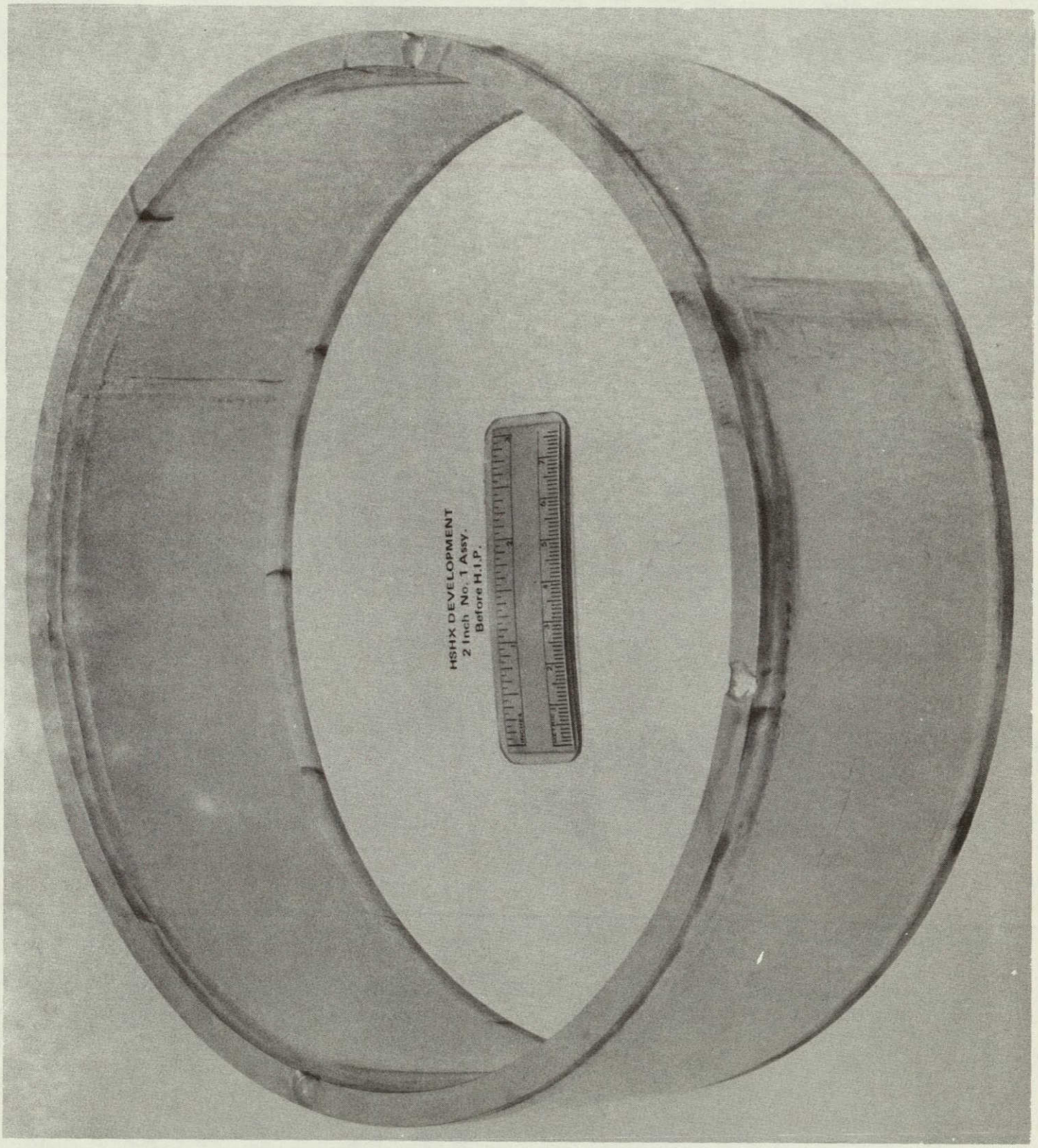

Figure 3-13

Photograph of Trial Part No. 1 Diffusion Welding Assembly Prior to Welding.

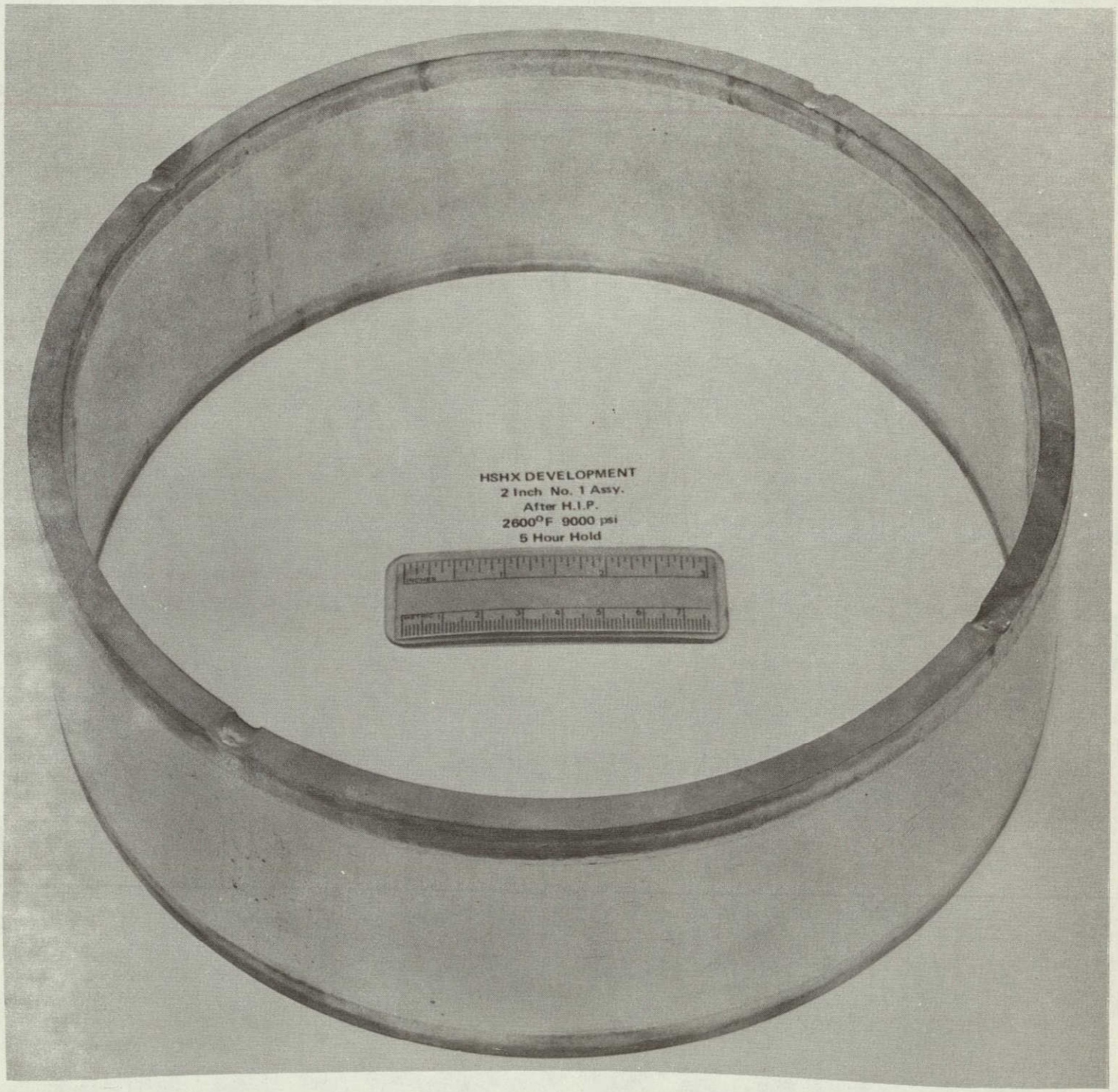

Figure 3-14

Photograph of Trial Part No. 1 Diffusion Welding Assembly After 5 Hour, 1700K and 62. MPa (2600°F and 9000 PSI) Welding Cycle.

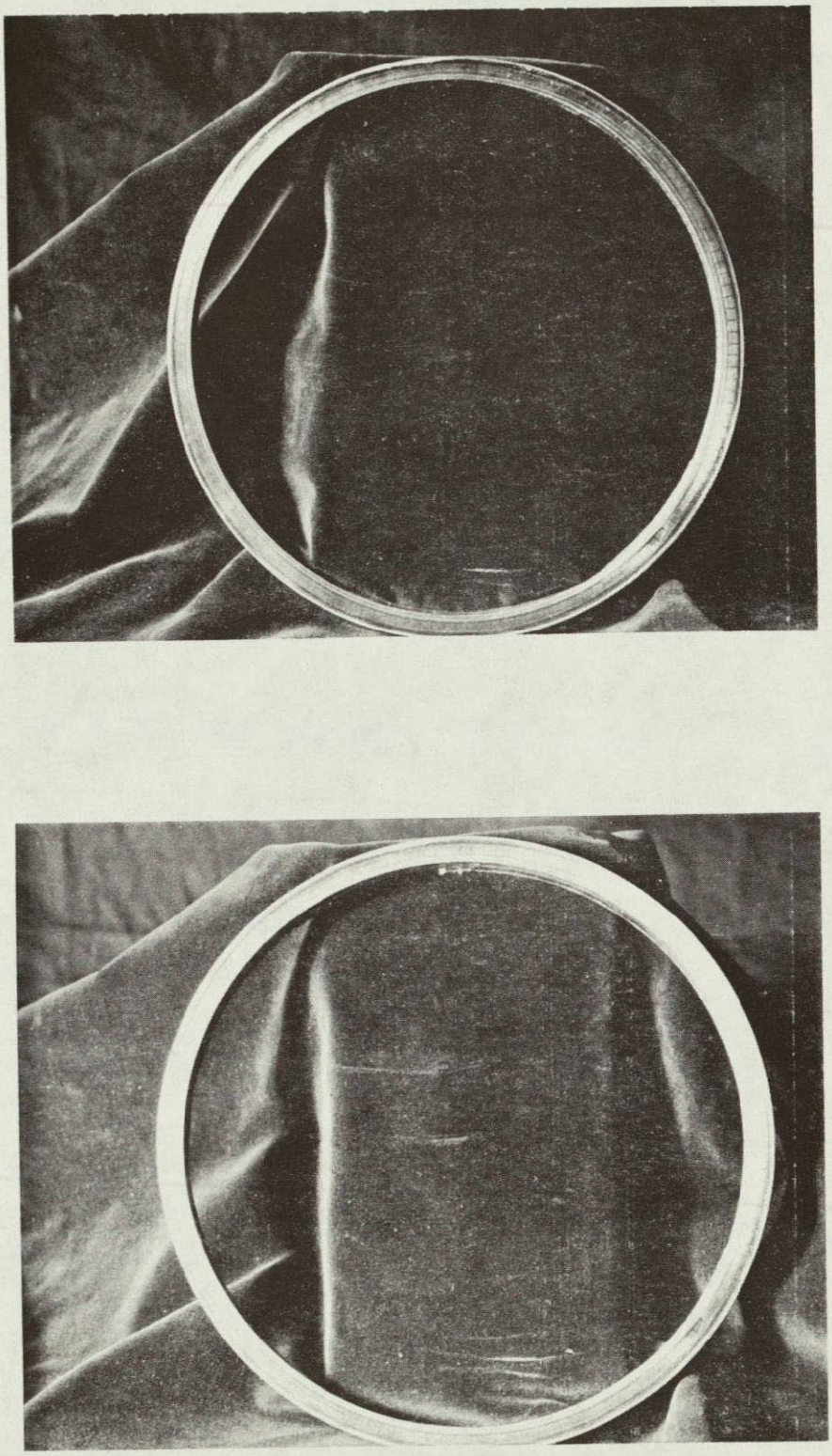

FIGURE 3-15

5. cm (2 IN) TRIAL PART #2 UPPER END RING

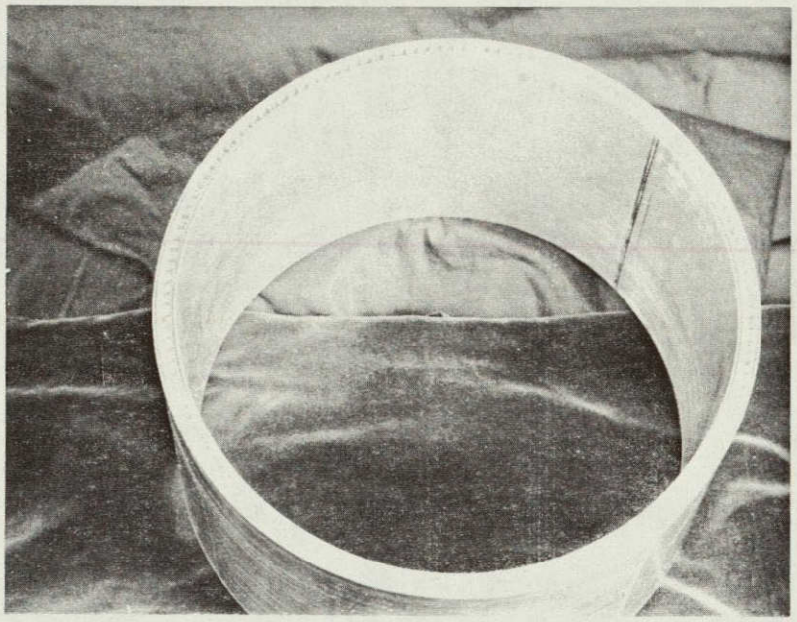

23. cm (9 IN) TRIAL PART PARTIALLY LEACHED FOR WELD PREP
THIS SECTION INCLUDES ONLY THE
LOWER, FULL LENGTH Mo BARS

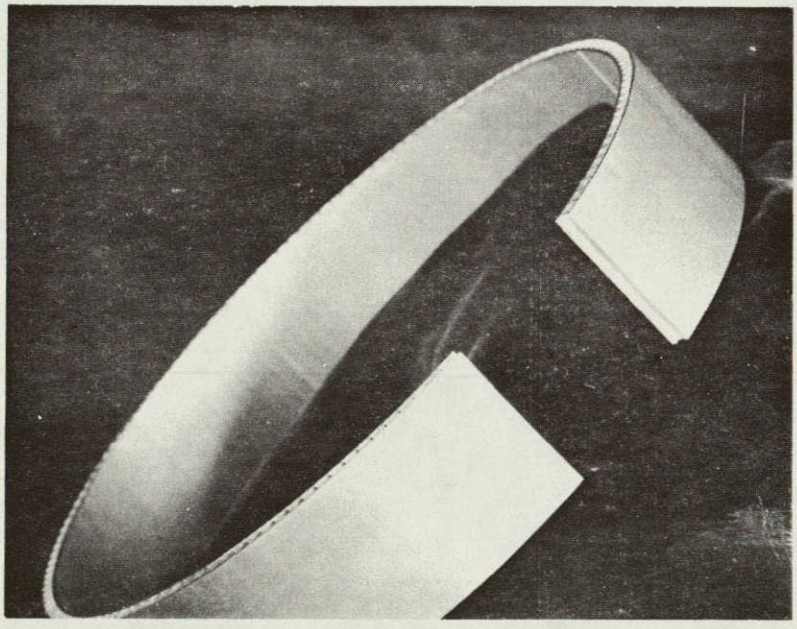

FIGURE 3-16 UPPER PORTION OF 23. cm (9 IN) TRIAL PART
INCLUDING SHORT LENGTH Mo BARS
AND Mo BAR JOINTS WITH SURFACE DIMPLES
(ALL Mo AND SEAL CYLINDERS HAVE BEEN REMOVED)

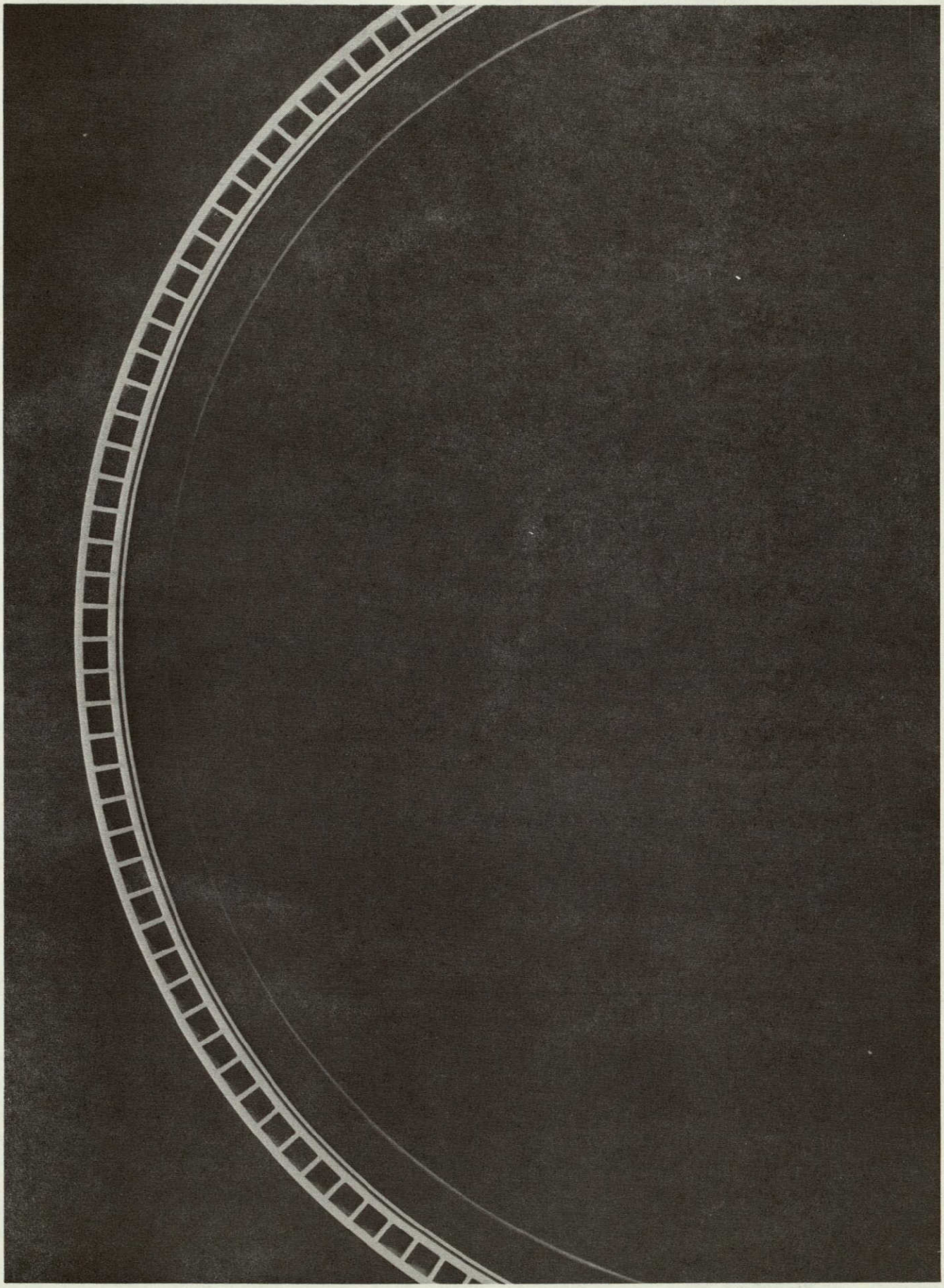

Figure 3-17

Diffusion Welded 5. cm (2 in) Trial Part No. 1 After Molybdenum Filler Bars and Outer Barrier Cylinders Removed.

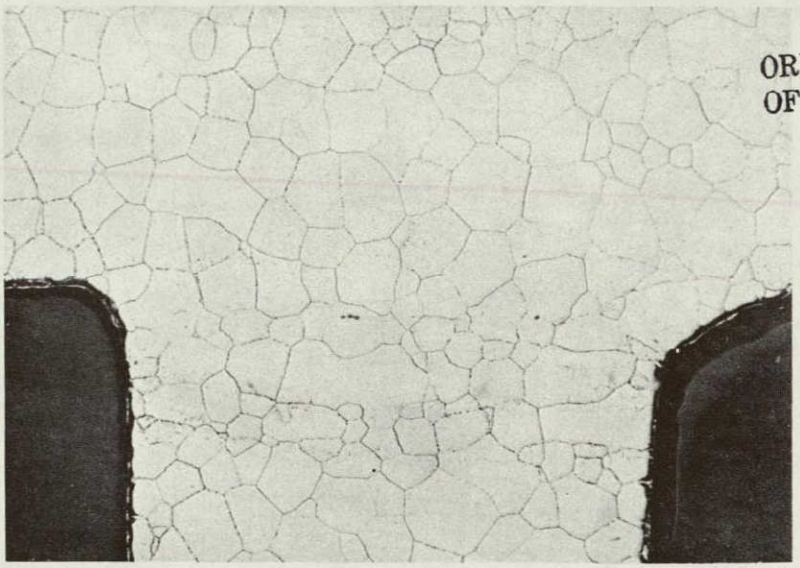

Specimen From Top Ring (100X)

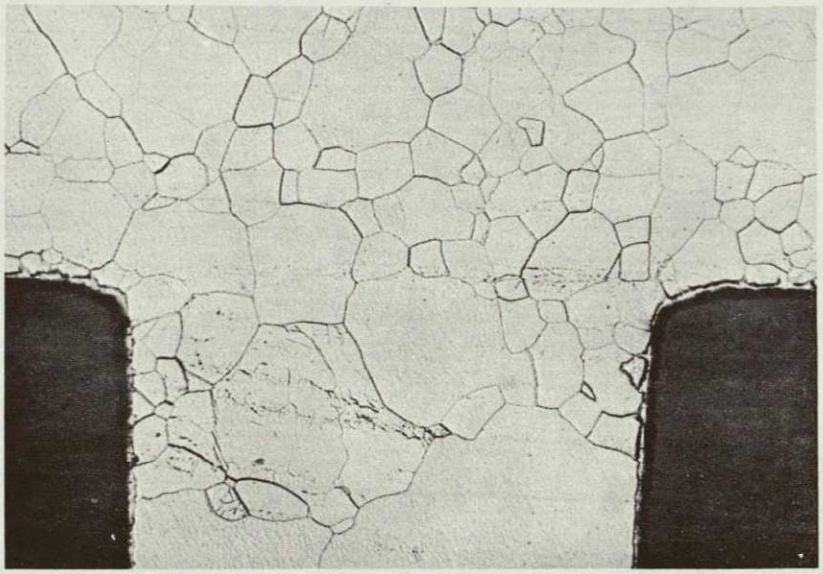

Specimen From Bottom Ring (100X)

Figure 3-18

Photomicrographs Showing Typical Microstructure of Diffusion Welds in the 23. cm (9 in) Trial Part.

In the initial attempt, fins were machined in several 3.18 cm x 3.18 cm (1.25 in x 1.25 in) segments of 0.64 cm (0.25 in) thick C-103 plate. Straddle milling was used to machine both sides of the fins simultaneously and thus minimize the tendency to break the fins. Galling and smearing occurred, primarily on the bottom surface of the slots between the fins. While this is not a weld interface surface, it nevertheless can affect the diffusion welding process if it retains entrapped debris or contaminants which can later contaminate surfaces to be welded.

In order to improve surface finish, machinability tests were conducted in which cutter type, coolant, feed rate, and cutter speed were varied. Two cutter sets were used. Both were 7.6 cm (3 in) diameter side milling cutters, 0.48 cm (0.18 in) wide, one with 32 staggered teeth (16 each side) and the other with 24 straight face teeth. Two coolants were used; one was sulfochlorinated mineral oil (Clear Tex 140) and the other a high lubricity water base-sol-oil (Norton Wheel Mate 803). Feed-rates were 0.004 cm (0.0015 in) and 0.008 cm (0.003 in) average per tooth, and cutter speeds were 49.5 and 86.4 surface cm per minute. Conventional milling procedures were used, and cuts made to full depth in one pass. A coolant pump was used which developed higher pressures than standard milling machine pumps in order to better flush away chips which might cause galling and tearing of the surface.

Although minor differences were noted in the surfaces obtained using various combinations of these four variables, galling and tearing still occurred and provided the possibility for entrainment of surface contamination. However, with careful solvent and acid cleaning followed by heat treatment in vacuum at 1480K (2200^{o}F) for 30 minutes, the finned pieces could be satisfactorily cleaned for diffusion welding.

Considerable improvement in the surface of the slot resulted when slots were milled in two passes rather than one. The initial pass cuts 0.318 cm (0.125 in) wide by 0.343 cm (0.135 in) deep slots, 0.5 cm (0.200 in) on center. The 0.064 cm (0.025 in) thick, 0.41 cm (0.160 in) high fins are formed during the second (final) pass by climb-straddle milling. Climb milling tends to discharge the chips away from the area being cut rather than into it.

Cutter failures were experienced with high speed steel cutters consequently carbide typed cutters were used on the deliverable hardware. A photograph of the fin machining operation of the inner cylinders of the three trial parts is shown in Figure 3-19.

This inner cylinder was separated into three segments, two of them were 5. cm (2 in) in overall length and one was 23. cm (9 in) in overall length. The parting grooves were machined prior to forming the fins. The depth of each slot was measured at four positions along its length while the segments were still on the mandrel used to hold the part during machining operations. These measurements indicate a variation of 0.015 cm (0.006 in) in slot depth over the entire cylinder. The molybdenum filler bars were tailored to this variation by grinding to appropriate thickness to obtain the desired ratio of fin to molybdenum bar height for diffusion welding.

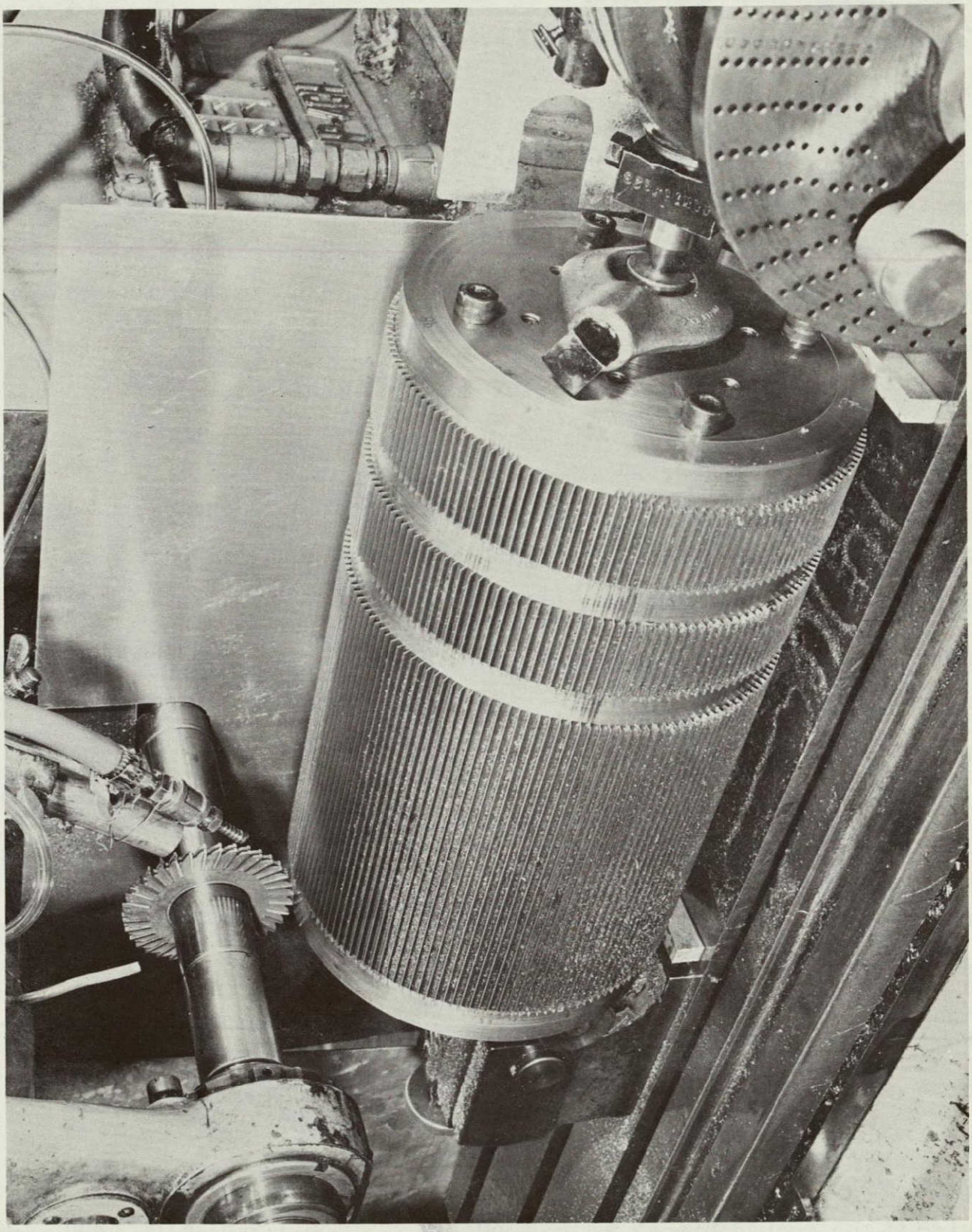

Climb Straddle Milling of Fins on Trial Part Inner Cylinders. (Note that some rough machined slots at the rear of the cylinder have not yet been finish machined.)

Figure 3-19

3.3 GAS TUNGSTEN ARC (GTA) WELDING

In the fabrication of the HSHX, several C-103 alloy parts are joined by welding. One example is the inner cylinder, which is formed by welding together two 1.3 cm (0.5 in) thick half-cylinders formed from plate stock. Another example is the scrolls. The outer-scrolls are formed from 0.13 cm (0.050 in) thick sheet and the inner-scrolls machined from heavy plate. The inner and outer halves are welded together; the toroid is then welded to the finned cylinder.

Because columbium alloys can be severely embrittled by interstitial elements (carbon, nitrogen, oxygen, and hydrogen) extreme care must be taken during the welding process to avoid contamination by these elements in the weldment. Welding is therefore accomplished by gas tungsten arc (GTA) welding in a vacuum purged inert atmosphere weld chamber or by vacuum electron beam (EB) welding.

Preliminary welding experiments were performed with the objective of determining the best method to use for each weldment (sheet-to-sheet, plate-to-plate, etc.), to optimize the welding parameters for each process, and to obtain data regarding shrinkage during welding, and weld strength.

Experience was first gained in welding unsupported 0.13 cm (0.050 in) thick C-103 sheet, simulating scroll assembly welds. Curved sheets, with rabbetted edges for self-fixturing, were joined by automatic GTA welding. The curved pieces were supported 2.5 cm (1 in) from each side of the weld joint by a curved fixture and tack welded at 7.6 cm (3 in) intervals prior to welding. Weld parameters were as follows:

Approx. Welding Current - 96 amps
Approx. Arc Voltage - 17 volts

Atmosphere - helium

Welding Speed - 54.6 cm/sec (21.5 in/min)

The weld appeared to be good visually as shown in Figure 3-20. The welded sheet was cut at the two locations shown in the figure and examined metallographically; location 1 included a surface irregularity. Montages of photomicrographs at the two locations are shown in Figure 3-21. The microstructure appears to be similar at both locations, and no evidence was noted that the presence of the surface irregularity was indicative of a potential problem.

Two pieces of 5. x 10. x 0.64 cm (2 x 4 x 0.25 in) C-130 plate were GTA welded along the 10. cm (4 in) dimension. Edges to be joined were prepped to provide a U-shaped joint with a 0.08 to 0.10 cm (0.030 to 0.040 in) land at the root. The two pieces were clamped in a fixture to prevent warpage during welding. The first weld pass or root pass was a manual fusion weld without the use of filler wire. Three more weld passes were required to fill the joint. The direction of travel was reversed for each pass in order to control warpage of the test plate due to weld shrinkage. Manual welding was accomplished using the following parameters:

Approx. Welding Current - 150-190 amps

Approx. Arc Voltage - 19-22 volts

No. of Passes to Complete Weld - 4

Atmosphere - Helium

Filler Wire - 0.23 cm (0.090 in) diameter C-103

Electrode - 0.24 cm (.090 in) 2% thoriated tungsten

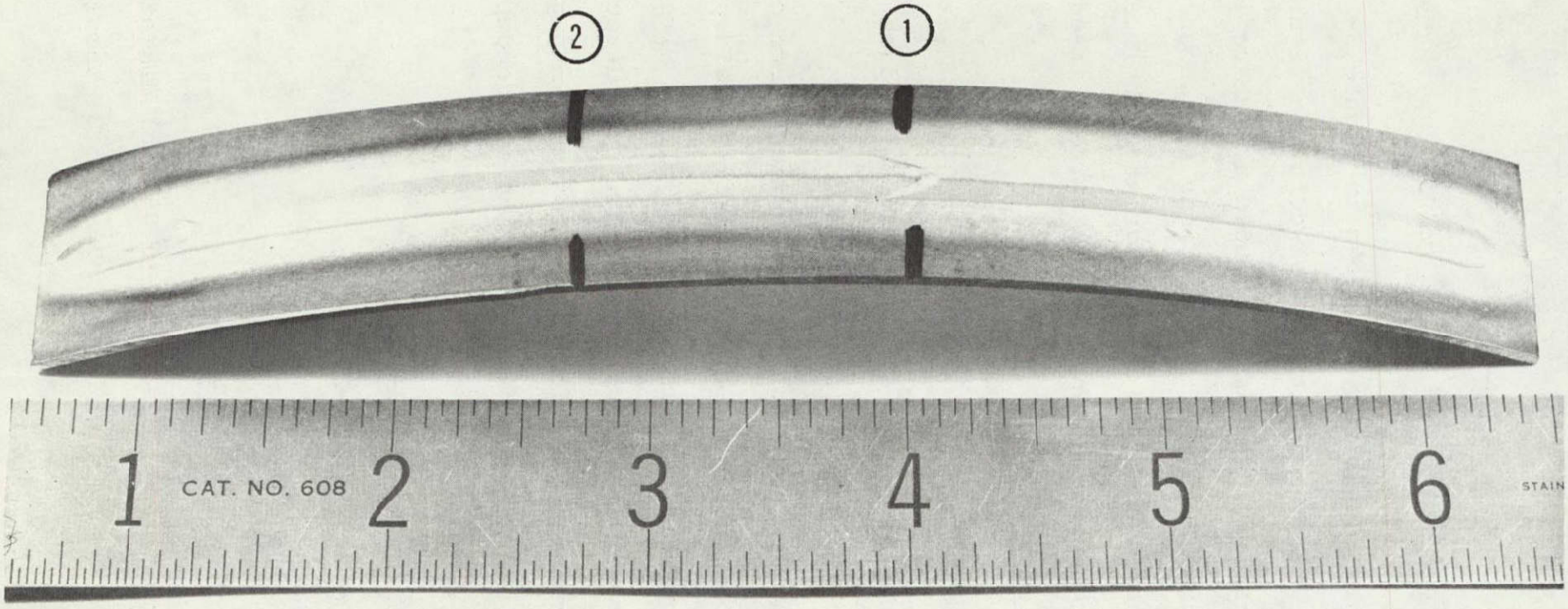

Figure 3-20. Automatic GTA Welded Curved 0.13 cm (0.050 Inch) Thick C-103 Sheets with Rabbetted Edges for Self Fixturing. Cuts were made at the Indicated Positions for Metallographic Examination.

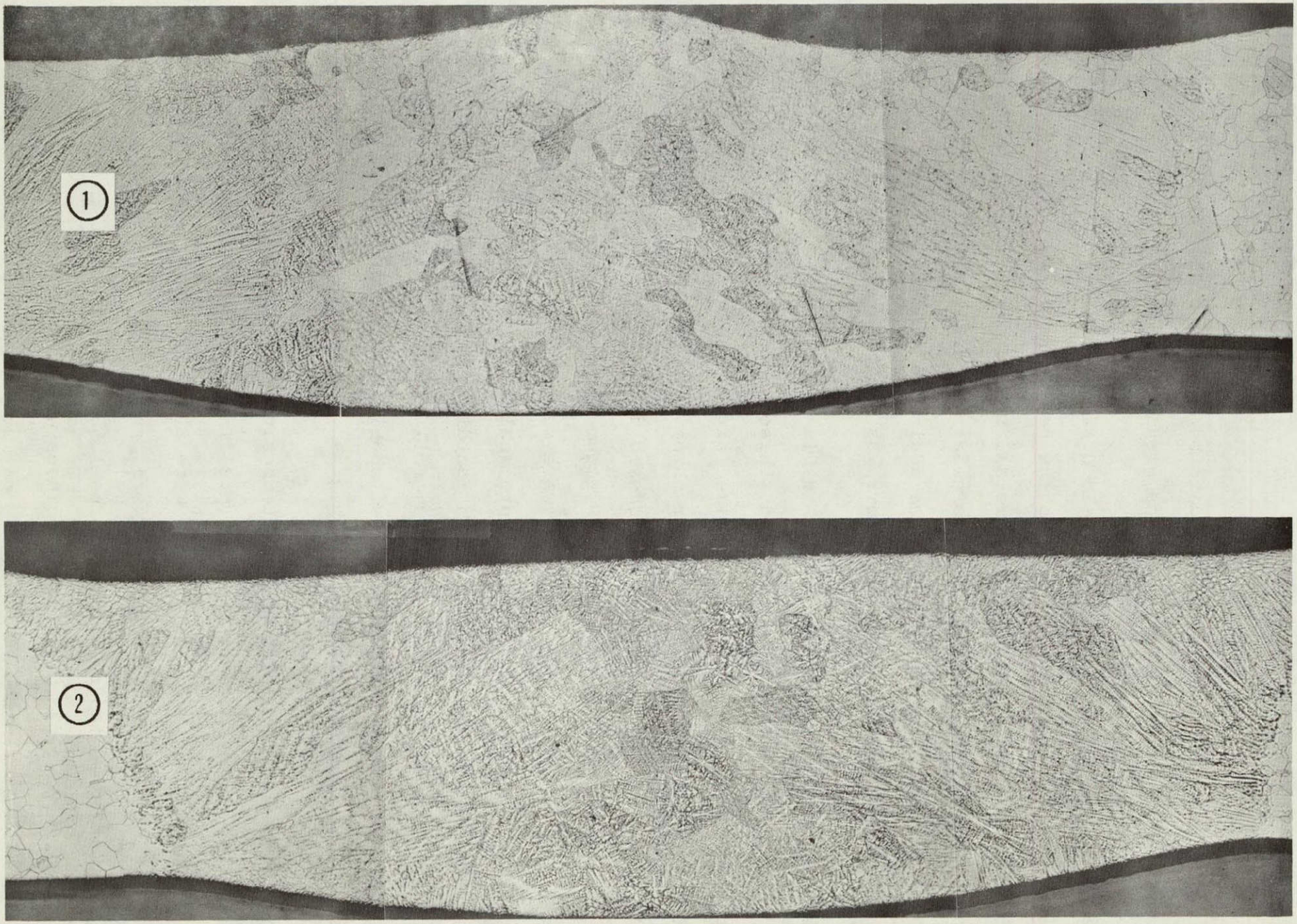

Figure 3-21. Photomicrographs of Automatic GTA Weld of Curved 0.13 cm (0.050-inch) Thick C-103 Sheet at Locations Shown in Figure 3-20. (50X)

The weld was radiographed and found to be free of cracks both before and after the weld reinforcement was ground off.

One welding trial made was to EB weld 0.64 cm (0.25 in) thick C-103 plate. It was necessary to defocus the beam considerably in order to obtain suitable flow of the fused metal, resulting in a large heat affected zone in the plate and a somewhat irregular weld. In view of the success with GTA welding, the additional effort needed to develop optimum EB welding parameters was not pursued.

C-103 alloy sheets 0.064 cm (0.025 in) in thickness were also GTA welded. After the welds were certified, these sheets were used to make mechanical test specimens for tensile, stress-rupture, and bend tests. All specimens were heat treated for three hours at 1700^{o}K (2600^{o}F) in vacuum to simulate the original proposed diffusion welding cycle. Some of the specimens were then aged in vacuum for 1000 hours at 1285K (1850^{o}F) to determine if the welds were susceptible to age embrittlement. During this aging, the specimens were sealed in an evacuated Cb-1Zr capsule. Specimens were wrapped in tantalum foil inside the capsule and the capsule also wrapped in tantalum foil inside the vacuum furnace. The capsule also contained bend test specimens made from 0.64 cm (0.25 in) thick welded plate.

Bend tests were conducted at room temperature on the four 0.064 cm (0.025 in) thick and four 0.64 cm (0.25 in) thick welded specimens, all of which had been aged. Specimens were 5. cm (2 in) in length and 1.3 cm (0.5 in) in width. Bend tests were performed in three point loading over a 110 degree mandrel and a radius 1.5 times the sheet thickness. Two of the 0.64 cm (0.25 in) thick specimens were tested with the weld face

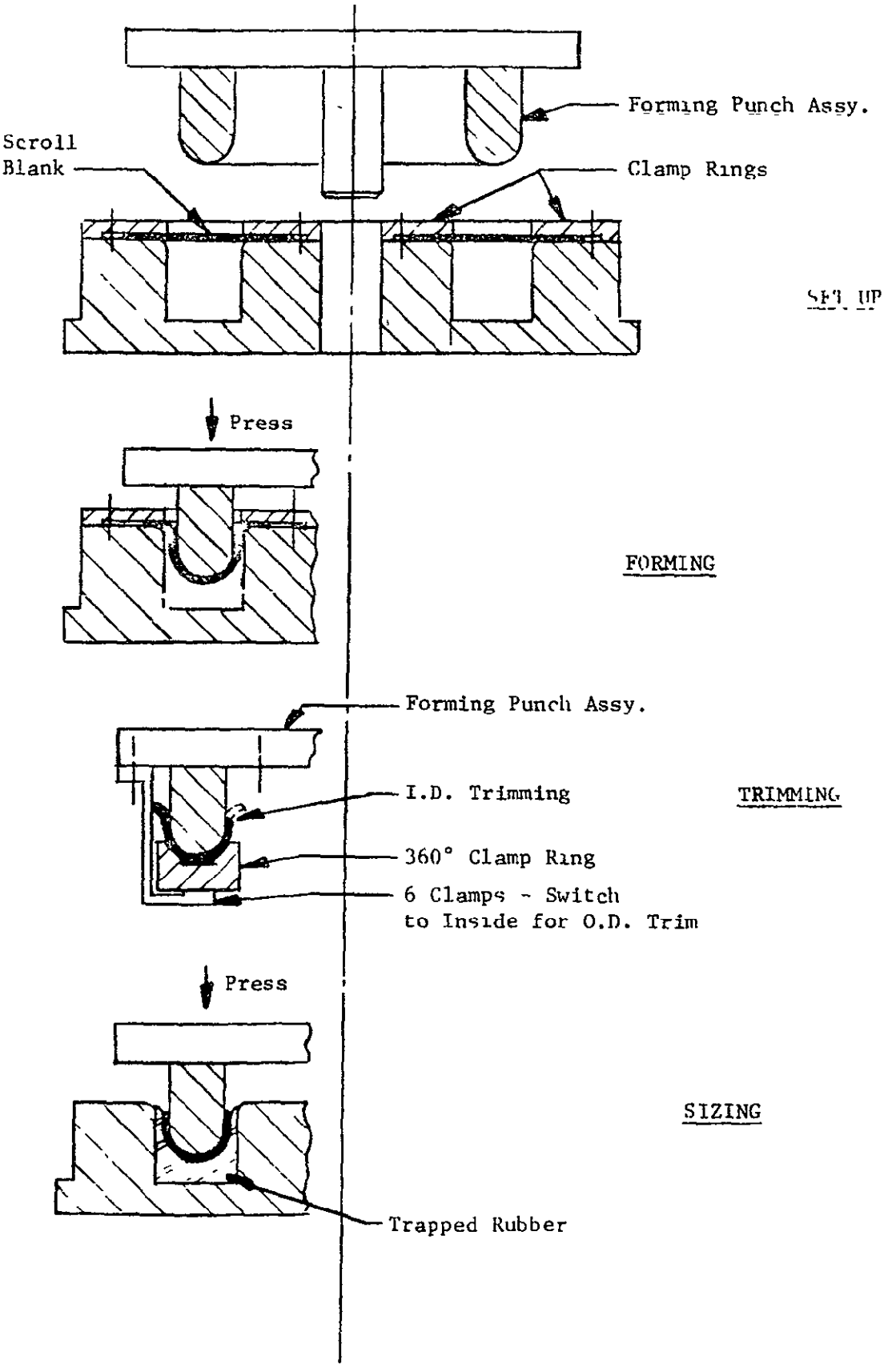

Figure 3-22 Forming Process for Toroid Halves.

freely during forming. The formed sheet is then stress relieved prior to final sizing.

After the excess metal has been trimmed off, the form is pressed into a trapped rubber mold. During this step, rubber static forces finish form the part closely about the male punch. Spring back is taken into consideration through the use of various thicknesses of formed aluminum sheet over the male mandrel.

In the initial trials, 0.076 cm (0.030 in) thick AISI 304 stainless steel was used to represent the C-103 because of its similar forming characteristics. In the earliest trial, some wrinkling of the outer edge was encountered as the radial inward movement of the metal induced circumferential contraction. A sturdier hold-down ring to prevent compressive buckling of the outer flange and minor rework of the die to form thicker sheet resulted in substantial improvement in quality of the trial parts. At this point the part was close to final print dimensions. Subsequent stress relief, trim and trapped rubber reforming gave good results and demonstrated that the part could be final sized in this manner, if required accuracy is not obtained in the initial drawing operation.

3.5 LEACHING

Leaching of the molybdenum filler bars from the diffusion bonded cylinder can be accomplished by simple immersion in appropriate acid solutions. This was determined in leaching tests using a tube to simulate a flow passage in the HSHX.

A tantalum tube, with an inside cross section approximately equal to that of an HSHX flow passage, was used to simulate the flow passage. This tube was filled with a total length of 23. cm (9 in) of molybdenum rod, the tube swaged snugly around the rod, and the lower end of the tube mechanically sealed by crimping. The tube was installed vertically in 345°K (165°F) leaching acid, GE Specification P4AYA20 Class C, which has the following composition by volume:

25% Nitric Acid

25% Sulphuric Acid

50% Water

The amount of molybdenum remaining in the tube was determined periodically by probing with a very fine wire. It was therefore unnecessary to remove the tube from the leaching bath or to significantly displace the acid within the tube to obtain leaching rate data. A near linear leaching rate of about 1.3 cm (1/2 in) per hour was measured. The 23. cm (9 in) length of molybdenum was removed in less than 20 hours. A control sample of Cb-103 approximately 0.64 x 0.64 x 1.3 cm (1/4 x 1/4 x 1/2 in) lost less than 0.1 milligram in weight during this exposure. There were no residues or deposits within the tube after leaching.

Alternate pickling solutions were also studied. These included the following by volume:

	Solution X	Solution Y
H_2SO_4	44%	30%
HNO_3	21%	3%
HCl	0.5%	-
Water	34.5%	67%

Solution X reacted at an exceedingly fast rate, leaching 23. cm (9 in) of molybdenum from the tube in 3 hours with no residue remaining. The possibility of chloride effects have not been evaluated; for this reason, this faster acting leachant is considered as a potentially excellent backup.

Solution Y produced a yellow/white deposit which slowed the reaction to a stop within two hours.

The cleanliness and reliability of the P4AYA20 Class C etchant fostered its selection for diffusion welded hardware in preference to Solution X or Solution Y.

3.6 CYCLIC PRESSURE TESTS

The purpose of the cyclic-pressure test was to demonstrate that diffusion welded joints of a specimen representing a segment of the diffusion welded cylinder of the HSHX can withstand one-hundred cycles from atmospheric pressure to 115 percent of the design pressure at a temperature of 1270°K (1825°F), which is in excess of predicted operating temperature.

The specimen was approximately 5. cm (2 in) wide and 7.6 cm (3 in) long as shown in Figure 3-23. The 0.013 cm (0.050 in) top plate actually consisted of two thicknesses of 0.064 cm (0.025 in) thick sheet which diffusion welded together during that process. Molybdenum filler bars

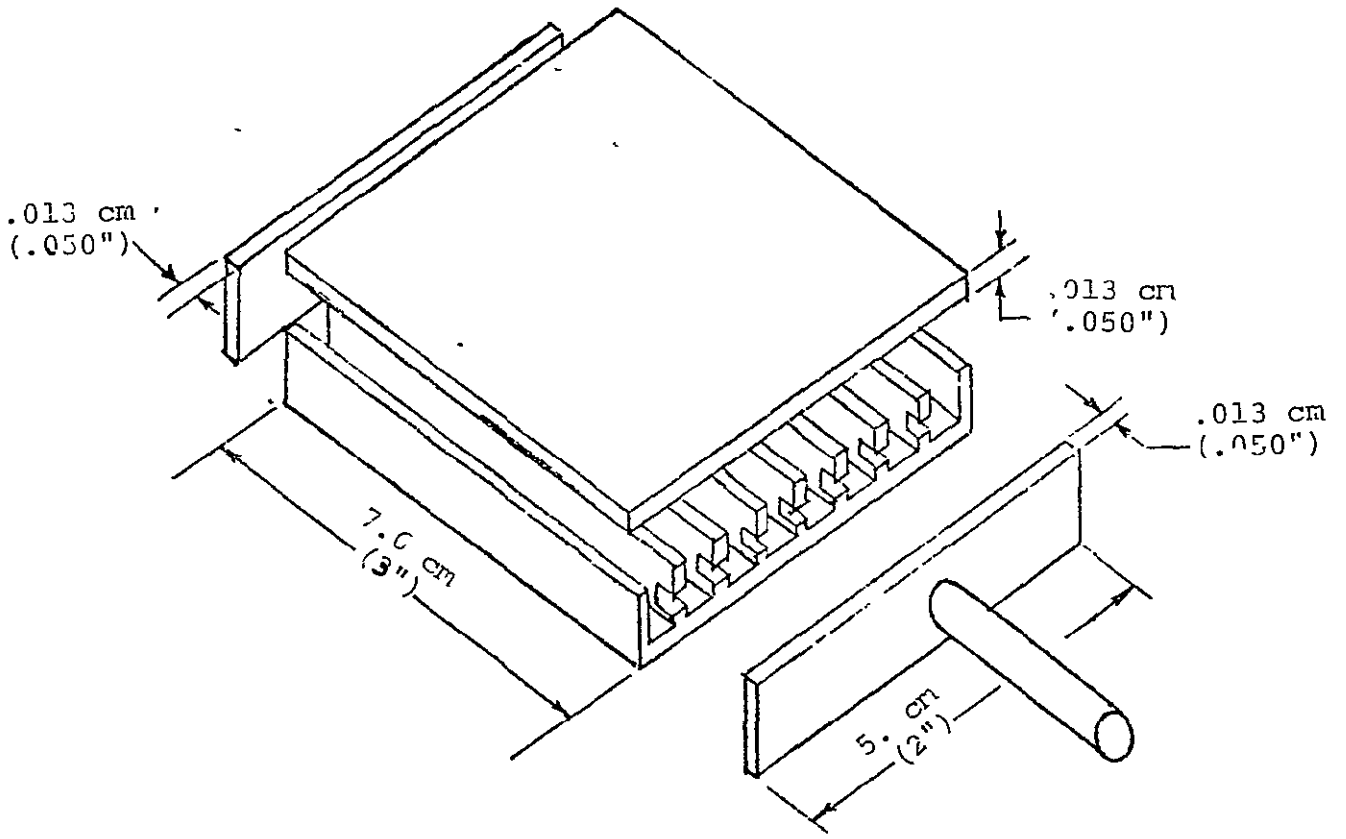

Figure 3-23 Cyclic Pressure Test Specimen for Diffusion Weld Joint Strength Evaluation.

0.0076 to 0.013 cm (0.003 to 0.005 in) shorter than the fin-height were positioned in the slots prior to diffusion bonding. These were leached out after diffusion welding. This specimen was one of several experimental specimens included in the earlier diffusion welding run #24 at Evendale. Autoclave conditions were 5 hours at 1700°K (2600°F) and 62. MPa (9000 psi) helium pressure. A photograph of the specimen is shown in Figure 3-24.

Prior to fabrication, a thin slice was cut from one end of the diffusion welded portion for metallographic evaluation of the weld interface. Although excellent diffusion welds were obtained in some of the specimens in this same diffusion welding run #24, the diffusion weld in the cyclic pressure test specimen contained some porosity as shown in Figure 3-25.

A schematic of the test set-up utilized to conduct the cyclic pressure test is shown in Figure 3-26. The specimen, wrapped in a layer of corrugated tantalum foil and positioned in a vacuum furnace, was connected to the vacuum/helium manifold through a 0.64 cm (0.25 in) diameter tube. As evident in Figure 3-26, the interior of the specimen could be evacuated by closing valves 2 and 3 and opening valve 1. It could be pressurized by closing valves 1 and 3 and opening valve 2. Pressure could be reduced to atmospheric by closing valves 1 and 2 and opening valve 3. A bubbler between valve 3 and atmosphere prevented back diffusion of air into the specimen. Prior to heating, the specimen was evacuated and back-filled with high purity (99.995% minimum) helium several times to remove all traces of air. During heatup, the interior of the specimen was under dynamic vacuum. After the temperature was stabilized at 1270°K (1825°F), helium was admitted into the specimen providing a .930 MPa (135 psi) pressure gradient across the specimen wall.

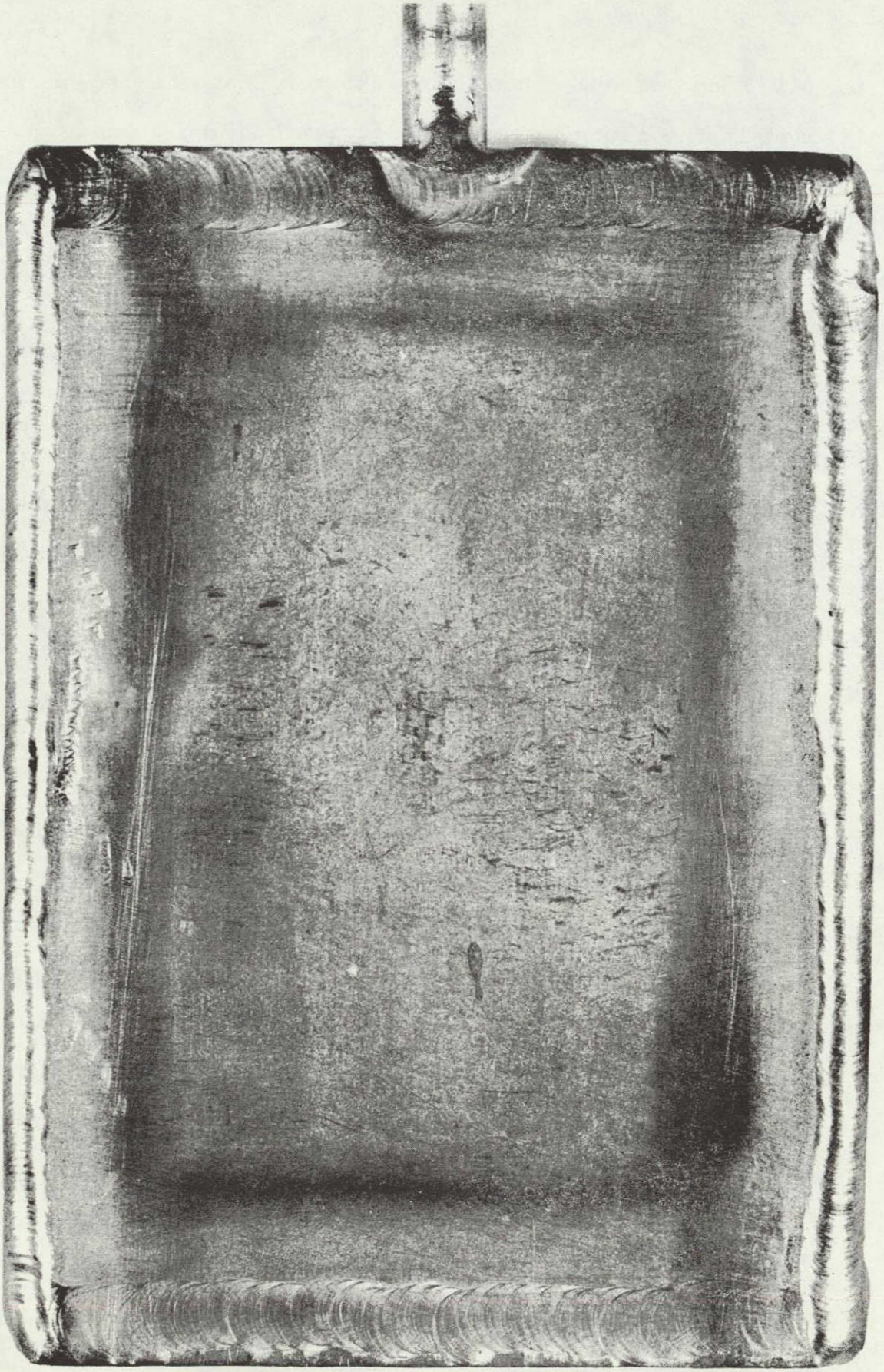

Figure 3-24 Photograph of Cyclic Pressure Test Specimen Before Testing (Approx 3X).

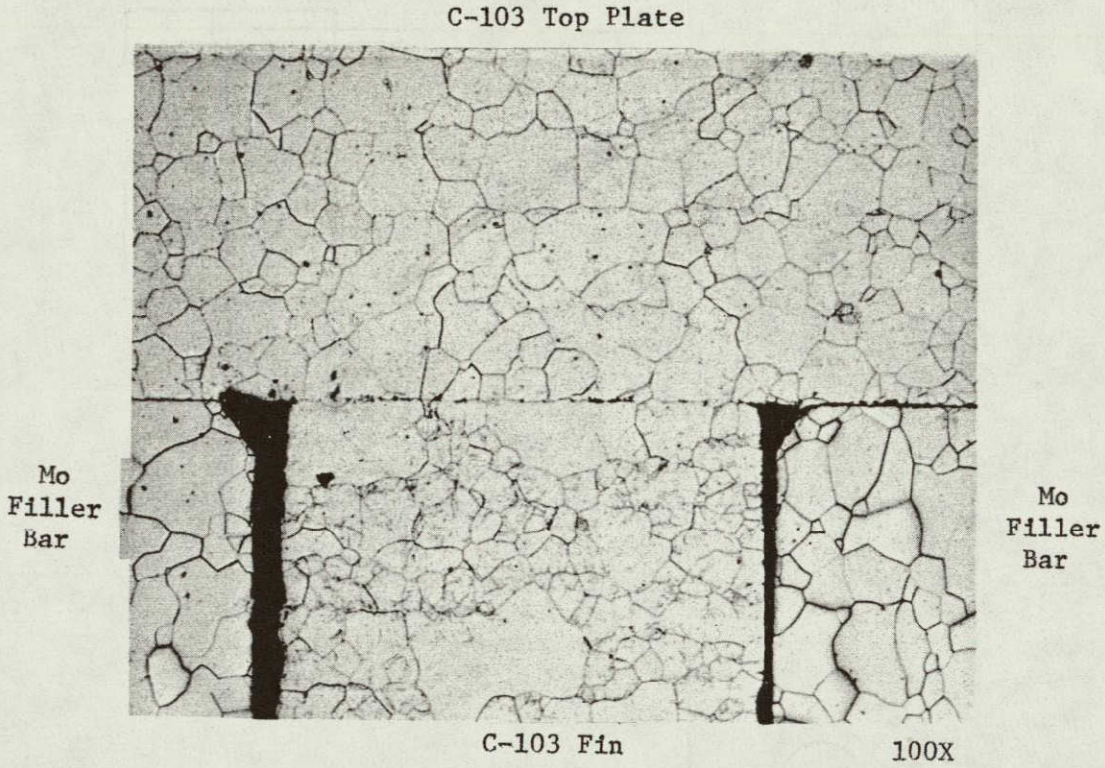

Figure 3-25 Microstructure of Diffusion Welded Joint of C-103 Fin and Top Plate Cyclic Test Specimen

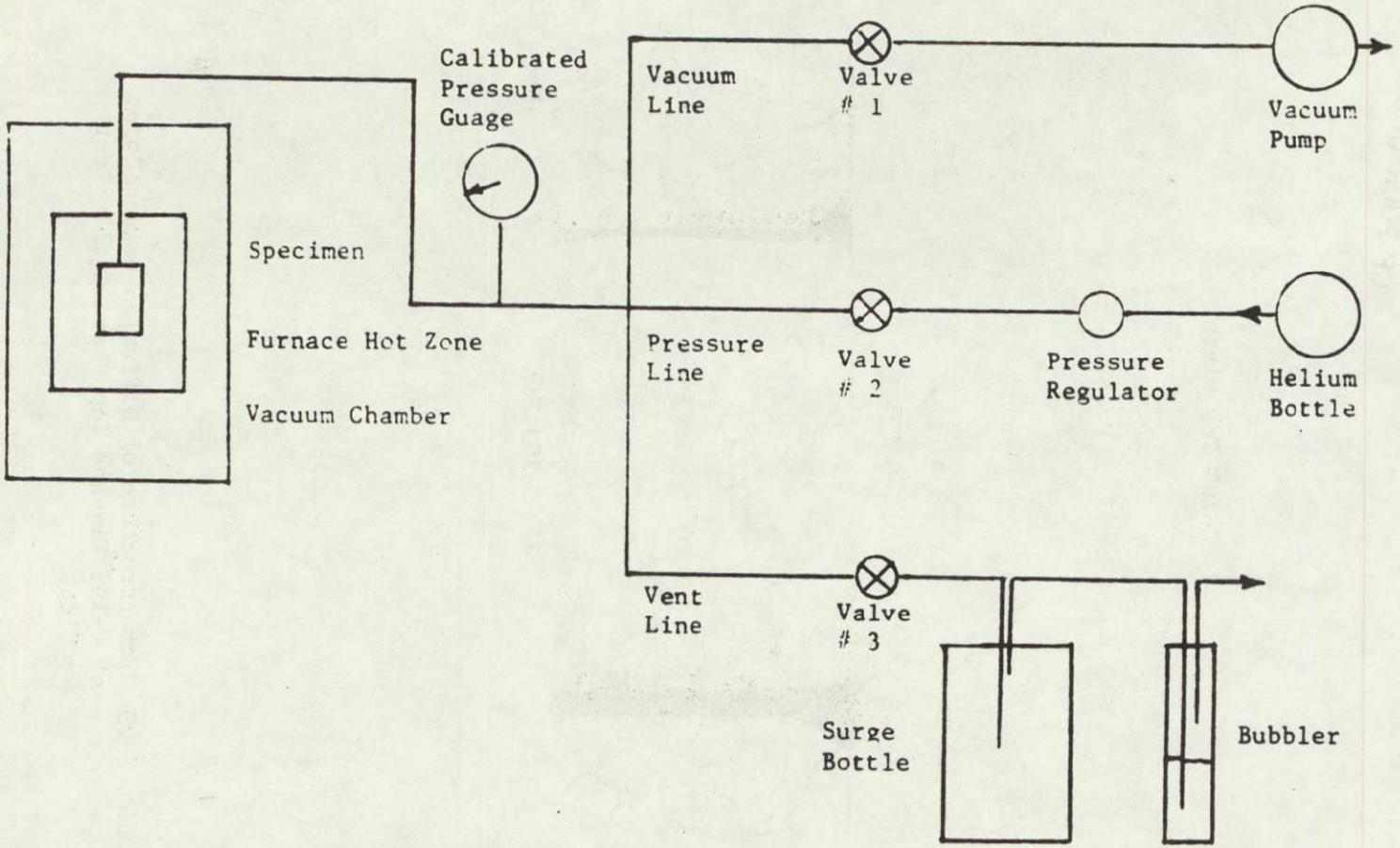

Figure 3-26 Schematic of Cyclic Pressure Test

Pressure was cycled between .93 MPa (135 psia) and atmospheric by alternately opening and closing valves 2 and 3. Pressure was cycled at a rate of about 10 times per minute. After the 100 cycles were completed, the specimen was evacuated prior to and during cooling to room temperature.

No significant change occurred in specimen appearance or thickness during the testing as indicated by measurements made at six different locations before and after testing. No weld failures occurred as measurable by holography; a holograph made after the cycling is shown in Figure 3-27.

Subsequent to the cyclic pressure testing, the specimen was pressurized internally at room temperature in 6.9 MPa (1000 psi) steps to failure. Pressure was applied using a hand-operated hydraulic pump attached to the specimen through small diameter tubing. During this phase of the testing, the specimen was mounted on the holography table, its back-plate bonded to a sturdy frame with epoxy. Holographs were made after each 6.9 MPa (1000 psi) step. Each holograph was made by two exposures of a single frame of film; the interference lines indicate a change in position of the surface at the time of the second exposure relative to its position at the time of the first exposure. If unwelded areas exist, circular interference lines will be present around these areas. Each interference line corresponds to a surface movement of approximately 0.3μm (12×10^{-6} in).

The holographs are shown in Figure 3-28. Shown below each holograph is the internal pressure at the time of each exposure and the maximum pressure attained between exposures. Holographs made with both exposures at

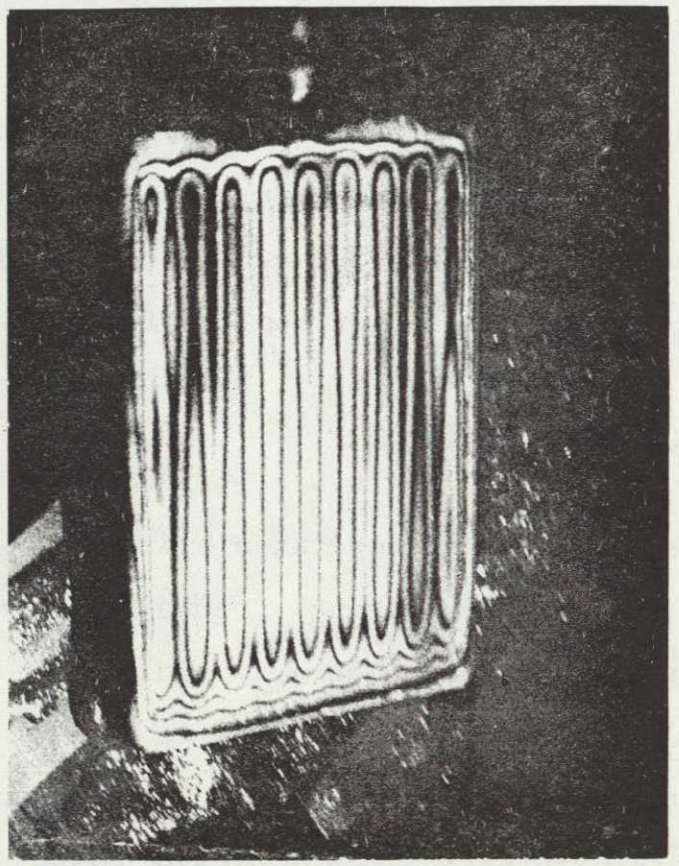

0/5.5 MPa
0/800 psi

Figure 3-27. Holograph of Cyclic Pressure Test Specimen After Testing Showing Diffusion Weld Integrity.

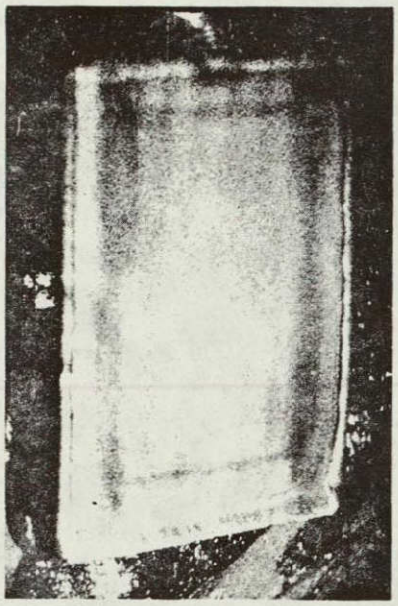

(a) 0/0 MPa
after 6.9 MPA
1000 psi

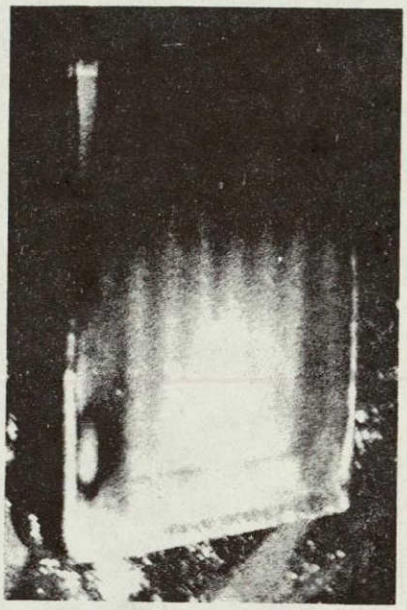

(b) 0/0 MPa
after 13.8 MPA
2000 psi

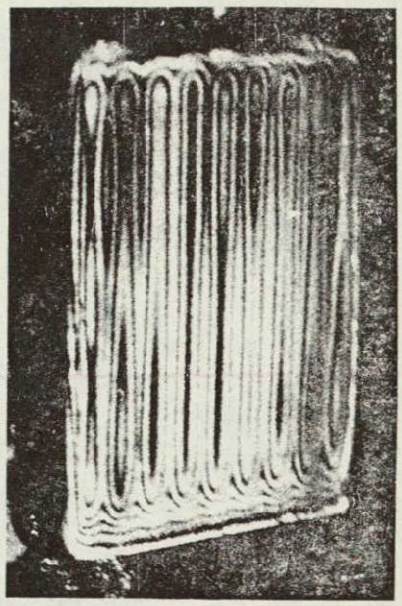

(c) 0/5.5 MPa
0/800 psi

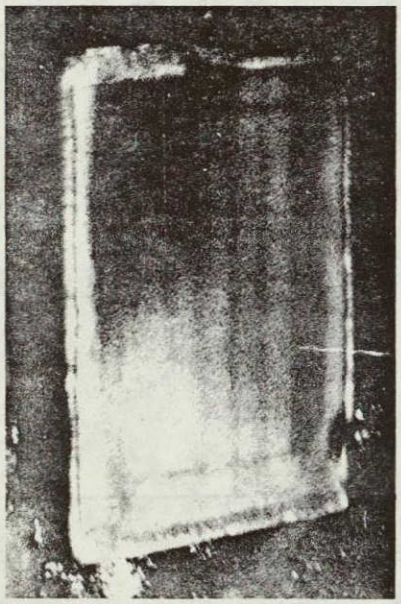

(d) 0/0 MPa
after 20.7 MPa
3000 psi

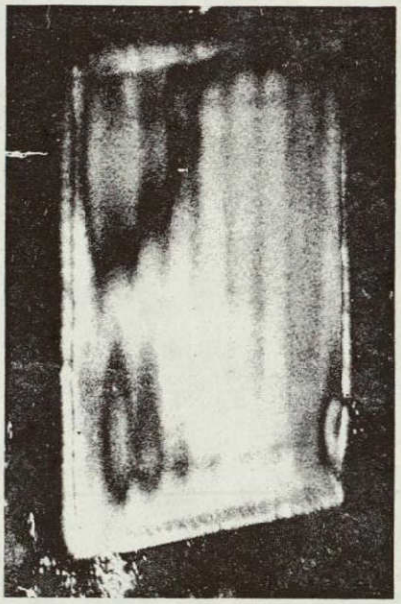

(e) 0/0 MPa
after 27.6 MPa
4000 psi

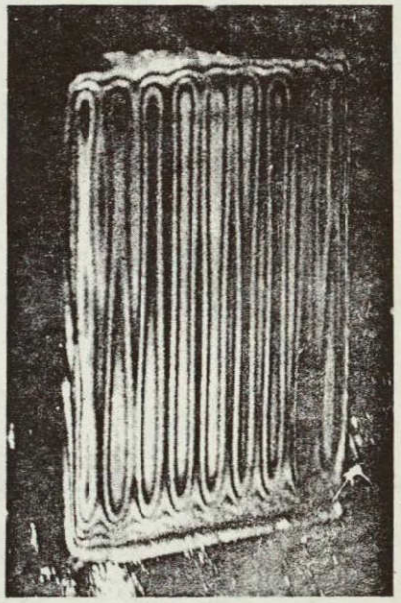

(f) 0/5.5 MPa
0/800 psi

Figure 3-28 **Holographs of cyclic pressure test specimen made at pressures indicated.**

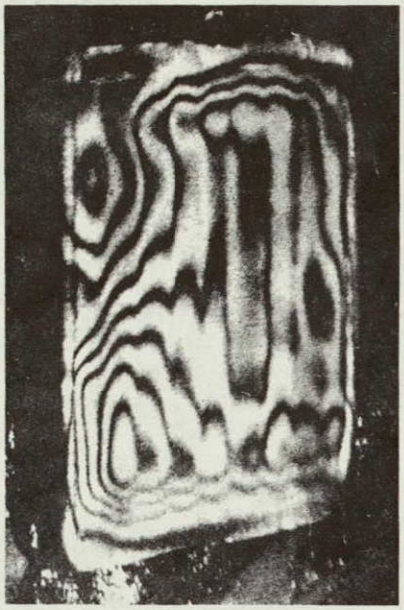

(g) 0/0 MPa
after 34.5 MPa
5000 psi

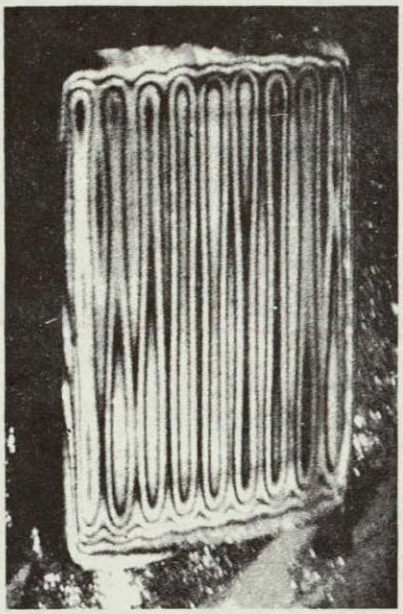

(h) 0/5.5 MPa
0/800 psi

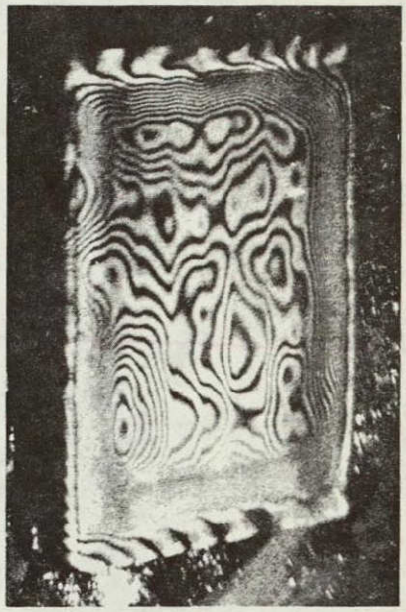

(i) 0/0 MPa
after 41.4 MPa
6000 psi

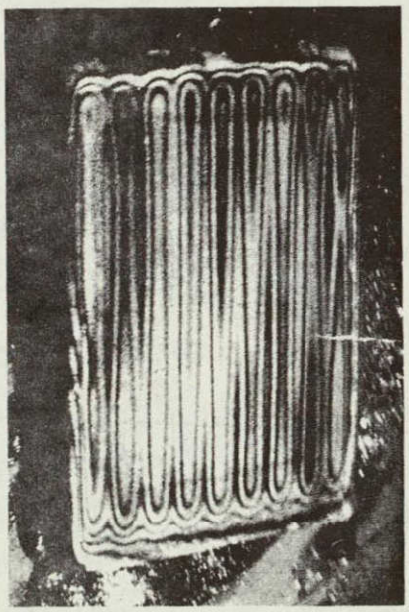

(j) 0/5.5 MPa
0/800 psi

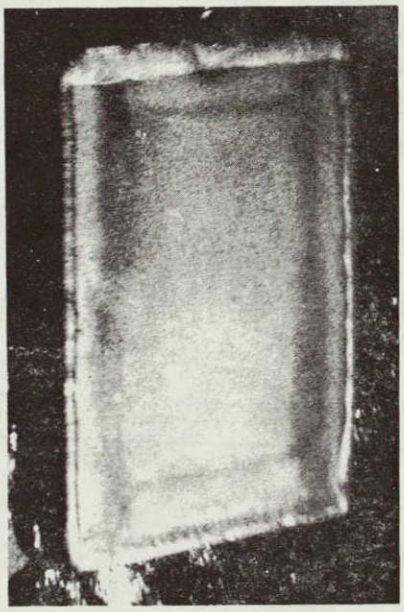

(k) 0/0 MPa
after 48.3 MPa
7000 psi

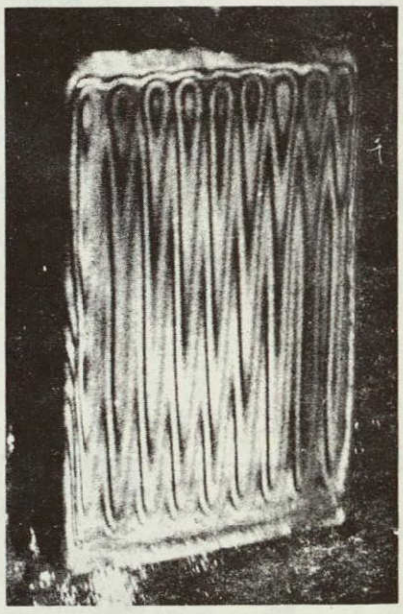

(l) 0/5.5 MPa
0/80- psi

Figure 3-28 (Cont'd). Holographs of cyclic pressure test specimen made at pressures indicated.

zero pressure show permanent deformation (if any) that occurred as the result of the pressure applied to the specimen between the two exposures. Those made with the initial exposure at zero pressure and the second exposure at 5.5 MPa (800 psig) show diffusion weld integrity.

The holographs in Figure 3-28 show that no significant permanent deformation occurred as the result of pressurizing the specimen to 6.9 MPa (1000 psig)(a). Some minor yielding occurred at the lower left corner at 13.8 MPa(2000 psig)(b); there was no failure of the diffusion welds as shown in the next holograph (c). The holograph (d) for 20.7 MPa (3000 psig) shows little or no change, but after 27.6 MPa (4000 psig)(e) minor additional permanent yield has occurred, but the integrity of the diffusion welds was not breached (f).

Additional yielding occurred at 34.5 MPa (5000 psig) as shown in Figure 6(g) with the welds still intact (h). Similarly, additional yielding occurred at 41.4 MPa (6000 psig)(i), with welds still intact (j). The absence of observable interference lines after 48.3 MPa (7000 psig) (k) indicates that a considerable amount of permanent deformation occurred and that the interference lines are not resolvable. The absence of circular interference lines in (l) indicates that no weld failures had occurred. The odd shapes of some of the interference lines can be attributed to motion of the back of the specimen. Since the back surface of the specimen was attached to a solid frame, any deformation that occurred on the back surface would move the entire front surface of the specimen also and contribute to interference lines in the holograms.

Failure of the specimen occurred at approximately 51.7 MPa (7500 psig) internal pressure, which corresponds to stresses in the fins (disregarding stress concentrations and welding stresses) of 310. to 345. MPa (45,000 to 50,000 psi). This is greater than the average room temperature yield stress of C-103, and is an encouraging indication of the high joint efficiency attainable by the diffusion welding process. It was also encouraging in view of the less-than-ultimate weld interface quality that existed in this particular specimen. Figure 3-29 shows the specimen after failure. The bulged surface is evident in Figure 3-29(a); also evident is a tear along the weld which joined the end plate to the finned section of the specimen. Rupture of the fins occurred at the weld between fins and top plate as shown in Figure 3-29(b). The coating on the back side of the specimen which is noticeable in the figure, is epoxy cement used to mount the specimen to a holder for holography during the destructive room temperature pressurization.

This cyclic pressure test demonstrated that a diffusion welded C-103 specimen, fabricated by procedures to be utilized in the manufacture of the HSHX, survived 100 pressure cycles to 115 percent of design pressure at 1270^{o}K(1825^{o}F) without loss of weld integrity.

It also showed that when the specimen was pressurized to failure at room temperature, the diffusion welds held until stresses exceeded average room temperature yield strength despite some porosity in the joint interface, demonstrating that high strengths are attainable by diffusion welding even under lower temperature and pressure diffusion welding conditions than those to be utilized in the manufacture of the HSHX.

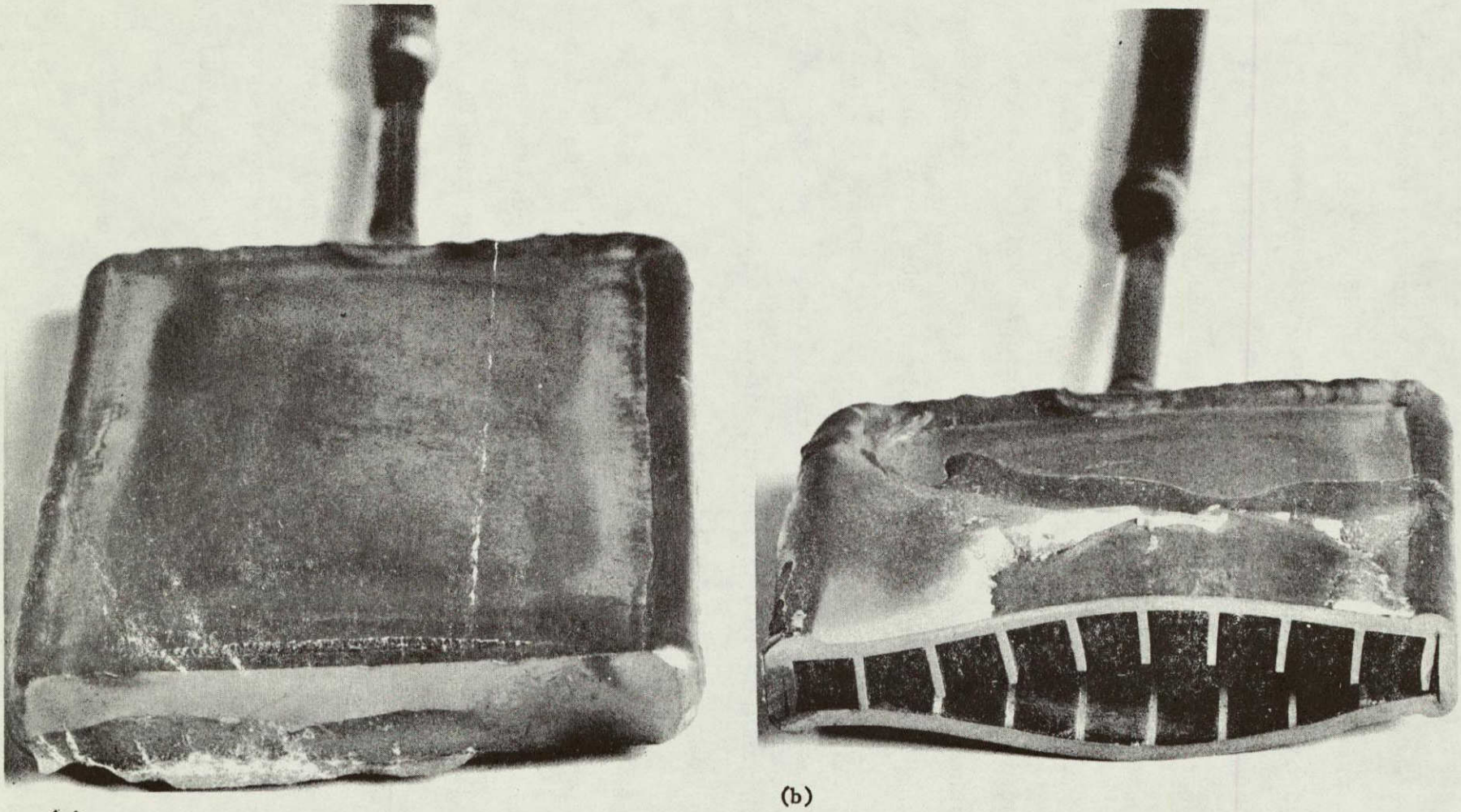

(a) (b)

Figure 3-29 Cyclic Pressure Specimen After Destructive Pressurization at Room Temperature: (a) Showing Bulged Surface and Tear Along Weld, and (b) Showing Separation of Fins From Top Plate at or Near Bond Line.

3.7 NON DESTRUCTIVE TEST (NDT) INSPECTION

The purpose of this effort was to demonstrate that ultrasonic techniques could be utilized for inspection of the integrity of HSHX bonds. Use of ultrasonics instead of holography would be simpler, less expensive and would make it unnecessary to pressurize the HSHX hardware (beyond levels expected during operation) during inspection procedures.

Preliminary ultrasonic testing was performed on trial diffusion welded specimens with voids created by the use of leachable molybdenum foil shims at the weld line interface. Using an Immerscope 721, a 1.9 cm (3/4 in) diameter focused transducer calibrated on a 0.051 cm (0.020 in) diameter hole at 80% amplitude on a 5 MHz sound beam, the front and rear surfaces of a 0.064 cm (0.025 in) thick sheet could be resolved. In welded areas between two 0.064 cm (0.025 in) thick sheets the rear face at 0.13 cm (0.050 in) could be identified and in void areas the interface at 0.064 cm (0.025 in) depth could be identified.

For purposes of calibration a "defect standard" was prepared in which voids of varying lengths in the diffusion welds were caused by use of molybdenum shims which were later leached out leaving the desired defect. This defect standard is depicted in Figure 3-30. As can be seen in Figure 3-31, a "C" scan trace of the longitudinal ultrasonic inspection of that standard, all the calibration defects can be detected except the very smallest, which is only 0.051 cm (0.020-inch) long. There is no certainty that the molybdenum shim used to develop this defect has been leached away. While the holographic method of inspection is an excellent

C-J

tool for determining distortion of the sheet metal surface during pressurization and pressure tests to failure, it was concluded that the ultrasonic method of inspection is most satisfactory for evaluating absence of contact in diffusion welds.

The quality of diffusion welds, that is the absence of porosity and evidence of grain growth across the interface cannot of course be determined by the ultrasonic scans. Diffusion weld quality is consequently obtained by metallographic inspection of numerous diffusion welds taken from specimens cut from the ends of diffusion welded cylinders. This in combination with ultrasonic scan of 100% of the diffusion weld areas provide an excellent assessment of the overall quality of the diffusion welds on delivered hardware.

SECTION 4

INSULATION/EMERGENCY COOLING/ AUXILIARY COOLING VERIFICATION

The insulation system identified for the Mini-Brayton HSA is a high temperature multifoil of the type developed by the Thermo Electron Corporation.

This multifoil insulation concept consists of many layers (60 in number required for the HSA) of thin metal foils (molybdenum and nickel) separated by high purity refractory oxide particles (calcia stabilized zirconia). Each layer of metal foil, which is typically 0.0013 cm (1/2 mil) thick, acts as a thermal radiation barrier. The oxide particles prevent adjacent foils from coming in contact forming a metal-to-metal conduction path. The oxide particles are a new microns in diameter and are sprayed onto one side of each foil. The coated foil is then fired under vacuum at a temperature of 1075K. The particle coatings are relatively sparse, and the low thermal conductivities of the oxides plus the high contact resistance between particles and foil minimize the conduction component of total heat transfer through the insulation.

The Emergency Cooling System (ECS) is designed to maintain acceptable heat source temperatures in event of a failure of the primary HSHX operational cooling mode. Failure to maintain temperatures of the iridium fuel cladding in the MHW-heat source below safe levels may result in a release of PuO_2 from the heat source.

The concept of an insulation blanket which melts when excessive temperatures are experienced is the approach to providing emergency cooling capability. Once a failure of the Mini-Brayton system takes place, all of the energy generated by the heat source is transferred through the melted and fused insulation blanket and then radiated from the outer HSA surface.

The Auxiliary Cooling System (ACS) is designed to limit the temperature of critical components while in a non-operating, fueled condition, such as on the Launch Pad.

Description of Test Program

Testing of the multilayer foil insulation was conducted to demonstrate experimentally that the multifoil insulation meets the system requirements of long life performance and environmental stability and that the emergency cooling concept is a viable approach.

The following tests were conducted: Thermal Conductivity, Vibration, Life Stability (including Thermal cycle), Material Compatibility and Small Scale Meltdown.

4.1 INSULATION LIFE STABILITY TESTS

The purpose of the life stability test series was to determine the thermal stability of Nickel-Zirconia multifoil insulation in the temperature range 1090 to 1255K (1500 to 1800°F). (Early in the program an all nickel foil blanket was contemplated.) A secondary purpose was to evaluate the effectiveness of the zirconia as separators by testing a sample without a zirconia coating.

The test program consisted of six tests of five all nickel multifoil insulation samples. Five tests of this series demonstrated the thermal stability of nickel-zirconia multifoil insulation for at least 1000 hours within the temperature range tested. The sixth test verified the thermal instability of bare nickel multifoil insulation at 1255K (1800^{O}F), which demonstrates the effectiveness of the zirconia as foil separators. A regression analysis supported the test data observations. Diagnostic disassembly of the 1145K and 1255K (1600 and 1800^{O}F) hot face samples has confirmed that no significant self-welding of adjacent foils occurred with the zirconia coated samples.

4.1.1 TEST SAMPLES AND TEST FACILITY

The life stability test sample consisted of a small cylinder and two planar ends of all nickel multifoil insulation, inner and outer cylindrical tantalum enclosures, a quartz lamp heater, and a base with ceramic standoffs.

The insulation sample consisted of a 5.1 cm (2.0 in) diameter, 8.26 cm (3.25 in) long cyinder and two planar end discs, 5.1 cm (2.0 in) in diameter. Each was composed of 60 layers of 0.0013 cm(0.0005 in) thick nickel foil coated on one side with a very disperse zirconia coating. The cylinder was wrapped around an uncoated nickel mesh support. The thickness of the cylindrical insulation was about 0.61 cm (0.24 in) thick and the planar ends were 0.2 cm (0.08 in) thick. Each planar end had a 1.3 cm (0.5 in) diameter hole thru which the heater was mounted. An inner tantalum cylinder with planar ends was the radiator. The test

sample was heated by a 500 watt quartz lamp about 1.3 cm (0.5 in) diameter and 10.2 cm (4 in) long. The lamp was mounted to an aluminum base plate with ceramic standoffs. The mounted quartz lamp and the completely assembled life stability test sample are shown in the photograph of Figure 4-1. Each test sample was instrumented with two tungsten/tungsten-rhenium thermocouples on the hot face (diametrically opposite) and two chromel-alumel thermocouples on the radiator (diametrically opposite). The instrumented test sample is illustrated on Figure 4-2.

The test samples were placed in a vacuum bell jar and tested at $\leq 10^{-3}$ pascals (Pa) (10^{-5} torr).

4.1.2 TEST RESULTS

As indicated, 1000 hour tests were conducted on four samples at hot face temperatures of 1090, 1145, 1200, and 1255K (1500, 1600, 1700, and 1800°F). Each of these samples was individually heated with about 40 watts. Approximately 20% of the heat flowed thru the sample, with the remainder being edge losses and losses thru the heater and thermocouple leads. After the test chamber was evacuated to about 10^{-4}Pa (10^{-6}torr), the samples were heated until the hot face temperatures reached the predetermined values. Then heater input was held constant and tests run for 1000 continuous hours. After this high temperature vacuum exposure, the samples were cooled to room temperature before exposure to ambient. The test data are plotted on Figures 4-3 thru 4-6 for 1090K thru 1255K (1500°F thru 1800°F), respectively. Raw test data given on sheet 1 of the figures consist of measured heater input power, measured hot and cold face temperature, and calculated ΔT. Normalized data given on sheet 2 of the figures were used as an evaluation tool and is described subsequently.

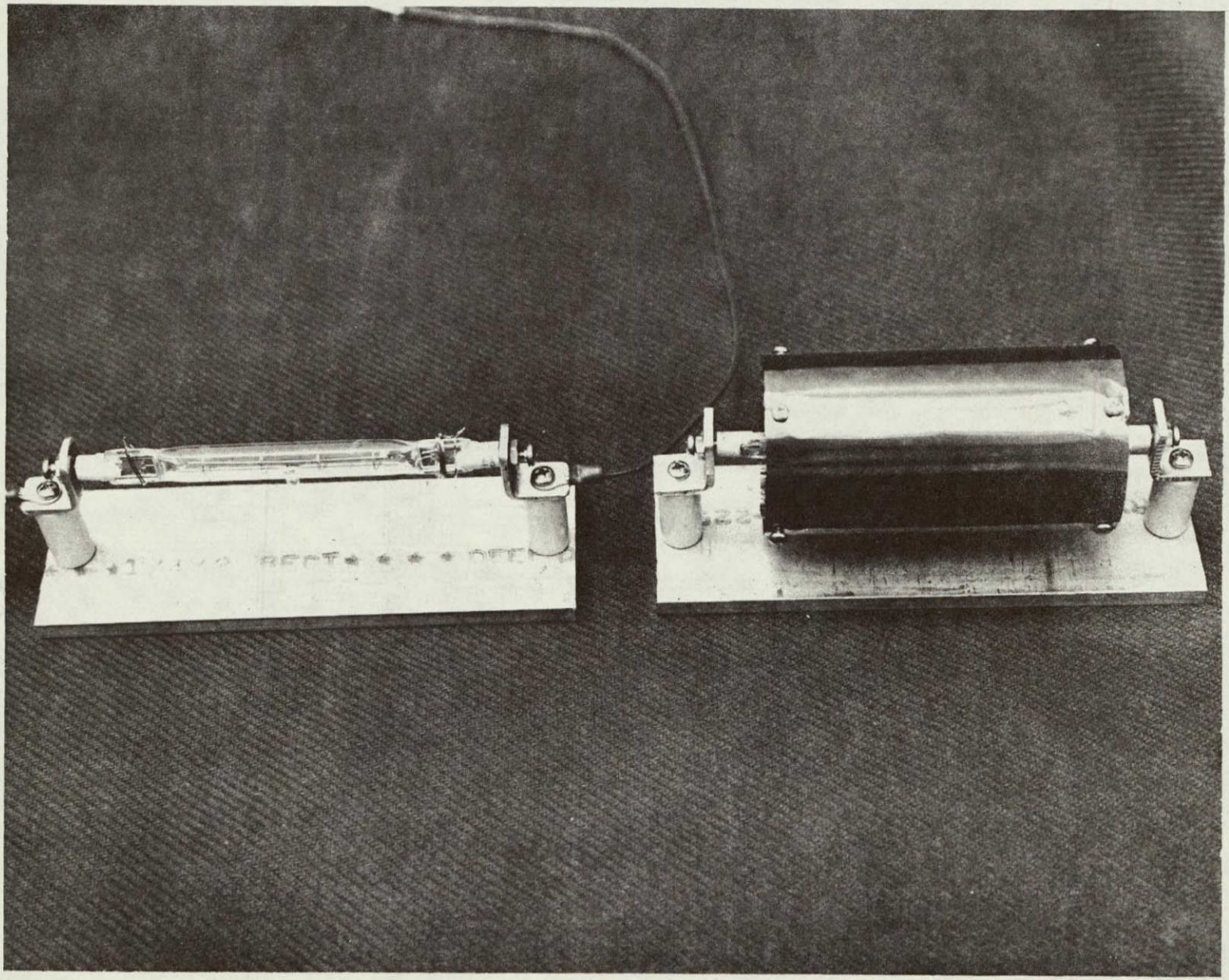

Figure 4-1 Life Stability Test - Sample Quartz Lamp Heater on Left And Fully Assembed Sample on Right

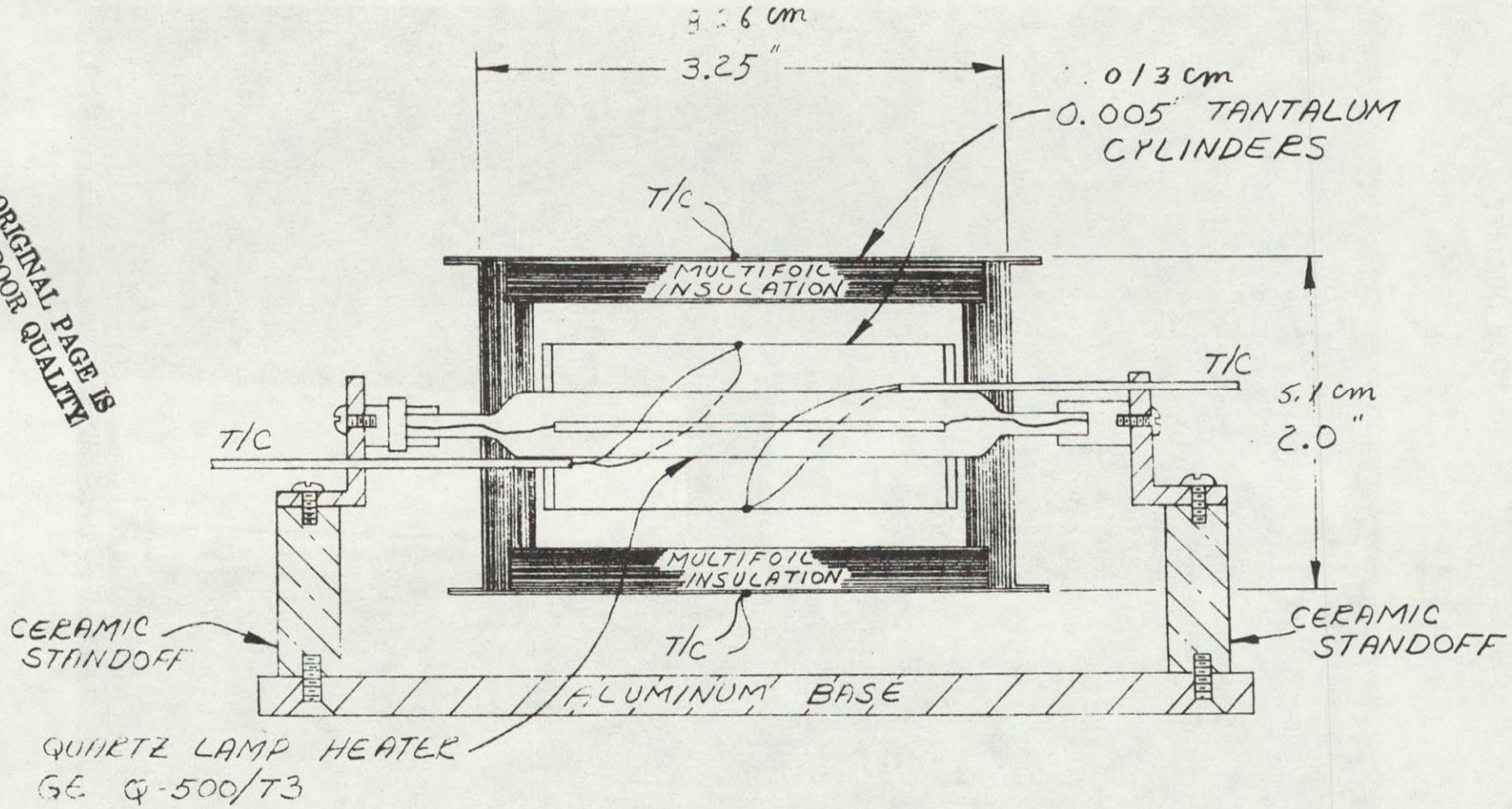

FIGURE 4-2 LIFE STABILITY TEST ASSEMBLY

Using standard statistical techniques, a linear regression analysis was performed to determine if raw and normalized hot face temperatures are time dependent. The regression analysis indicated, at a 95% confidence level, that for three of the five nickel-zirconia tests (1145K (1600°F), 1255K (1800°F) and thermal cycling) the hot face temperature is not time dependent. The 1090K (1500°F) test exhibited a slightly negative slope of a least square fit vs. time, but that sample was later tested in the thermal cycling test and exhibited no time dependence. The 1200K (1700°F) test exhibited a slightly positive slope of a least square fit vs. time, indicating an appreciation of performance with time. The overall assessment of the regression analysis is that all five nickel-zirconia tests demonstrated thermal stability over a minimum of 1000 hours, with one sample being tested for a total of about 2500 hours.

The thermal instability of the bare nickel foil is manifest in the raw and normalized data of Figure 4-8, where the hot face drops, indicating increasing thermal conductivity. The cold face rises with time, indicating that as the thermal conductivity increases, progressively more of the heat flows thru the sample.

A diagnostic disassembly was performed on three of the five samples (1145K (1600°F) and 1255K (1800°F) nickel-zirconia and the 1255K (1800°F) bare nickel). The nickel-zirconia samples were disassembled by removing the two planar ends and then unwrapping the cylinder. With both zirconia samples some sticking was observed between the edge of the planar ends and the edge of the cylinder. The sticking was most prevalent to the nickel screen (uncoated) around which time the cylinder was wound. All end layers were separable, although the three innermost layers of the 1255K (1800°F)

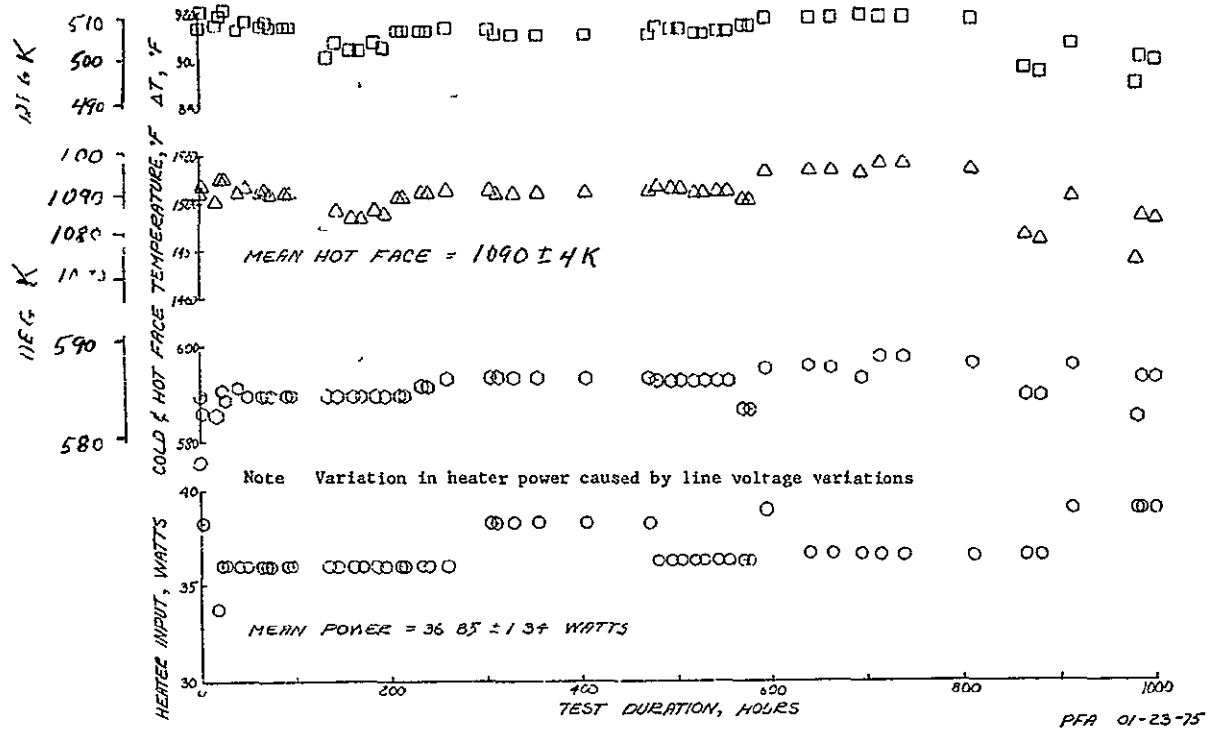

FIGURE 4-3 RAW & NORMALIZED LIFE STABILITY TEST DATA - 1090K HOT FACE
SHEET 1 OF 2

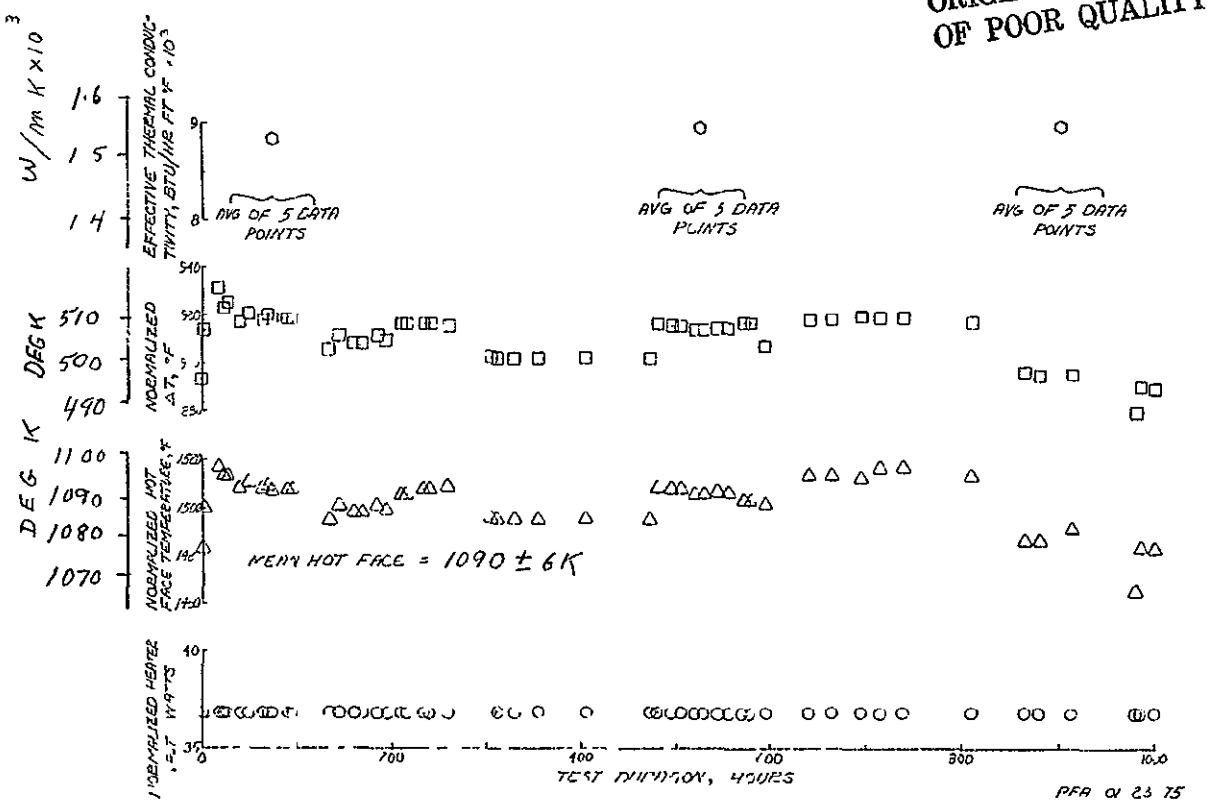

FIGURE 4-3 RAW & NORMALIZED LIFE STABILITY TEST DATA - 1090K HOT FACE
SHEET 2 OF 2

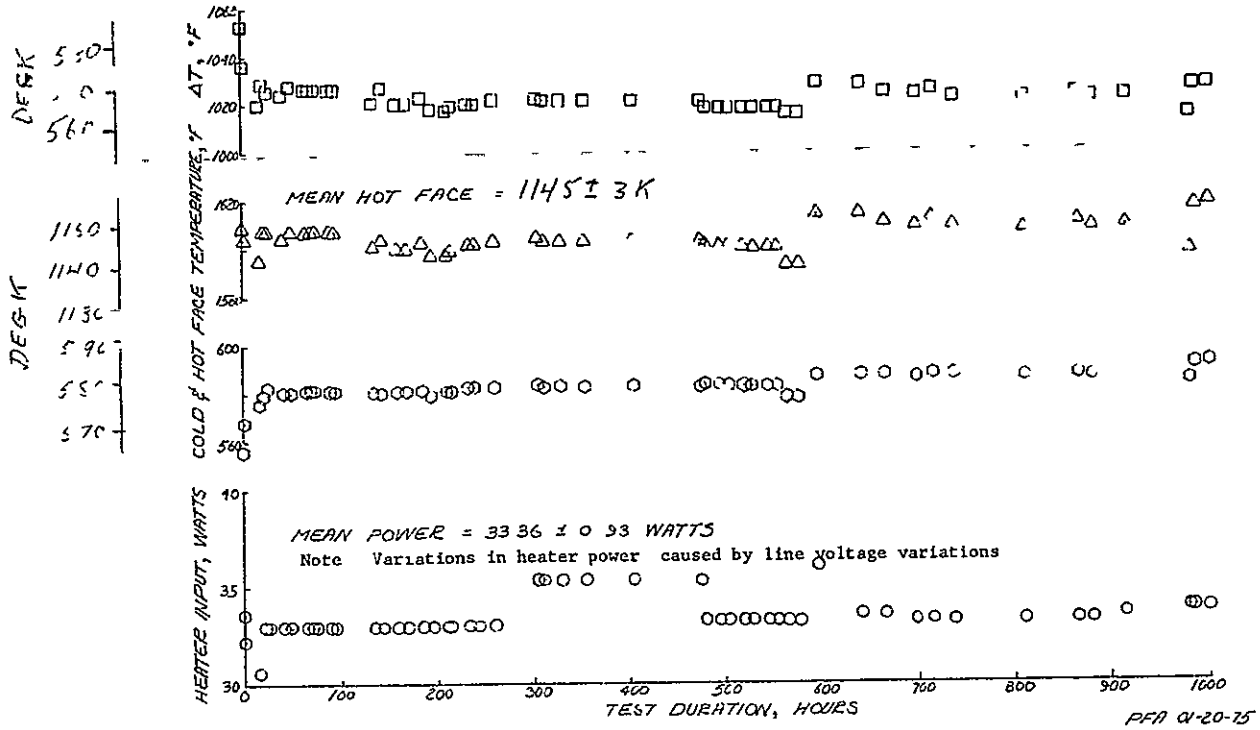

FIGURE 4-4 RAW & NORMALIZED LIFE STABILITY TEST DATA - 1145K HOT FACE
SHEET 1 OF 2

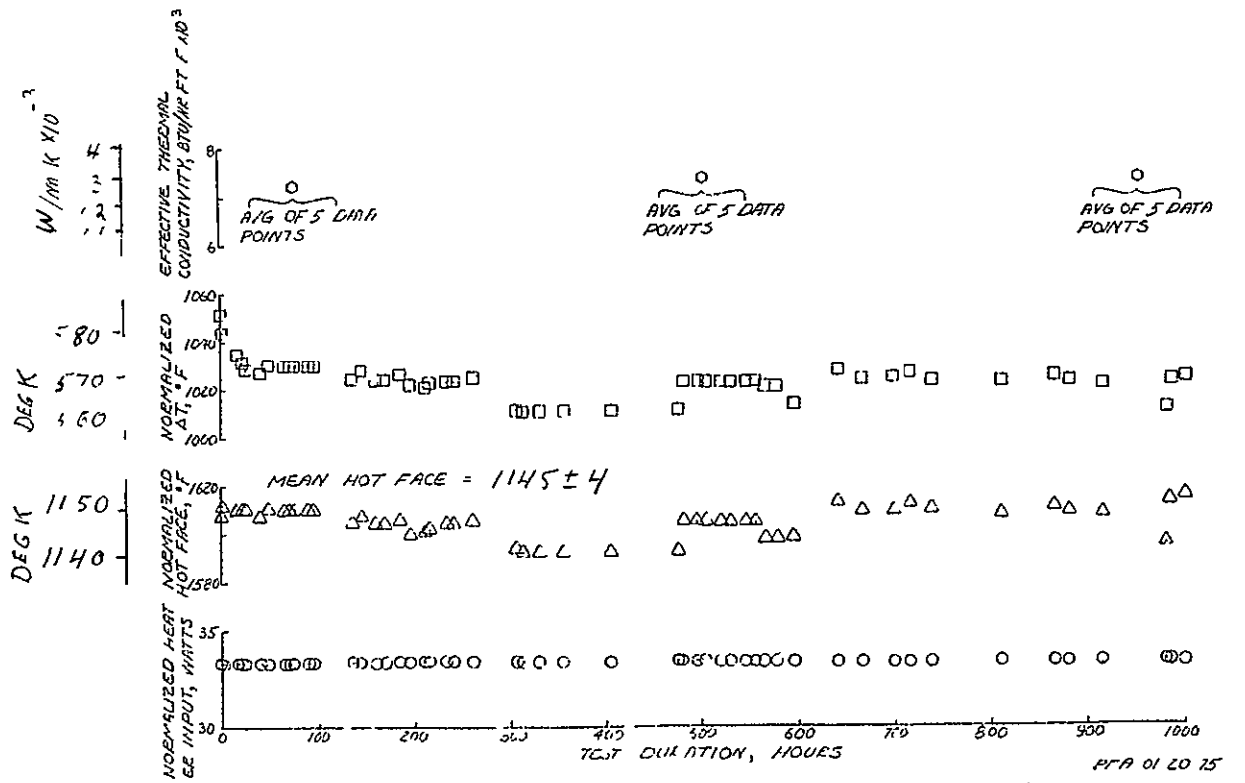

FIGURE 4-4 RAW & NORMALIZED LIFE STABILITY TEST DATA - 1145K HOT FACE
SHEET 2 OF 2

ORIGINAL PAGE IS
OF POOR QUALITY

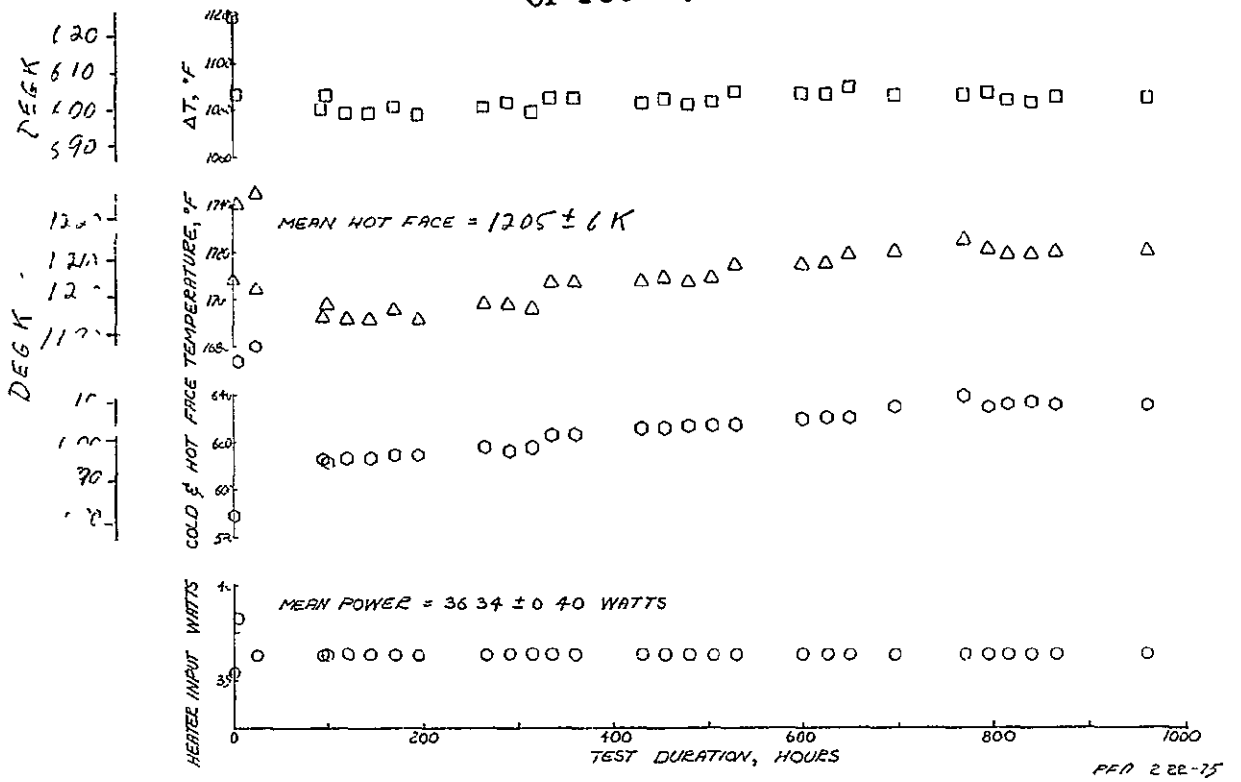

FIGURE 4-5 RAW & NORMALIZED LIFE STABILITY TEST DATA - 1205K HOT FACE
SHEET 1 OF 2

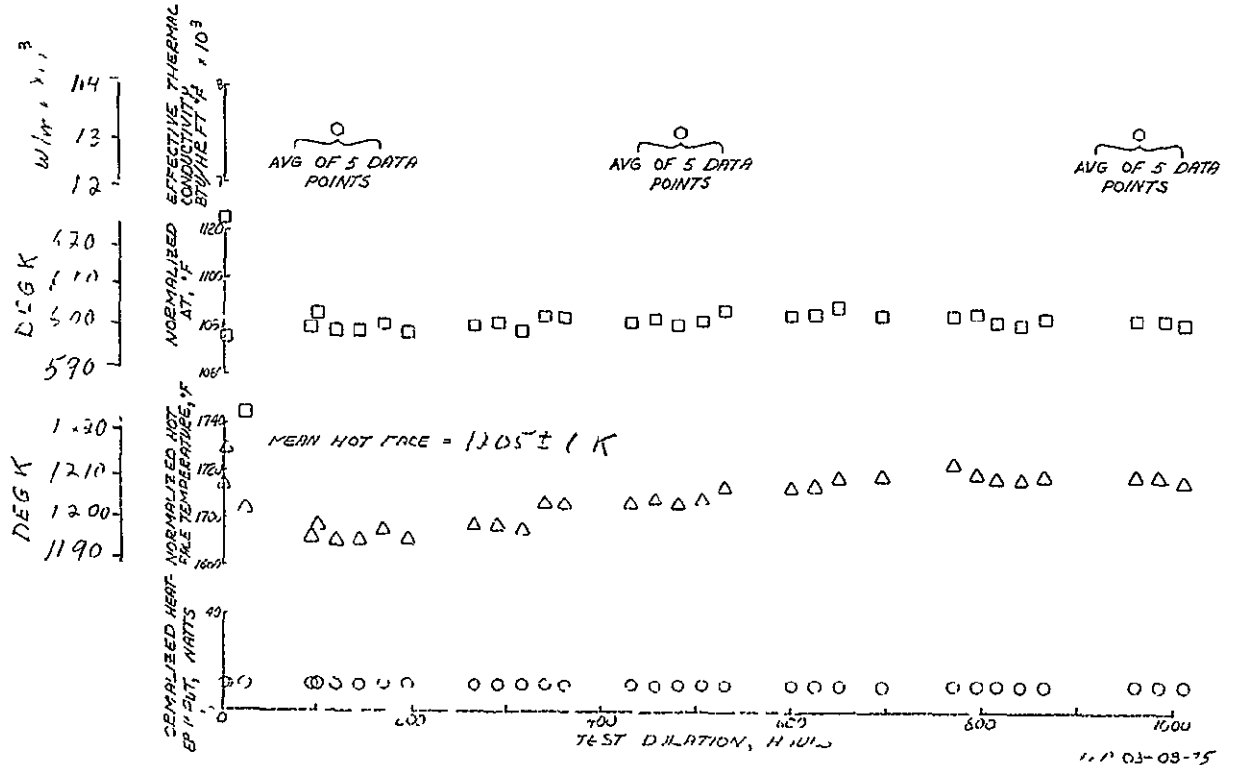

FIGURE 4-5 RAW & NORMALIZED LIFE STABILITY TEST DATA 1205K HOT FACE
SHEET 2 OF 2

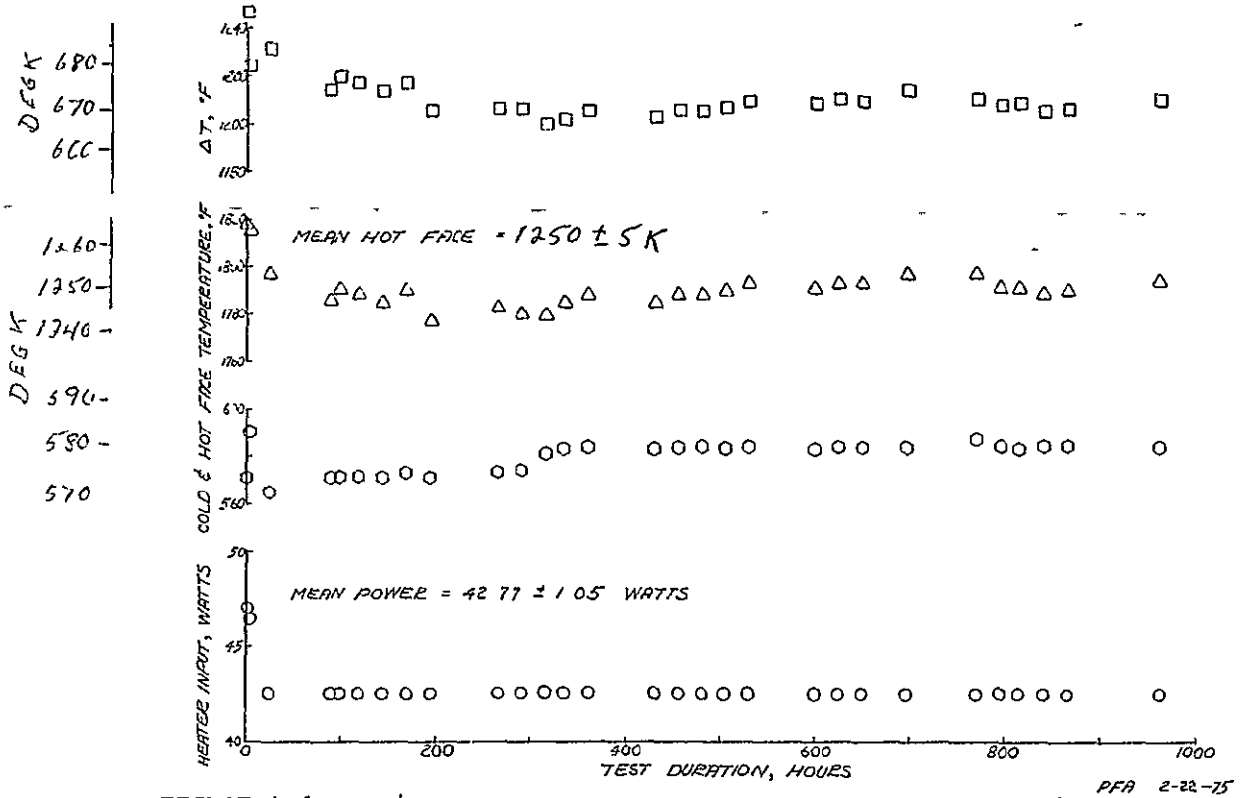

FIGURE 4-6 RAW & NORMALIZED LIFE STABILITY TEST DATA - 1255K HOT FACE
SHEET 1 OF 2

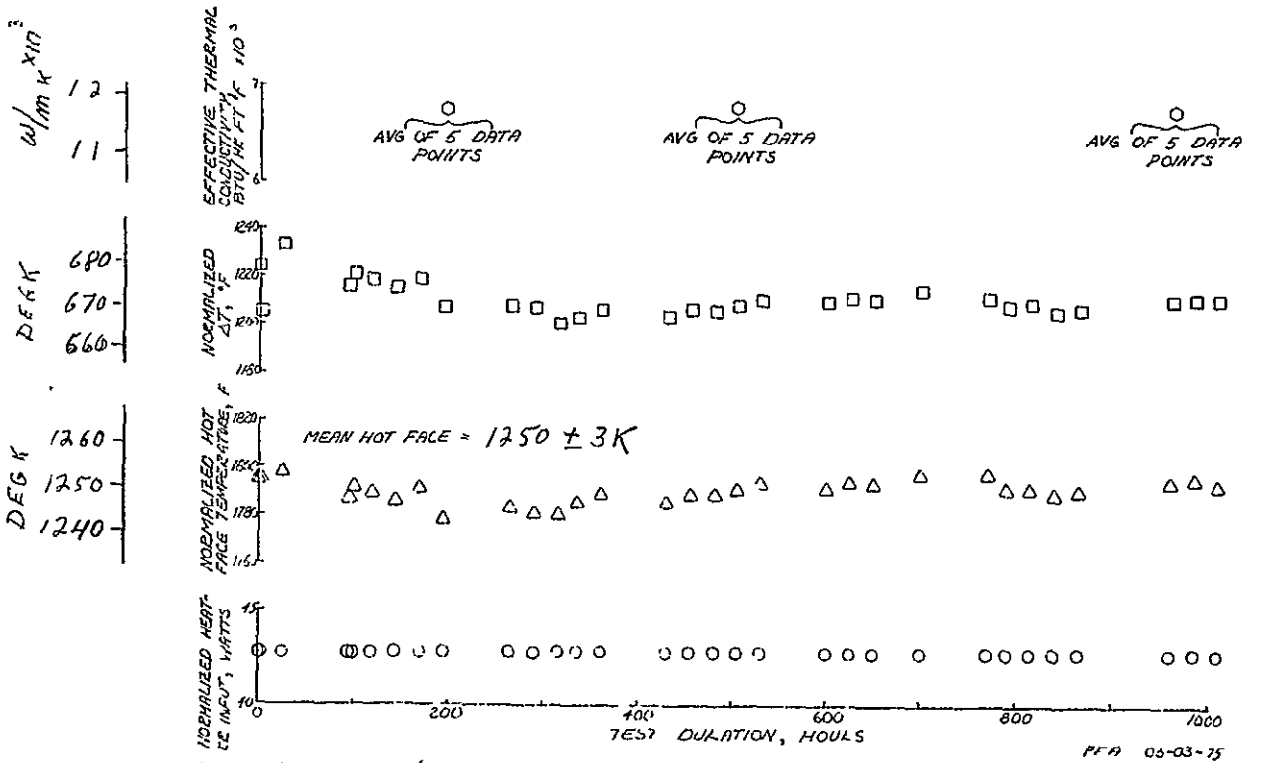

FIGURE 4-6 RAW & NORMALIZED LIFE STABILITY TEST DATA - 1255K HOT FACE
SHEET 2 OF 2

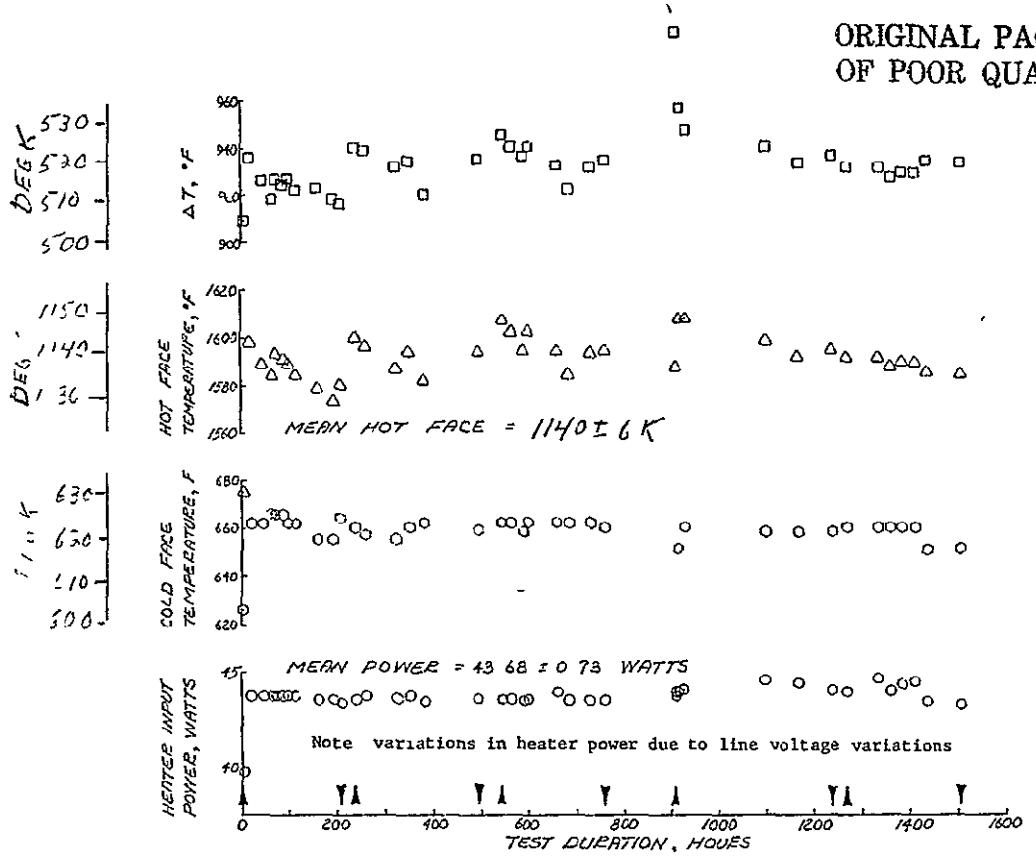

PFA 01 24-75

FIGURE 4-7 RAW & NORMALIZED LIFE STABILITY TEST DATA - 1145K THERMAL CYCLE
SHEET 1 OF 2

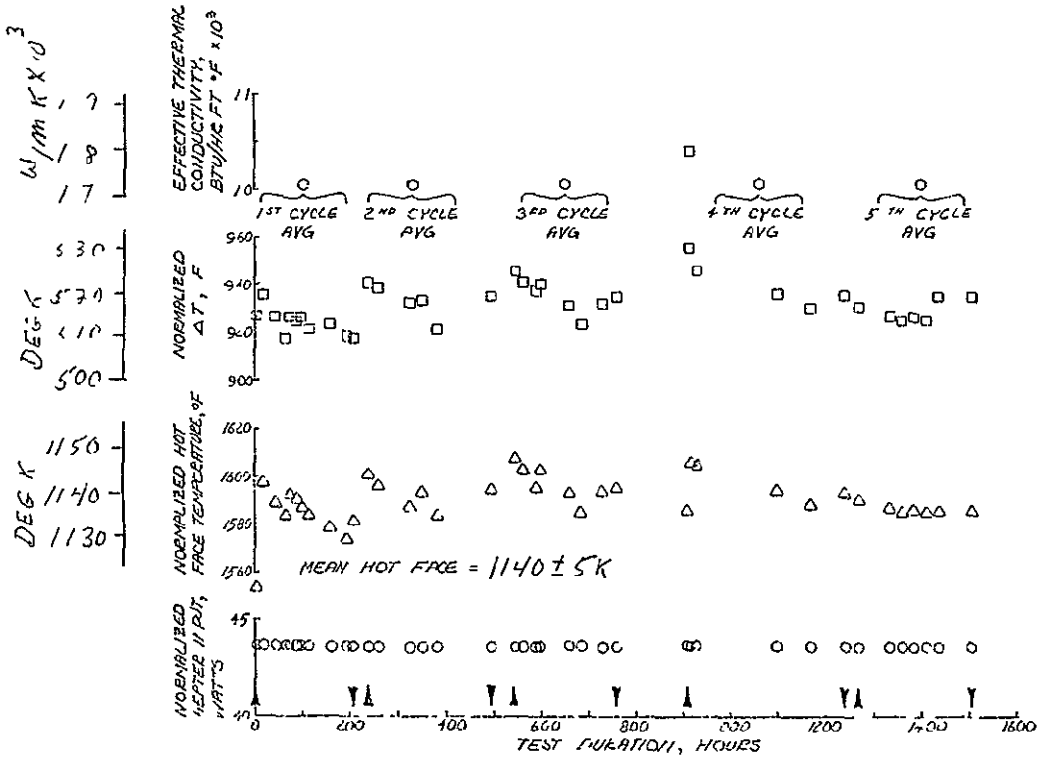

PFA 0-24-75

FIGURE 4-7 RAW & NORMALIZED LIFE STABILITY TEST DATA - 1145K THERMAL CYCLE
SHEET 2 OF 2

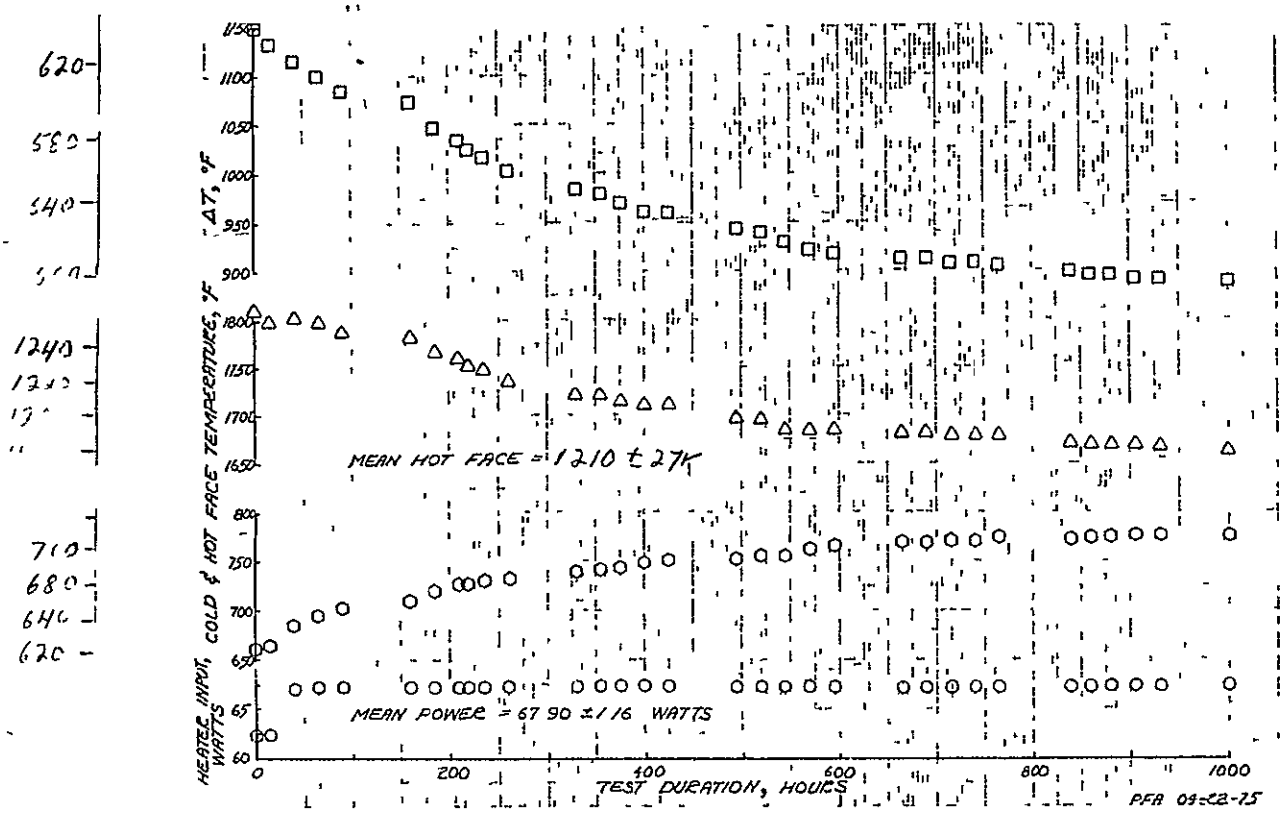

FIGURE 4-8 RAW LIFE STABILITY TEST OF BARE NICKEL FOIL @ 1255K HOT FACE
SHEET 1 OF 2

ORIGINAL PAGE IS
OF POOR QUALITY

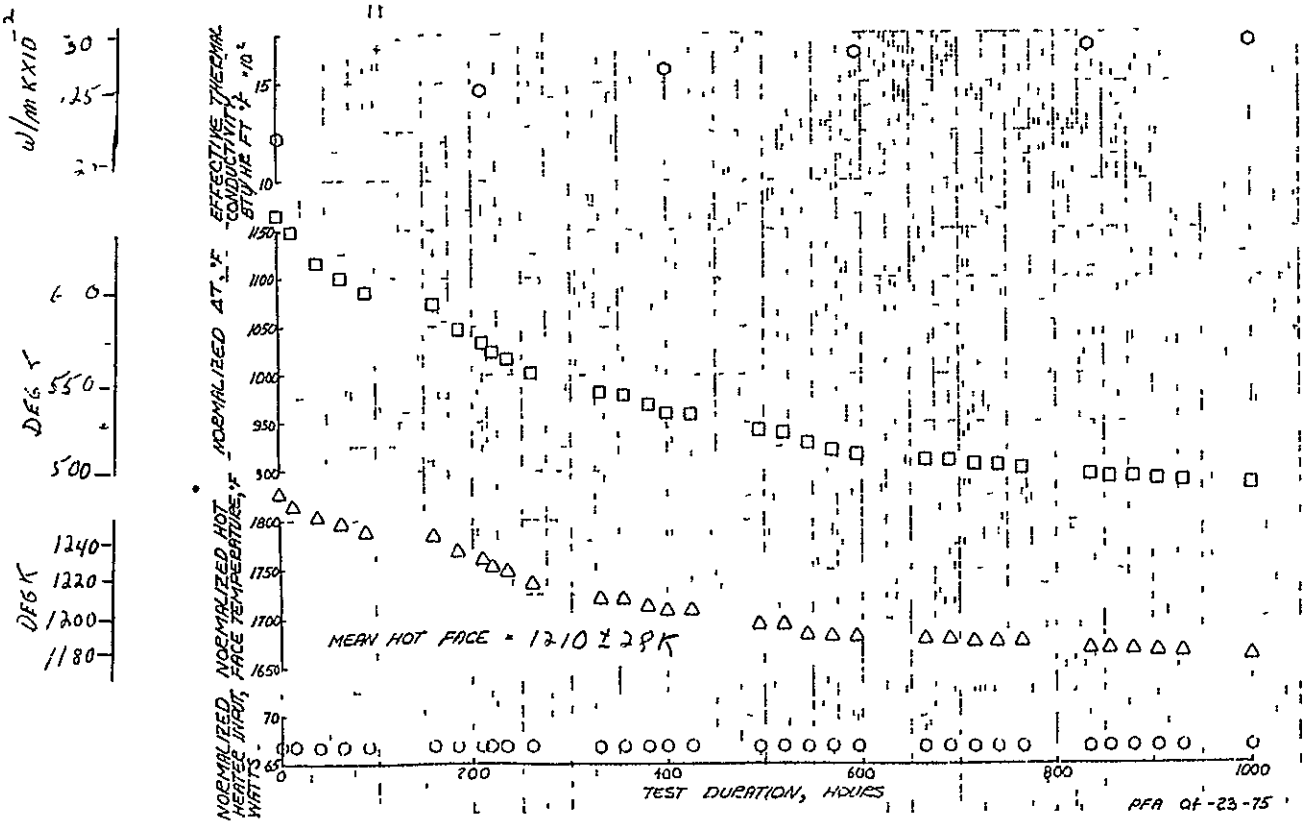

FIGURE 4-8 NORMALIZED LIFE STABILITY TEST OF BARE NICKEL FOIL @ 1255K HOT FACE
SHEET 2 OF 2

sample were sticky. For both these samples, the 60 layer foil cylinder was completely unwound. Some sticking near the edges was observed. With the 1255K (1800°F) sample, some local sticking near the center of the sample was noted at about the 10th layer from the inside, which continued to the innermost layer. This was apparently caused by slight projections in the foil (caused by the screen support) which resulted in local metal to metal contact. The innermost layer of the 1145K (1600°F) sample stuck to the nickel screen but was removed, leaving an embossed screen pattern on the foil. The innermost layer of the 1255K (1800°F) sample welded to the screen and could not be removed. The external appearance of the 1255K (1800°F) sample showing the outer tantalum cylinder prior to unwrapping is shown in the photograph of Figure 4-9. The internal appearance of the sample is shown on Figure 4-10.

The bare nickel foil sample was disassembled after 1000 hours at 1255K (1800°F) hot face. The external surface of the sample had a darkened appearance. The cylinder was unwrapped to determine the extent of the self-welding. Self-welding was evident as far out as the 60th layer of the 60 foil sample. After unwrapping four layers, and observing more severe self-welding as the unwrapping proceeded, further unwrapping became impractical without severe tearing occurring.

The appearance of the planar end discs was considerably different. The inner surface of both end discs was darkened and crinkled. Self-welding was prevalent thru all 60 layers and evidence of vaporization of the nickel was noted.

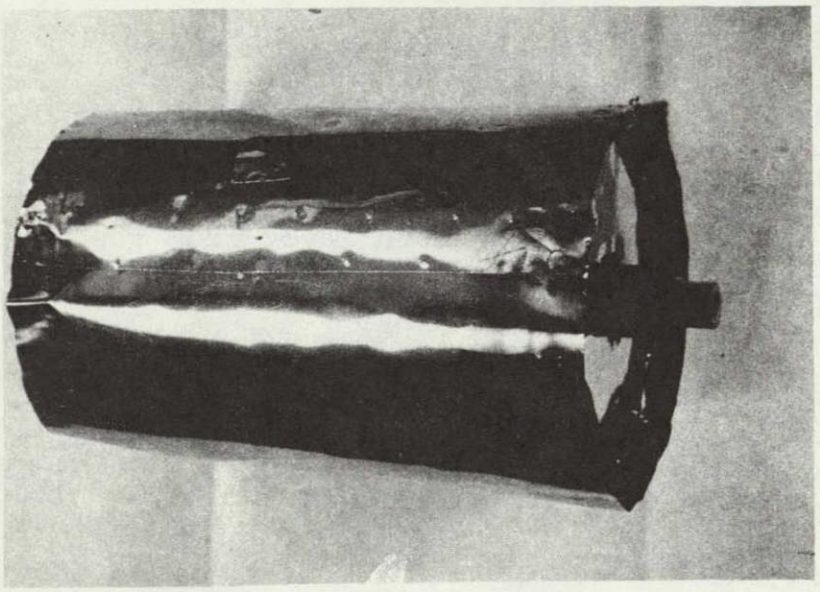

FIGURE 4-9. EXTERNAL APPEARANCE OF 1255K (1800°F) LIFE STABILITY TEST SAMPLE PRIOR TO DIAGNOSTIC DISASSEMBLY

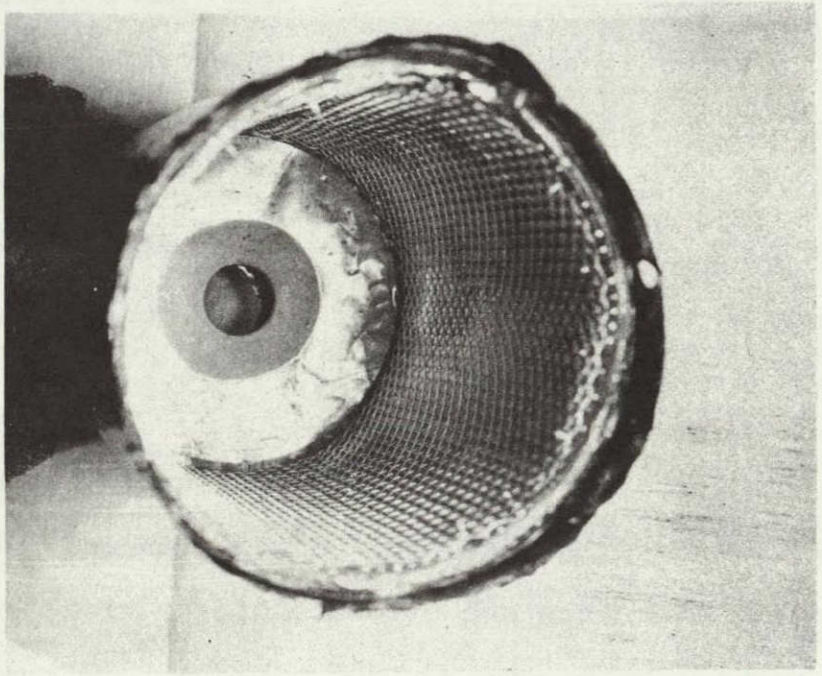

FIGURE 4-10. INTERNAL APPEARANCE OF 1255K (1800°F LIFE STABILITY) TEST SAMPLE DURING DIAGNOSTIC DISASSEMBLY

The overall assessment of the diagnostic disassembly of the three samples is that no significant self-welding of the zirconia coated foils occurred during 1000 hours or more of operation in vacuum at elevated temperature in excess of predicted operational temperatures. The massive self-welding observed with the bare nickel (no zirconia) foil sample proves the effectivenss of the zirconia particle separators.

Although this macroscopic evaluation of the zirconia coated nickel foil indicated thermal stability at high temperature, material compatibility tests which were conducted subsequent to the tests described revealed some potential chemical instability of Ni/ZrO_2 which could occur over the 7 year life time. The results of these material compatibility tests, discussed in 4.4, led to a conservative design modification which restricted the nickel foil to lower temperatures.

4.2 INSULATION THERMAL CONDUCTIVITY TESTS

The purpose of the thermal conductivity tests was to:

- Measure the effective thermal conductivity of 60 layers of nickel-zirconia multifoil insulation in vacuum.
- Assess the effect, if any, of a vibration environment on the effective thermal conductivity of the multifoil insulation.
- Assess the expected Auxiliary Cooling Subsystem (ACS) performed by measuring thermal conductivity of insulation backfilled with inert gases at 1 atm pressure.

Thermal conductivity measurements were performed on two sets of multi-foil thermal insulation. Each set consisted of two separate stacks of 0.0013 cm (0.0005 in) thick individual nickel foils separated by zirconia particles sprayed on one face of each foil. The 10.2 cm (4.0 in) diameter stacks were nominally 0.13 cm (0.050 in) thick as tested at 6.9 kPa/1.0 psi contact pressure and each contained 60 individual foils. The four separate samples (stacks) were identified by the tags 1D, 2D, 5D, and 6D respectively.

The measurements were made by the guarded hot plate technique. This technique has an accuracy of $\pm$ 5% across its temperature range of 115K to 1255K (250°F to 1800°F). A set of two sample stacks was required, consequently, the average data for the two stacks is reported. The test samples consisted of two sets each of the twin stacks, as fabricated, and then the same two sets remeasured after a vibration test. After an extensive error analysis, beyond that required for the ASTM C177 method[1], the final results were normalized for the effects of radial edge losses in this extremely anisotropic material. Test data is given in Figures 4-11 and 4-12. Figure 12 shows results for conductivity in Krypton and Xenon gas which were made in tests subsequent to the first set of data given in Figure 4-11. The following is a summary of the results:

- The effective thermal conductivity in a vacuum is 6.4 x 10^{-3} watts/m K (3.7 x 10^{-3}Btu/hr ft ^{o}F) at a mean temperature of 1016K (1369^{o}F), with average hot and cold faces of 1222K (1740^{o}F) and 813K (1003^{o}F), respectively, and with an average compressive load of 6.9 kPa/1.0 psi. This is in substantial agreement with the TECO reported effective conductivity of 6.69 x 10^{-3} watts/m K (3.87 x 10^{-3} Btu/hr ft^{o}F). Performance of the insulation in the HSA should result in lower effective thermal conductivity in the absence of compressive loads.

- The measured effective thermal conductivity of the insulation in inert gases at ~1 ATM is greater than the conductivity of the gas alone by a factor that ranges from 1.45 for helium to 2.74 for argon. Therefore use of the pure gas conductivity in ACS analyses will give conservative results.

- The vibration testing had no significant effect on effective thermal conductivity for the four samples tested. Therefore, degradation of insulation due to launch vibrations is not anticipated (see 4.3).

- Multifoil insulation is extremely anisotropic, with a ratio of the lateral conductivity (parallel to the layers) to the through conductivity (perpendicular to the layers) being 10000 to 1, indicating the great importance of joint design to minimize edge losses.

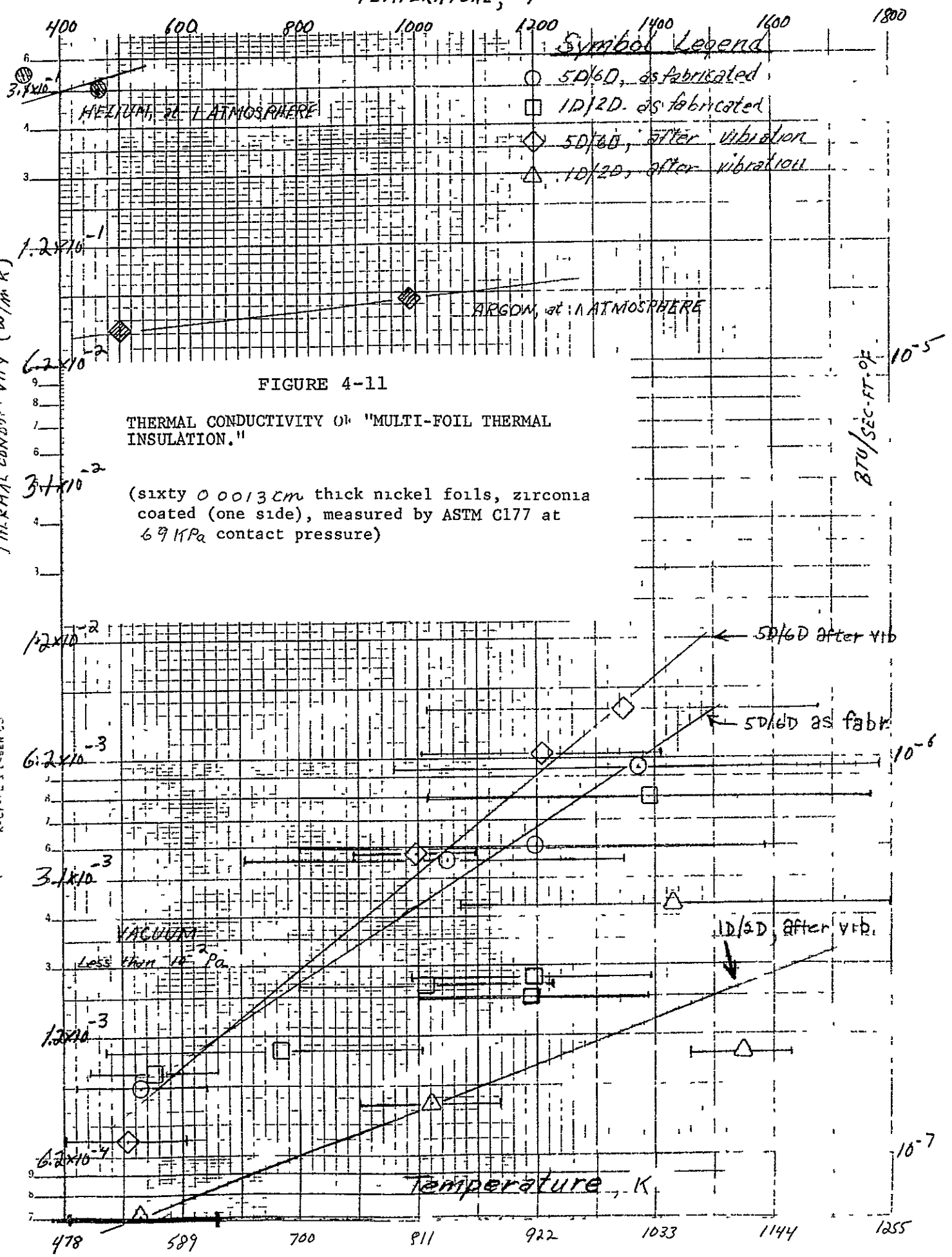

FIGURE 4-11

THERMAL CONDUCTIVITY OF "MULTI-FOIL THERMAL INSULATION."

(sixty 0.0013 cm thick nickel foils, zirconia coated (one side), measured by ASTM C177 at 69 kPa contact pressure)

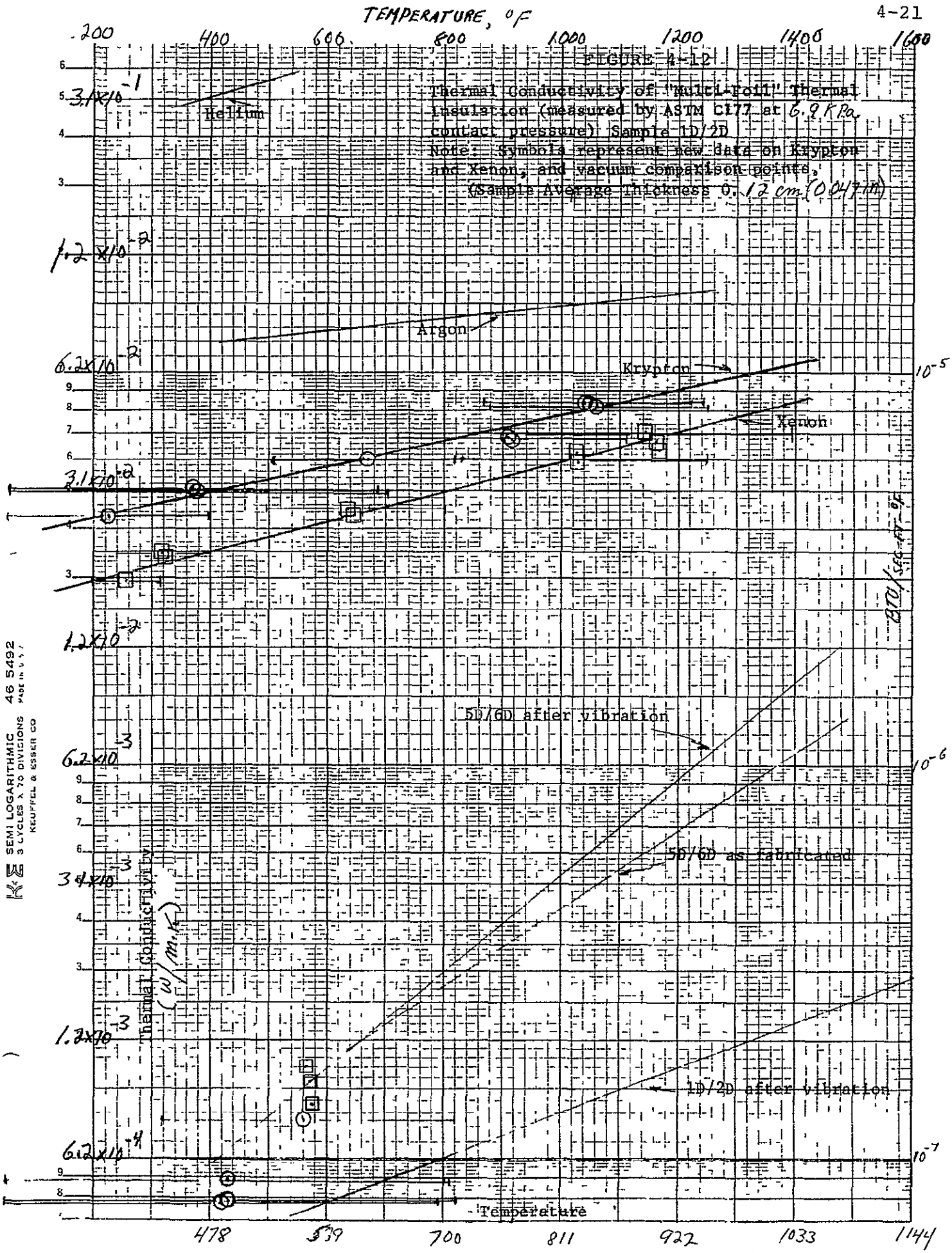

FIGURE 4-12

Thermal Conductivity of 'Multi-Foil' Thermal Insulation (measured by ASTM C177 at 6.9 KPa contact pressure) Sample 1D/2D

Note: Symbols represent new data on Krypton and Xenon, and vacuum comparison points.

(Sample Average Thickness 0.12 cm (.047 in)

SEMI LOGARITHMIC 46 5492
3 CYCLES X 70 DIVISIONS MADE IN U.S.A.
KEUFFEL & ESSER CO

4.3 INSULATION VIBRATION TESTS

The purpose of these vibration tests on insulation samples was to evaluate the ability of the zirconia particles to adhere to the foil during worst case vibration environment associated with potential space missions.

Six samples were procured from Thermo Electron Corporation for these tests. The samples were 10.2 cm (4 in) diameter disks composed of 60 layers of 0.0013 cm (.0005 in) nickel foil coated with zirconia. Four underwent vibration (samples 1D, 2D, 5D and 6D) and two were used as conductivity standards. During vibration some of the samples were heated to anticipated temperatures at launch.

The maximum zirconia weight loss in the worst case, due to the entire vibration test spectrum was 2.5% of the total original zirconia weight. Conductivity measurements made before and after vibration testing show no significant change, verifying that vibration is not deleterious to the performance of insulation system.

4.3.1 TEST DESCRIPTION

The vibration test program was conducted in two parts. The first part was a "survey test" to determine vibration and zirconia particle adherance characteristics of the insulation system for nominal environments. The second part of the vibration test program was a "capability test" to determine insulation system vibration survivability up to 20g's, which is far in excess of potential mission environments. Weights were recorded immediately before and after each test to determine zirconia weight loss.

In the "survey test", the multifoil samples were subjected first to a 1g, 15 minute, sinusoidal sweep from 10-500-10 Hz in the plane of the sample (x axis) and then perpendicular to the plane of the sample (y axis). Then the samples were subjected to a typical mission 3 minute random vibration spectrum (Figure 4-13) in both the x and y axis.

In the "capability test" the multifoil samples were subjected to a series of 15 minute sinusoidal sweeps from 10 to 20 Hz to 500 Hz and back to 10 or 20 Hz. The initial 1g level in these tests were increased in steps after each sweep, to a maximum value of 20g's in the final sweep as follows:

Test Sequence Number, N	g Level	Frequency
1	2 g's	10-500-10 Hz
2	3 g's (1)	"
3	5 g's	"
4	10 g's	"
5	20 g's (2)	20-500-20 Hz

(1) samples #1-D and #2-D not tested at 3g's

(2) the lower limit of 20 Hz for the 20g test was required because of displacement limitation during vibration

Two of the samples were vibrated along the plane of the samples, the other two samples were vibrated perpendicular to the plane of the samples. As previously indicated, the objective of the "capability tests" was to determine if there was a sinusoidal vibration level at which the samples would break down, (i.e., lose significant amounts of zirconia).

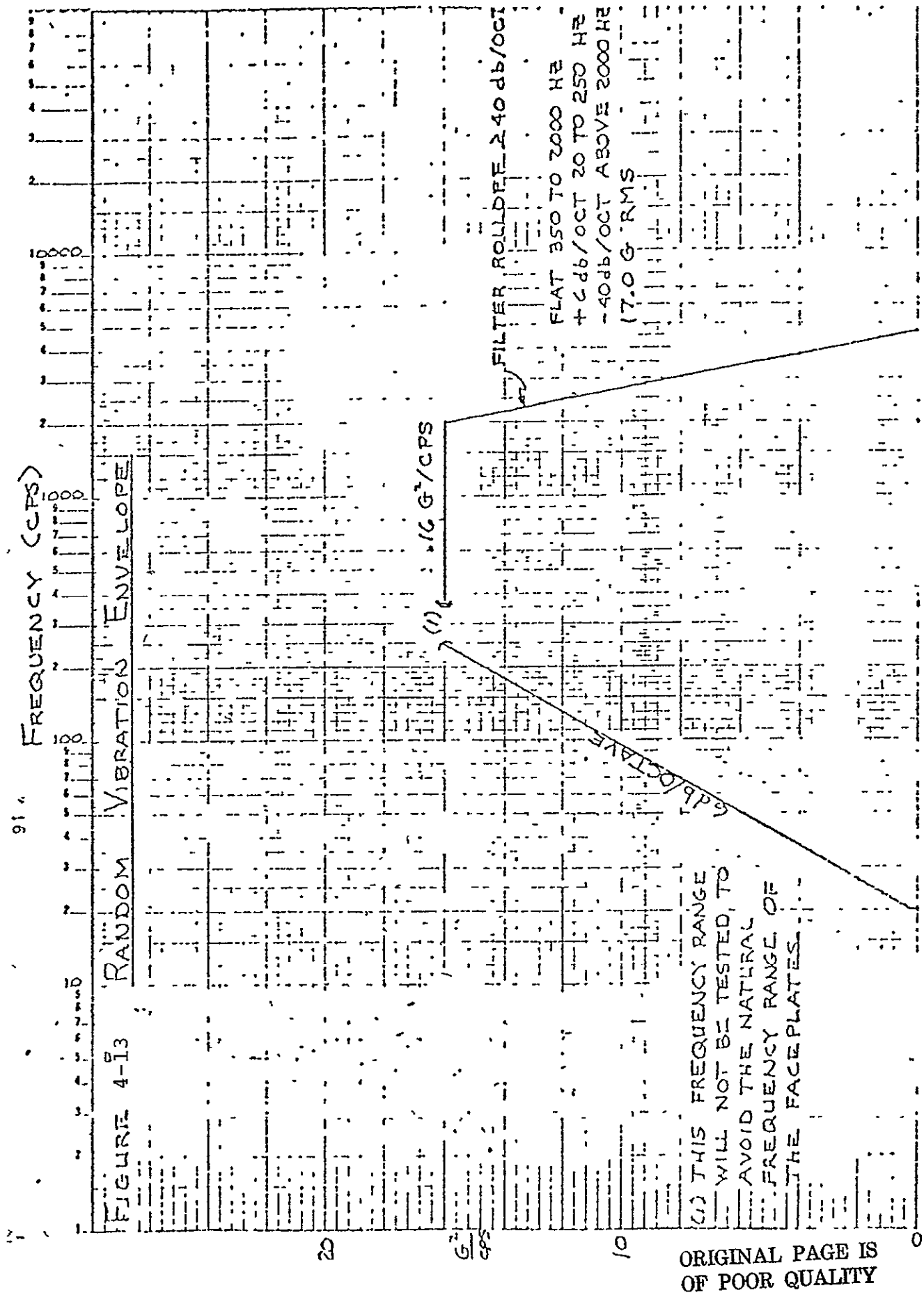

FIGURE 4-13

Test specimens were fixed to a support plate which was bolted to a C-150 shaker table as shown in the sketch of Figure 4-14. A radiant heating fixture (also shown in Figure 4-14), supported off a separate "A" frame, was held in close proximity to (but never in contact with) the insulation sample during vibration. Photographs of the test fixture and test set up are shown in Figures 4-15, 4-16 and 4-17. A screen, evident in the photographs, was affixed to the bottom of the heater to prevent any MinK heater insulation particles from falling on to the vibration sample.

4.3.2 TEST RESULTS

The tests were conducted during the following time periods:

January 22, 1975	- Samples 5-D and 6-D subjected to 1 g sine survey test.
February 6, 1975	- Samples 5-D and 6-D subjected to random survey and capability tests (sine sweeps up to 20 g's)
February 11-14, 1975	- Samples 1-D and 2-D subjected to complete spectrum of tests

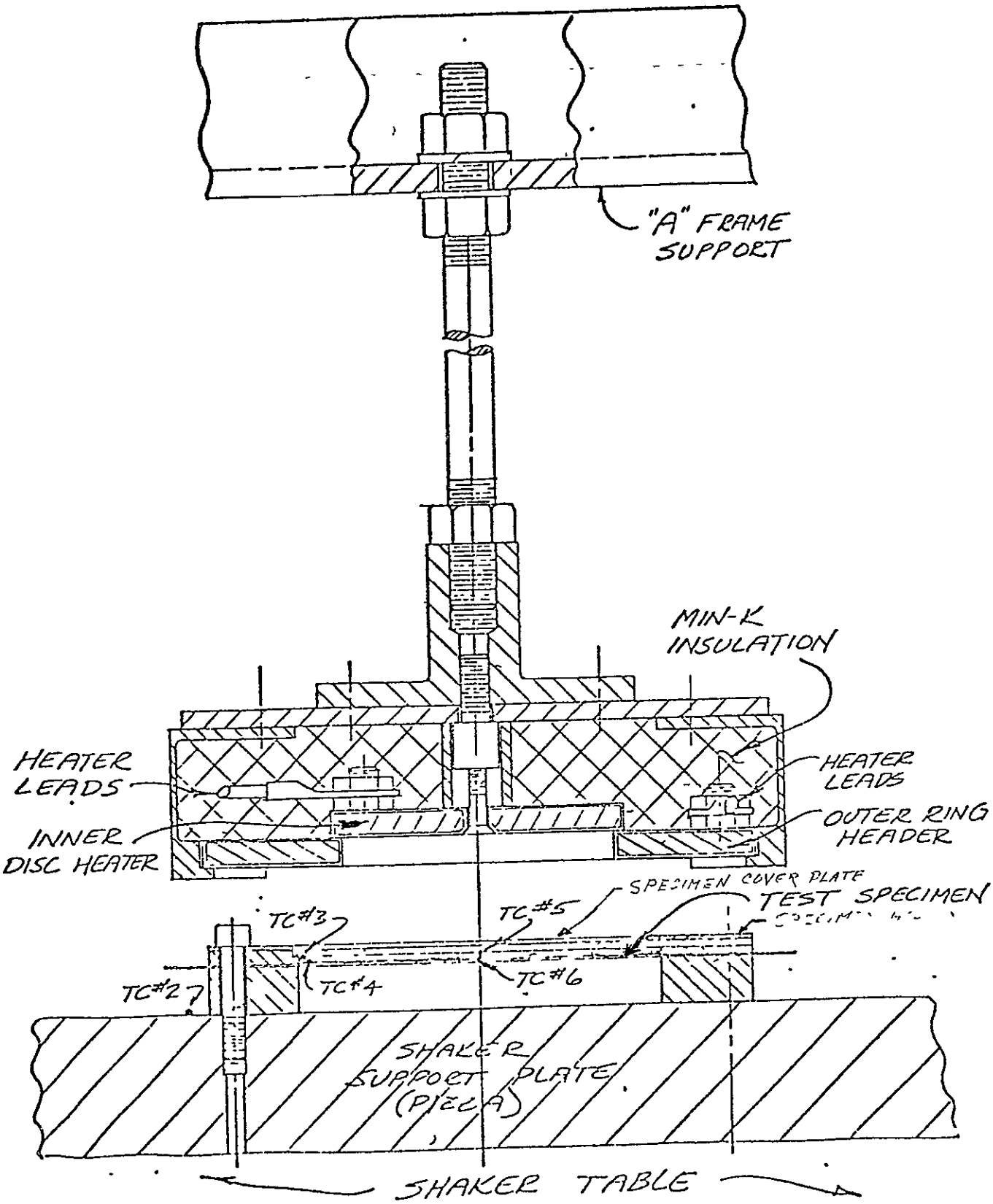

FIGURE 4-14 INSULATION VIBRATION TEST SET-UP

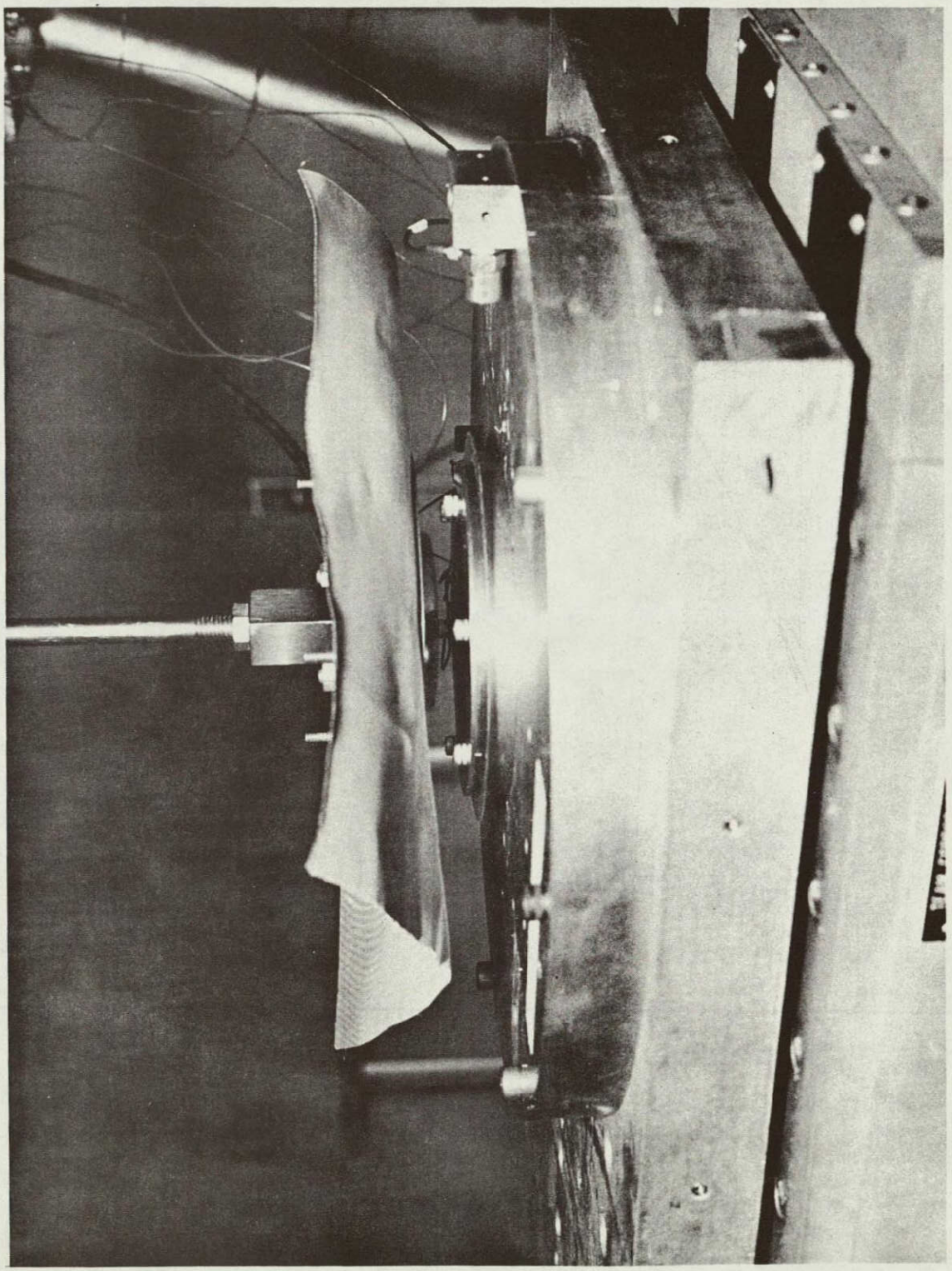

Figure 4-15. Vibration Test Fixture

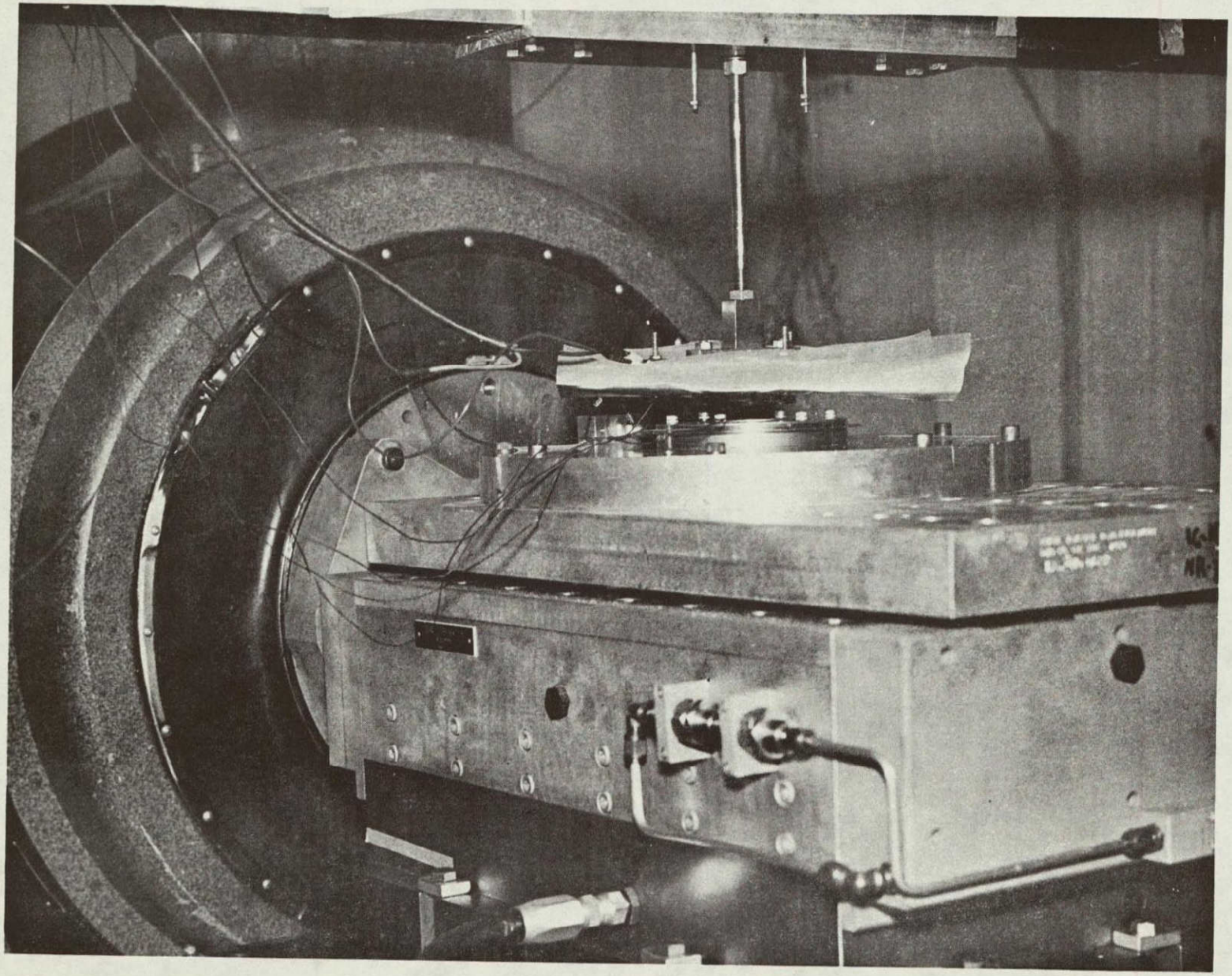

Figure 4-16. Vibration Test Fixture

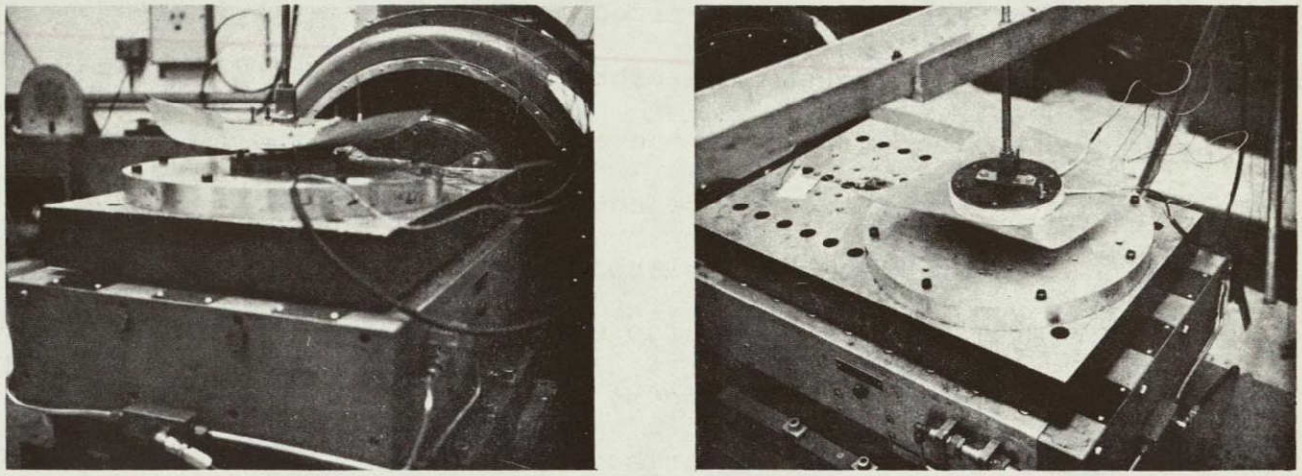

Figure 4-17. Vibration Test Fixture Photos Showing Setup For Vibrating Along The Plane Of The Sample

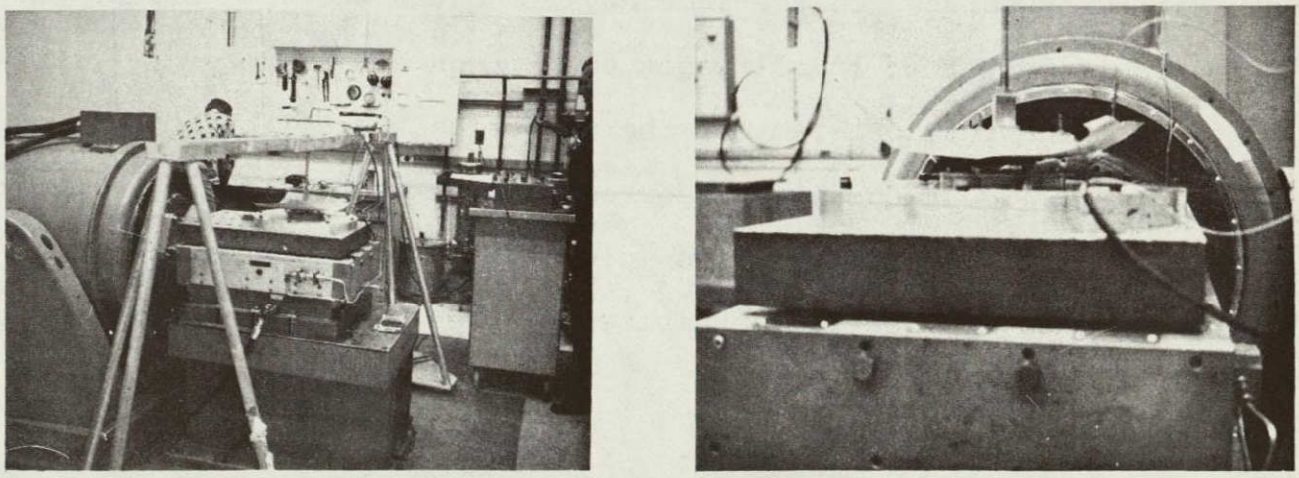

The samples were heated during the tests to hot face temperatures ranging from 340K (150°F) to 590K (605°F). A summary of the temperature profiles during vibration is given in Table 4-1. The results of weight measurements are summarized in Table 4-2. In all instances the weight measured prior to the vibration tests exceeded the weight certified by the vendor. It is conjectured that this is due to adsorption of water vapor (samples were not maintained and stored in a closely controlled environment. Normal laboratory room temperature and humidity conditions prevailed). It was also noted that weight measurements differed before and after storage periods, ranging from days to weeks, in between tests. This is also attributed to changes in humidity and resultant adsorption or evaporation of H_2O. One sample (6-D) apparently lost 20 mg during a 2 week storage period. The significant observation from the weight measurements is that the immediate loss of weight after a vibration test (which would be attributed to loss of zirconia particles) was in every case essentially negligible. The largest loss in zirconia weight for the worst case (sample 6-D) was 2.5% after a series of separate vibration surveys on the same day without a storage period. It is also significant that in all cases the zirconia area density after completing the test program met the prescribed specification limits for the insulation. It was also observed that, samples 1-D and 2-D which were held at higher temperatures (closer to predicted temperatures) than the other two samples, exhibited smaller weight losses after vibration.

TABLE 4-1 TEST SPECIMEN TEMPERATURE READINGS BEFORE AND AFTER VIBRATION TESTS DEG K

		Sample 1-D				Sample 2-D				Sample 5-D				Sample 6-D			
		Top Center	Top Edge	Bottom Center	Bottom Edge	Top Center	Top Edge	Bottom Center	Bottom Edge	Top Center	Top Edge	Bottom Center	Bottom Edge	Top Center	Top Edge	Bottom Center	Bottom Edge
SURVEY TEST																	
	Before	540	398	330	319	505	370	332	320	339				339			
1G Sine, X axis	After	403 *	368	322	315	505	372	335	322								
	Before	503	380	329	320	517	385	332	323	342				342	317	307	305
Random, X axis	After	547	398	338	325	517	387	333	325					340			
	Before	493	376	326	319	479		328	323	339				339			
1G Sine, Y axis	After	477	368	330	320	472	375	329	324								
	Before	472	372	329	324	474	375	329	324	342				342	318	303	302
Random, Y axis	After	474	375	330	324		378	332	325					342	317	304	302
CAPABILITY TEST **																	
	Before	497	411	340	333	589	439	342	328	342	317	304	302	343	318	301	300
2G sine	After	503	417	344	339	590	442	344	335					343	318	301	300
	Before	DELETED 3 G TESTS								342	318	304	302	345	324	300	299
3G Sine	After	FOR 1-D AND 2-D												344	320	302	302
	Before	464	394	335	332	589	433	335	332	342	318	304	302	346	319	303	302
5G Sine	After	470	400	339	336	585	434	342	337					346	324	303	303
	Before	507	413	335	330	592	454	342	335	339				343	317	303	303
10G Sine	After	528	420	345	340	569	440	343	337	347				337	314	304	304
	Before	484	393	337	329	589	446	343	339	142				345	320	306	305
20G Sine	After	488	404	340	335	542	436	346	341					342	318	307	305

Blank Spaces Indicate no Data Recorded

* Heater Shorted Out During Tests.

** Samples1-D and 5-D vibrated along Y axis in capability test
Samples 2-D and 6-D vibrated along X axis in capability test

Table 4-2 Insulation Vibration Test Sample Weight Data

	Sample Weight				Weight Loss (-) or Gain (+)							
	1-D	2-D	5-D	6-D	1-D		2-D		5-D		6-D	
	gms	gms	gms	gms	gms	Fraction of Original Zirconia	gms	Fraction of Original Zirconia	gms	Fraction of Original Zirconia	gms	Fraction of Original Zirconia
SAMPLE PREP												
Bare Foil Weight	53.4550	53.2113	53.5328	54.4329	-	-	-	-	- -	-	-	-
After Zr_2O_2 Spray	53.5905	53.3616	53.7312	54.5932	+.1355	1.0	+.1503	1.0	+.1984	1.0	+.1603	1.0
SURVEY TEST												
After Cond. Test	53.5930	53.3632	53.7334 (2)	54.5992 (2)	+.0025	+.018	+.0016	+.011	+.0022	+.011	+.0060	+.037
After 1G Sine, X-Axis	53.5930	53.3632	53.7326 (3)	59.5962 (3)	.0000	+.000	.0000	.000	-.0008 (3)	-.004	-.0030 (3)	-.019
After Random, X-Axis	53.5931	53.3630	53.7285	54.5744	+.0001	+.001	-.0002	-.001	-.0030	-.015	-.0209	-.130
After 1G Sine, Y-Axis	53.5932	53.3632	53.7315	54.5953	+.0001	+.001	+.0002	+.001	-.0011	-.006	-.0009	-.006
After Random, Y-Axis	59.5923	53.3632	53.7247	54.5736	-.0009	-.007	.0000	.000	-.0038	-.019	-.0008	-.005
CAPABILITY TEST (1)												
After 2G's Sine	53.5932	53.3632	53.7241	54.5742	.0000	.0000	.0000	.000	-.0006	-.003	+.0006	+.004
After 3G's Sine	Deleted		53.7240	54.5717	-	-	-	-	-.0001	-.001	-.0025	-.016
After 5G's Sine	53.5930	53.3632	53.7236	54.5717	+.0007	+.005	.0000	.000	-.0004	-.002	.0000	.000
After 10G's Sine	53.5927	53.3620	53.7233	54.5111	-.0003	-.002	-.0012	-.008	-.0003	-.002	-.0006	-.004
After 20G's Sine	53.5930	53.3632	53.7223	54.5709	+.0003	+.002	+.0012	+.008	.0000	.000	-.0002	-.001
Total Weight Loss					+.0025	+.018	+.0016	+.011	-.0079	-.040	-.0223	-.139

(1) Samples 1-D and 5-D vibrated along Y-axis in capability tests.
Samples 2-D and 6-D vibrated along X-axis in capability tests.

(2) Samples 5-D and 6-D underwent 1G sine tests along the Y-Axis before random along the X-axis.

(3) Sample 5-D weighed 53.7315 grams after test on 1/22/75 and 53.7269 grams prior to test on 2/6/75.
Sample 6-D weighed 54.5953 grams after test on 1/22/75 and 54.5750 prior to test on 2/6/75.

As indicated in Section 4.2, thermal conductivity measurements made before and after the tests showed no significant change in effective thermal conductivity.

It is concluded from these tests, which subjected the insulation to vibration environments far in excess of that anticipated during launch, that the zirconia coated foil will not suffer any degradation in thermal performance due to loss of zirconia.

4.4 MATERIAL COMPATIBILITY TESTS

The objectives of the material compatibility tests were two fold, first to determine the long term effect of interaction between the nickel foils in the insulation blanket and the C-103 HSHX and second to evaluate the long term stability of the materials that comprise the insulation blanket. These are described briefly below.

4.4.1 EFFECT OF NICKEL VAPORIZATION ON C-103 HSHX

The ability of the HSHX to retain its mechanical properties and ductility over the operational life of the system requires that the C-103 columbium base alloy not be significantly contaminated during operation. Potential sources of contamination include, principally, the nickel which can vaporize from the multifoil insulation, and also the outgassing of CO and other vaporous species from the dense graphite isotope heat components. Contamination from these graphite components will be controlled by procedures developed on the Multi Hundred Watt (MHW) program in which high temperature outgassing in vacuum and protection of the baked out components in inert gas was employed.

A significant level of analytical effort and some brief experiments were performed to evaluate the possible effects of nickel vapor transfer and diffusion into the C-103 HSHX. In order to scope the problem the worst case situation - one in which the insulation blanket is comprised entirely of nickel foils - was investigated. The highest rates of nickel vaporization would occur from the foil at the hotter end of the HSHX; bulk diffusion of the nickel into the columbium alloy heat exchanger is also greater at the hotter end. However, grain boundary

diffusion of nickel into the columbium alloy at the colder end of the HSHX could be appreciable and could result in considerable grain boundary embrittlement if it occurred. The formation of brittle intermetallics and their effect upon ductility and strength were also a concern. The magnitude and consequences of such vapor transport, diffusion and embrittlement are discussed in the following paragraphs.

4.4.1.1 NICKEL VAPOR TRANSPORT

Nickel vaporization rates were calculated from the hottest portion of the nickel foil insulation, and a cosine function distribution of this vapor to various positions along the axial length of the HSHX was determined. The calculations were reiterated to determine the nickel vapor contributions to various points along the HSHX from progressively colder portions of the inner nickel foil insulation sleeve, and estimates were made of the effects of such axial vapor flow to colder ends of the system. The Ni vapor impingement rate was thus calculated to be 1.98 μm/yr at the hot side insulation temperature of 1182K (1668°F) and 691×10^{-4} μm/yr at the low temperature end of 1038K (1408°F). This equilibrium rate decreases by a factor of about 290 from the hot to the cold end. However, this neglects the net line-of-sight flux of Ni down the temperature gradient to the cold end. The magnitude of this effect for the design geometry was estimated numerically with a model calculation which indicates that deposition rates of nickel or columbium at the cold end would be increased by only about 10% above the uncorrected value.

4.4.1.2 NICKEL CONCENTRATION GRADIENTS IN C-103 AND GRAIN BOUNDARY DIFFUSION

The nickel concentration gradients were calculated on the hot end of the HSHX as affected by nickel vapor arrival rates and as influenced by bulk diffusion and grain boundary diffusion, and an estimate was made of the depth of embrittlement due to formation of intermetallics. For Ni concentrations up to the solubility limit, the diffusion coefficient is representable by $D = 9.3 \exp(-80{,}400/RT)$ cm^2/sec. Published work[2] on Cb-Ni diffusion couples and on high-rate vapor condenstation of Ni on Cb indicate that overall diffusion coefficients may be as much as two orders of magnitude higher once CbNi and other intermetallic compounds are formed. The Ni diffusion penetration was calculated with the boundary condition of constant Ni deposition rate appropriate to that temperature. According to these initial calculations, at 1182K diffusion penetration after ten years would be to a depth of about 40 micro meters (μm) and the surface Ni concentration would reach 57 atomic percent. At 1038K the depth would be about 4 μm and the surface concentration would be about 4 atomic percent. These calculated surface concentrations exceed the solubility limit of $\sim$ 1% thus, the formation of a surface layer of intermetallic compound would be expected. Once the surface layer of intermetallic compound is formed, diffusion rates would be significantly higher. If the supply of Ni were unlimited, the thicknesses of compound layers formed would be about ten times the penetration depths calculated above. However, the growth of the compound layer is limited by the vapor transfer rate of Ni to the columbium alloy. The layer thickness was initially estimated by assuming that all of the Ni deposited forms a surface layer of CbNi. This pre-

dicted a 50 μm thick layer at 1182K and 0.2 μm at 1038K in a ten year period. It has been reported by the Russians and subsequently observed in experiments outlined below that the compound formed is Cb_5Ni, instead of CbNi; thus, the layer would of course be much thicker, or about 250 μm thick. This initial estimation was refined further by the experimental work and additional calculations reported in detail below to indicate 164 μm (.0065 in.) thickness of embrittled layer in 10 years.

The published Cb-Ni diffusion studies report no significnt grain-boundary diffusion. However, they were at diffusion temperatures 110K to 165K (200 to 300°F) higher than those anticipated in the heat exchanger. No appropriate data exist on grain-boundary diffusion of Ni in C-103. However, the activation energy for grain-boundary diffusion was estimated by analogy with data for b.c.c., Fe, along with estimates of the extent of the penetration. Such calculations suggest that, at the hot end, bulk diffusion out of the grain boundaries will limit grain-boundary penetration to twice the bulk penetration. At 1038K, grain-boundary diffusion would be relatively more important, but its effect will be limited because of the very limited supply of Ni. It is not possible, without experimental effort, to predict how significant this grain boundary penetration would become.

4.4.1.3 NICKEL/C-103 DIFFUSION EXPERIMENTS

Two experiments were performed to evaluate the ductility of C-103 alloy containing nickel additions.

The first experiment involved preparation of small arc melted buttons of C-103 containing 0, 2-1/2 and 5 weight percent of nickel. The alloy without nickel was ductile under cold forming whereas those with progressively higher nickel contents were progressively embrittled.

The second experiment involved sputtering of about 2 μm of nickel on the surface of 1.3 x 5. x 0.064 cm (0.5" x 2" x .025") C-103 sheet, diffusing this nickel into the C-103 at a temperature of 1323K (1922°F) (below the Ni-Cb eutectic temperature of 1448K (2147°F) for a period of 63 hours and conducting bend tests with the surface containing the diffused nickel in tension. An intermetallic phase about 19 μm thick was identified by x-ray diffraction as Cb_5Ni. In a 3t bend test at room temperature, cracks formed in the area containing the intermetallic phase, but these did not propagate into the base alloy. Photomicrographs of these specimens before and after bend test are shown in Figures 4-18 through 4-21. This second experiment permits a reassessment of the effects of nickel diffusion into columbium.

The presence of Cb_5Ni confirms the Cb rich portion of the Cb-Ni phase diagram reported by Russian workers.[3] Results by Duerden and Hume-Rothery[4] do not show the appearance of Cb_5Ni. It is clear that such a Cb rich phase increases the possible conversion rate of C-103 into

compounds under conditions where the Ni supply rate controls the kinetics. Under these Ni-deficient conditions the expected phases would be on the Cb rich end of the phase diagram.

Gross estimates of the diffusion coefficients were obtained from Ni condensation, growth[5] on Cb and Ni-Cb diffusion couples[6] in which the CbNi + $CbNi_3$ phases form. These yield $D \sim 3.3 \times 10^{-13} \frac{cm^2}{sec}$ at 1182K which is obtained using data calculated from the Russian work[5] and a $D \sim 1 \times 10^{-11}$ measured at 1348K (1967°F) from a diffusion couple $(4Dt)^{\frac{1}{2}}$ distance[6]. A D of 1.7×10^{-11} cm^2/sec can be extrapolated from the Russian data[5] at 1373K and 1273K for CbNi + $CbNi_3$ layers. These two estimates at 1182K vary 2 orders of magnitude. The actual phase found in this work was Cb_5Ni, which melts at 1623K rather than 1843K and presumably has a lower activation energy and higher diffusion rate than CbNi. The 12 fold coordination radii for Ni and Cb are 1.25Å and 1.47Å respectively and so Ni is probably the diffusion species in whatever compounds form because of its smaller atomic radii. In contrast to the high diffusion values estimated above for the compounds, the coefficient for Ni in Cb is given by $D = 9.3 \exp(-80,400/RT)$[7] and yields a much lower value of $D = 1.2 \times 10^{-14}$ $cm^2/sec.$ at 1182K (1668°F).

The phase observed in the Ni-G103 diffusion couple heat treated at 1323K (1922°F) for 63 hr. was Cb_5Ni. The 2 μm thick Ni coating was completely converted into Cb_5Ni within this time. The resulting Cb_5Ni layer is approximately 19 μm thick and allows a lower limit of D in Cb_5Ni at 1323K to be made by using

$$(4Dt)^{\frac{1}{2}} \gtrsim 19. \times 10^{-4} \text{ cm},$$

$$D \gtrsim 4 \times 10^{-12} \text{ cm}^2/\text{sec}.$$

The Ni vapor impingement rate J_{Ni} at 1182K is

$$J_{Ni} = 5.8 \times 10^{-11} \text{ atom/cm}^2\text{sec},$$

or $$1.83 \times 10^{19} \text{ atoms/cm}^2\text{yr}.$$

The Cb conversion rate into Cb_5Ni may then be 5 times the nickel impingement rate which results in a maximum thickness conversion rate for Cb of

$$\dot{d}(Cb) = 16.4 \text{ μm/yr.} = 0.00064 \text{ in/yr.}$$

At the end of a 10 year lifetime the Cb_5Ni could be almost 164 μm thick and a coarse estimate of the minimum value of D required for the compound formation rate to be controlled by Ni vapor impingement on the free surface can be now made. Assuming $\ell = (4Dt)^{\frac{1}{2}}$,

$$\frac{d\ell}{dt} = \frac{D^{\frac{1}{2}}}{t} = \frac{2D}{\ell} \quad .$$

For this velocity to be equal to the maximum Cb consumption rate of 16.4 μm/yr (0.00064 in/yr.)

$$\dot{d}(Cb) = \frac{2D}{\ell} \ ,$$

$$D = \frac{1}{2} \times 16.4 \frac{\mu m}{yr} \times \frac{164 \ \mu m}{3.15 \times 10^7 \text{ sec/yr}} \ ,$$

or $$D = 4.3 \times 10^{-13} \text{ cm}^2/\text{sec}.$$

This must be the diffusion coefficient in order for impingement to be controlling. Since this diffusion coefficient is lower than the earlier estimated diffusion coefficients, Ni vapor impingement, rather

than diffusion, would control the conversion rate of Cb into Cb_5Ni up to the end of the C-103 part service life.

The Cb conversion rate is 16.4 μm/yr and results in 0.01651 cm (0.0065 in) mils) conversion in 10 yr., 0.013 cm (0.005in) in 7.7 yr., 0.0077 cm (0.003 in) in 4.6 yr. and 0.0013 cm (0.0005 in) in 0.8 yr.

The diffusion and bend experiments indicated, as would be expected, that brittle intermetallics would form if nickel vapors are allowed to diffuse into C-103 in sufficient quantity to exceed the solubility limit. The basic ductility of the base alloy, however, is sufficient to prevent propagation of the crack into the base alloy even under significant plastic deformation. Avoiding nickel transfer from the foil to the HSHX is clearly very desirable.

The initial diffusion calculations indicated that replacement of the first two 0.0013 cm (0.0005in) Ni layers (of an all nickel foil insulation system) with Cb would be effective if only CbNi were formed. The foils would stop the Ni flux at the low temperature - 1038K (1408°F) - end. At 1182K (1668°F) the Ni flux through the 0.0013 cm (0.0005 in) Cb would be negligible until the foil is converted into CbNi or Cb_5Ni (this would require about 5 years if CbNi were formed but only 1 year if Cb_5Ni were formed.) The diffusion of Ni through this additional barrier layer would then also reduce the final impingement rate of Ni vapor on the second Cb layer and ultimately upon the Cb heat exchanger. Thus, while use of two intervening layers of 0.0013 cm (0.0005 in) columbium alloy foil would prove effective in reducing nickel transfer

in the case of CbNi formation, the formation of Cb_5Ni dictates a single layer of 0.013 cm (0.005in) foil which would provide much longer delay in initiating nickel transfer of an all nickel foil insulation system. A conservative approach in the baseline insulation system utilizing molybdenum foils to replace the nickel foils in the region of high temperature would be to incorporate an inboard columbium foil to getter any Ni vapor that may reach it.

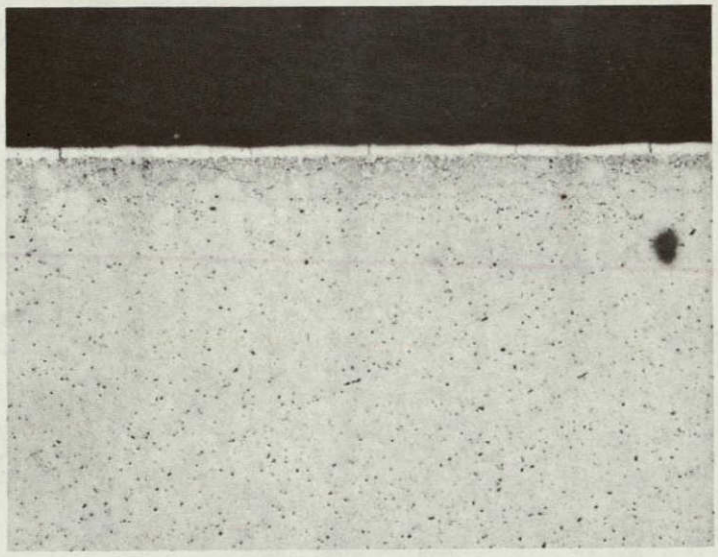

Figure 4-18 C-103 Sputtered With 2 μm of Nickel and Vacuum Heat Treated for 63 Hours at 1323K (1922°F). Mag: 150X

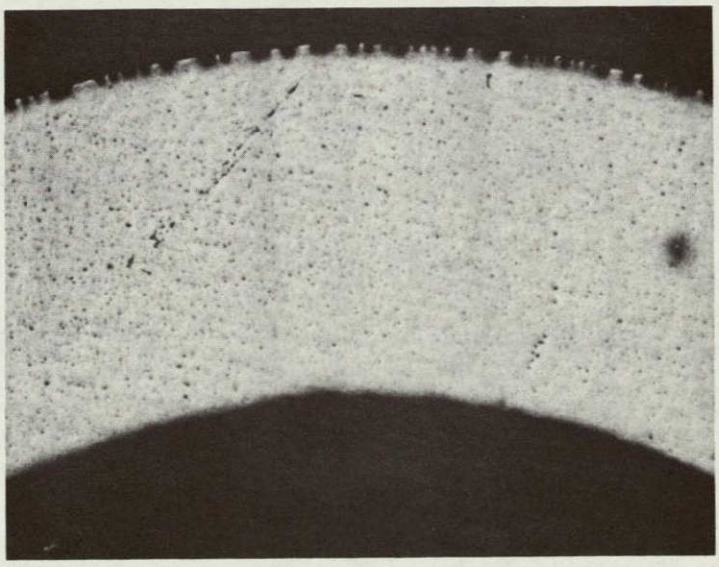

Figure 4-19 C-103 Sputtered with 2 μm of Nickel Vacuum Heat Treated for 63 Hours at 1323K (1922°F) and Bent Over a 3t Radius. Mag: 75X

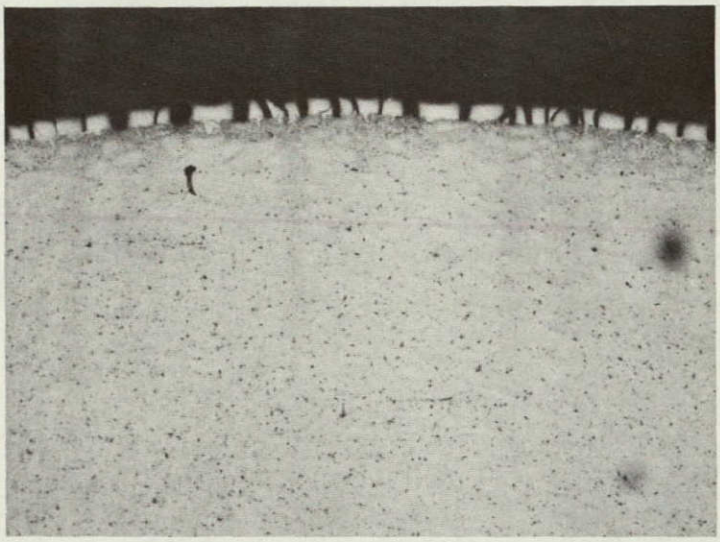

Figure 4-20 C-103 Sputtered With 2 μm of Nickel, Vacuum Heat Treated for 63 Hours at 1323K (1922°F) and Bent Over a 3t Bend Radius. Mag: 150X

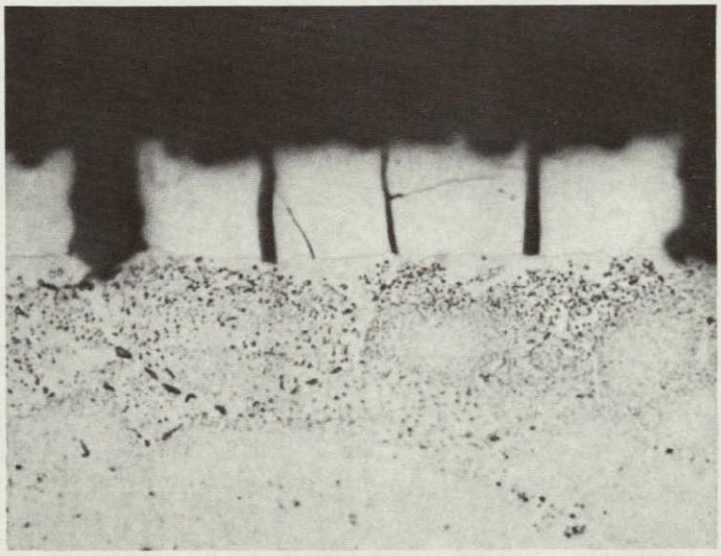

Figure 4-21 C-130 Sputtered With 2 μm of Nickel, Vacuum Heat Treated for 63 Hours at 1323K (1922°F) and Bent Over a 3t Bend Radius. Mag: 750X

4.4.2 INSULATION MATERIAL COMPATIBILITY TESTS

The 1000 hour "Life Stability" tests discussed in 4.1 revealed no apparent degradation in thermal performance of a scaled down cylindrical configuration of nickel foil in which a temperature gradient (similar to that expected during operation) existed across the foils. Nonetheless, because of the long life (7 year) requirement, further tests were performed to determine if any insulation material interactions would occur that were not observed in the macroscopic evaluation of the "Life Stability" test specimens. In this new series of material compatibility tests a sizeable number of square shaped capsules (also referred to as crucibles) were prepared in which different combinations of flat foils and ZrO_2 were arranged. The configuration of the flat foils and ZrO_2 within the crucibles were arranged to investigate nickel, molybdenum, columbium (≡ niobium, Nb) and ZrO_2 interfaces and interactions, characteristics of zirconia coated vs. uncoated foils, 5% ZrO_2 vs. 50% ZrO_2 coverage, wet vs. dry zirconia and effect of nickel purity. The capsules were subjected to accelerated life tests in an evacuated oven temperature of 993K/720°C, 1223K/950°C and 1323K/1050°C. All foils and materials in a capsule were essentially at the same temperature, that is, no temperature gradient was intentionally imposed across the foil pocket. A tungsten weight was incorporated to assure good contact.

In the first series of tests a combination ZrO_2 coated nickel, molybdenum and columbium (Nb), foils were tested at 993K/720°C, 1223K/950°C and 1323K/1050°C for approximately 170 hours. Figure 4-22 gives the matrix of configurations and test conditions. All nickel and niobium foils were

0.0013 cm (0.0005 in) in thickness except the high purity nickel which was 0.013 cm (0.005 in). The molybdenum foils were 0.0025 cm (0.001 in) thick. The purpose of this first test series was to: (1) determine the safe long term operating temperature for nickel foil; (2) determine if molybdenum can act as a diffusion barrier between nickel and columbium; (3) determine if moisture accumulated during storage is a potential problem; and (4) determine if a heavy coverage of zirconia on nickel foils decreases self welding. Figure 4-23 through 4-28 show photomicrographs of typical cross sections of the foils. The general conclusions that were reached by a study of the capsules and the photomicrographs are as follows:

1. There is evidence of nickel vaporization at 993K /720°C although the amount was quantitatively unmeasurable after 168 hours. An upper limit on the operation of nickel for long term dependability on the HSA should be $\sim$ 993K/720°C.

2. There was no evidence of self-welding of nickel foils with a 5% ZrO_2 coating at 993K /720 °C.

3. Self-welding of nickel foils with a 5% ZrO_2 coating at 1223K /950 °C was severe after 168 hours.

4. A heavy coating (50%) of ZrO_2 is effective in reducing self-welding; e.g., at 1223K /950 °C no welding was evident. Thinning of the nickel foils however was more severe with the heavy ZrO_2 coating indicating some reduction of ZrO_2 by Ni. Additionally use of a heavy ZrO_2 coating would undoubtedly degrade the thermal performance of the insulation due to conductive effects across the ZrO_2.

FIGURE 4-22

Ni/Mo/Nb/CaO: ZrO_2 COMPATIBILITY TEST CAPSULES

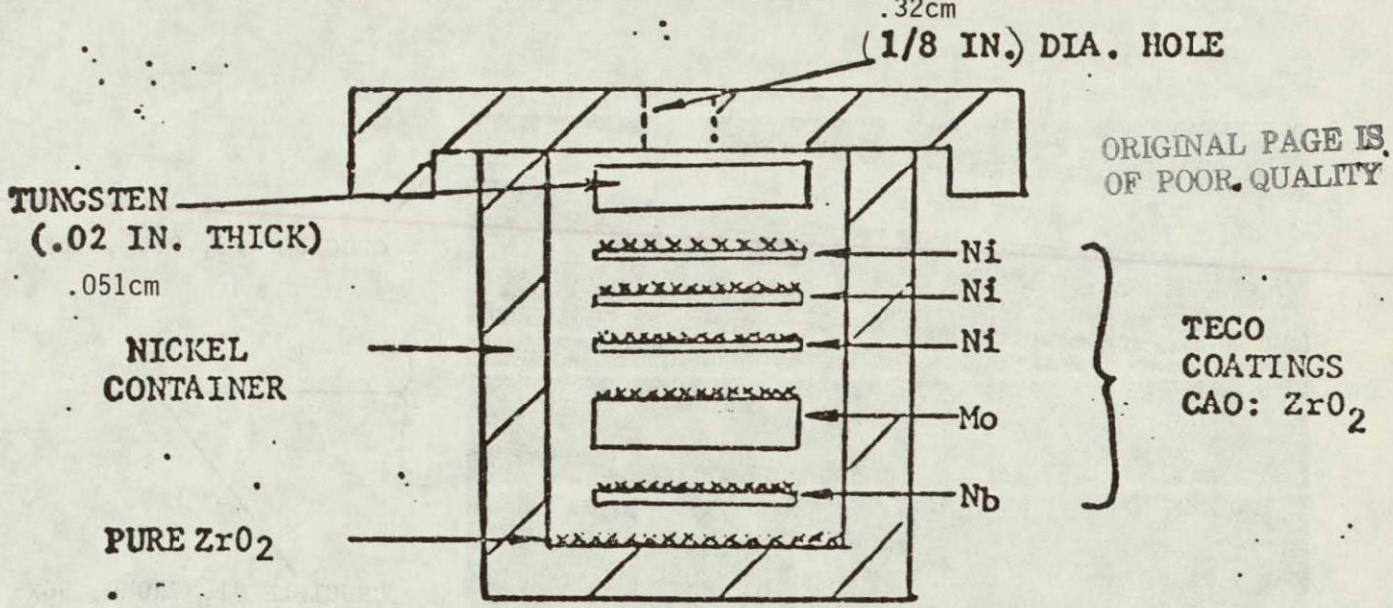

CAPSULE NUMBER	COATING COVERAGE	TESTING TEMPERATURE	REMARKS
1	4 to 6%	720°C	Outgassed 1 hr. @ 500°C prior to test
2	4 to 6%	950°C	Outgassed 1 hr. @ 500°C prior to test
3	4 to 6%	1050°C	Outgassed 1 hr. @ 500°C prior to test
4	4 to 6%	950°C	Exposed to H_2O prior to test
5	4 to 6%	1050°C	Exposed to H_2O prior to test
6	50%	950°C	Outgassed 1 hr. @ 500°C prior to test
7	50%	1050°C	Outgassed 1 hr. @ 500°C prior to test
8	4 to 6%	950°C	High purity nickel outgassed 1 hr. @ 500°C prior to test
9	4 to 6%	1050°C	High purity nickel outgassed 1 hr. @ 500°C prior to test

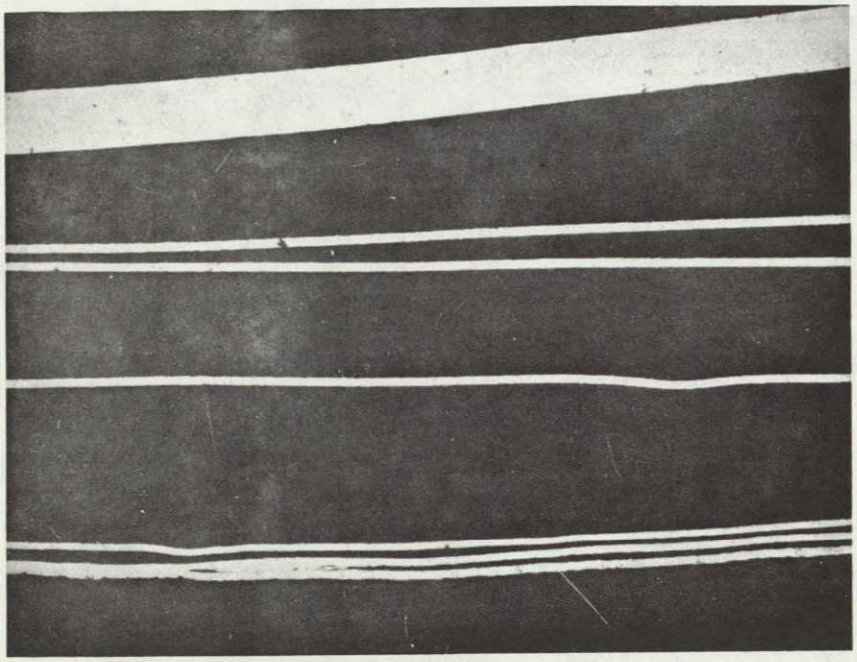

CRUCIBLE #8, 950°, 56X

CRUCIBLE #1, 720°C, 56X

CRUCIBLE #2, 950°C, 56X

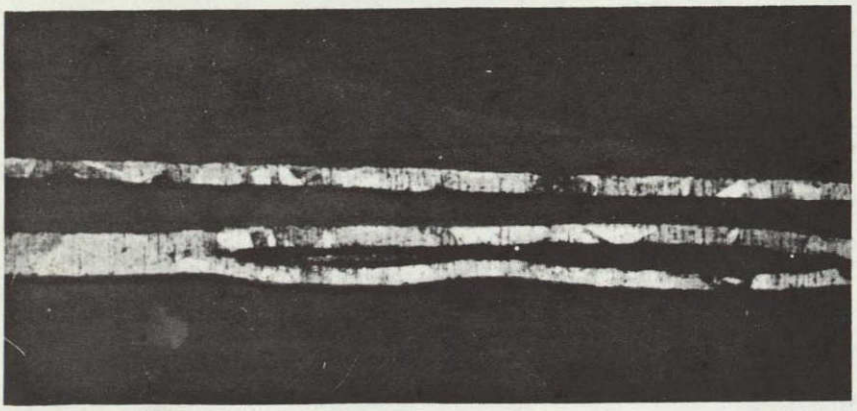

CRUCIBLE #2
(120X)
(ETCHED)

Ni/Ni/Ni/Mo/Nb//Ni

FIGURE 4-23 TYPICAL CROSS SECTIONS OF Ni FOILS

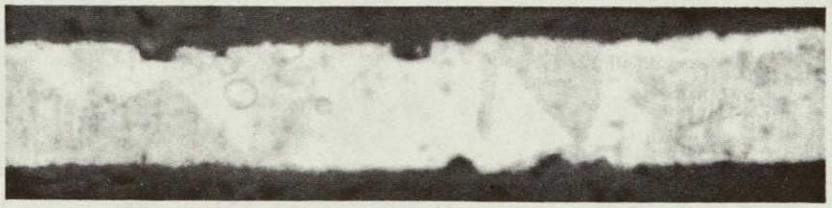

5% $CaO:ZrO_2$ COATED SIDE
AVG. THK'S. - .0013cm
MIN. THK'S. - .001cm
(1160X) (720°C)
CRUCIBLE #1

5% CaO ZrO_2 COATED SIDE
MAX. THK'S. - .0013cm
MIN. THK'S. - .0066cm
(1160X) (950°C)
CRUCIBLE #2

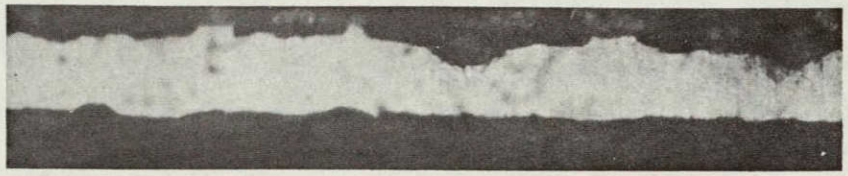

50% $CaO:ZrO_2$ COATED SIDE
MAX. THK'S. - .0013cm
MIN. THK'S. - .0005cm
(920X) (950°C)
CRUCIBLE #6

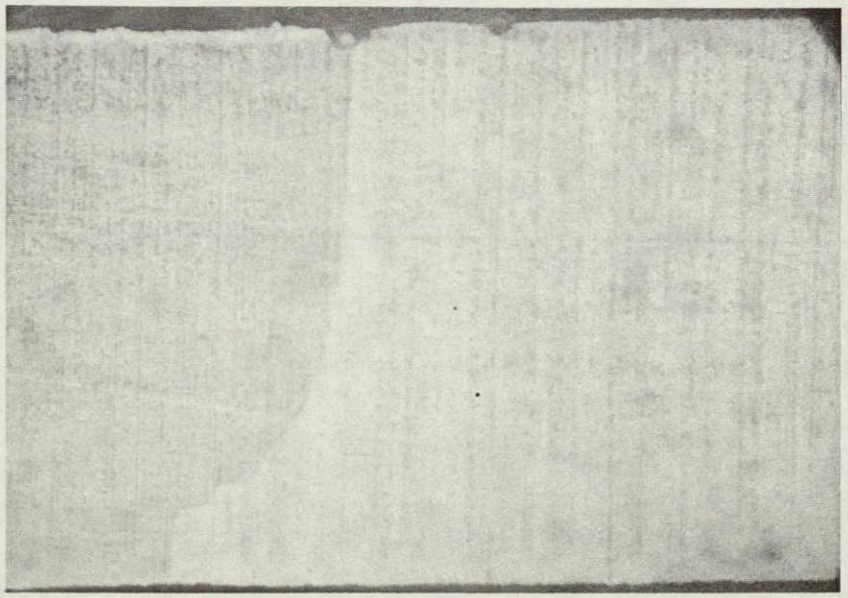

5% $CaO:ZrO_2$ COATED SIDE
MAX. THK'S. - .013cm
MIN. THK'S. - .012cm
(580X) (950°C)
"HIGH" PURITY Ni

FIGURE 4-24 TYPICAL CROSS SECTIONS OF NICKEL FOILS Ni/Ni/Ni/Mo/Nb//Ni

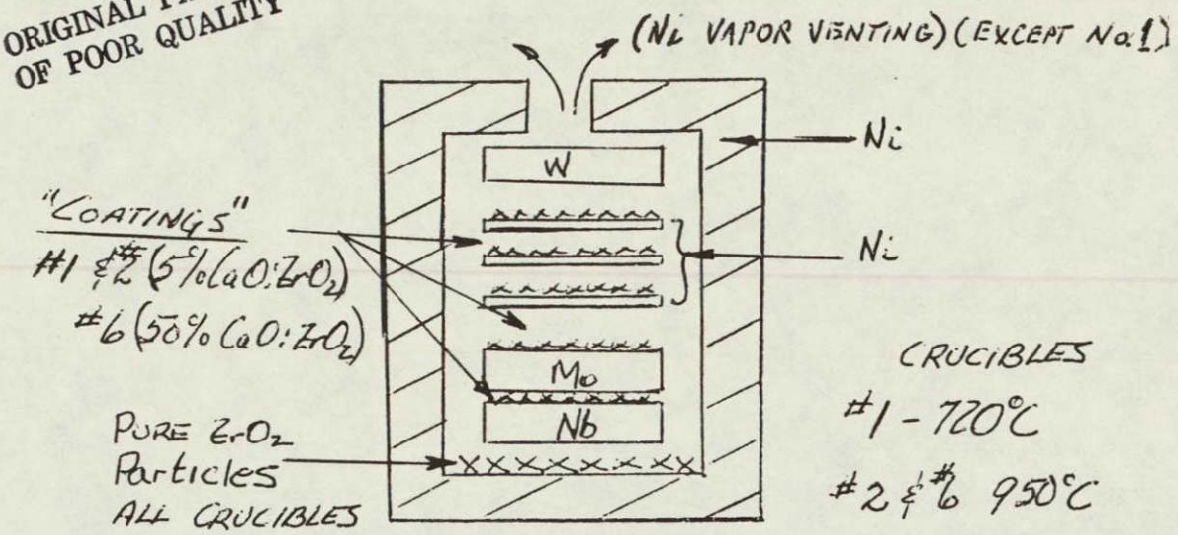

Niobium

No Ni Observed
$CaO:ZrO_2$ Visible

1160X

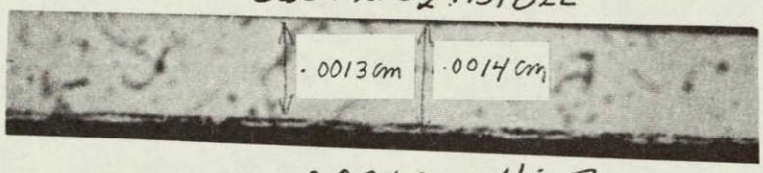

FACING Mo
#1
FACING Ni

~.0001 cm Ni PRESENT.

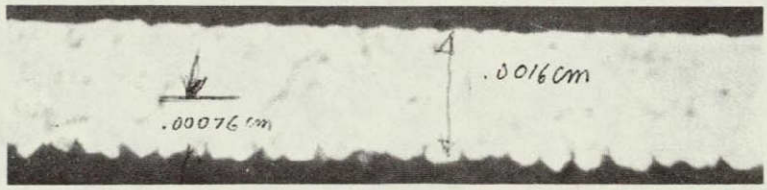

.0005 in. PRIOR TO TEST.
UNETCHED #2
Growth ~.00014 in.

#2

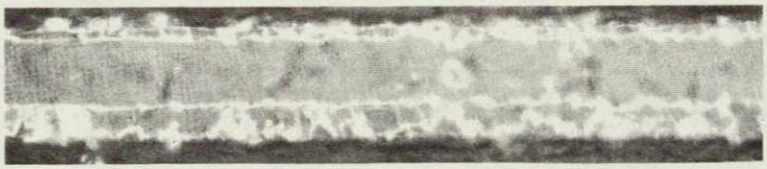

FACING Mo
ETCHED #2
FACING Ni

Ni PENETRATION SAME AS #2 EXCEPT LESS SCREAMING (Mo Side).

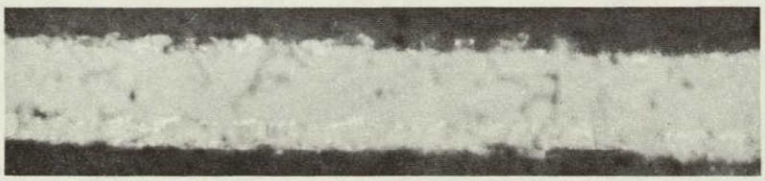

FACING Mo
#6
FACING Ni

FIGURE 4-25 TYPICAL CROSS SECTIONS OF NIOBIUM FOILS

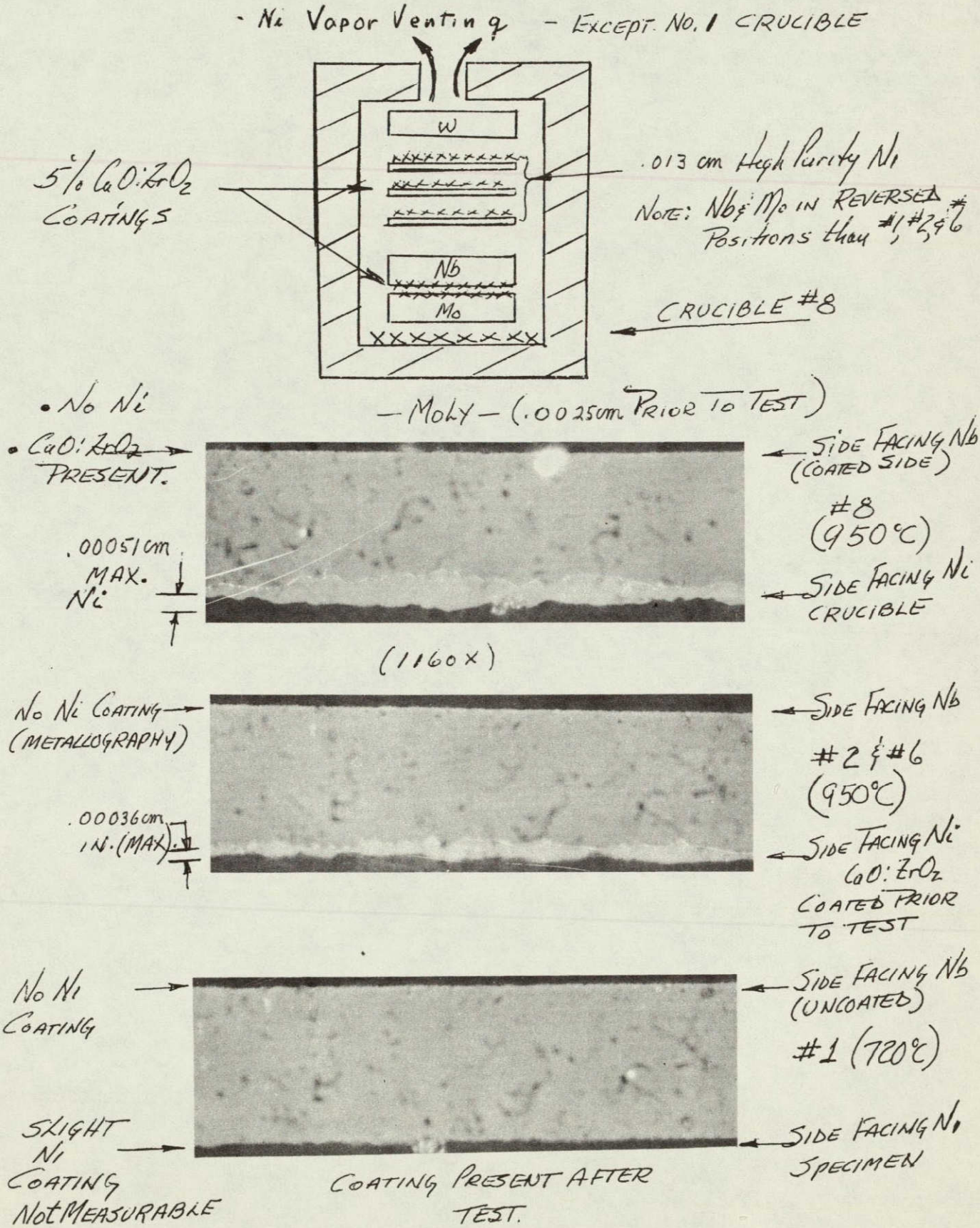

FIGURE 4-26 TYPICAL CROSS SECTIONS OF MOLYBDENUM FOILS

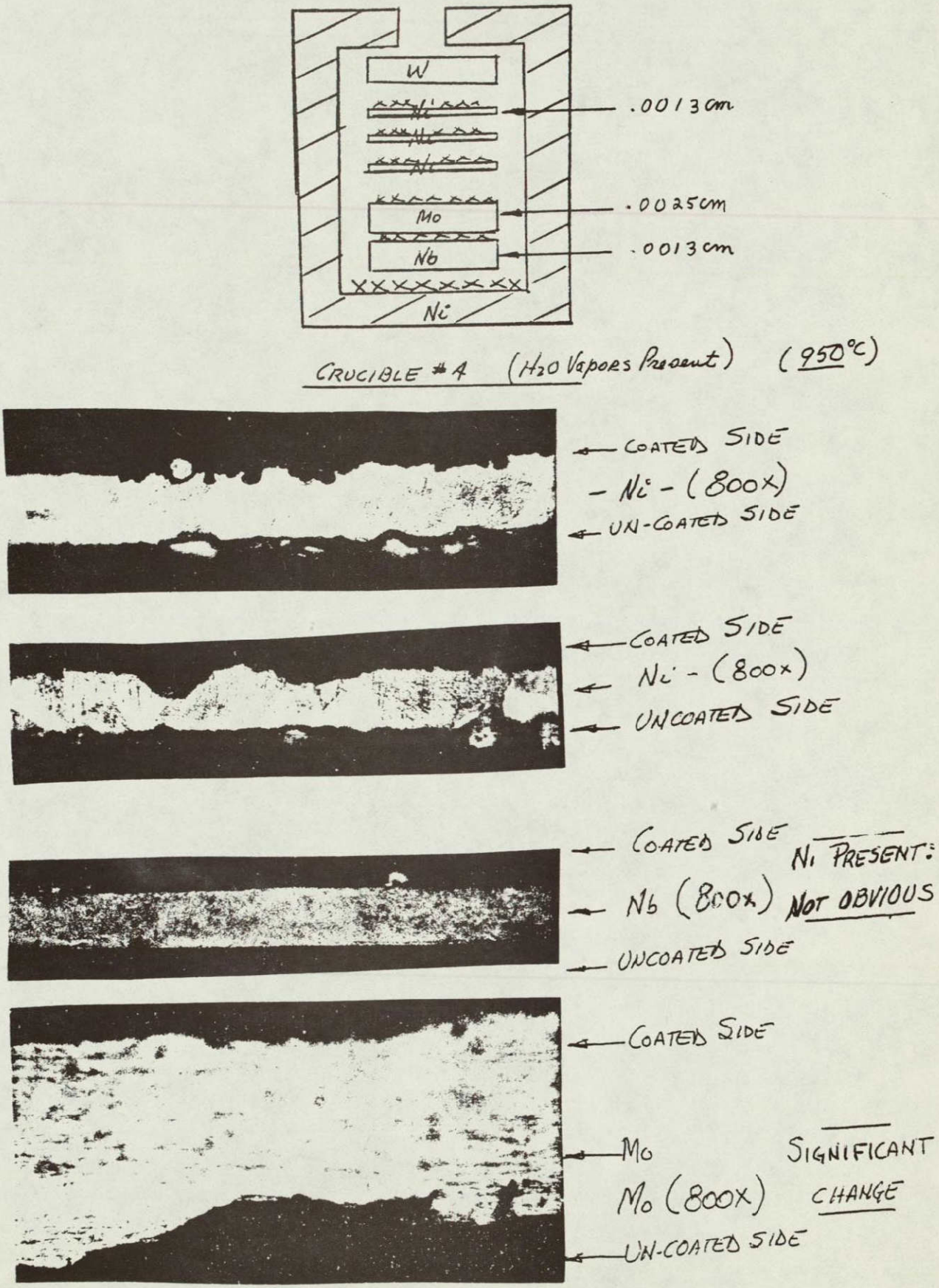

FIGURE 4-27 TYPICAL CROSS SECTIONS OF FOILS EXPOSED TO H_2O

ORIGINAL PAGE IS
OF POOR QUALITY

EVENDALE

CRUCIBLE
#5

1050°C
(H_2O VAPOR
PRESENT)

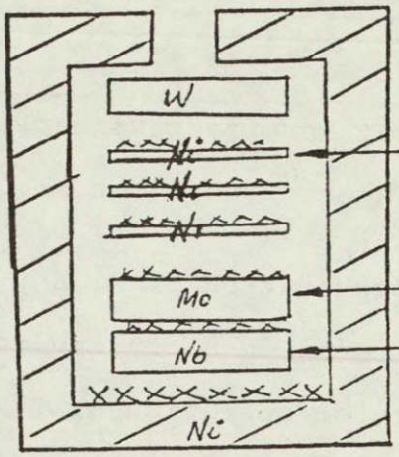

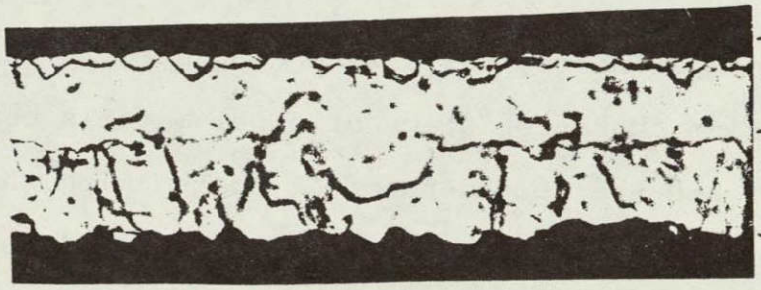

(EXTENSIVE SELF WELDING TO 3RD Ni SPECIMEN)

FIGURE 4-28 TYPICAL CROSS SECTIONS OF FOILS EXPOSED TO H_2O

5. Molybdenum foil is not an effective barrier between Ni and Nb if it is discontinuous around the Nb.

6. H_2O causes serious degradation of Ni and Mo. Consequently, the foil should be stored in a dry environment and baked out prior to assembly or operation at temperature.

7. Use of high purity nickel foil does not minimize evaporation of nickel. Its use is not recommended.

The second series of material compatibility tests were conducted to determine the interaction characteristics of uncoated nickel and molybdenum foils. It was found that at 993K/720°C there was no evidence of evaporation of nickel of self-welding of the foils whereas at 1223K/950°C there was substantial evaporation of nickel and self-welding of the foils. All of the Mo foils were coated with nickel.

The third series of material compatibility tests were conducted to determine, separately, the interaction characteristics of niobium foils coated with 5% calcia stabilized ZrO_2 and the molybdenum foil coated with the ZrO_2. It was found that at 1223K/950°C there was no welding of foils or measurable reaction with the ZrO_2 although it appeared from the color of the ZrO_2 in the bottom of the crucibles that ZrO_2 is more stable with Mo than with Nb. This conclusion was reinforced by examining the pure ZrO_2 in the bottom of the capsules which were tested. The color change and porosity of the ZrO_2 particles give an indication of the reduction of the ZrO_2. Figures 4-29 through 4-32 show enlarged photographs of the

ZrO_2 particles taken from the bottom of various capsules. The general conclusions reached from a study of these results are as follows:

1. Pre test exposure of zirconia to H_2O vapor is severely damaging.
2. Exposure to a temperature of 1223K/950°C reduces pure ZrO_2 faster than a temperature of 993K/720°C.
3. Reduction evolves release of gas, probably O_2.
4. Mo and Nb alone cause less reduction of ZrO_2 than combinations of Mo-Ni and Nb-Ni foil with ZrO_2.

Some further tests on oxide stability were conducted at 1223K/950°C and 1323K/1050°C. Various combinations of foil material, pure ZrO_2 and calcia stabilized ZrO_2 were heated for approximately 170 hours at a pressure of 1.3×10^{-5} Pa (10^{-5}torr). Additionally, single, double and triple wraps of Nb foil around Nb, and Mo foil around Nb, were included in some of the crucibles to determine the effectiveness of these in protecting Nb from interaction with nickel. Some typical observations and photomicrographs of crucibles with wrapped foils tested at 1323K / 1050°C are shown in Figure 4-33 through 4-38. General conclusions reached from this series of tests are as follows:

1. Mo foil with calcia coated ZrO_2 is stable at 1323K/1050°C.
2. Combinations of Mo and Ni foil with calcia stabilized ZrO_2 is stable at 1223K/950°C but not at 1323K/1050°C.
3. Combinations of Nb and Ni foils with calcia stabilized ZrO_2 is not stable at 1223K/950°C.
4. Calcia stablized ZrO_2 is more stable than pure ZrO_2.

5. Complete Nb wraps around an Nb specimen is somewhat more effective in protecting the Nb specimen from Ni penetration because of the gettering behavior of the protective Nb wraps. Nonetheless if a sufficient number of Mo protective wraps are used the Nb specimen can be protected from nickel interdiffusion.

It is interesting to note that compatibility tests of Ni, Mo and Nb foils conducted at Battelle - Columbus Laboratories and at NASA-Lewis Research Center indicated that Ni-Nb foil combinations were more resistant to diffusional welding (i.e. self-welding) at 1223K/950^{o}C than Ni-Mo or Ni-Ni combinations. It was surprising that Ni-Nb did not weld while the Ni-Mo did weld in view of the fact that the reported intermetallic growth rates of Ni-Nb are substantially higher than Ni-Mo. It is believed that the reason for this seemingly behavior is due to more intimate contact of the Ni-Nb foils than the Ni-Mo foils. It is considered that such differences in behavior do not lend confidence to observations of non-welding in either foil combination if the behaviors are very reflective of uncontrollable differences in contact and the foils do weld (interdiffuse) when in contact.

The overall conclusions from the material compatibility studies at GE, NASA and Battelle relating to the design of the insulation blanket can be summarized as follows:

- Nickel foil should be limited to 993K/720^{o}C or less to avoid self-welding of foils and instability of ZrO_2 with Ni.

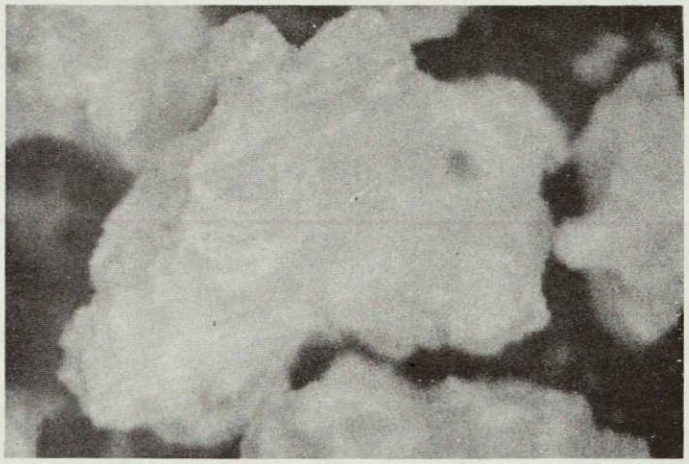

PURE ZrO_2
AS-RECEIVED CONDITION
(35X)
PARTICLES WHITE

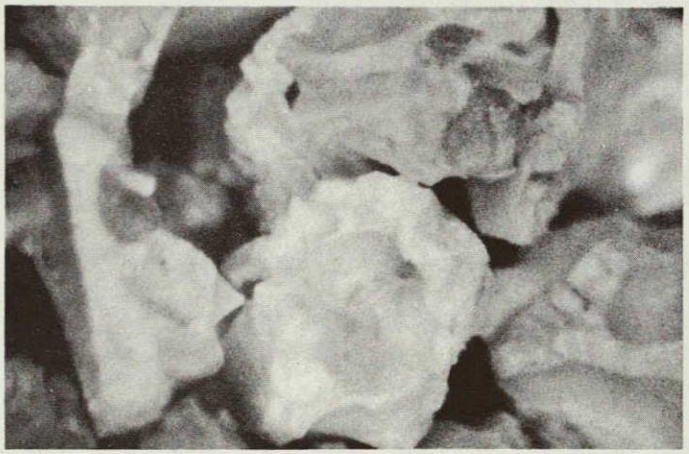

PURE ZrO_2
CRUCIBLE #22 (950°C)
ALL MOLY SYSTEM
PARTICLES GRAY
(NO BLACK PARTICLES)
(35X)

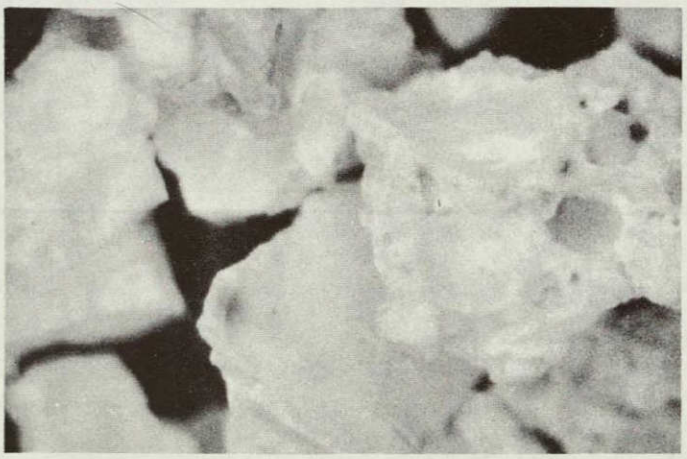

PURE ZrO_2
CRUCIBLE #20 (950°C)
ALL Nb SYSTEM
PARTICLES GRAY
(NO BLACK PARTICLES)
(35X)

FIGURE 4-29 REDUCTION OF PURE ZrO_2 BY Mo AND Nb AT 950°C

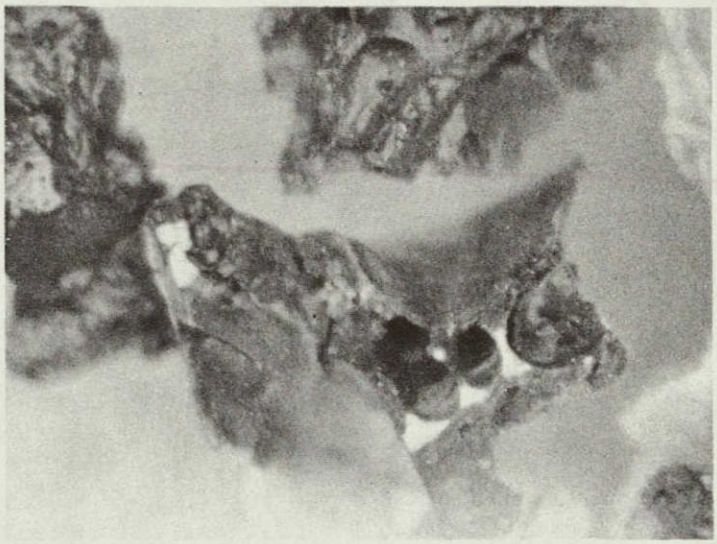

PURE ZrO_2
CRUCIBLE #2 (950°C)
(35X)
Ni/Ni/Ni/Mo/Nb//ZrO_2
PARTICLE GRAY & BLACK
BLACK PARTICLE SHOWN

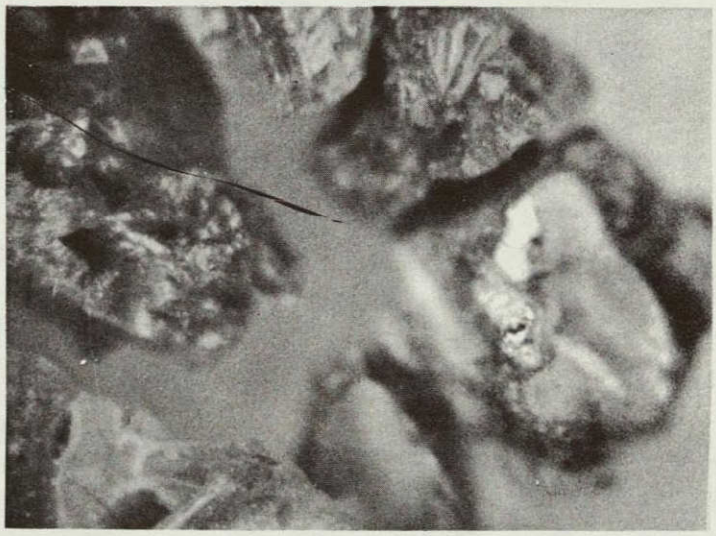

PURE ZrO_2
CRUCIBLE #15
(35X)
Ni/Mo/Ni/Mo/Ni//ZrO_2 Ni
PARTICLES GRAY & BLACK
BLACK PARTICLE SHOWN
NOTE "NICKEL STUCK TO ZrO_2"

FIGURE 4-30 REDUCTION OF ZrO_2 BY Ni AND BY Ni/Nb AT 950°C

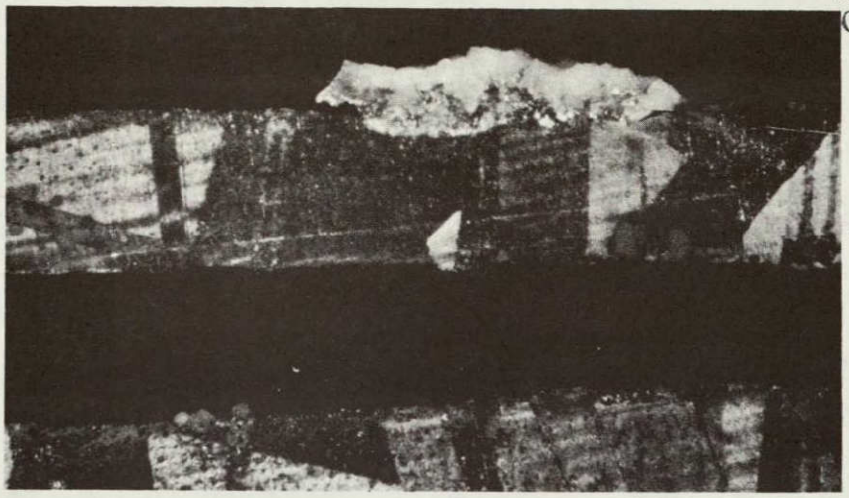

(230X)

"PURE" ZrO_2 STUCK ON BOTTOM OF Ni CRUCIBLE
CRUCIBLE #2, 950°C
Ni/Ni/Ni/Mo/Nb//Ni

INSIGNIFICANT STICKING OF "PURE" ZrO_2 ON BOTTOM OF Ni CRUCIBLE #8, 950°C
Ni/Ni/Ni/Nb/Mo//Ni

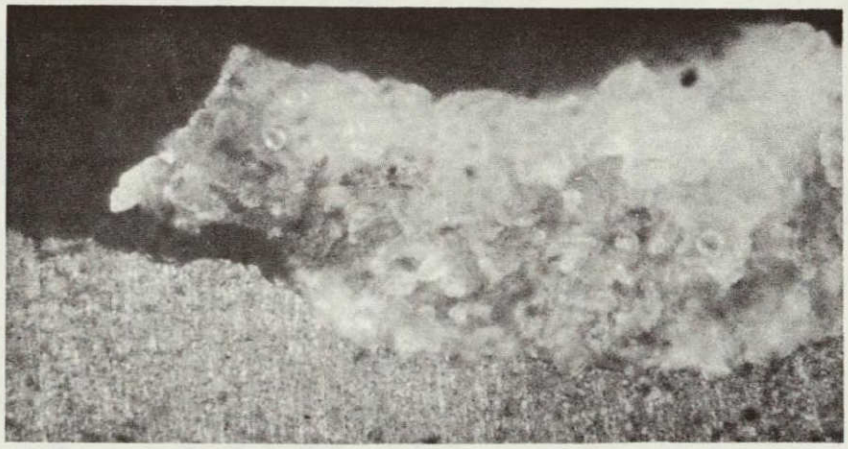

"PURE ZrO_2 ON Ni CRUCIBLE #2
(950°C) (920X)
(UNETCHED)

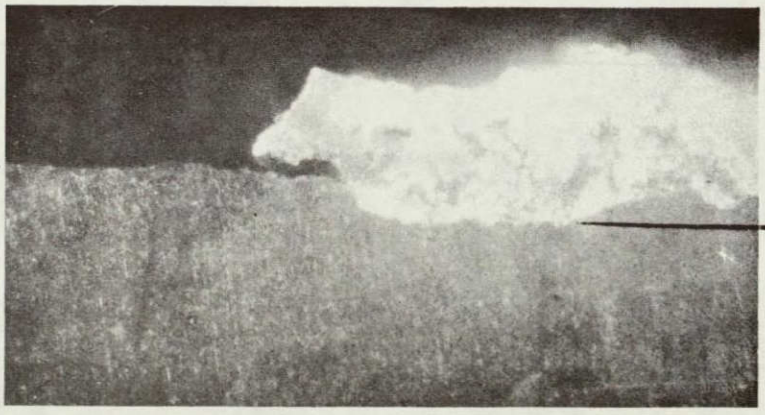

CRUCIBLE #2
(460X)

.009cm

.008cm

FIGURE 4-31 REDUCTION OF ZrO_2 BY Nb AND ACCELERATED EVAPORATION OF Ni

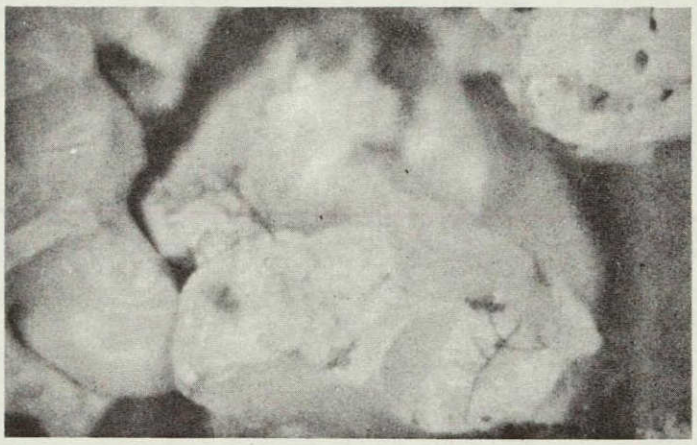

PURE ZrO_2
CRUCIBLE #1 (720°C)
Ni/Ni/Ni/Mo/Nb//ZrO_2 Ni
(35X)
PARTICLES WHITE & GRAY
GRAY PARTICLE SHOWN

PURE ZrO_2
CRUCIBLE #14 (720°C)
Ni/Mo/Ni/Mo/Ni/ZrO_2 Ni
(35X)
PARTICLES WHITE & GRAY
GRAY PARTICLE SHOWN

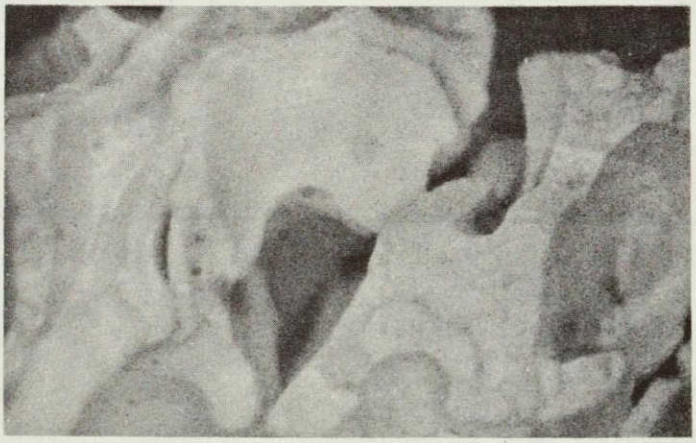

PURE ZrO_2
CRUCIBLE #14 (720°C)
WHITE PARTICLE SHOWN
(35X)

FIGURE 4-32 REDUCTION OF PURE ZrO_2 BY Ni AND Ni/Nb AT 720°C

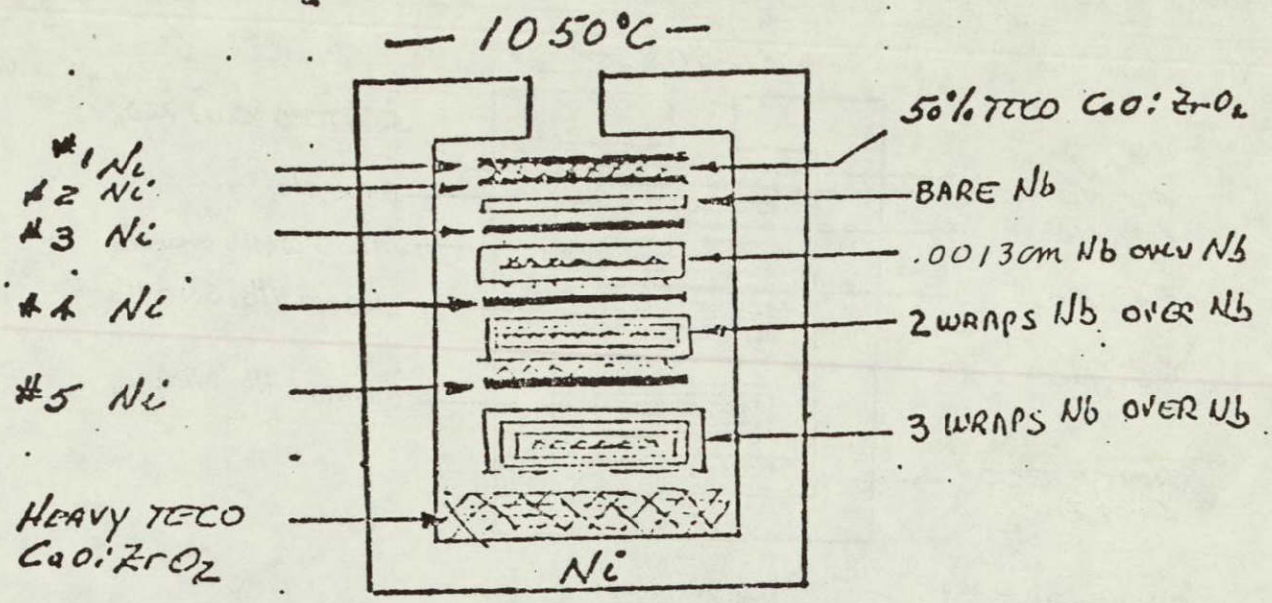

CRUCIBLE #1

OBSERVATIONS

ORIGINAL PAGE IS
OF POOR QUALITY

- TECO POWDER - DRAK GRAY AND SINTERED
- #1 Ni - GAINED APPROX. 0.00051 TO 0.0013 cm THK'S. (TOP ETCHED, BRIGHT BOTTOM-DULL)
- #2 Ni - LOST APPROX. 0.0025 cm THK'S.
- #3 Ni - LOST APPROX. 0.003 cm THK'S.
- #4 Ni - LOST APPROX. 0.0038 TO 0.0051 cm THK'S.
- #5 Ni - NO CHANGE TOP SHINNY
- BARE Ni DID NOT STICK TO BARE Nb ; 50% $CaO:ZrO_2$ PREVENTED Ni/Ni Bonding.
- SINGLE WRAPPED Nb SPECIMEN - COMPLETELY PENETRATED WITH Ni
- DOUBLE WRAPPED Nb SPECIMEN - METALLIC LOOKING Ni PENETRATION ~0.
- TRIPLE WRAPPED Nb SPECIMEN - Ni PENETRATION ~ 0.
- 50% $CaO:ZrO_2$ VISIBLE BETWEEN SPECIMENS (#1 AND #2)
- BARE Nb GAINED 0.0076 cm (CENTER) 0.015 cm (EDGES)
- BOTTOM OF CRUCIBLE APPARENTLY RUNNING HOTTER THAN TOP OF CRUCIBLE

FIGURE 4-33 OBSERVATIONS OF CRUCIBLE #1 TESTED AT 1323K/1050°C

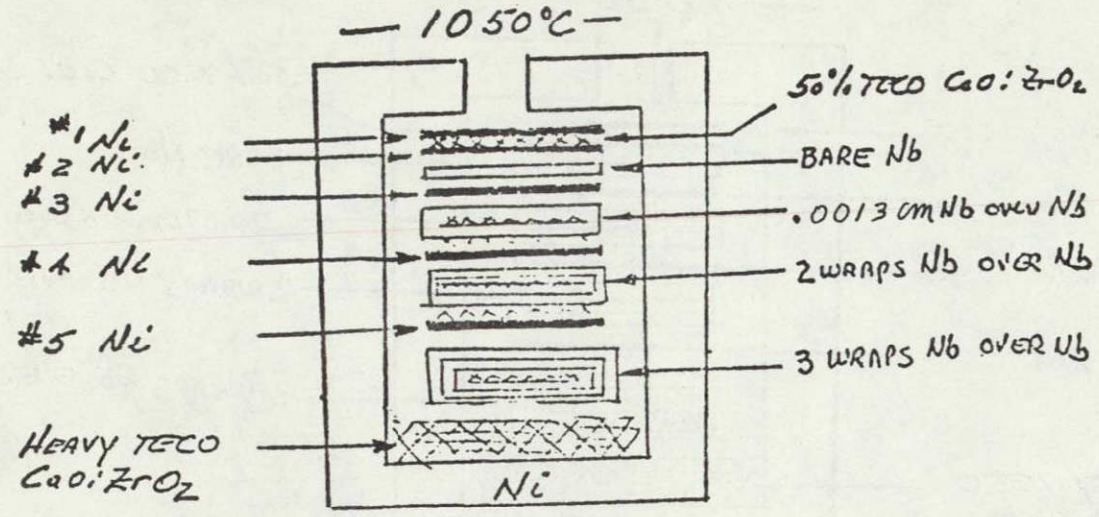

CRUCIBLE #1

OBSERVATIONS

COATED SIDE

SINGLE Nb WRAPPED Nb SPECIMEN (1590X)

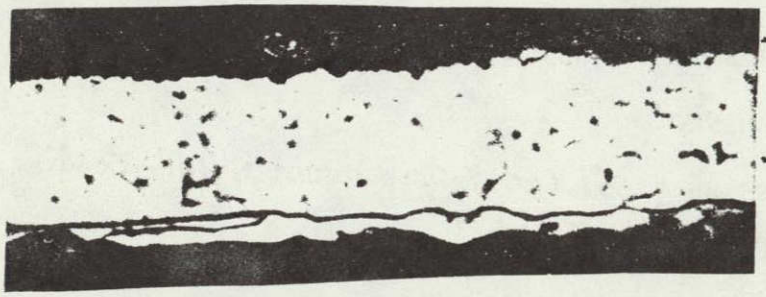

COATED SIDE

DOUBLE Nb WRAPPED Nb SPECIMEN (1590X)

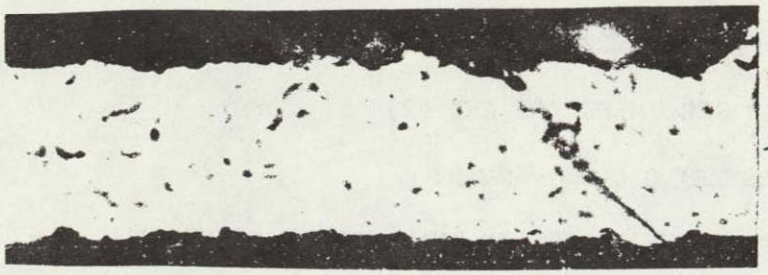

COATED SIDE

TRIPLE Nb WRAPPED Nb SPECIMEN (1590X)

No Ni VISIBLE

FIGURE 4-34 TYPICAL CROSS SECTION OF Nb WRAPPED Nb FOILS AT 1323K/1050°C

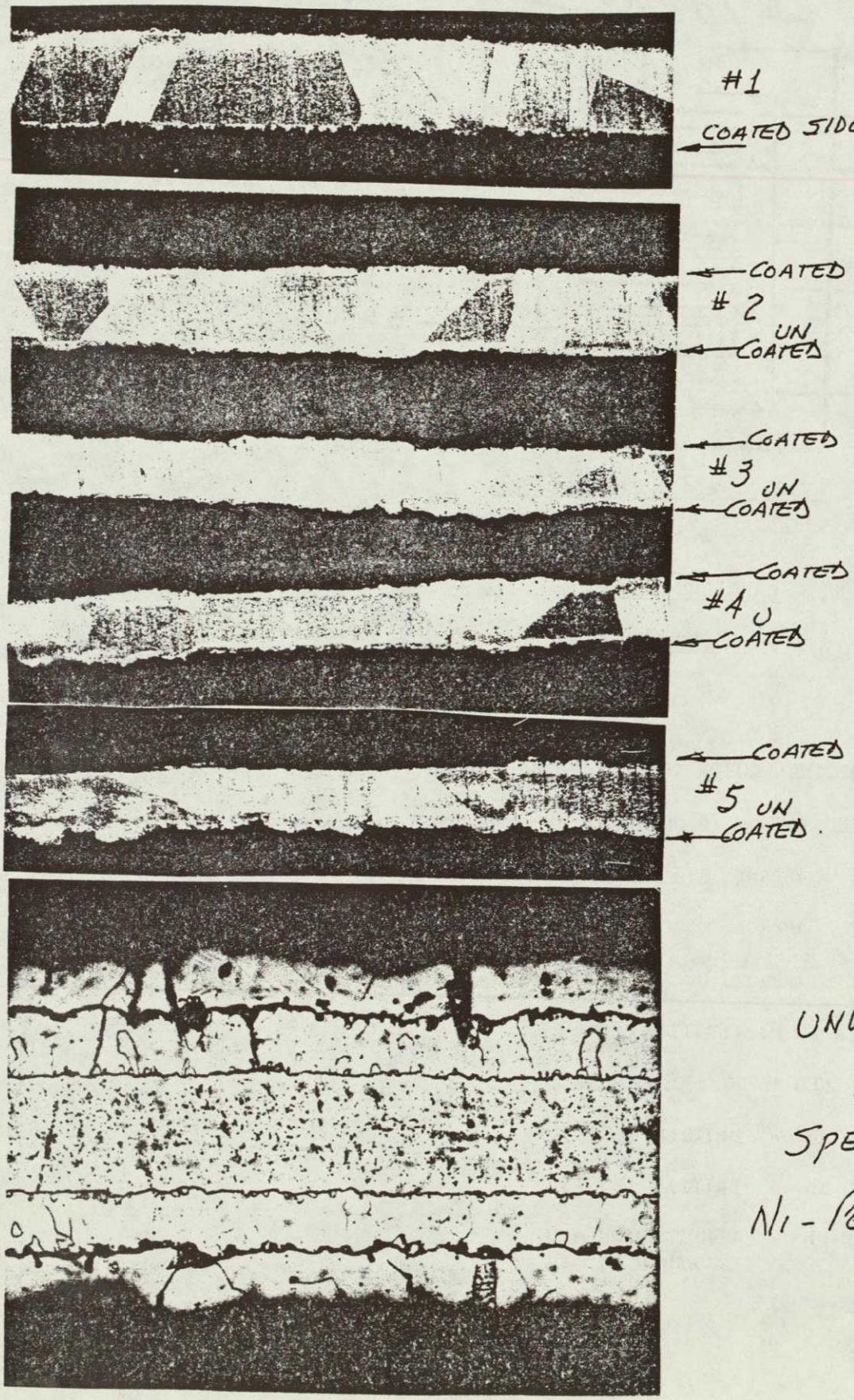

FIGURE 4-35 TYPICAL CROSS SECTION OF Ni FOILS AND UNWRAPPED Nb FOIL AT 1323K/1050°C

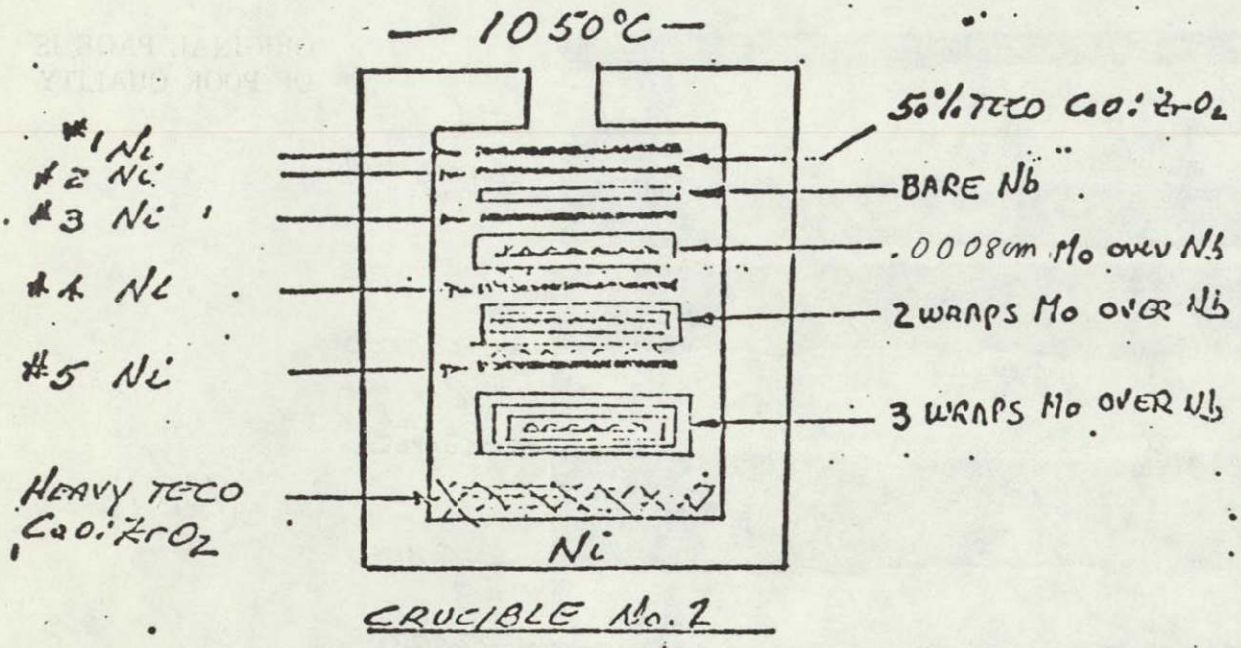

CRUCIBLE #2

OBSERVATIONS

- TECO POWDER ORIGINAL COLOR (Mo MORE STABLE WITH $CaO:ZrO_2$ THAN Nb)
- #1 Ni - GAINED APPROX. 0.0005 TO 0.0013 cm THK'S.
- #2 Ni - LOST APPROX. 0.0025 cm THK'S.
- #3 Ni - LOST APPROX. 0.0025 TO 0.0038 cm
- #4 Ni - LOST APPROX. 0.0025 TO 0.0038 cm
- #5 Ni - STUCK TO Mo (BRITTLE)
- BARE Nb - GAINED APPROX. 0.0076 cm
- SINGLE WRAPPED Nb - BRITTLE (LOST)
- DOUBLE WRAPPED Nb - BRITTLE (LOST)
- TRIPLE WRAPPED Nb - PENETRATION = 0.
  GROWTH = 0.

FIGURE 4-36 OBSERVATIONS OF CRUCIBLE #2 TESTED AT 1323K/1050°C

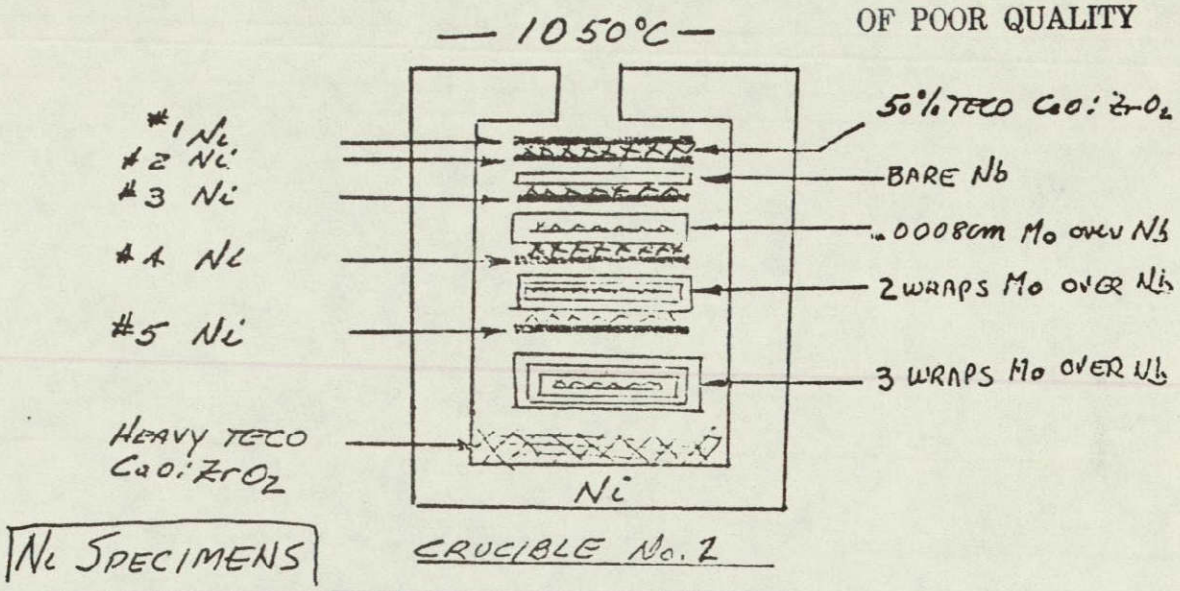

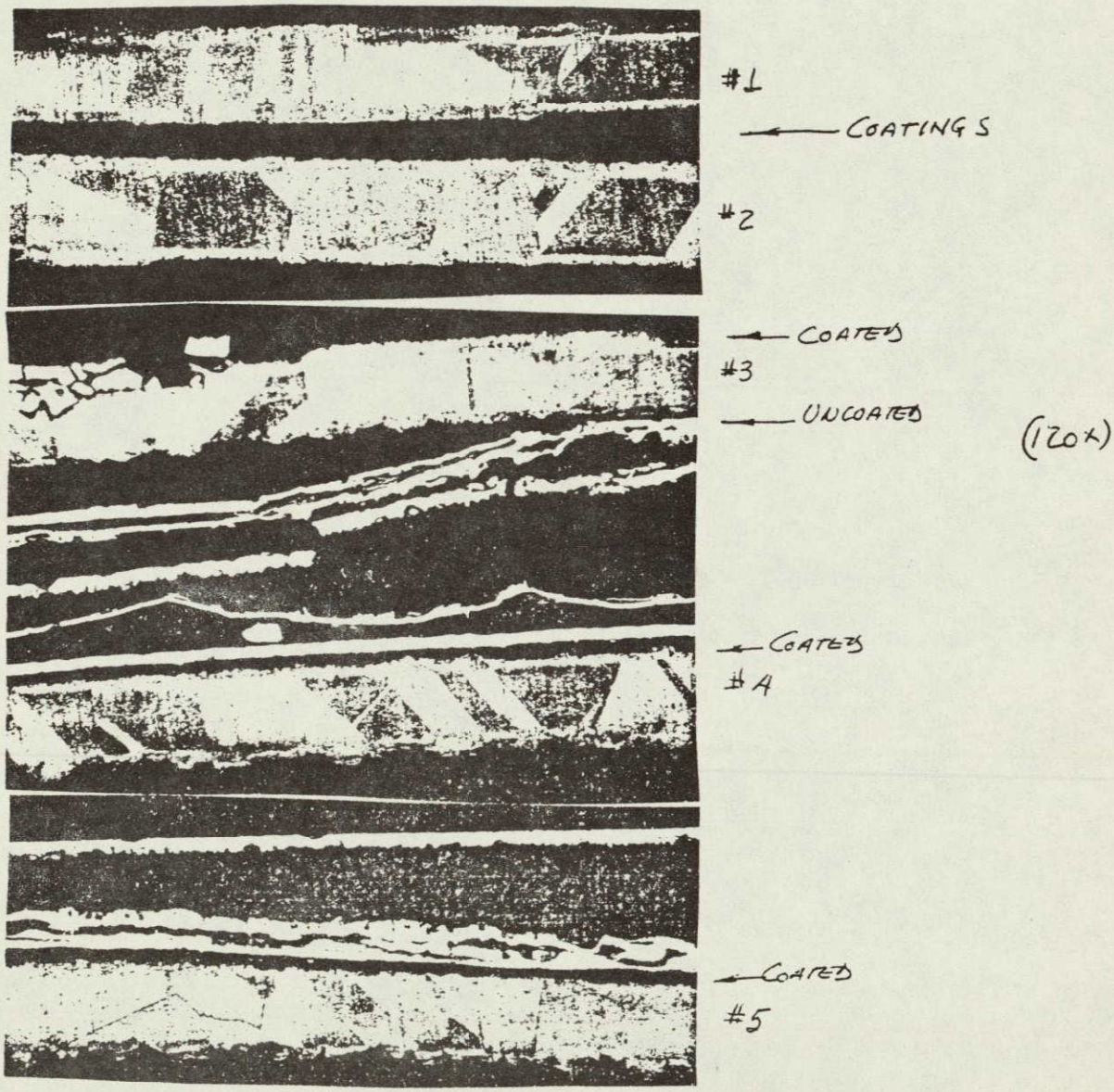

FIGURE 4-37 TYPICAL CROSS SECTIONS ON Ni FOILS FROM CRUCIBLE #2 TESTED AT 1323K /1050°C

CRUCIBLE #2 - Mo FOIL BARRIER STUDY
1050°C

ORIGINAL PAGE IS
OF POOR QUALITY

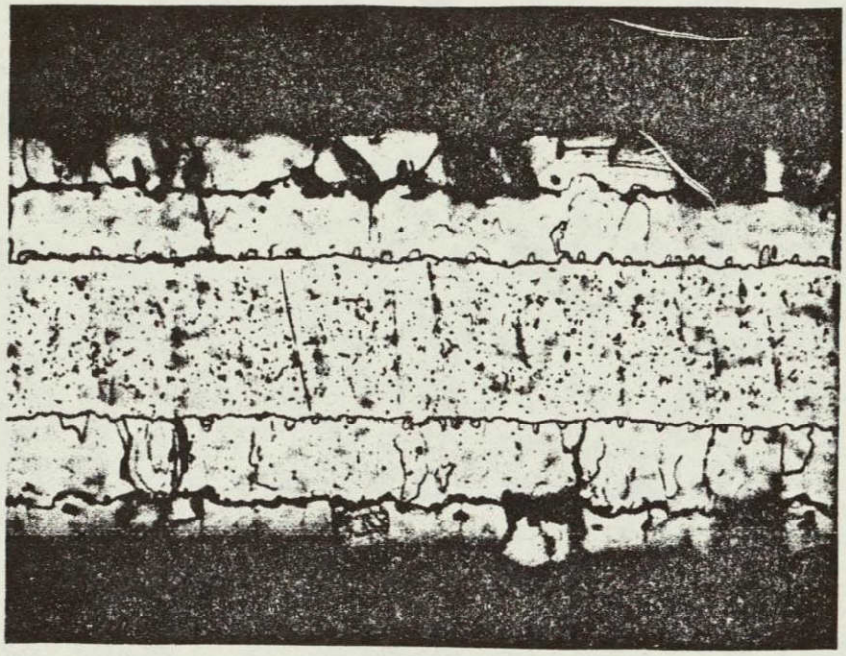

(290X)

BARE Nb SPECIMEN SHOWING
Ni PENETRATION (BOTH SIDES)

FIGURE 4-38 TYPICAL CROSS SECTION OF Nb FOIL WRAPPED IN Mo TESTED AT 1323K/ 1050°C

- Calcia stabilized ZrO_2 should be utilized since it is more stable than pure ZrO_2.
- ZrO_2 is more stable with Mo than with Nb, hence for a very conservative design approach (ignoring melt down requirements for emergency cooling) the use of Mo foils at temperatures greater than 993K/720°C or some lesser upper level seems warranted for ground performance tests.
- Care should be taken to assure that the ZrO_2 is dry.
- Use of very high purity nickel foil has no effect on reducing nickel evaporation or foil self-welding.
- Final design of the insulation system for a flight system would require long term stability tests on subsize or full size foil blankets in the actual design configuration.

4.5 INSULATION MELTDOWN TESTS

The purpose of the insulation meltdown tests was to demonstrate the Emergency Cooling System (ECS) concept for the HSA. Two "small scale" tests were conducted ; the first meltdown test was of an all nickel foil (60 layer) configuration and the second was a combination of columbium and nickel layers, a design which was under consideration at the time of the test. A description of the tests and the results are discussed in the following paragraphs.

4.5.1 SMALL SCALE MELTDOWN TEST OF ALL NICKEL FOIL CONFIGURATIONS

One of two extra life stability test samples (see Figure 4-39) was selected for this 60 layer all Ni small scale meltdown test to provide a preliminary evaluation of the Mini-Brayton HSA ECS. The test specimen was heated with a tungsten wound heater. Instrumentation included two tungsten-rhenium T/C's, one on the inner tantalum cylinder (as illustrated) and the other on the 30th layer of insulation (not shown), and two chromel-alumel T/C's, both on the outer tantalum cylinder. The sample was placed in a vacuum chamber which was evacuated to about 1×10^{-4} Pa (10^{-6} torr), and the sample was heated to a hot face temperature of about 1255K (1800^{o}F).

In the first test attempted, the ECS activation was simulated by applying 320 watts to the heater. This thermal input caused a rapid heatup of the inner tantalum cylinder to about 2200K (3500^{o}F), at which time the instrumentation began reading erratically. Shortly afterwards, (about 5 minutes), the heater burned out. Diagnostic disassembly revealed that the mullite heater core had fused and deformed, shorting out the tungsten winding. Melting/vaporization of the sample had been initiated at four locations around the center of the cylindrical sample, as shown in the photographs of Figures 4-40 and 4-41, and on the inside of both end caps. No molten material was noted during this test, and no molten residue was observed during disassembly, it is believed that evaporation caused the material removal.

The heater was rebuilt using a tungsten wire and the test re-initiated. After a stable hot face was achieved (1215K (1725^{o}F), 40.5 watts), the emergency load was simulated (226.1 watts).

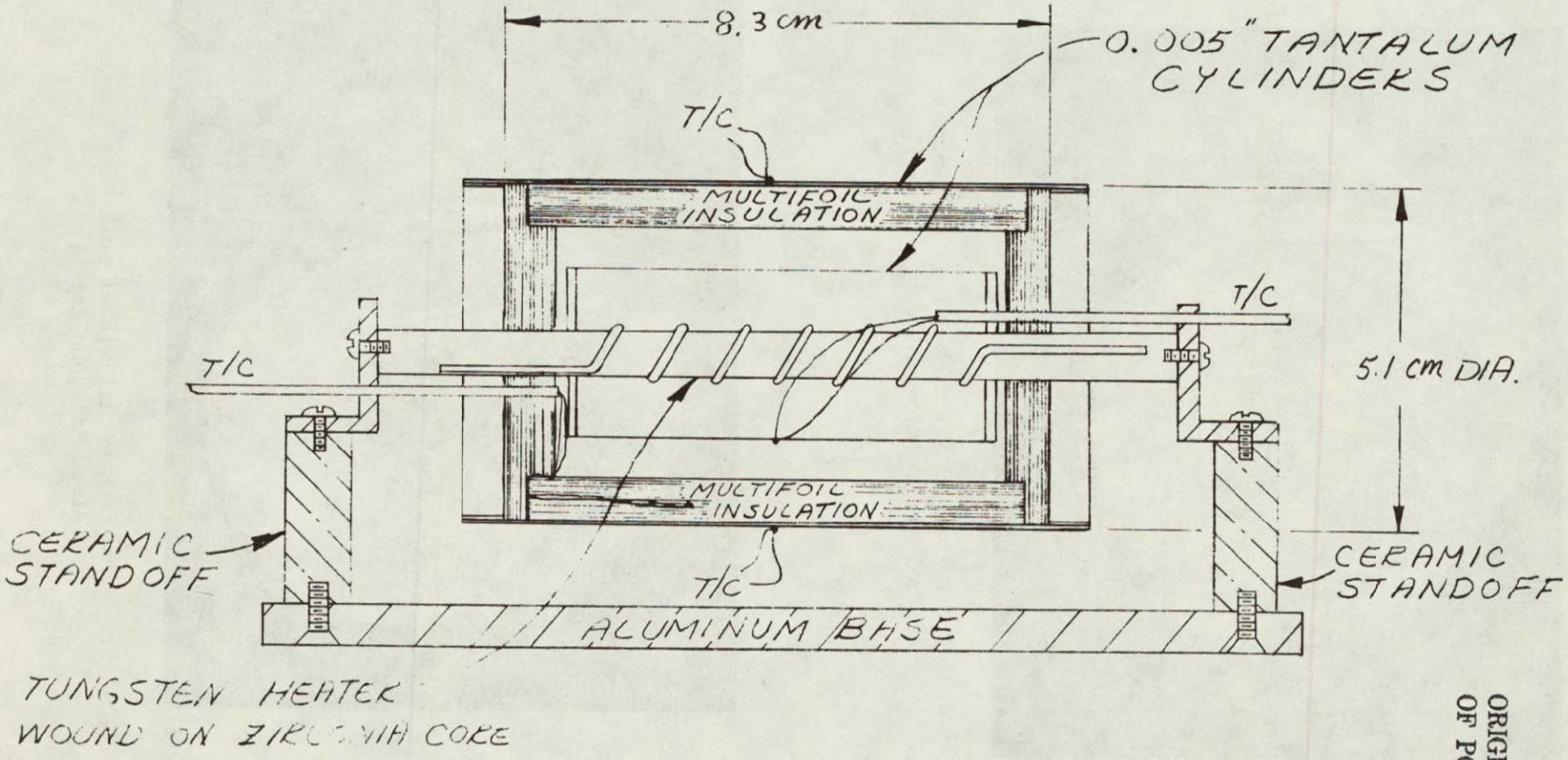

(HORIZONTAL DURING TEST)

FIGURE 4-39. ALL NICKEL FOIL SMALL SCALE MELTDOWN TEST ASSEMBLY #1

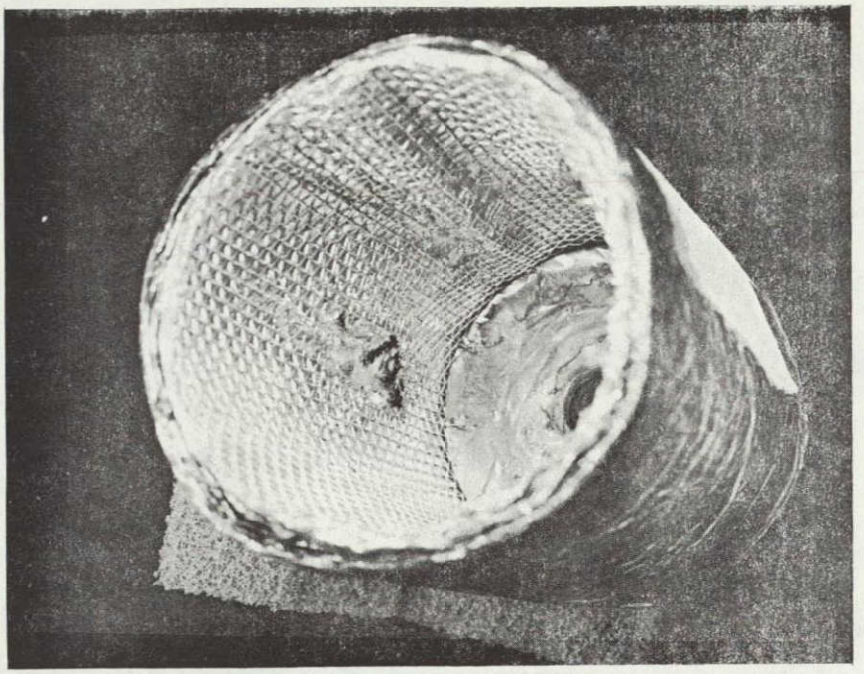

Figure 4-40. Photograph of All Nickel Foil Test Sample After First Meltdown Attempt

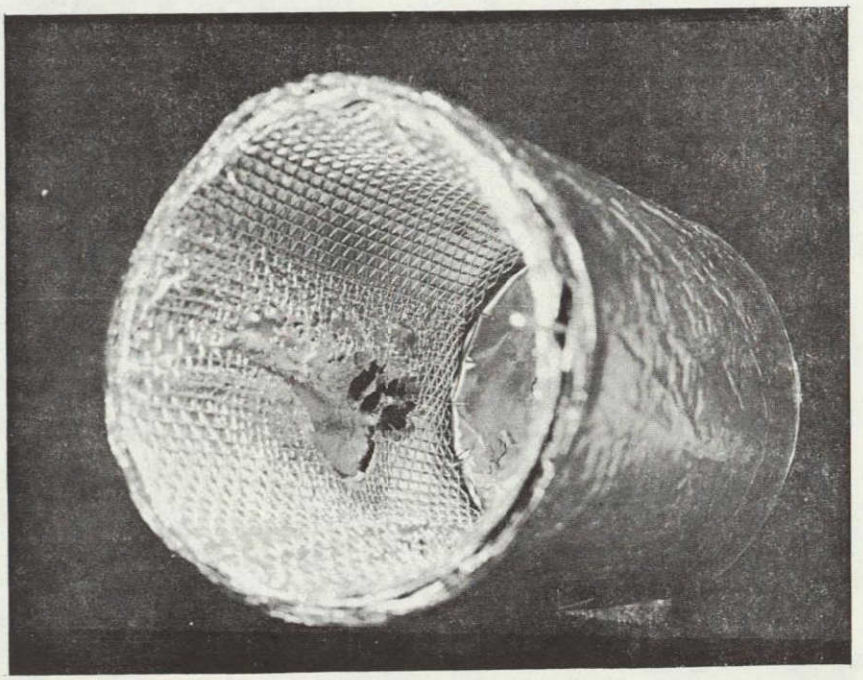

Figure 4-41. Photograph of All Nickel Foil Test Sample After First Meltdown Attempt

After 15 minutes, the tantalum inner liner reached 1740K (2660°F), and melting/vaporization commenced. The inner Ta liner fluctuated between 1830K (2830°F) and 1660K (2525°F) for 30 minutes as melting/vaporization proceeded, until the heater again burned out. The 30th layer reached a peak temperature of 1690K (2585°F) (shy of the 1730K (2650°F) phase change temperature of nickel) just at heater burnout. A recorder chart of these temperatures is presented on Figure 4-42. No molten nickel was observed during this meltdown test. Evaporation of the nickel foil was obvious as the glass bell jar became noticeably darker as the test proceeded. Following cooldown, the test specimen was diagnostically disassembled. The tantalum foil cold face was visibly darkened and was probably due to vapor deposited nickel (see Figure 4-43). One planer end of the insulation was removed and partial fusing all around the joint was observed (see Figure 4-44). The tungsten heater wire was observed to be broken near one end of the assembly. Melting/vaporization was initiated over 90% of the inner circumference near the center of the cylinder (see Figure 4-45) and appeared to have progressed about midway through the insulation blanket in spots. In an attempt to determine how deeply melting/vaporization had proceeded into the insulation cylinder, the blanket was unwound from the outside. Table 4-3 presents the cogent observations. Self-welding of adjacent foils was observed as far out as the 56th layer and increased in magnitude as the unwrapping proceeded. By the time the 44th layer was reached, three larger solidly fused areas of foil were encountered which prohibited further unwrapping.

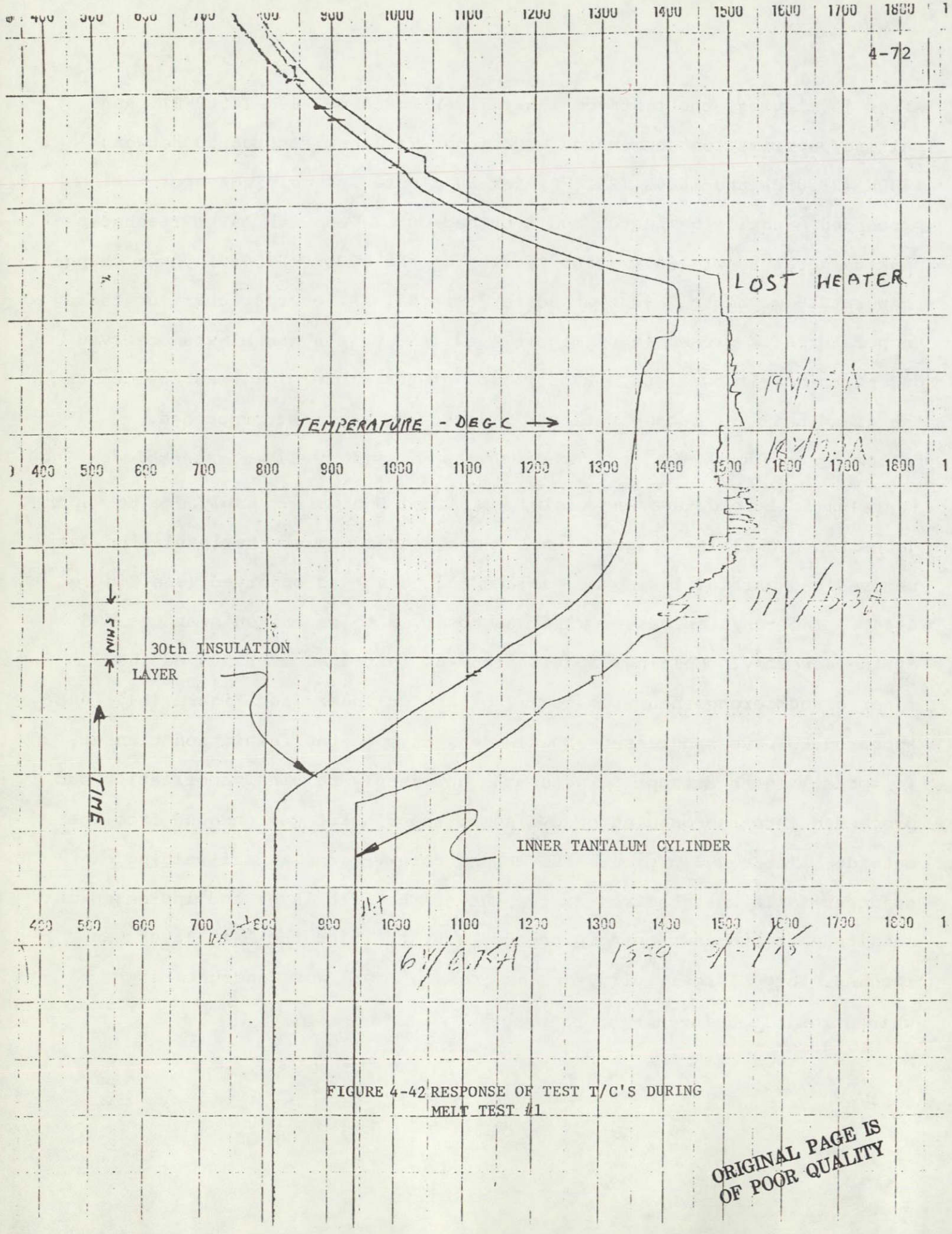

FIGURE 4-42 RESPONSE OF TEST T/C'S DURING MELT TEST #1

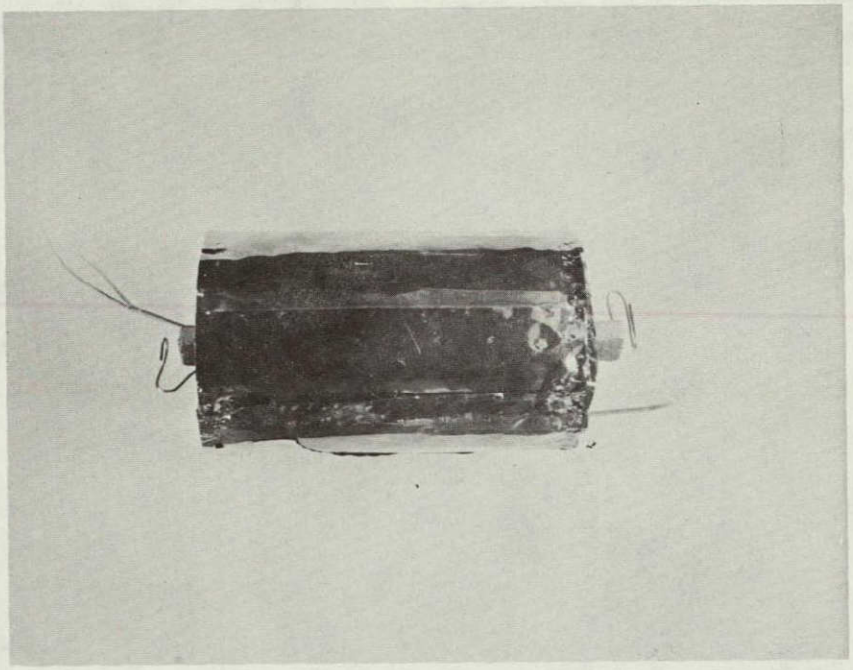

Figure 4-43. Tantalum Foil Outer Cylinder - Note Darkened Appearance Due to Vapor Deposited Nickel

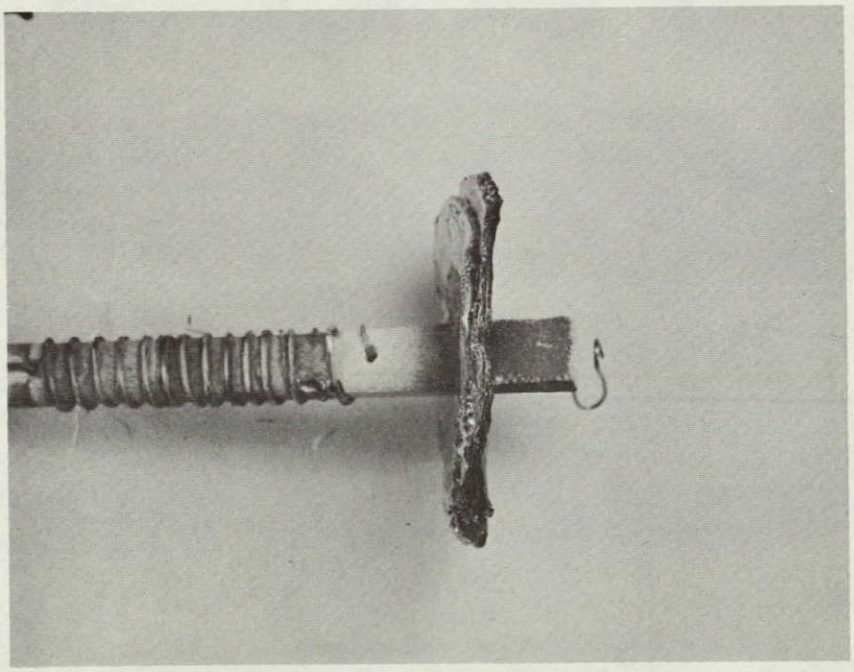

Figure 4-44. Planar End Insulation and Heater Assembly - Note Fused Edge of Insulation

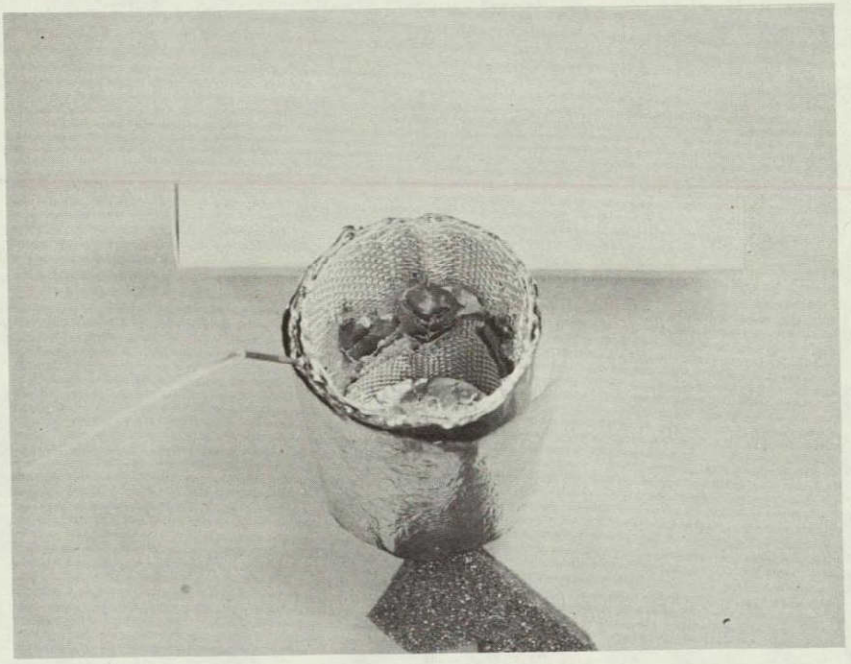

Figure 4-45. Melting/Vaporization of Nickel Screen and Insulation Blanket Cylindrical Section

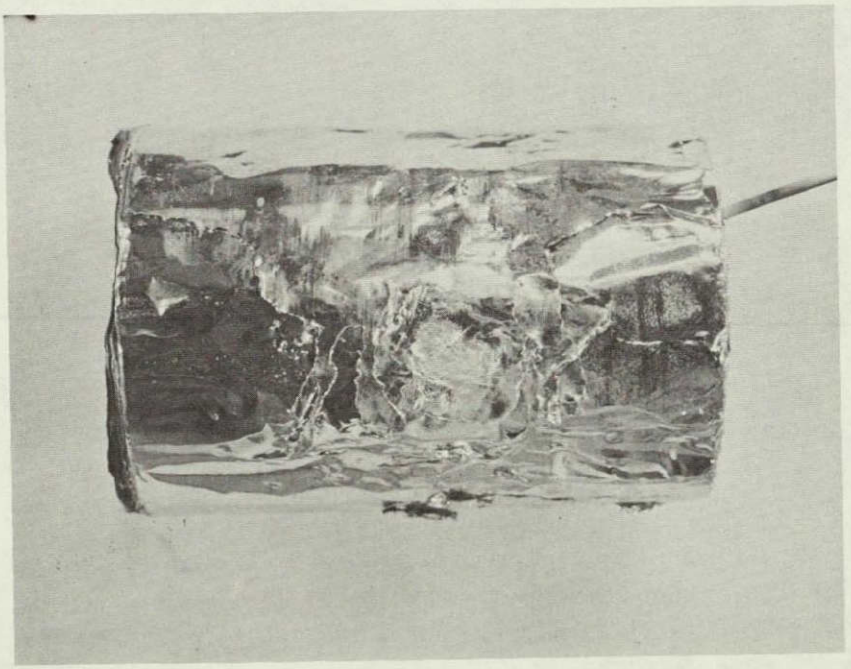

Figure 4-46. Typical Solidly Fused Area of Multifoil Insulation at 44th Layer

TABLE 4-3 CHRONOLOGY OF ALL NICKEL TEST SPECIMEN DIAGNOSTIC DISASSEMBLY

Layer from Outside	Layer from Inside	Observations
3½	56	Beginning of self-welding
11	49	Encountered difficulty in unwrapping
14½	45	Encountered solidly fused area
15	45	Encountered second solidly fused area ~120° past above
16	44	Encountered third solidly fused area; no further unwrapping possible

Due to the exceptionally high temperatures involved in this small scale configuration, continuous tungsten heater performance was tenuous, so much so that a complete meltdown was never achieved during this test. However, a graphite heater used in a later small scale melt test of the columbium nickel foil configuration did not burn out and that test was run to completion as discussed below.

4.5.2 SMALL SCALE MELTDOWN TEST OF COLUMBIUM-NICKEL FOIL CONFIGURATION

The insulation material compatibility tests indicated that nickel foil should be limited to the low temperature region of the insulation blanket. During the time frame when those tests were being conducted and before a design decision was made to incorporate molybdenum foil for the Ground Demonstration HSA Hardware, it was considered prudent to subject a candidate columbium-nickel foil small scale cylindrical specimen to meltdown

conditions. The primary objective was to verify that melting would be initiated at the Nb-Ni eutectic temperature of 1448K (2147^{o}F), an improvement in the meltdown characteristics of the all nickel foil system.

The test configuration was similar to the first meltdown test except that a graphite heater was incorporated and the insulation foil material was altered as shown in Figure 4-47. The insulation cylinder consisted of 36 inboard columbium foils followed by 24 layers of nickel foil. The planar end caps were molybdenum foil since these layers need not necessarily melt to achieve successful emergency cooling operation. Figure 4-48 gives the test temperature history of thermocouples distributed in the insulation specimen. It is evident that when the Ni/Nb interface at the 36th foil reached the nickel-columbium eutectic temperature a very sudden decrease in temperature occurred indicating a reaction that essentially spoiled the insulation characteristics of the foil blanket as would be expected if melting/vaporization occurred. At this point the test specimen was observed to flash red hot. Photographs of the insulation blanket specimen after the meltdown test are given in Figures 4-49 and 4-50. The melting and fusion of the foils into a solid mass is evident. A photomicrograph of a cross section of the blanket is shown in Figure 4-51. The solid fusing of the columbium foils and melting and solidification of the nickel foils is graphic.

FIGURE 4-47 - SMALL SCALE MELT DOWN TEST ASSEMBLY #2

(HORIZONTAL DURING TEST)

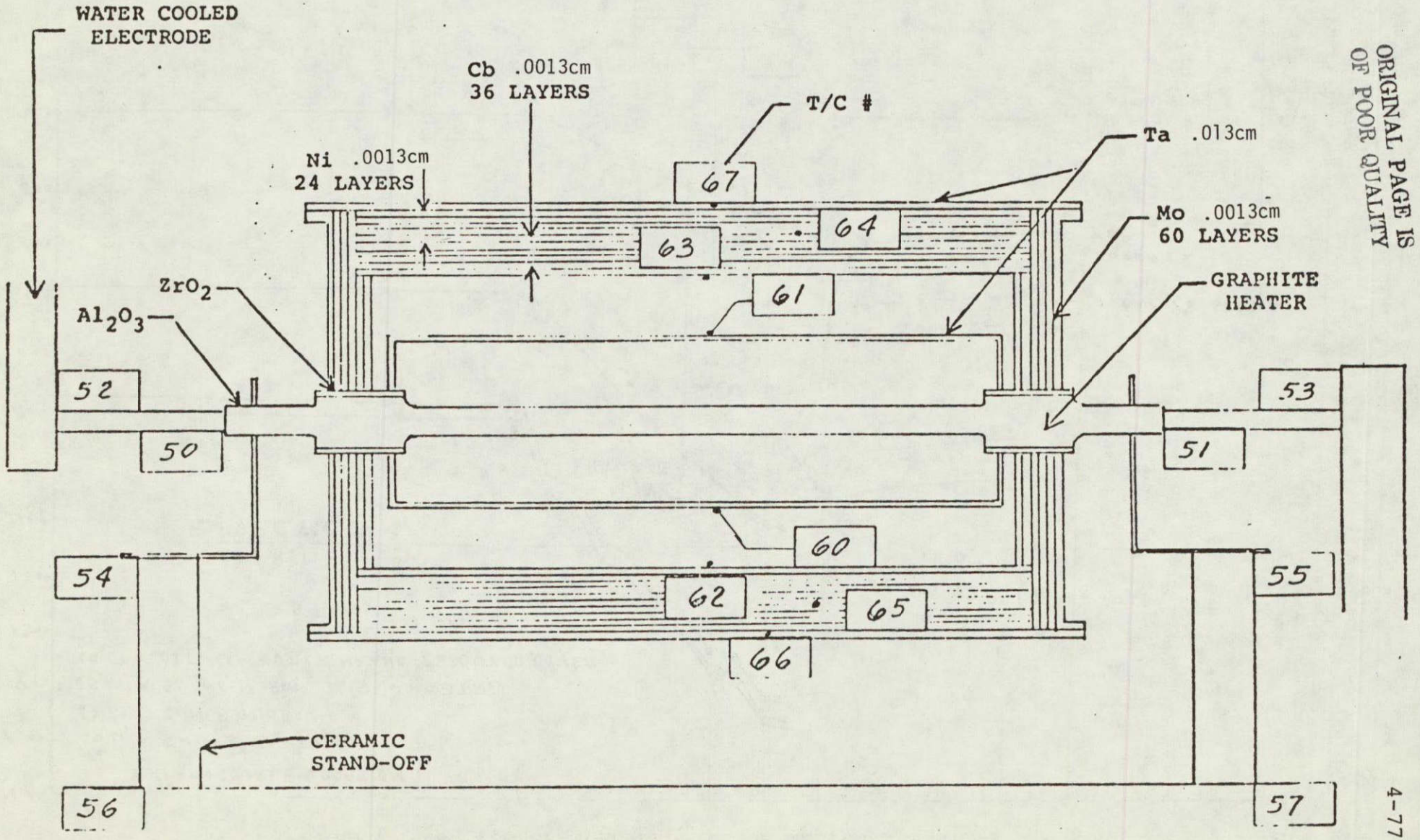

FIGURE 4-48 TEMPERATURE PROFILE OF MELTDOWN TEST #2

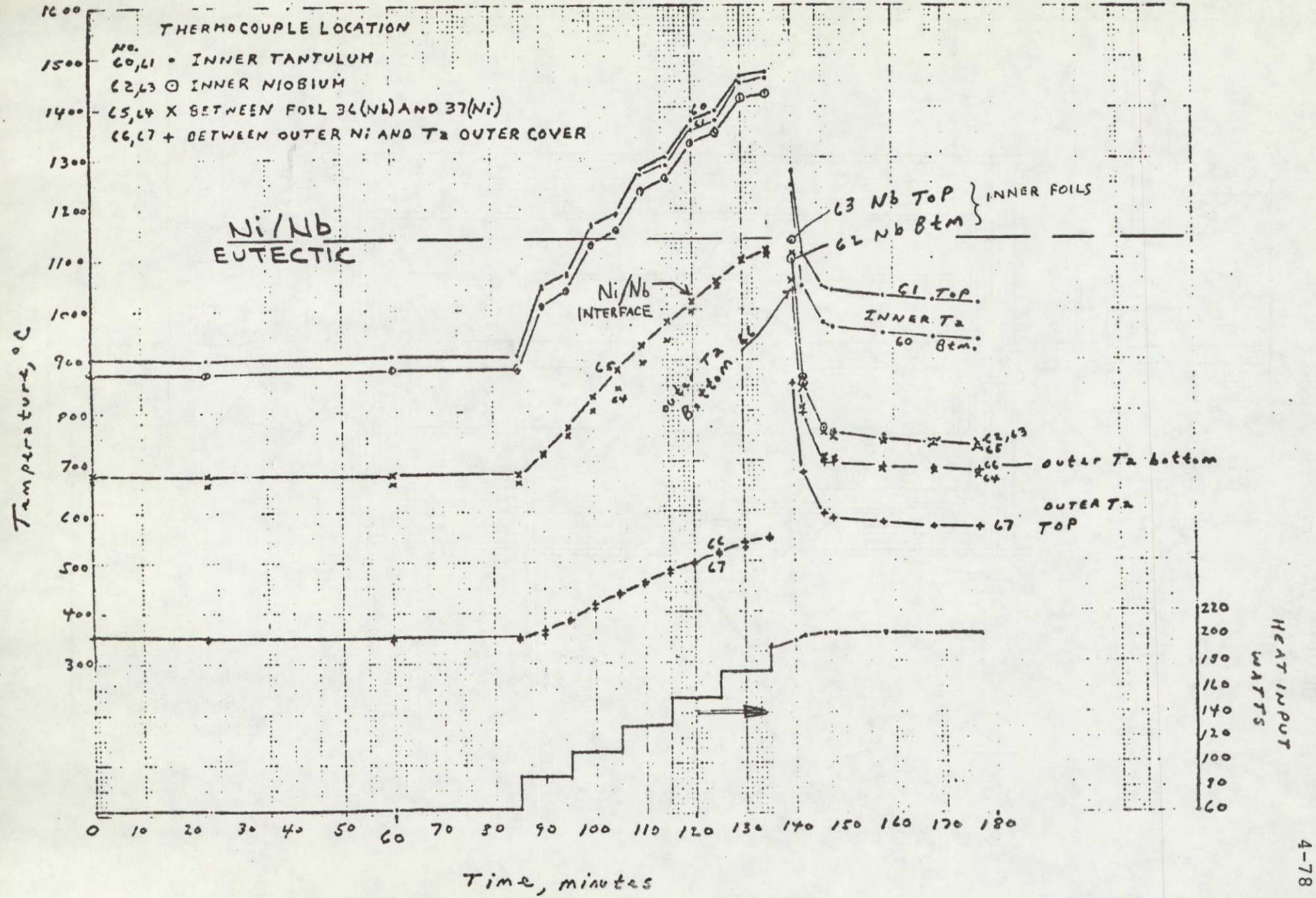

FIGURE 4-49

INSULATION SPECIMEN AFTER MELT DOWN TEST #2

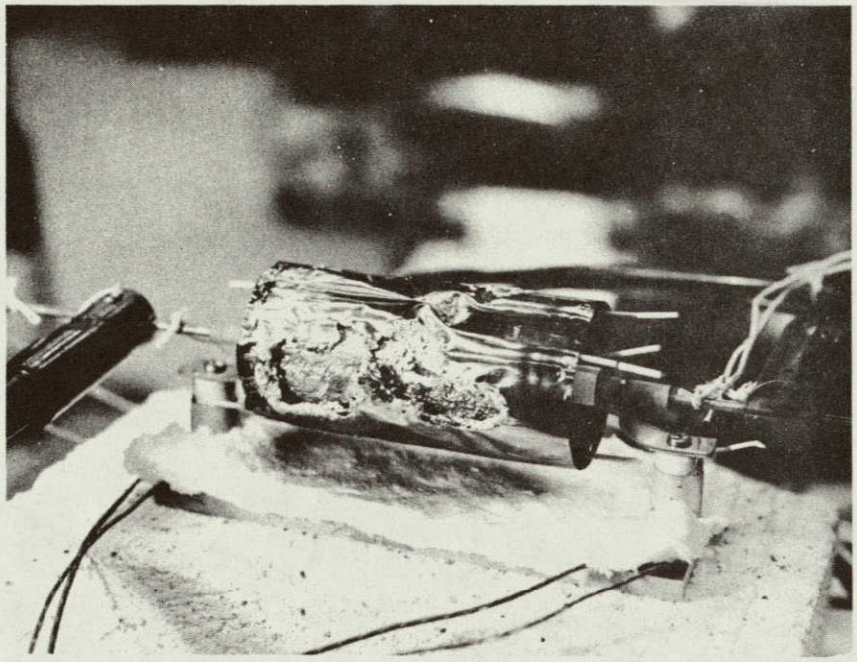

BOTTOM VIEW TURNED 90° POST MELT

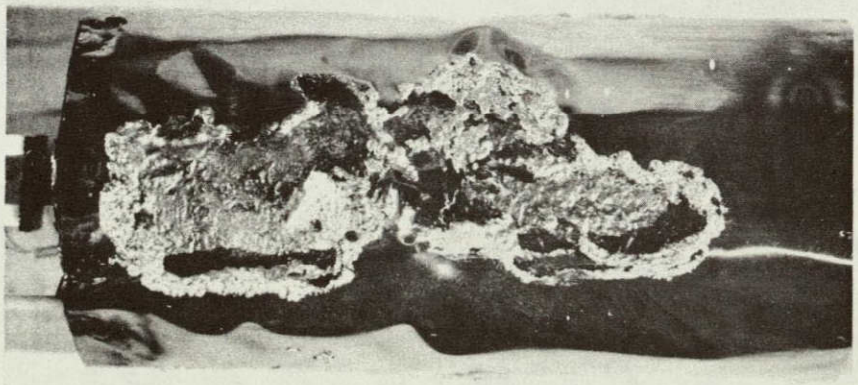

FIGURE 4-50

END VIEW OF SPECIMEN AFTER MELT DOWN TEST #2
VIEW WITH ONE END CAP REMOVED

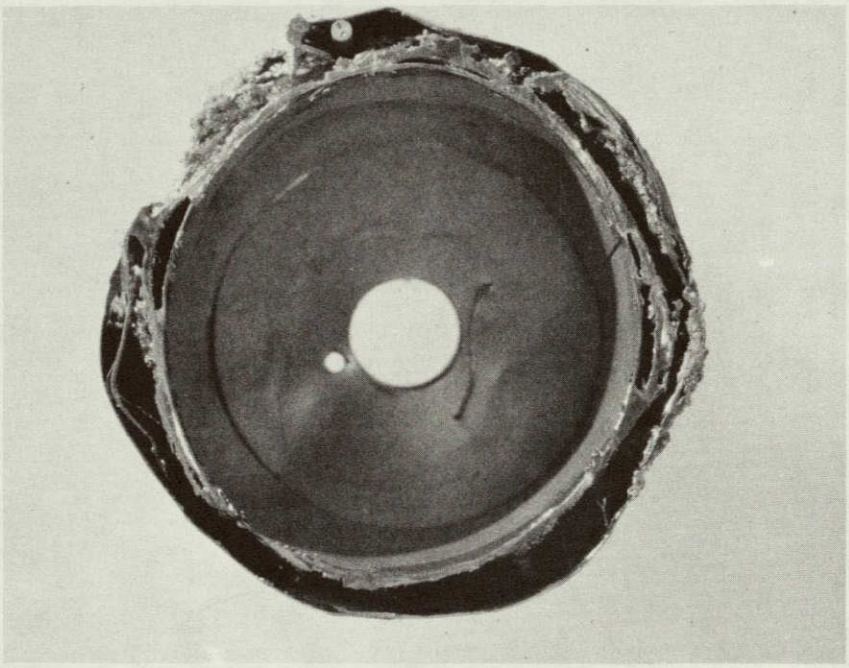

FIGURE 4-51

PHOTO MICROGRAPH OF CROSS SECTION OF INSULATION AFTER MELT DOWN TEST #2

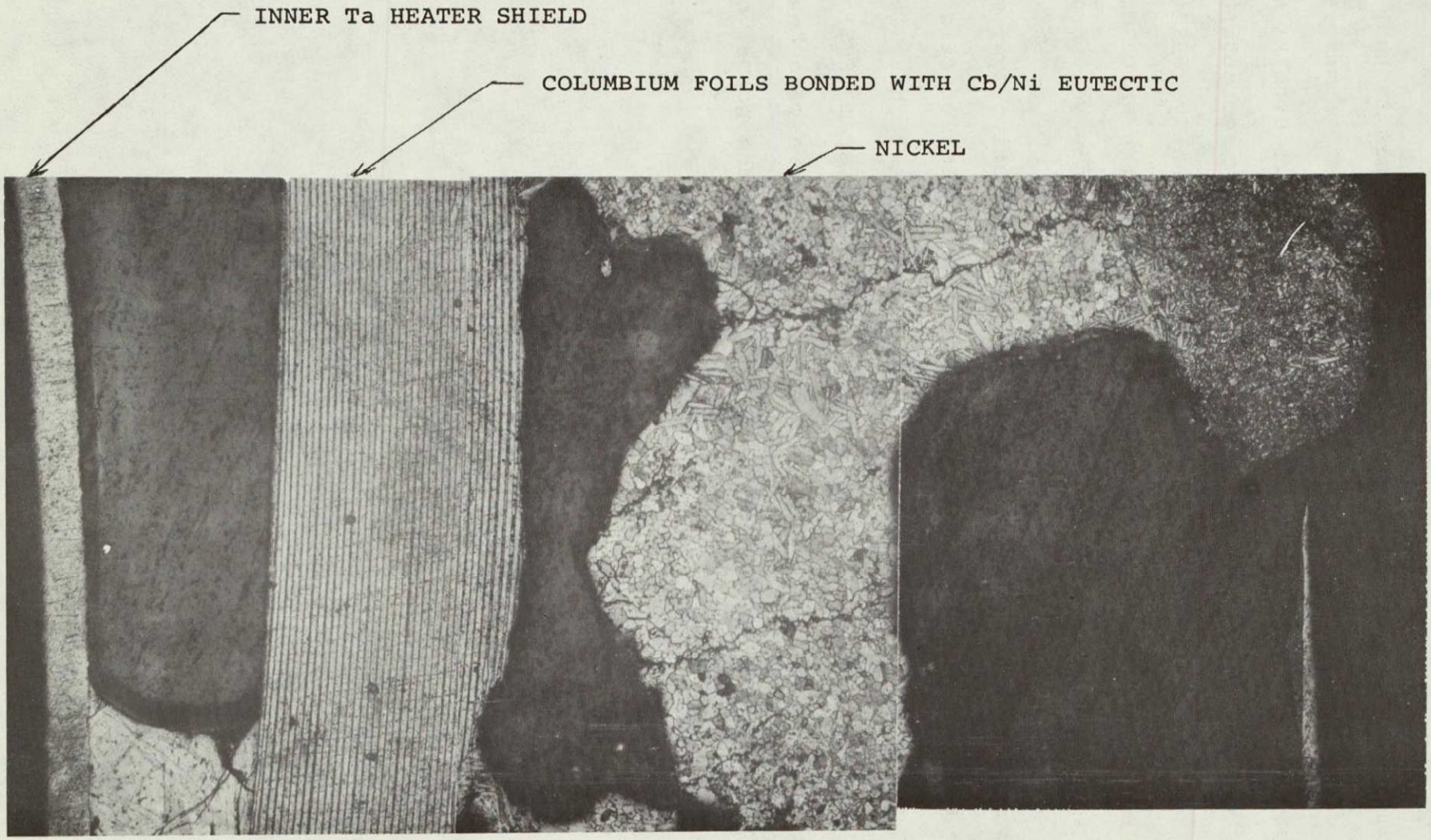

A very significant conclusion from both meltdown tests is that the self-welding of adjacent foils in the ECS mode will assist in maintaining a safe heat source PICS (iridium fuel clad) temperature even if melting is incomplete. The fusing shorts out the insulation by increasing the thermal conductivity several orders of magnitude. Analytically determined emergency mode temperature response of the heat source which does not account for the self-welding phenomenon is undoubtedly very conservative.

It would appear from the test results that an insulation system which incorporates multi-material foils will spoil when the eutectic temperature is reached at the interface. This would suggest that with judicious selection, some tailoring of the Emergency Cooling System (ECS) activation temperature is possible in the flight design to assure safe heat source temperatures, as well as long life stability during the normal operation of the HSA.

(2) Thermal Cycling - The HSA shall have the capability to withstand a minimum of 100 startup-shutdown thermal cycles.

(3) Working Fluid - The Brayton cycle gas shall be a mixture of He and Xe having a molecular weight of 83.8.

(4) Heat Source - The basic fuel sphere assemblies (FSA) shall be as developed for the multi-hundred watt-radioisotope thermoelectric generator. The MHW-HS consists of 24 PuO_2, graphite covered, iridium clad fuel spheres suitably spaced and supported in a cylindrical canister having an overall diameter of 18.26 cm (7.19 in) and overall length of 43.10 cm (16.99 in).

(5) Heat Source Heat Exchanger - The HSHX shall be fabricated from the columbium base C-103 alloy and designed to transfer 2400 w(t) to the working fluid at a flow rate of 0.57 Kg/sec. (0.126 lb/sec.). The working fluid enters the HSHX at 980K (1305^{o}F) and exits at 1144K (1600^{o}F). The maximum pressure drop shall be no more than 0.0015 MPa (0.22 psi) at an operating pressure of 0.243 MPa (35.3 psia).

The HSHX shall be designed for a maximum of two percent creep in the radial direction (1% axial) for the design life.

The HSHX, manifolds and ducting providing containment of the working fluid, shall be designed for zero leakage for the design life. The maximum permissible measured leak rate for a fabricated unit shall not exceed one times ten to the minus 6 standard cc/sec. of helium following pressure and performance testing.

(6) Auxiliary Cooling System (ACS) - The ACS is required to provide cooling of the HS during all non-operational phases of the power system and limit temperatures of all HSA surfaces exposed to the atmosphere. There are two design criteria for the ACS. The maximum temperature of exposed surface of the HSA shall not exceed 466K (380°F) while on the launch pad to prevent possible ignition of fuel vapors present during pre-launch operations. The maximum temperature of all refractory alloys exposed to air shall not exceed 523K (483°F) to preclude oxidation.

(7) Emergency Cooling System (ECS) - The ECS shall maintain the isotope heat source at a safe temperature in the event of a failure of the power conversion system, such as a loss of the working fluid. During the transient condition after onset of an emergency condition, the Heat Source Post Impact Containment Shell (PICS) shall not exceed times and/or temperatures which would cause breaching of the PICS and release of the isotopic fuel. Upon reaching a steady state condition after ECS activation the PICS temperature shall not exceed 1773K (2732°F). The threshold temperature for ECS activation shall not exceed 1755K (2700°F).

(8) Weight - The HSA shall be designed for minimum weight with a goal for a flight worthy system not to exceed a maximum limit of 40.8kg (90.0 lbs).

5.1.3 C-103 CREEP STRENGTH CRITERIA

During the design phase of the HSHX the available applicable C-103 creep data was utilized to size the HSHX structure for the creep criteria stated in 5.1.2. At the time of the design an allowable 1% creep strength for the specified design life, of 22.6 MPa (3038 psi) was estimated from the available creep data and was so specified for the heat exchanger structure. As additional test data became available from the NASA material test program it became apparent that the original extrapolated 1% creep strength was over-estimated by a factor of approximately two. Consequently some of the original margin built into the design was diminished as a result of the updated 1% creep allowable. These design margins are discussed in 5.3. The latest NASA creep data is shown in Figure 5-1.

5.1.4 STRUCTURAL LOADING CRITERIA

The Heat Source Assembly is designed for a load factor of 50g acting along each of the three principal axes. This load factor was derived from dynamic response characteristics of similar spacecraft designs (LES 8/9). The insulation support frames need not be required to meet the 50g criteria because of their isolation due to the insulation foils. The frames can be designed for a 15 g load factor acting along each of the principal axes.

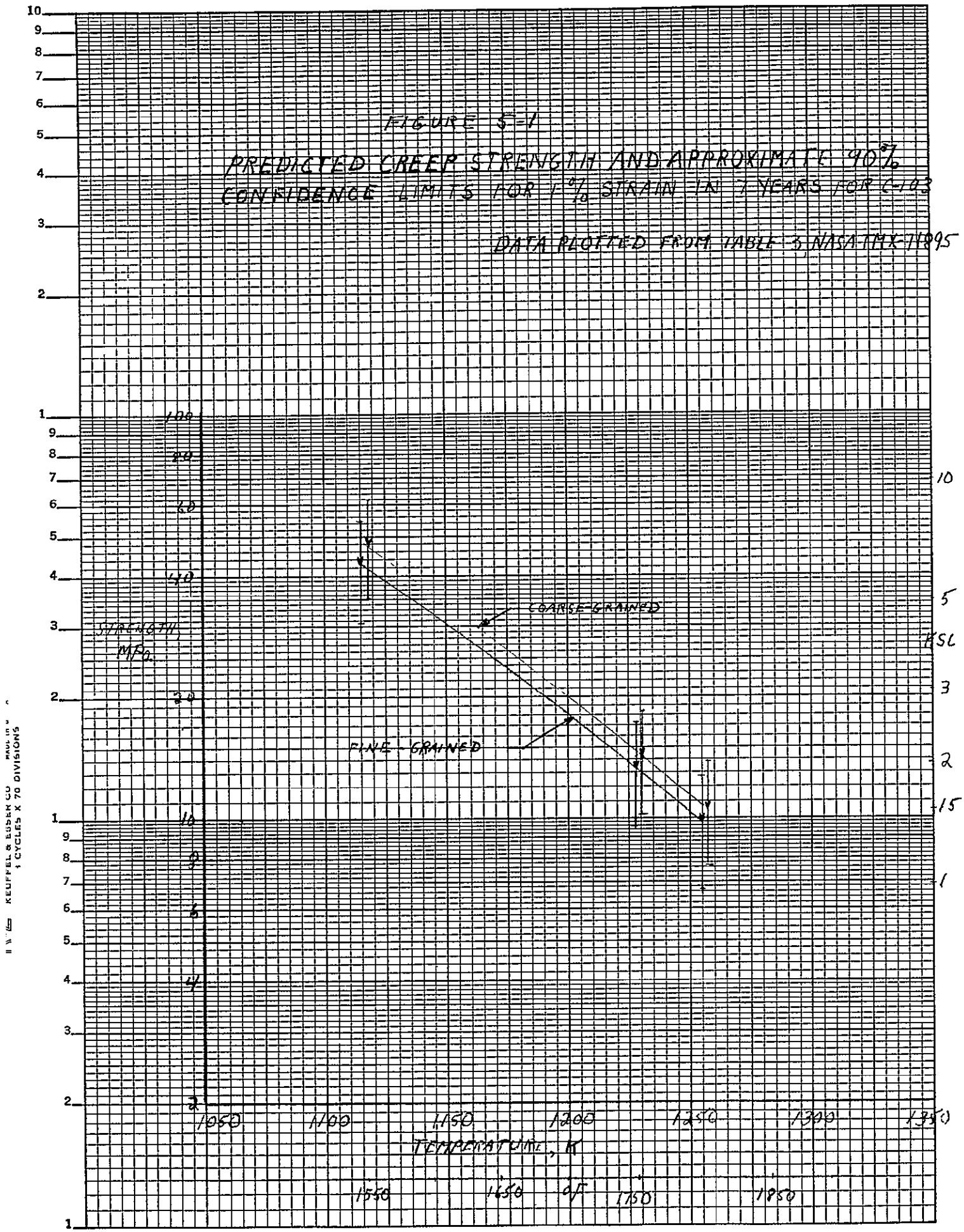
FIGURE 5-1
PREDICTED CREEP STRENGTH AND APPROXIMATE 90% CONFIDENCE LIMITS FOR 1% STRAIN IN 1 YEARS FOR C-103
DATA PLOTTED FROM TABLE 3 NASA TMX-11895
COARSE-GRAINED
FINE-GRAINED
STRENGTH, MPa
TEMPERATURE, K
1050
1100
1150
1200
1250
1300
1350
1550
1650
1750
1850
100
80
60
40
30
20
10
9
8
6
4
3
2
1
10
5
3
2
1.5
1
KSI

5.1.5 SAFETY CRITERIA

The safety design criteria relating to explosion, re-entry and impact environments, specified for the MHW Heat Source, which are given in Section 5.2 Volume I of NASA CR 121223, apply to the Titan IIIC mission HSA design. Additional safety requirements which apply to the temperature response of the Heat Source in the HSA configuration are as follows:

1. During an orbit operation the Heat Source external surface (girdle) temperature shall not exceed 1373K (2012°F). This is based on the MHW Specification for the Heat Source. This requirement shall also apply if the HSHX inlet temperature is increased to 1200K (1700°F).

2. During on pad operations, the external surfaces of the HSA shall not exceed 466K (380°F). This is to preclude auto-ignition of booster propellants. Additionally the maximum temperature of all refractory alloys exposed to air shall not exceed 523K (483°F) to preclude oxidation.

3. During the transient and steady state conditions after onset of an emergency condition, the Heat Source Post Impact Containment Shell (PICS) shall not exceed temperatures which could cause breach of the PICS and release of the isotopic fuel. These temperature limitations are time dependent and are as follows:

TABLE 5-1

PICS TEMPERATURE LIMITS

TEMPERATURE RANGE	MAXIMUM TIME AT TEMPERATURE
1773-1873K	10 Hours
1673-1773	50
1573-1673	200
1473-1573	1000
>1323K	On Impact

5.2 HSA CONFIGURATION

The HSA, without the Electric Heat Source (which is provided under the BIPS program contract) is shown in Figure 5-2 (Dwg. 47E313000). The HSA external housing, Figure 5-3 (Dwg. 47J313060), is a right cylinder, with rings on both ends to which are bolted elliptical domes shown in Figure 5-4 (Dwg. 47E313030). The housing and domes are fabricated from stainless steel for the ground demonstration tests.

Protruding from the cylindrical section near each end are 38.1 mm (1.5 in.) ID columbium alloy (C-103) tubes - inlet and outlet ports for the Heat Source Heat Exchanger. These tubes are joined to the housing by a bellows system to allow for thermal expansion differentials. Protruding from each dome are electrical connectors. The aft dome contains the thermocouple connectors primarily from the heat exchanger. These thermocouples should not have to be disturbed since the aft dome does not need to be removed once assembled. The forward dome which is removed to insert and/or remove the EHS or shipping support spacer, has the connectors for the EHS power leads. Thermocouple leads from the EHS and

forward end enclosure and preload screw are brought out through an additional connector in the forward end dome. However these thermocouples might have to be replaced each time the dome is removed because of their fragile nature.

Inconel "C" seals are used throughout the housing assembly to provide a leak-tight unit.

The mounting interface of the HSA consists of three self-aligning uniball bearings on the forward housing and one uniball bearing on the aft dome.

Internally, the HSA consist of provision for an Electric Heat Source (EHS), to be mounted in the center of the housing and supported through inconel preload screws to titanium end enclosures (spiders), Figure 5-5 (Dwg. 47C313092), on each end. The end enclosures in turn are mounted to the housing end ring flanges. This whole assembly is preloaded by tightening down the forward preload screw. This is necessary to keep the heat source under compression for all load conditions. The Heat Source Heat Exchanger (HSHX) encloses the volume around the EHS and is mounted off the EHS. During shipment of the assembly, in the event an EHS is not available, a shipping support spacer supports the HSHX.

The HSHX shown in Figure 5-6 (Dwg. 707E839), is made of columbium alloy (C-103) and consist of two circular headers, 238.76 mm (9.40 in.) center-

line diameter, 38. mm (1.50 in.) inside diameter. The headers are spaced 403.86 mm (15.9 in.) on centers and joined together by concentric cylinders (the HSHX core) with 148 flow vanes for Brayton working fluid flow. As indicated previously, each header has one port which penetrates the housing to provide connection to the rest of the Mini-Brayton System. The ports, at each end of the HSHX, are in line with each other.

Insulation for the HSA consists primarily of zirconium coated molybdenum and nickel multi-foil sheets wound over a C-103 columbium alloy cylinder This insulation cylinder is installed on the I.D. of the housing. The insulation is shown in Figure 5-7 (Dwg. 47D313043). Zirconium coated molybdenum multi-foil disks mounted between C-103 columbium alloy disk support (Figure 5-8, Dwg. 47C313038) are used on each end between the HSHX and the spiders to insulate the ends.

The C-103 HSA bellow assembly is shown in Figure 5- 9 (Dwg. 47C313008). A bellow assembly is installed over the inlet and outlet ducts to seal the HSA for auxiliary cooling. The bellows provide for thermal expansion of the housing during warmup after power is applied to the Electric Heat Source (or after an isotope heat source is assembled into the HSA in the case of a flight system). The bellows are qualified by proof pressure tests at 0.276 MPa (40 psi), thermal cycling to 1035K (1400^{o}F) three times, mechanical cycling 1000 times with $\pm$ 0.254 cm ($\pm$ 0.10 in) offset in two orthogonal axes and then leak testing to 10^{-9} std cc helium/sec.

FOLDOUT FRAME 1

FOLDOUT FRAME 2

ORIGINAL PAGE IS OF POOR QUALITY

ORIGINAL PAGE IS OF POOR QUALITY

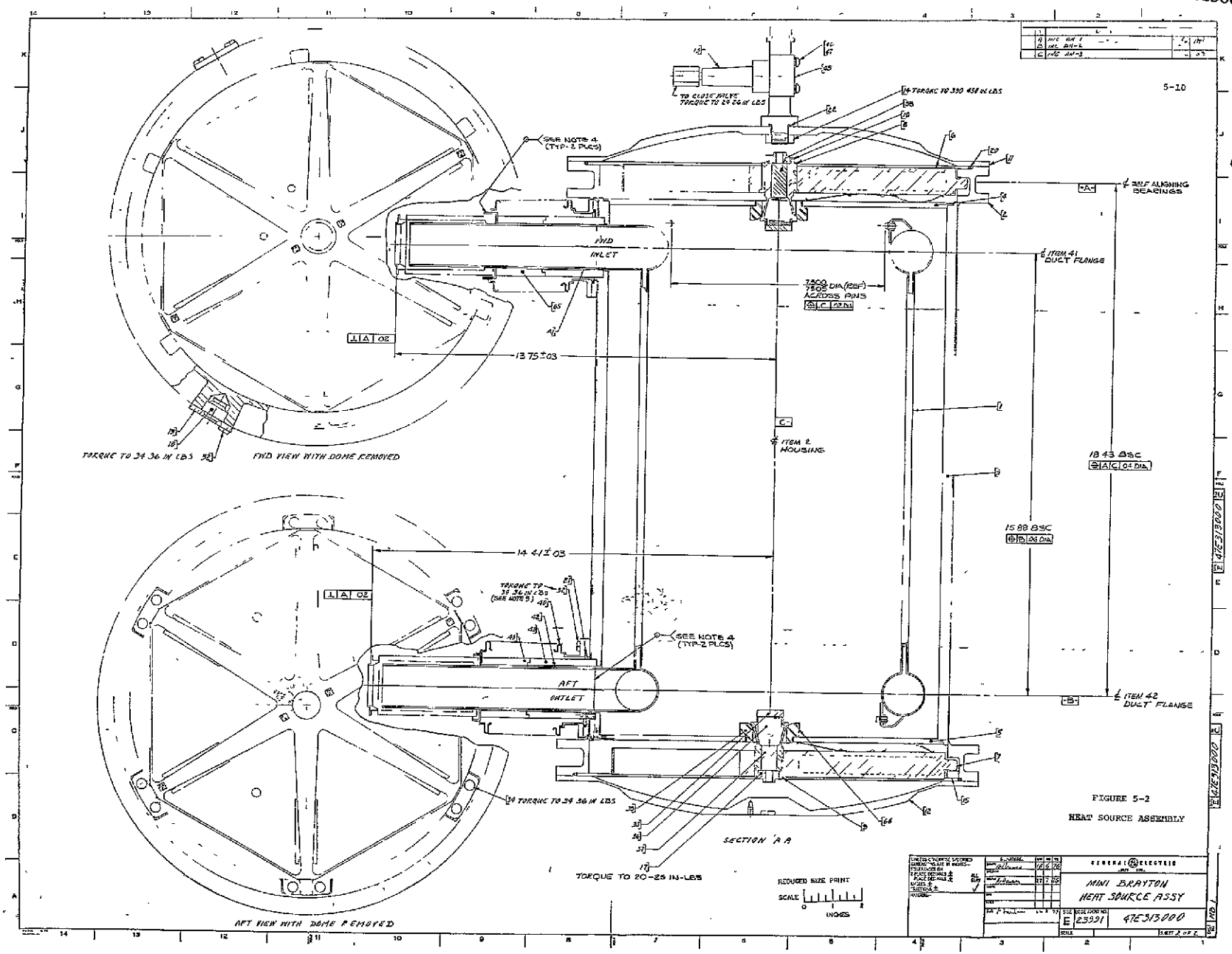

FIGURE 5-2

HEAT SOURCE ASSEMBLY

FOLDOUT FRAME 1

FOLDOUT FRAME 2

ORIGINAL PAGE IS OF POOR QUALITY

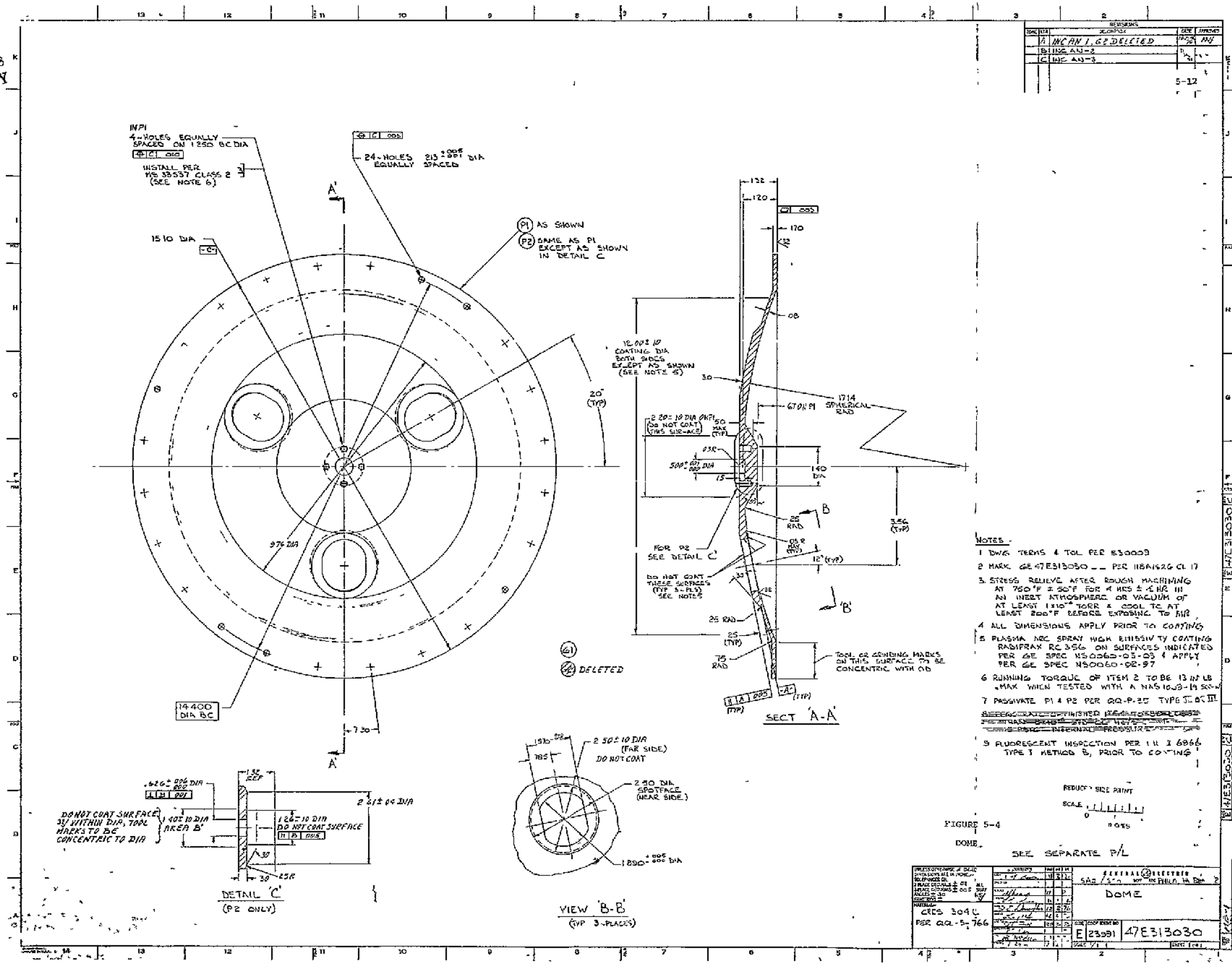

FIGURE 5-4 DOME

FOLDOUT FRAME

ORIGINAL PAGE IS
OF POOR QUALITY

FOLDOUT FRAME 2

47C313022 C

ZONE	LTR	DESCRIPTION	DATE	APPROVED
	C	INC. AN'S -1, -2 & -3		

5-13

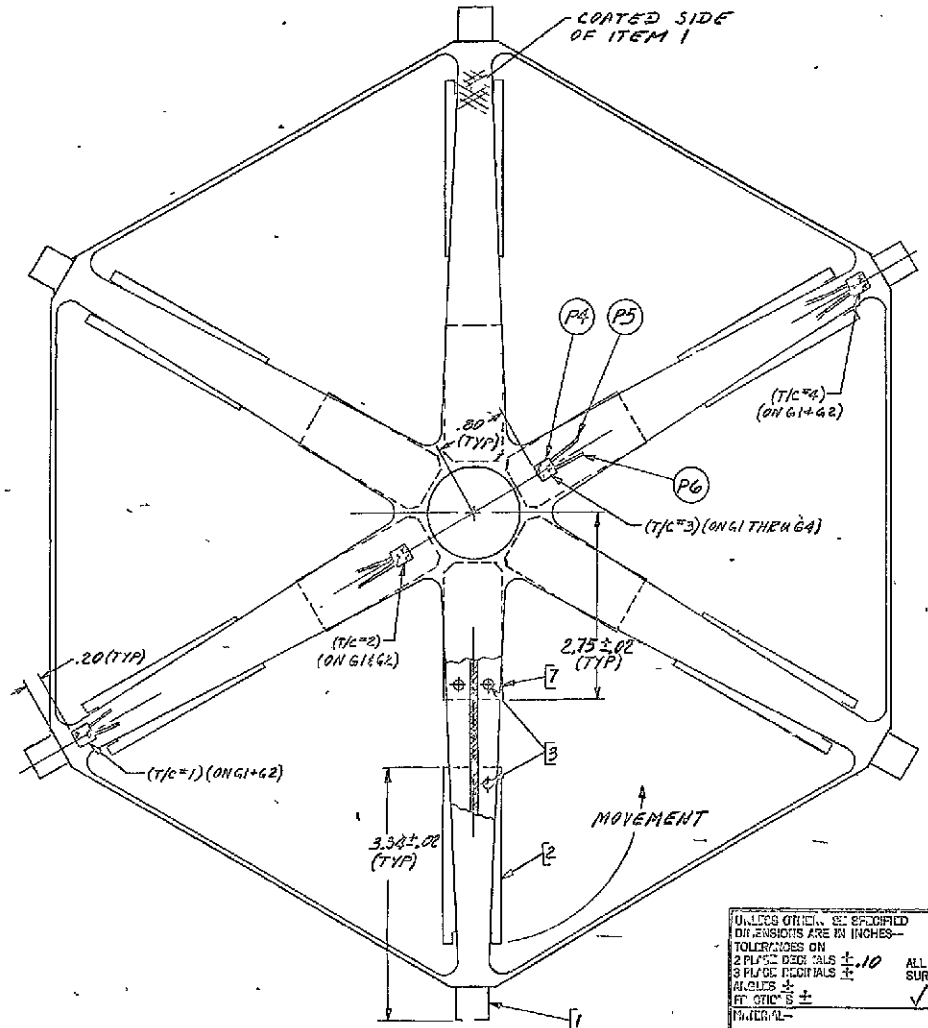

FIGURE 5-5
END ENCLOSURES

NOTES:

1. DWG TERMS & TOL PER S30009.
2. MARK "GE47C313022G_" PER 11BA1526, CL17.
3. SPRINGS, ITEM 2&7, TO BE CENTERED ON WEB OF ITEM 1 WITHIN .02 AND .066-.072 DIA HOLES MADE IN ITEMS 1&2 AND 1&7. ITEM 2 TO BE FREE TO MOVE AFTER FORMING HEAD ON ITEM 3.
4. HIGH EMISSIVITY COATING TO BE REMOVED FOR T/C AND RETAINER INSTALLATION, COATING REMOVAL SHALL NOT EXCEED AN AREA OF .30 IN. X .30 IN. T/C WIRES, P5 & P6, TO HAVE THEIR ENDS WELDED AND TWISTED TOGETHER 2 TO 5 TURNS. T/C JUNCTION TO BE POSITIONED UNDER RETAINER, P4, AND RETAINER WELDED TO ITEM 1 A MIN OF 3. PLACES.

REVISION STATUS TABULATION

							REV STATUS OF SHEETS
						CV	
		PL 60	PL 61	PL 62	PL 63	SH	

SEE SEPARATE PL

UNLESS OTHERWISE SPECIFIED DIMENSIONS ARE IN INCHES— TOLERANCES ON 2 PLACE DECIMALS ±.10 3 PLACE DECIMALS ± ANGLES ± FRACTIONS ± MATERIAL—	ALL SURF. ✓

DES		15	6 76
CHKD		7	9 76
APP'D		26	8 76
PROJ		31	8 76
MFG		31	8 76
PIECE P.C.		16	8 76
STRESS		20	8 76
QA		26	8 76
PD		1	9 76

GENERAL ELECTRIC
ESP&SSD DEPT LOC. PHILA PA

END ENCLOSURE WITH THERMOCOUPLES

SIZE	CODE IDENT NO	47C313022
C	23991	

SCALE 1/1 SHEET 1 OF 1

DWG NO 47C313022 REV C

FORM-P (5-73) PRINTED IN U.S.A.

FOLDOUT FRAME 1

ORIGINAL PAGE IS
OF POOR QUALITY

FOLDOUT FRAME 2

ZONE	SYM	REVISIONS DESCRIPTION	DATE	APPROVAL
	A	GENERAL CHANGES PER CN 1349	[illegible]	[illegible]
	B	GENERAL CHANGES PER CN 1351	[illegible]	[illegible]
	C	GENERAL CHANGES PER CN 1361	[illegible]	[illegible]
	D	CHANGES PER CN 1368	[illegible]	[illegible]
	E	CHANGES PER CN 1370	[illegible]	[illegible]
	F	CHANGES PER CN 1377	[illegible]	[illegible]
	G	CHANGES PER CN 1781	[illegible]	[illegible]

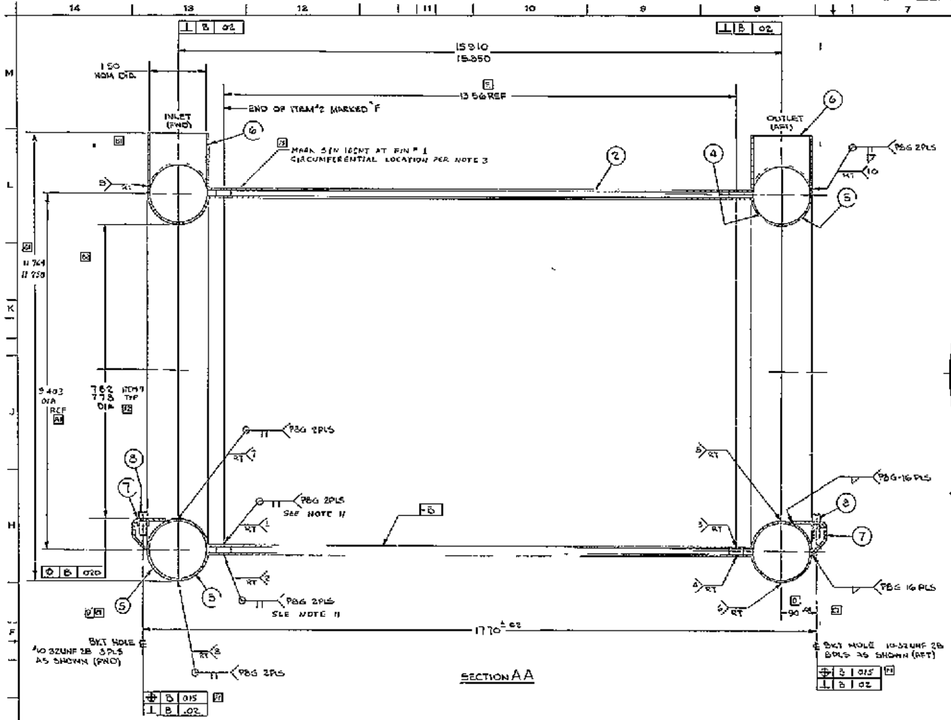

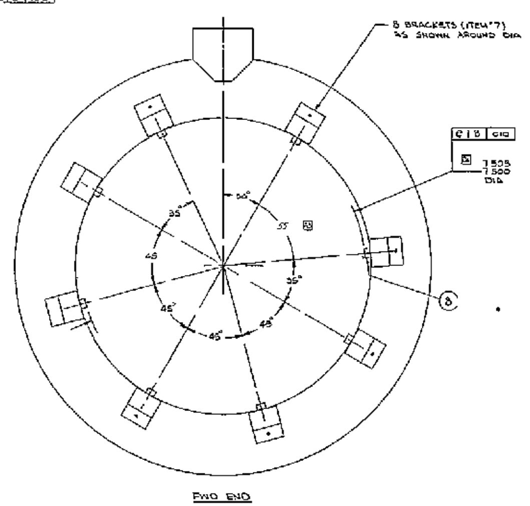

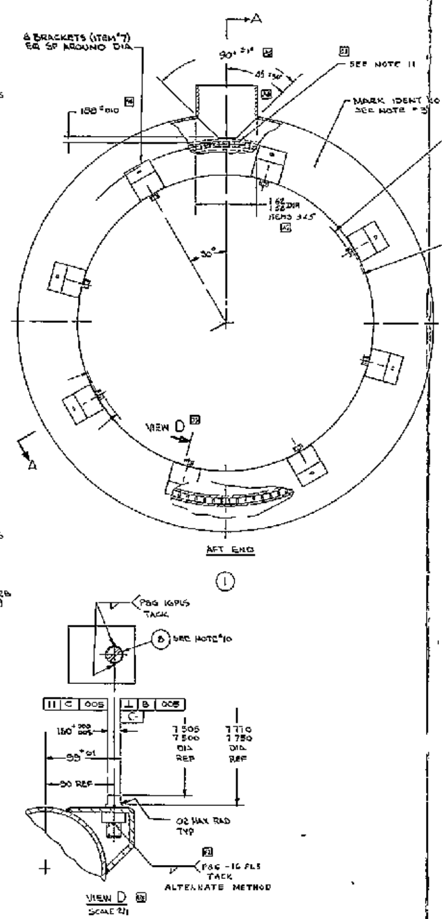

11 ALIGN HOLES IN PARTS 3 & 4 WITH CHANNELS IN PART 2 BEFORE WELDING

10 THREAD MOUNTING STUDS (ITEM #8) IN PLACE
TACK WELD AS SHOWN IN VIEW D
FINISH MACHINE 8 FWD STUDS (ZONE D9)
FINISH MACHINE 8 AFT STUDS (ZONE K3 L3, D6)

9 HELIUM LEAK TEST PER GE P3CYA16
LEAK RATE SHALL NOT EXCEED 10^{-6} STD CC He/SEC

8 DOUBLE WRAP IN .001 THK TANTALUM FOIL AND POST WELD ANNEAL PER GE P10CYA8 AT 2200°F FOR 1 HOUR

7 CLEAN OUTSIDE OF ASSY PER GE-P8AYA20, CLASS B PRIOR TO POST WELD ANNEAL

6 RADIOGRAPH INSPECT WELDS MARKED RT__ PER GE P3AYA14 NO LINEAR INDICATIONS PERMITTED POROSITY UP TO 0.015 DIAM PERMITTED IF SEPARATED FROM ADJACENT POROSITY BY 0.050 AND NO MORE THAN 3 PER 1 INCH LENGTH. POROSITY UP TO 0.005 DIAM PERMITTED IF SEPARATED BY 0.025 FROM ADJACENT POROSITY AND NO MORE THAN 6 PER 1 INCH LENGTH. STRINGER POROSITY 0.005 DIAM OR LESS PERMITTED IF NO LONGER THAN 1/16 INCH IN LENGTH, SEPARATED FROM ADJACENT POROSITY BY 0.025 AND NOT MORE THAN ONE SUCH STRINGER PER INCH

5 WELD PER GE P8GYA11

4 CLEANLINESS AND HANDLING PER GE P4BYA12

3 MARK IDENT NO PER GE P23AYA11, METHOD 7A3

2 SHOP AND TOL PER GE P1YA15

1 INTRP OF DWG PER GE P1YA16

FIGURE 5-6
HEAT SOURCE HEAT EXCHANGER

G04	G03	G02	G01	ITEM NO.	ZONE	SYM	IDENTIFICATION NO	NOMENCLATURE OR DESCRIPTION	MATERIAL OR NOTE
	16	16	16	8	F5		152B4027P1	MOUNT STUD	
	16	16	16	7	H7		152B4[illegible]P1	BRACKET	
	2	2	2	6	M7		152B4653P1	PORT	
	2	2	2	5	L7		101D9561P1	SCROLL, OUTER	
	1			4	L6		101D9580P6	SCROLL, INNER	
		1		4	L6		101D9580P4	SCROLL, INNER	
			1	4	L8		101D9580P2	SCROLL, INNER	
	1			3	F13		101D9580P5	SCROLL, INNER	
		1		3	F13		101D9580P3	SCROLL, INNER	
			1	3	M8		101D9580P1	SCROLL, INNER	
	1			2	L9		101D9560P3	CYLINDER	
		1		2	L9		101D9560P2	CYLINDER	
			1	2	L9		101D9560P1	CYLINDER	
	X			1	F5			ASSEMBLY	
		X		1	F5			ASSEMBLY	
			X	1	F5			ASSEMBLY	

QTY REQD

LIST OF MATERIAL

UNLESS OTHERWISE SPECIFIED DIMENSIONS ARE IN INCHES TOLERANCES ON
FRACTIONS ± DECIMALS ± ANGLES ±
ALL SURFACES ✓
MATERIAL
C LOSNAUD COLUMBIUM ALLOY

ASSEMBLY
HEAT SOURCE
HEAT EXCHANGER

GENERAL ELECTRIC
ASD
CINCINNATI, O

SCALE FULL

707E839 G

17287

FOLDOUT FRAME

ORIGINAL PAGE IS
OF POOR QUALITY

FOLDOUT FRAME 2

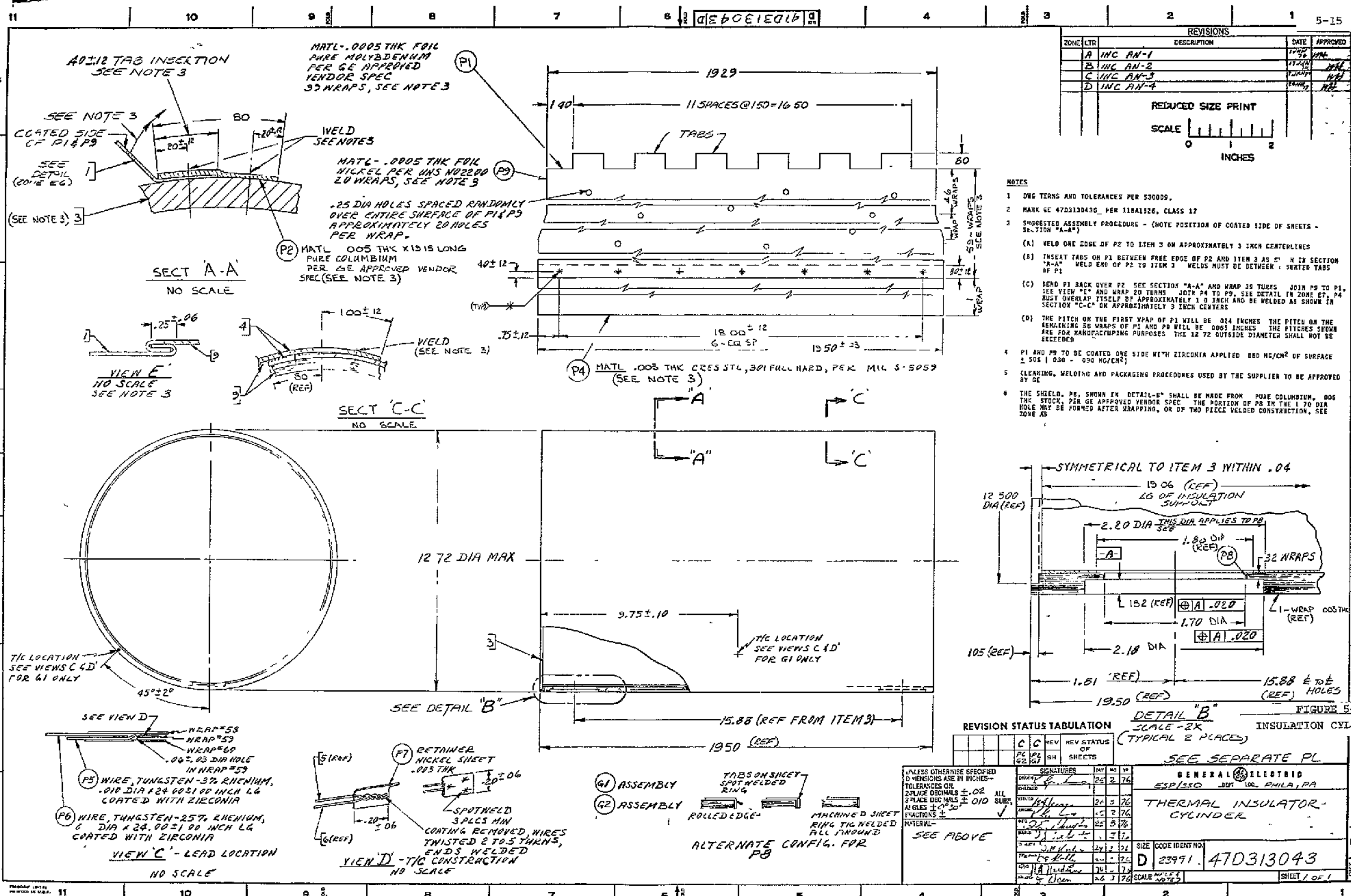

FIGURE 5-7
INSULATION CYLINDER

ORIGINAL PAGE IS
OF POOR QUALITY

FOLDOUT FRAME 1 | FOLDOUT FRAME 2

SIZE C 47C313038 REV E

REVISIONS				
ZONE	LTR	DESCRIPTION	DATE	APPROVED
	A	INC AN-1	14 VIAY 76	
	B	INC AN-2	17 JUN 76	
	C	INC AN-3	7 JAN 77	
	D	INC AN-4	24 JAN 77	
	E	INC AN-5		

MATL. NOTE-
P1, P5 & P9, .015 STOCK COLUMBIUM 103 ALLOY
P3, P4, P7, P8, P11 & P12, .0005 STOCK PURE MOLIBDENUM
MATERIALS PER SUPPLIER SPEC APPROVED BY GE

NOTES:-(CONT)

5. P3, P4, P7, P8, P11 & P12 TO HAVE 8 HOLES-.25 DIA., RANDOMLY SPACED OVER ENTIRE SURFACE. CARE MUST BE TAKEN DURING ASSEMBLY NOT TO ALIGN HOLES OF ADJACENT LAMINATIONS. (HOLES B, C & D MAY BE COUNTED IN THE 8 HOLE TOTAL)

NOTES:-

1. DWG TERMS & TOLERANCES PER 530009
2. MARK "GE47C313038G_" PER 118A1526, CLASS 17
3. ITEMS 2, 6 & 10 & P3, P4, P7, P8, P11 & P12 TO BE COATED ONE SIDE WITH ZIRCONIA HAVING AN APPLIED DENSITY OF .060 MG/CM² OF SURFACE ± 50% (.030-.090 MG/CM²)
4. CLEANING & PACKAGING PROCEDURES USED BY THE SUPPLIER TO BE APPROVED BY GE.

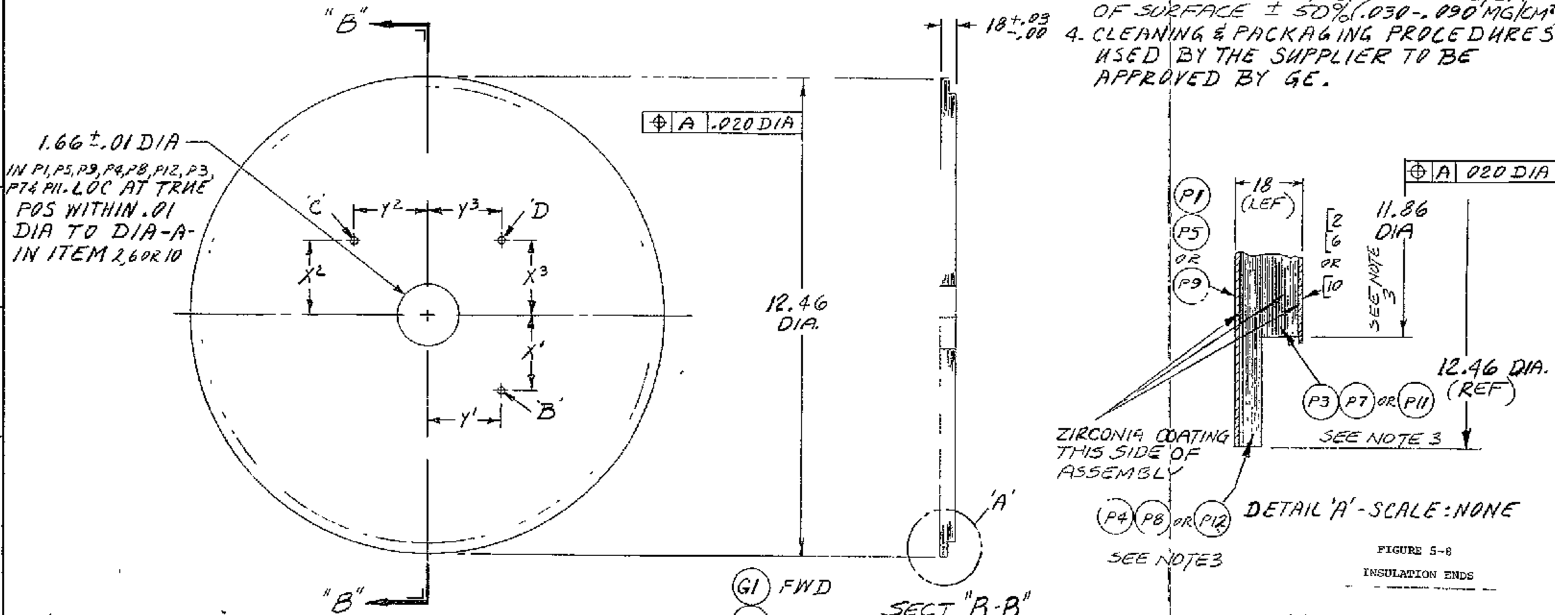

FIGURE 5-8
INSULATION ENDS

DIM X' & Y' ARE BASIC. HOLES LOC AT TRUE POS WITHIN .01 DIA IN RELATION TO HOLES 'B', 'C' & 'D' IN ITEM 2, 6 OR 10.

SUFFIX NO.	X'	Y'	DIA 'B' +.010 -.000	X²	Y²	DIA 'C' +.010 -.000	X³	Y³	DIA 'D' +.010 -.000
G1	4.060	0	.250	2.000	0	.266	1.000	1.732	.266
G2	4.060	0	.312	2.030	3.516	.312	2.030	3.516	.312
G3	4.060	0	.359	—	—	—	—	—	—

REVISION STATUS TABULATION

B	—	—	REV	REV STATUS OF SHEETS
PL G3	PL G2	PL G1	SH	

UNLESS OTHERWISE SPECIFIED DIMENSIONS ARE IN INCHES—
TOLERANCES ON
2 PLACE DECIMALS ± .02
3 PLACE DECIMALS ± .010
ANGLES ±
FRACTIONS ±
ALL SURF ✓

MATERIAL—
SEE MATERIAL NOTE

SIGNATURES		DAY	MO	YR
DRAWN	C S BROSZ	31	8	75
CHECKED	D Y Schmidt	15	9	75
ISSUED		26	3	76
ENGRG	D Y Schmidt	15	9	75
MFG		25	3	76
MATLS	R E	8	10	75
STRESS	D T Fox	17	9	75
THERMAL	R T Allen	15	9	75
DFA		7	10	75
PROGRAM		10	10	75

GENERAL ELECTRIC
ESP/SSO DEPT. LOC. PHILA, PA.

THERMAL INSULATOR - END

SIZE C CODE IDENT NO 23991 47C313038
SCALE HALF & NOTED SHEET 1 OF 1

DIST TO MB-1

FN-503-F (11-70) PRINTED IN U.S.A.

FOLDOUT FRAME

ORIGINAL PAGE IS
OF POOR QUALITY

FOLDOUT FRAME

SIZE		REV
C	47C313008	A

SOURCE OF SUPPLY

SUFFIX	VENDOR PART NO	VENDOR	FSCM
P1	74523	METAL BELLOWS CO SHARON, MASS	07699

REVISIONS

ZONE	LTR	DESCRIPTION	DATE	APPROVED
	A	INC - AN-1	HRL	17MAY76

5-17

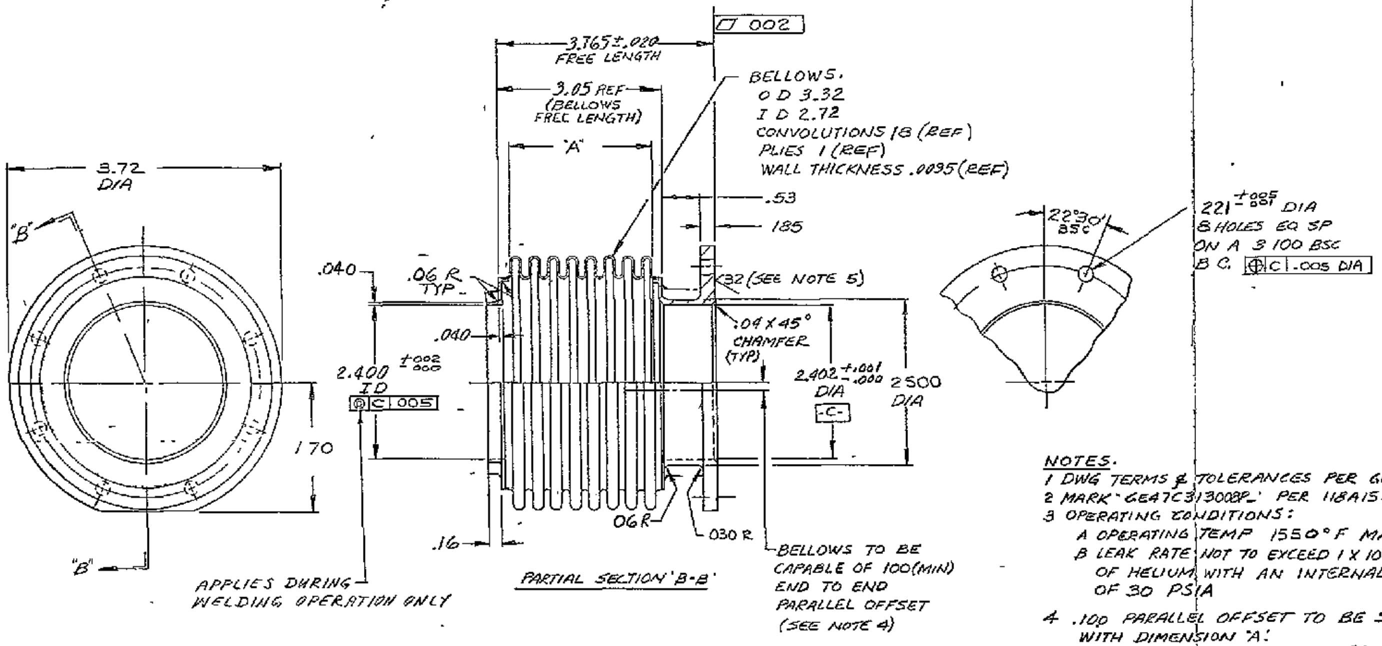

DIM "A" (SEE NOTE 4)
FREE LENGTH = 2.75
EXTENDED LENGTH = 2.85 MIN
COMPRESSED LENGTH = 2.65 MAX

NOTES.
1 DWG TERMS & TOLERANCES PER GE SPEC 530009
2 MARK "GE47C313008P_" PER 118A1526 CL 16 OR 17
3 OPERATING CONDITIONS:
   A OPERATING TEMP 1550°F MAX
   B LEAK RATE NOT TO EXCEED 1×10^{-7} scc/sec OF HELIUM WITH AN INTERNAL PRESSURE OF 30 PSIA
4 .100 PARALLEL OFFSET TO BE SIMULTANEOUS WITH DIMENSION "A".
5 TOOL OR GRINDING MARKS TO BE CONCENTRIC WITH O.D.

FIGURE 5-9
HSA BELLOWS

(P1)

SOURCE CONTROL DRAWING

ONLY THE ITEMS LISTED ON THIS DRAWING IN THE "SOURCE OF SUPPLY" TABULATION HAVE BEEN TESTED AND APPROVED BY ISAO FOR USE ON B T P S EQUIPMENT. A SUBSTITUTE ITEM SHALL NOT BE USED WITHOUT PRIOR WRITTEN APPROVAL BY ISAO

NO CHANGES SHALL BE MADE TO THE DESIGN, CONFIGURATION, MATERIAL, PARTS OR MANUFACTURING PROCESSES WITHOUT PRIOR WRITTEN APPROVAL OF PURCHASING

UNLESS OTHERWISE SPECIFIED DIMENSIONS ARE IN INCHES—
TOLERANCES ON
2 PLACE DECIMALS ±.02
3 PLACE DECIMALS ±.005
ANGLES ±0°30'
FRACTIONS ±
ALL SURF. 125 √

MATERIAL—
COLUMBIUM 103
PER GE APPROVED
VENDOR SPEC

SIGNATURES	DAY	MO	YR
DRAWN [signature]	9	3	76
CHECKED			
ISSUED [signature]	22	3	76
ENGRG [signature]	18	3	76
MFG [signature]	18	3	76
MATL [signature]	22	3	76
STRESS [signature]	22	3	76
THERMAL [signature]			
P.A. [signature]	19	3	76
PROG [signature]	22	3	76

GENERAL ELECTRIC
ISAO/SS DEPT LOC BLDG B, PHILA PA

BELLOWS

SIZE	CODE IDENT NO	
C	23991	47C313008

SCALE NONE SHEET 1 OF 1

DIST TO MB-1

5.2.1 ASSEMBLY PROCEDURE

The external configuration of the HSA consists of a stainless steel cylinder 32.41 cm (12.76 in.) I.D. with 0.081 cm (0.032 in.) thick walls. On each end of the cylinder is attached a flange for assembly of the elliptical end dome and end enclosure support.

The multi-layer foil insulation cylinder is inserted into the housing and supported on the forward end by a welding assembly fixture end plate. Next, the HSHX is attached to the aft end plate of the welding fixture and is installed into the housing. The HSHX is then moved off center as far as possible by means of the welding fixture.

Government furnished (GFE) extension ducts are welded to the inlet and outlet ports; the HSHX is then returned to the housing centerline position. Molybdenum multifoil insulation is then wrapped around the inlet/outlet extension ducts and the housing bellows and "C" seals slid over this. The inboard flange of each bellows is then bolted to the housing with "C" seals in place. The outboard lip of each of the two bellows is then welded to a "Z" ring on the inlet/outlet extension ducts. With the forward end of the HSHX supported by the welding fixture, the Electric Heat Source graphite supports are installed. Next the multifoil end insulation, pre-load screw, barriers, bearing disks and end enclosure are installed and T/C's leads are fed thru the insulation. The assembly is then turned over and the forward end welding fixture plate is removed.

The EHS is installed and the graphite heat source supports put in place. The pre-assembled end enclosure, pre-load screw and multi-foil end insulation are now installed while feeding EHS power leads thru the multi-foil. At this point the assembly is pre-loaded by torquing the pre-load screw.

The EHS power cables are now connected to EHS leads. T/C leads and power cables are routed to connectors mounted in the elliptical end dome. Also mounted on the forward end dome is a valve assembly which is used for gas management and auxiliary cooling. The dome and "C" seal are then attached to the housing flange and torqued.

Aft end T/C's are now routed to connectors mounted in aft end dome. The dome and "C" seal are bolted and torqued to housing flange, the system is now vacuum sealed and ready for testing.

5.3 STRUCTURAL ANALYSES AND DESIGN

This section contains brief descriptions of the structural analyses and design trade-offs of the HSHX and HSA support components.

5.3.1 HSHX DESIGN

5.3.1.1 HSHX Joint Header Configuration Trade Off and Analysis

Detailed stress analyses were performed to determine the optimum HSHX configuration (lowest weight and ease of fabrication) which meets the 1% creep stress design criterion.

Stress analyses were performed on five different toroidal header design concepts. Four design concepts were finalized to the point where they met a prescribed 21 MPa (3000 psi), 1% creep stress allowable at 1255K (1800^{o}F) at 100,000 hours used in early design trade-offs. Two of these designs, the common center line (℄) with conical interface, and common ℄ with no fillet radii were found to be feasible designs. The common ℄ with no fillet radii design (Figure 5-10) was selected as the most attractive due to its low stress levels, 12 MPa (1.784 psi) maximum stress, and low weight, 2 kg (4.4 lbs.) for both headers. It consists of a cylindrical center section (core) with toroidal headers at each end. The cylindrical section is composed of an inner cylinder with machined fins to form flow channels and an outer cylinder, welded together using the hot isostatic pressure process. The core and toroidal headers are gas tungsten arc welded together to form the HSHX pressure vessel assembly.

FIGURE 5-10

HEAT EXCHANGER

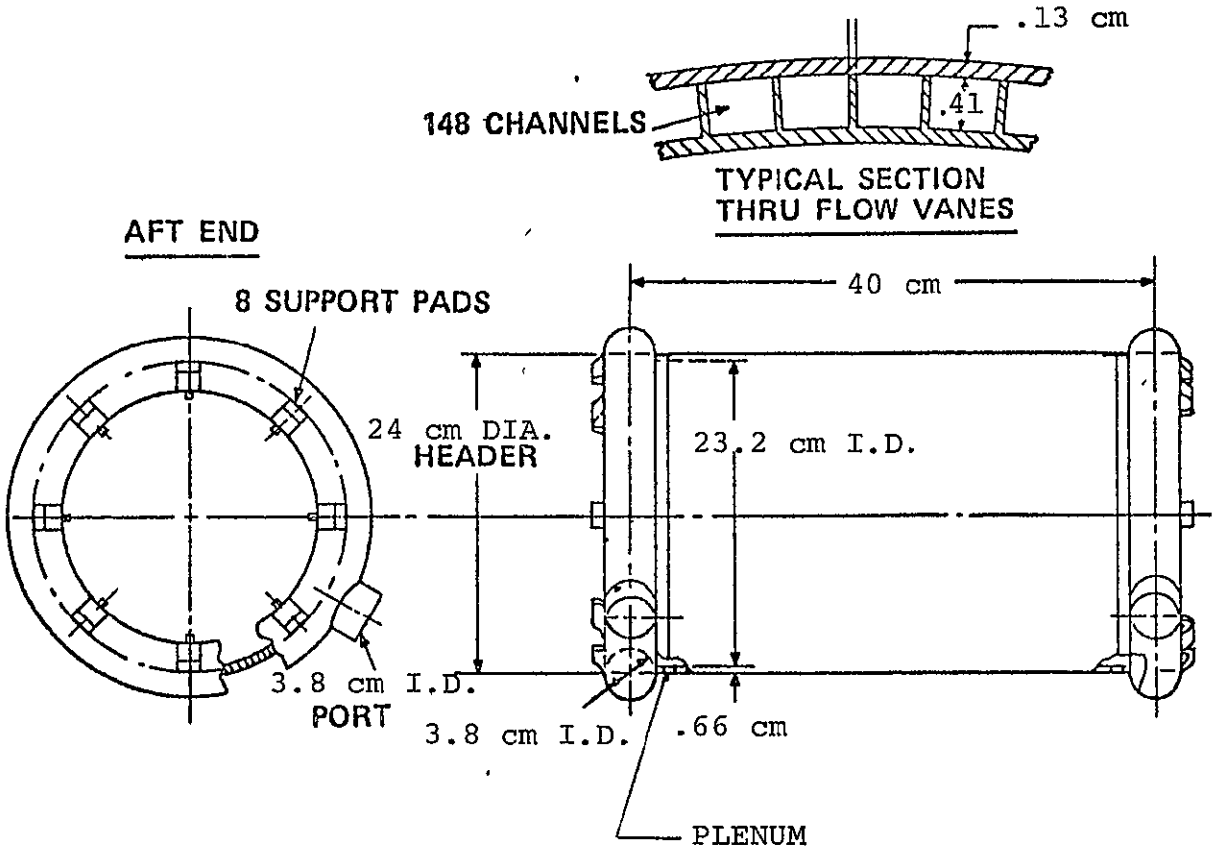

Stress analyses were performed to determine the stress levels in the toroids and at the joint between the toroids and the cylindrical-fin center section. The stress analysis utilized the "SNAP" computer program, (Reference 8), a finite element program utilizing shells of revolution with axisymmetric loading.

This common ℄ design was analyzed for three variations: a) a full fillet radii, b) a conical interface, and c) no fillet radii.

Sketches of these basic variations are shown in the first column of Figure 5-11. In order to meet the "early" 21 MPa (3000 psi) allowable stress level, the configuration of each design variation would have to be radically altered to those shown in the second column of Figure 5-11 with the exception of the selected Configuration #c.

FIGURE 5-11 COMMON CENTER LINE HEADER VARIATIONS

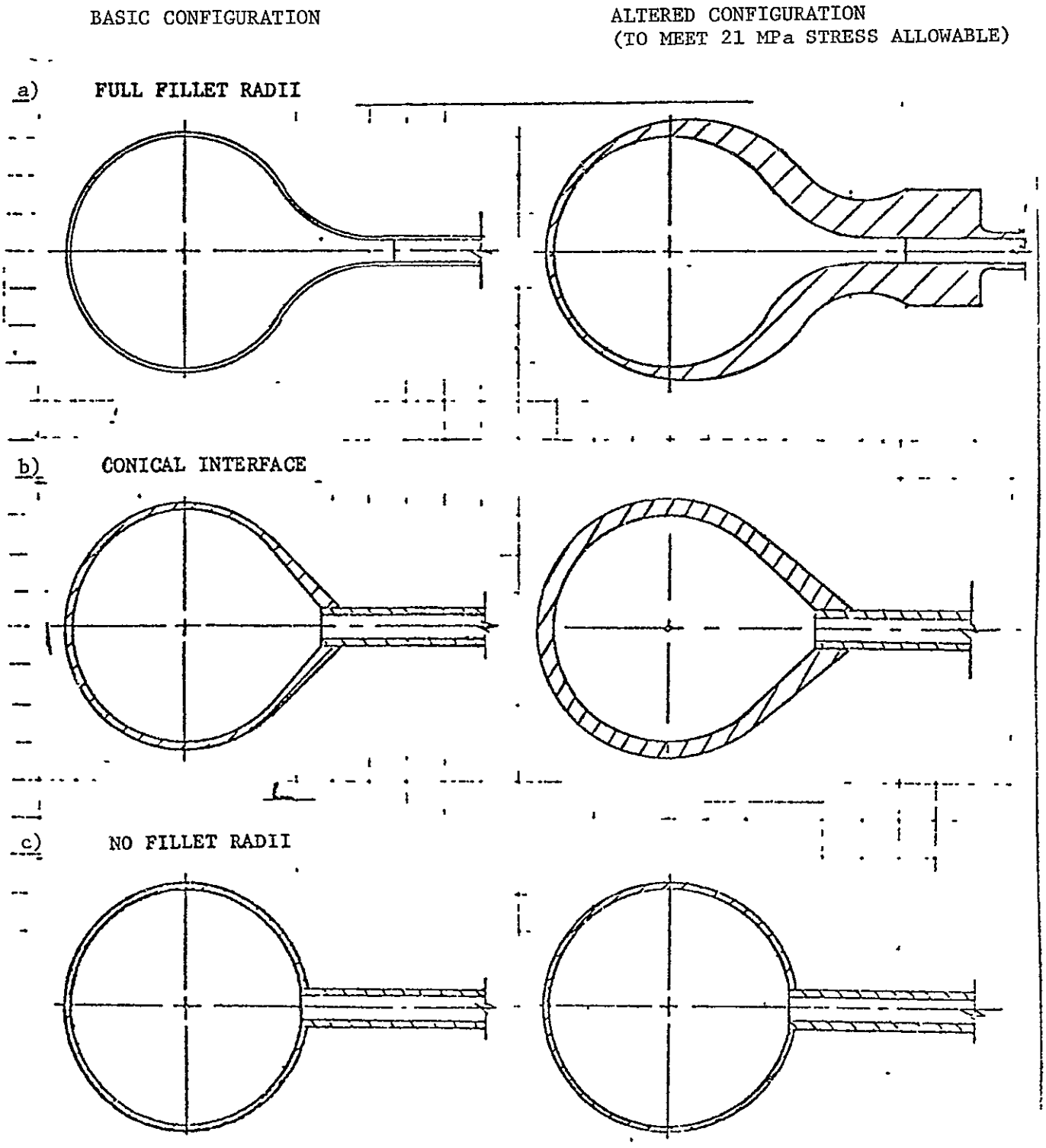

(Approximately to Scale)

The following table shows pertinent data from the configuration computer run for each variation which resulted in the lightest weight HSHX that meets the 3000 psi creep allowable for the particular design variation.

TABLE 5-2 SUMMARY OF HSHX DESIGN VARIATIONS
(SEE FIG. 5-11)

DESIGN VARIATION	MAX. STRESS IN HEADER		HEADER WEIGHT		EASE OF MANUFACTURE	SECTION THICKNESS	
	MPa	ksi	kg	lbs		cm	in
a	21	3.0	8.8	19.4	Difficult	.13-.89	.05-.35
b	21	3.0	5.0	11.1	Easier	.25-.57	.10-.225
c	12	1.8	2.0	4.4	Easiest	.13	.05

The selected HSHX design common ℄ without fillet radii is clearly the lightest weight design with the lowest stress profile and undoubtedly the simplest to fabricate from among the designs. The calculated header stress of 12 MPa (1784 psi) and plenum (see Figure 5-10) stress of 17 MPa (2488 psi) results in margins of safety of respectively 0.55 and 0.1 for a maximum allowable stress of 19 MPa (2774 psi), the original contractual specification of 1% allowable creep at 1270K (1825°F) for 10 years. Reevaluation of design margins based on the updated NASA creep test data extrapolations and revised lifetime requirements are given in Table 5-3. This table shows the predicted stress levels and temperatures in the critical regions of the HSHX. The "starved" region represents those flow channels where the flow rates are lowest due to pressure drop variations. These are the highest predicted HSHX operational temperatures. The latest NASA creep test data extrapolated to 7 years (the revised

TABLE 5-3

HSHX STRESS SUMMARY

HSHX REGION	PREDICTED MAX TEMP.				PREDICTED MAX STRESS				ESTIMATED 1% - 7 YR CREEP STRESS (FINE GRAIN)				DESIGN MARGIN			
	Nominal Flow		Starved Region		0 41 MPa (60 psi)		0 79 MPa (115 psi)		At Starved Temp.		28K(50°F) Higher Than Starved Temp		At Starved Temp		28K(50°F) Higher Than Starved Temp	
	K	°F	K	°F	MPa	PSI	MPa	PSI	MPa	PSI	MPa	PSI	0.41 MPa (60 PSI)	0.79 MPa (115 PSI)	0 41 MPa (60 PSI)	0.79 MPa (115 PSI)
CORE	1175	1655	1190	1685	4 8	691	8 2	1190	20	2900	15	2175	3.2	1.4	2 1	0.8
PLENUM	1195	1690	1210	1720	8 9	1298	17	2488	16	2320	12	1740	0.8	0	0 3	-0 3
HEADERS	1215	1730	1235	1760	6 4	931	12	1784	12	1740	9	1305	0 9	0	0 4	-0 3

HSA lifetime requirements) are shown for both the "starved" temperatures and for temperatures 28K above these maximum HSHX operational temperatures. The two pressure levels 0.41 MPa and 0.79 MPa for which HSHX stress levels are given represent the 1.3 KW BIPS system pressure (the anticipated operational pressure for the HSA's) and the HSA contractual design specification respectively. It is evident that with the reduced 1% creep strength allowables, the diffusion welded core still has large positive design margins. At the anticipated BIPS system operational pressure the headers and plenum area also exhibit positive design margins, even at temperatures exceeding the maximum predicted operational levels by 28K. At the HSA design specification pressure (0.79 MPa), the stress levels in the headers and plenum are just about at the 7 yr-1% creep stress allowable at the maximum predicted temperature levels. At a temperature 28K higher, however, they exhibit negative design margins.

5.3.1.2 EFFECT OF UNWELDED FINS

The purpose of this analysis was to determine the extent of lack of welding of fins to the outer HSHX cylinder that could be tolerated without exceeding design limits. The results are given in Figure 5-12 which shows the maximum stress levels as a function of unwelded fin length. Table 5-4 summarizes the results of the analyses, giving the maximum fin and shell stresses for cases without any fins unwelded up through the condition of three adjacent fins without welding.

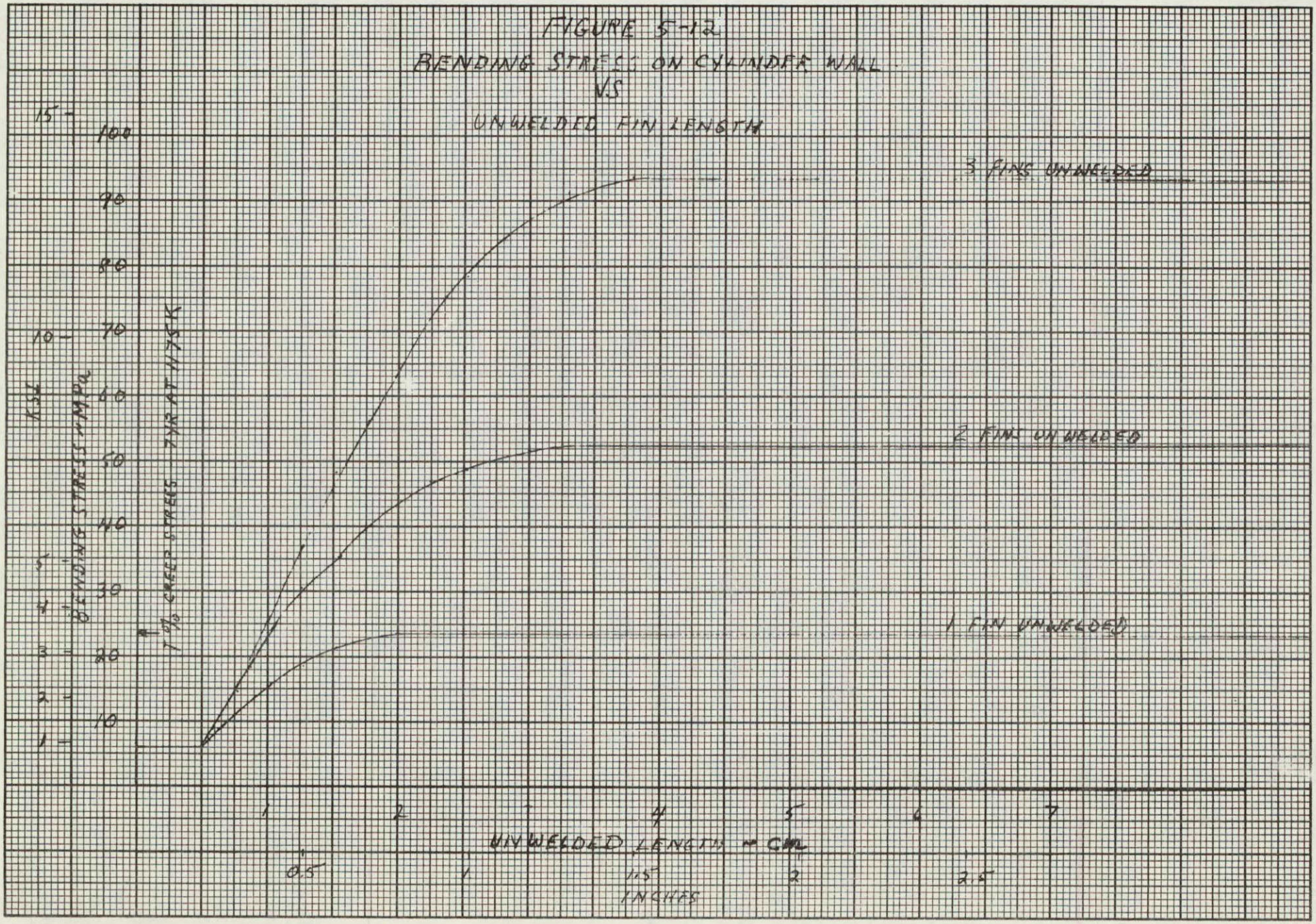

TABLE 5-4

HSHX MAXIMUM STRESS LEVELS FOR UNWELDED FINS
(AXIAL PLUS BENDING)

NUMBER OF FINS UNWELDED	MAXIMUM TENSILE FIN STRESS MPa	PSI	MAXIMUM TENSILE SHELL STRESS MPa	PSI
0	6.5	946	8.2	1190
1	16.3	2364	23.4	3388
2	33.5	4864	52.4	7597
3	53.9	7812	93.3	13537
every other fin	14.8	2144	31.2	4532
every third fin	17.0	2462	24.0	3488

The maximum stress of 24 MPa (3488 psi) for the case of every third fin completely unwelded along its axial length is approximately equal to the 1% 7 yr creep stress at 1175K (1655^{o}F) which represents the nominal maximum predicted operational temperature in the diffusion welded region of the HSHX. Thus, for the 0.79 MPa (115 psi) specification pressure of the HSA, a situation in which every third fin is totally unwelded would result in stresses in the diffusion welded section of the HSHX at about the 1% creep limit.

TABLE 5-5

EFFECT OF PARTIAL WELDING

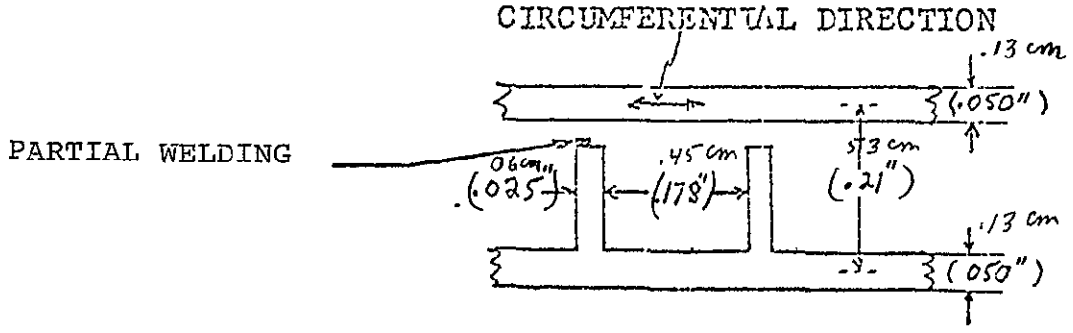

PRESSURE LEVEL	0.41 MPa (60 PSI)	0.79 MPa (115 PSI)
Direct Tension Stress in Fin - Full Weld (Bending Stress not considered)	2.9 MPa (427 PSI)	5.6 MPa (819 PSI)
1% - 7 Yr. Fine Grain Creep at 1175K (1655°F) = 23 MPa (3360 PSI)		
Margin of Safety with Stress Concentration Factor K_t = 2.0	2.9	1.1
Minimum Circumferential Weld Length with K_t = 2.0	.016 cm (.0064 in)	.031 cm (.0122 in)

The Columbium alloy support joints are simple shear clips spaced every 45° (except for the forward end) around the periphery of the two parts. Each support joint consists of a bracket with a stud welded to the heat source heat exchanger. The stud interfaces with the mating support on the heat source.

The mating surfaces of all the brackets forms a 19 cm (7.5 in) circle about the heat source heat exchanger and heat source center lines.

5.3.2 HSA SUPPORT STRUCTURE

5.3.2.1 Housing

The purpose of this analysis was to structurally size the housing which is the primary support for the HSA.

A flight design beryllium housing (actual GDS hardware is stainless steel to minimize cost) was analyzed for inertia loads due to launch and for accident explosion blast over pressure loads. Maximum calculated stresses are in the range of 207 MPa (30,000 psi) tension and 5 MPa (700 psi) shear. These loads are within material allowables.

The HSA housing serves the following purposes:

1) It provides a sealed container for auxiliary cooling on the pad and protects components from external environments in space, and
2) It supports the HSA.
3) It provides the mechanical mounting points to the BIPS hardware.

The housing consists of a cylindrical section and end domes. The cylindrical section consists of a thin walled cylinder with integral end rings. The end rings include a radial "U" ring section for

attaching the end dome. The end rings serve three functions; the first of these is to stiffen the cylindrical section and reduce relative motion between the spherical segmented end domes and the cylindrical section. The second function of the ring section is to react heat source and heat source heat exchanger launch loads.

The heat source heat exchanger is attached to the heat source by a series of clips at each end as discussed in the previous paragraph. The heat source is held in place by end enclosure supports at each end.

The third function of the housing is to transmit launch loads to the heat source assembly mounting points and hence to the BIPS hardware.

Housing loads were calculated for the three launch orientations; 1) 50 g's applied radially up at the ℄ of the heat source assembly, 2) 50 g's applied radially to the side at the ℄ of the heat source assembly, and 3) 50 g's applied axially at the ℄ of the heat source assembly, (Fifty g's was the load criteria for the MHW-RTG). In addition, housing loads were calculated for a 45 psi blast over pressure (Figure 5-1 of reference 9). The maximum stresses as indicated previously were within beryllium allowable stress levels.

5.3.2.2 End Enclosures

The purpose of this analysis was to verify the structural integrity of the heat source end enclosures which are essentially the same as the MHW-RTG end enclosures.

These titanium end enclosures were structurally analyzed for inertia design loads of 50 g's applied to the heat source along any axis. The assembly showed positive margins of safety for these conditions.

The heat source end enclosures shown previously in Figure 5-5 (Drawing 47C313092), support the heat source and the heat source heat exchanger and react the inertia loads transmitted by them. These loads are then transmitted to the heat source assembly housing.

The end enclosures consist of a hub to which the heat source is mounted and six radial legs equally placed around the hub. The enclosures are made from titanium alloy (Ti-6AL-2Sn-4Zr-2Mo).

End enclosure loads were calculated for three launch orientations; 1) 50 g applied radially up at the heat source assembly center line, 2) 50 g applied radially to the side at the heat source assembly center line, and 3) 50 g applied axially at the heat source assembly center line.

5.4 HYDRAULIC ANALYSIS

The hydraulic analysis of the HSHX included a pressure drop and flow distribution analysis of the core, headers, inlet and exit ducts, and an evaluation of the square to circular transition from the core to the header. Uniform flow distribution in the core requires that the static pressure profiles in the inlet and exit headers be parallel, i.e., each core flow channel have the same static pressure drop. The HSHX configuration has inlet and outlet ducts on the same side, providing a "U" shaped flow path through the core. Heyda and Fulton, Reference 10, have done extensive analytical work on this flow configuration and their loss factors and balancing techniques have been employed.

As flow enters the core, the velocity in the inlet header steadily decreases along its length. This deceleration results in a static pressure rise along the inlet header, which in the "U" shaped flow configuration somewhat offsets the loss in the outlet header.

Figure 5-13 presents the results of computer predicted flow distribution on pressure drop for inlet and outlet header diameters of 3.8 cm (1.5 in) and a HSHX nominal flow of 0.053 kg/sec. (0.117 lb./sec.). A recovery factor (β) of 0.75 was used for the inlet header, and a 2.0 velocity head loss (γ) was assumed in the exit header. Fluid channel flow rates vary from 0.93 to 1.14 times the average flow. Since flow thru the core is laminar, flow is very nearly proportional to ΔP; therefore, Figure 5-13 provides a good graphical representation of the core flow distribution. The strong effect of inlet and exit duct size on overall

HSHX pressure drop can be clearly seen. For the nominal flow of 0.053 Kg/sec., inlet and outlet ducts of 3.2 cm (1.25 in.) yield an overall ΔP of about 1.86 kPa/0.27 psi as compared with 1.24 kPa/0.18 psi for 3.8 cm meter (1.5 in.) diameter ducts, the latter being the selected duct size for the design.

Flow could be balanced by increasing the pressure rise in the inlet header or by decreasing the loss in the outlet header. Theoretically uniform flow header sizes can be readily calculated by balancing the header diameters as follows:

$$\frac{D_{INLET}}{D_{EXIT}} = \left(\frac{\beta}{\gamma}\right)^{\frac{1}{4}}$$

where: D_{INLET} = Inlet Header Diameter

D_{EXIT} = Exit Header Diameter

β = Inlet Header Recovery Factor = 0.75

γ = Outlet Header Velocity Head Loss = 2

Hence $\frac{D_{INLET}}{D_{EXIT}} = 0.78$

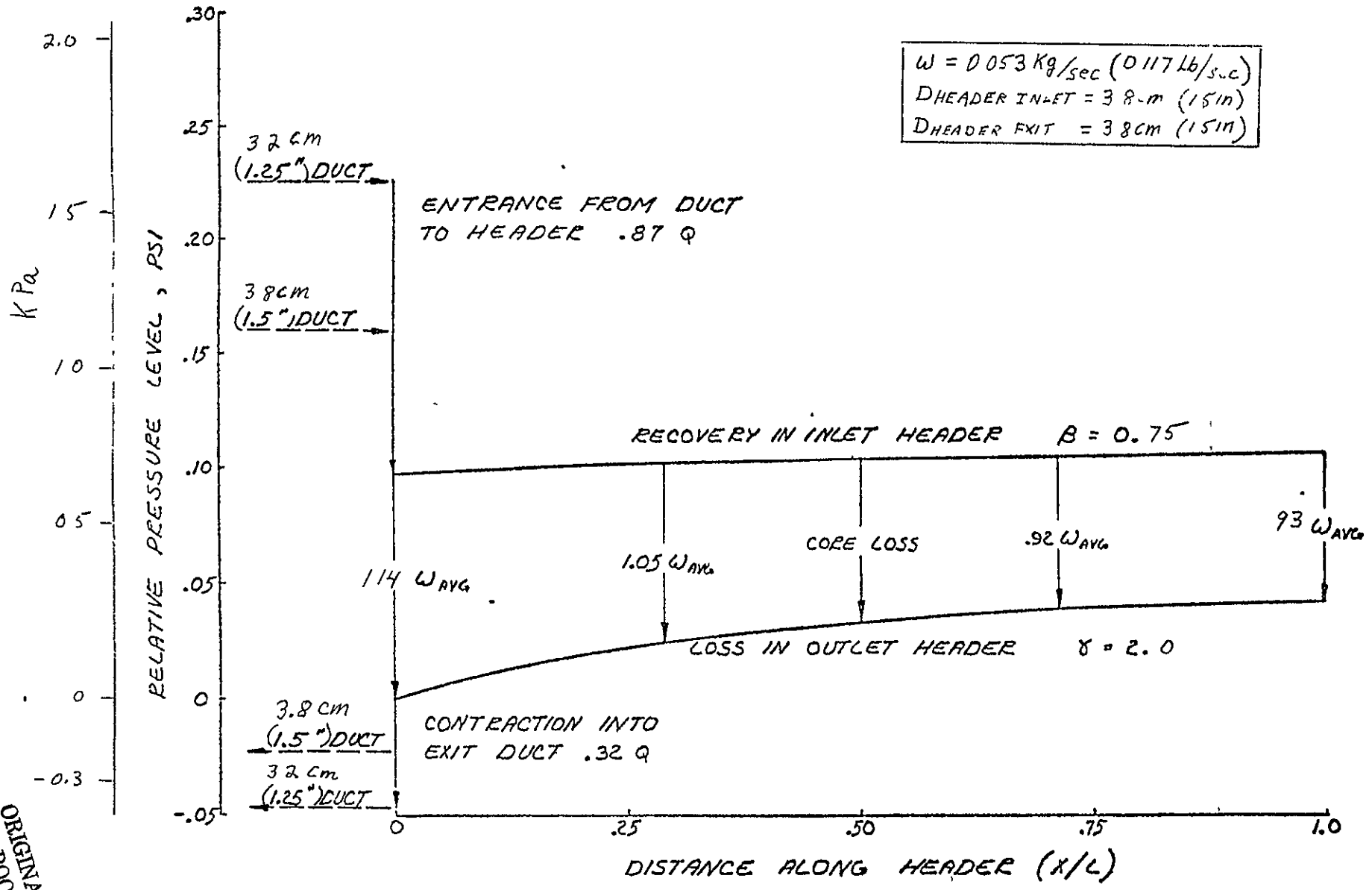

FIGURE 5-13 HSHX PRESSURE PROFILE

Uniform flow distribution could thus be achieved by maintaining the 3.8 cm (1.5 in.) diameter inlet header and increasing the exit header diameter to 4.9 cm (1.92 in.) or by maintaining the 3.8 cm diameter exit header and decreasing the inlet header diameter to 3.0 cm (1.17 in.). Increasing the outlet header diameter would be the safest approach, since the flatness of the resultant pressure profiles does not necessitate so accurate a determination of β and γ . It is questionable if the potential ΔP reduction from uniform flow is worthwhile in view of the large entrance and exit duct losses. Attaining perfectly uniform flow at the expense of additional tooling, cost, and weight associated with a larger diameter exit header is not warranted. Therefore uniform diameter inlet and exit headers were selected with a diameter of 3.8 cm (1.5 in.).

In order to facilitate fabrication of the HSHX machined inner header, circular flow channel holes are incorporated. The circular holes in the header are .41 cm (0.16 in.) diameter and are .64 cm (0.25 in.) long with a .82 cm (0.32 in.) long plenum section separating them from the rectangular core. The circular inlet holes increase the core ΔP by .16 kPa (0.023 psi) while the flow imbalance ΔP in the headers decreases .04 kPa (0.005 psi) for a net increase of .12 kPa (0.018 psi). This is considered a reasonable ΔP penalty for the greatly simplified and reliable fabrication of round rather than rectangular holes in the machined header fittings.

All of the above analysis has been based on the nominal flow rate of .053 kg/sec. (0.117 lb/sec.). The flow rate may be as large as 0.057 kg/sec. (0.126 lb/sec.). For flow rates close to the nominal value,

a close approximation of ΔP can be made by multiplying by the square of the flow ratio. The pressure drop thus is predicted to be 1.4 KPa (0.2 psi) at the nominal flow of 0.053 Kg/sec. (0.117 lb/sec.) and 1.6 KPa (0.23 psi) for the specification flow of 0.057 Kg/sec. (0.126 lb/sec.).

Various options to decrease the pressure drop below 1.4 KPa by varying the header dimensions were studied. These were invariably found not justifiable because of weight and cost penalties.

5.5 THERMAL ANALYSES

The purpose of the thermal analysis of the HSA was to

- Provide inputs to the design of the HSA
- Evaluate HSA thermal performance during normal operation
- Analytically evaluate performance of the Emergency Cooling System (ECS)
- Analytically evaluate performance of the Auxiliary Cooling System (ACS)

One, two, and three dimensional thermal models, programmed for computer usage, were utilized in the thermal studies. Simple one dimensional models were used early in the program to perform parametric sensitivity studies. The detailed two dimensional models were based on the Multi-Hundred Watt (MHW) ¼ sphere model of the isotope heat source and were utilized primarily to predict the isotope heat source component temperatures, e.g., the PICS (iridium fuel clad) response to activation of the ECS. The three dimensional models were developed to provide a detailed temperature map of the HSA and to determine the heat balance, the ACS response and the response to transients (startup, launch and shutdown). Brief descriptions of the salient thermal studies are presented in the following paragraphs.

The analytically predicted thermal performance of the preliminary design is divided into four areas: nominal operation, ACS, ECS, and transient analyses.

5.5.1 NOMINAL OPERATION

The two dimensional thermal model is illustrated on Figure 5-14. Nominal operational temperatures near the exit are listed in Table 5-6.

The three dimensional model of the preliminary design, on which are labeled the predicted temperatures, is given on Figure 5-15. This profile represents nominal flow conditions with the HSA radiating to the surrounding space radiator at 345K (160°F). Insulation hot face temperatures range from 1055K (1440°F) near the inlet to 1170K (1650°F) near the exit. The temperature distribution through the insulation is shown on Figure 5-16. If nickel foil is to be limited to 923K/650°C (a conservatively safe temperature) then it is evident from the figure that nickel foil must be limited to the outer 20 layers of the blanket. The temperatures predicted by the two and three dimensional models indicate that all HSA materials are operating within a requisite range.

An analysis was performed to evaluate the effect of non-uniform HSHX flow distribution on the circumferential temperature differential and to determine the allowable limits for circumferential gradients in the critical components.

The 3D preliminary design thermal model was used to obtain an accurate representation of the circumferential gradient. The baseline case is that with the flow ratio, defined as the ratio of flow in any given channel to the average channel flow, equal to 1.0. This case was shown on Figure 5-15 as the nominal case.

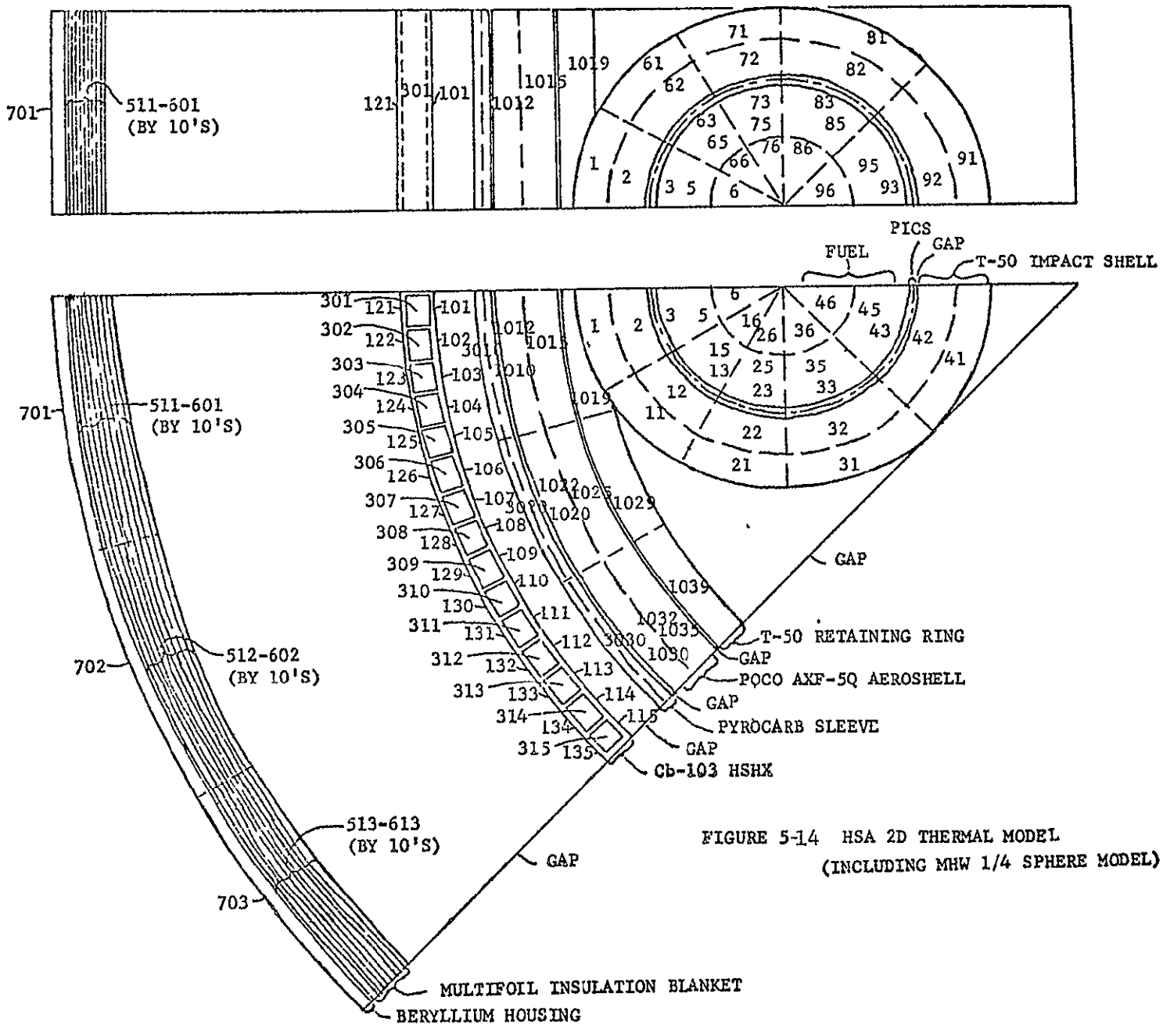

FIGURE 5-14 HSA 2D THERMAL MODEL
(INCLUDING MHW 1/4 SPHERE MODEL)

ORIGINAL PAGE IS
OF POOR QUALITY

TABLE 5-6. NORMAL OPERATING TEMPERATURES NEAR THE EXIT END OF THE HSA (TWO DIMENSIONAL MODEL)

COMPONENT	NODE NUMBER	TEMPERATURE K (^{O}F)
Fuel Center	96	1645 (2500)
PICS	93	1505 (2250)
T-50 Impact Shell	91	1425 (2110)
Heat Shield Surface	3010	1295 (1870)
HSHX Inner Wall	101	1195 (1690)
Helium Xenon	301	1100 (1515)
HSHX Outer Wall	121	1165 (1640)
Inner Insulation	601	1160 (1630)

FIGURE 5-15

HSA TEMPERATURE PROFILE DURING NORMAL OPERATION

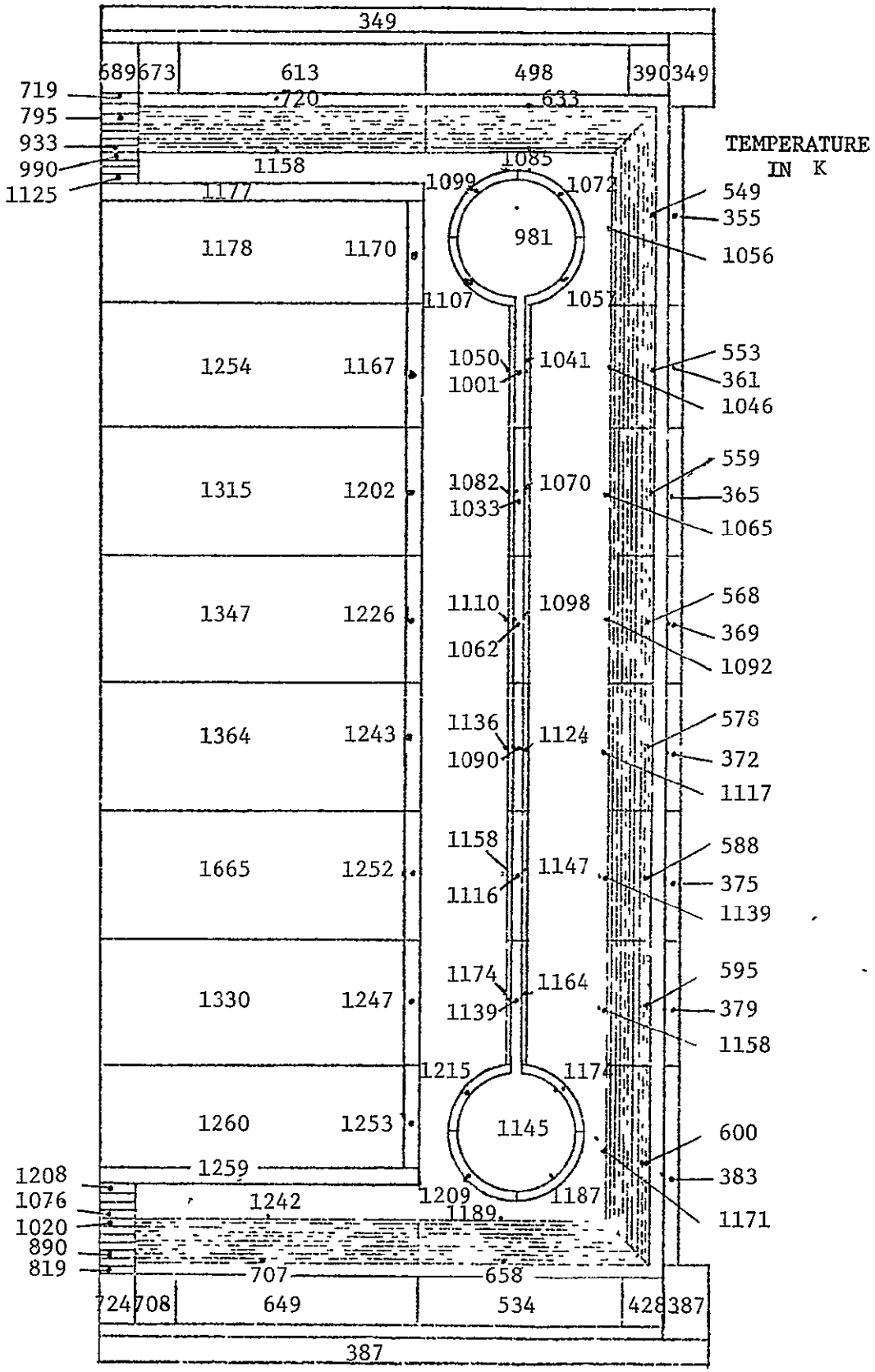

FIGURE 5-16

HSA INSULATION TEMPERATURE PROFILE

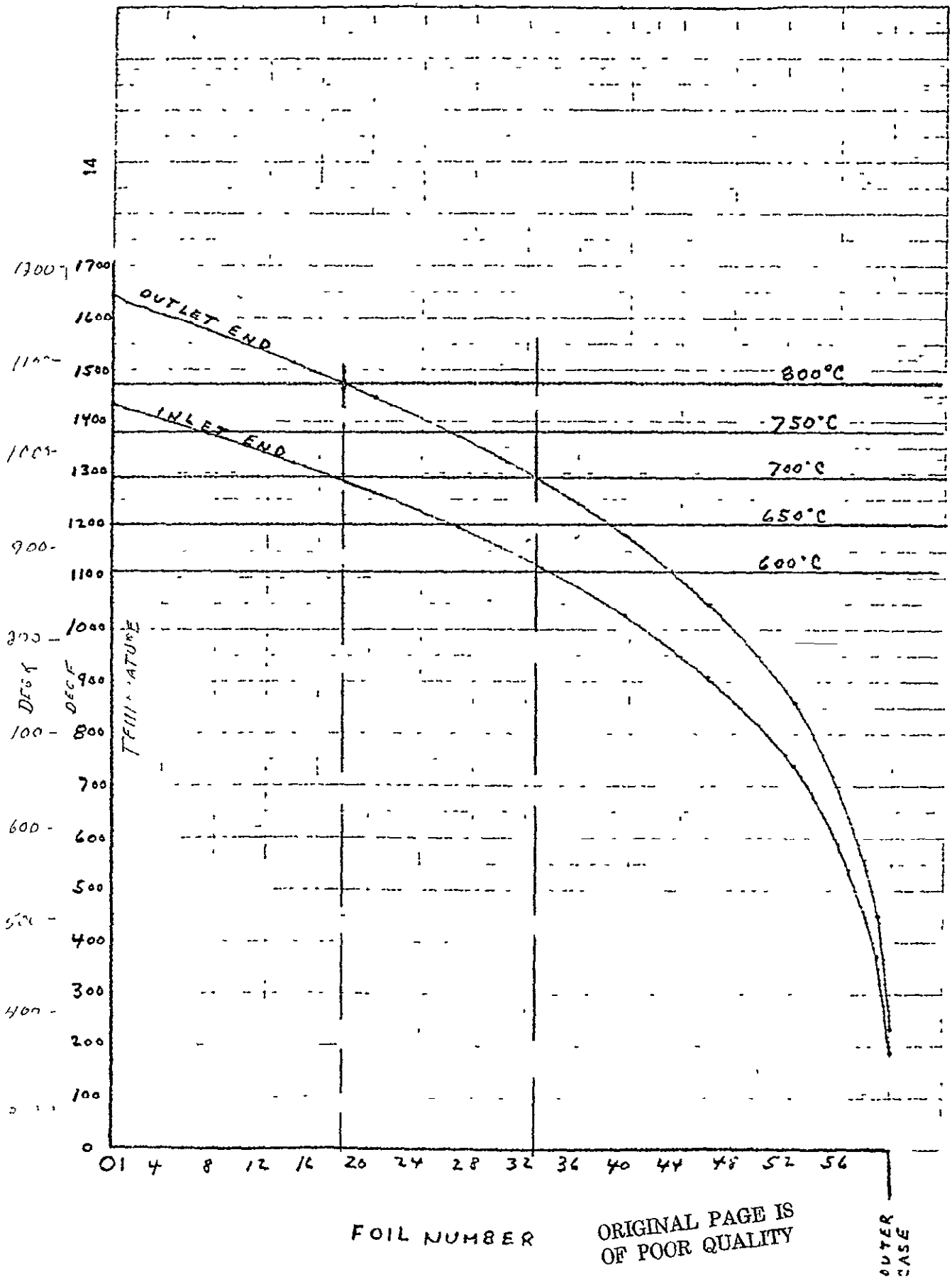

The 3D model consists of a 1/8 wedge of the HSA; thus each computer run represents 1/4 of the circumferential temperature gradient. Circumferential conduction is included within but not between wedges. Since the nominal case represents the midpoint of the flow distribution range (1.14 to 0.93 of the nominal flow rate), the two extremes were analyzed to complete the profile. Actually extremes of 1.22 and 0.89 of the flow rates (which represent conservatively high and low extremes) were used in the temperature analyses. Results of this study indicate maximum circumferential temperature differentials of approximately 35K ($60^{o}F$) on the heat source and the HSHX. The location of the maximum ΔT is near the exit header.

The fluid exits the HSHX at about 1145K ($1605^{o}F$), which is very close to the specified Brayton turbine inlet temperature. Since the working fluid is heated as high as 1175K ($1660^{o}F$) in the region of lean flow, this indicates adequate mixing prior to exiting the HSHX.

Since there are no specified allowable limits for circumferential temperature gradient, a scoping study was performed to determine a rough magnitude of permissible limits. MHW reentry analyses of the heat source have shown that a circumferential surface gradient of 1110K ($2000^{o}F$) is tolerable. Preliminary structural analysis of the HSHX has indicated that a 165K ($300^{o}F$) longitudinal gradient produces a negligible stress. Thus, it appears that circumferential temperature gradient on the order of 35K ($60^{o}F$) in the heat source and the HSHX is tolerable.

The HSA contract requires that the heat source surface temperature not exceed 1373K (2012°F) during normal operation, even if the HSHX inlet temperature is raised 55K (100°F) to 1035K (1405°F).

The 3D thermal model was utilized to determine if this requirement is met. For HSHX inlet and exit temperatures of 1035K (1405°F) and 1200K (1700°F) respectively, which correspond to a 55K (100°F) higher turbine inlet temperature, the maximum heat source surface temperature is 1315K (1905°F). This is approximately 60 K (110°F) lower than the contract requirement. Thus the contract required temperature limit is met even with the optional higher turbine inlet temperature of 1200K/1700°F.

5.5.2 AUXILIARY COOLING SYSTEM (ACS)

It is required that the ACS maintain any surface exposed to the external environment below the booster fuel auto ignition temperature of 465K (380°F). To determine if this requirement is met an analysis was conducted under the assumption that the HSA housing is exposed to the external environment. The internal volume of the HSA is charged with 1 atmosphere of helium to provide a low resistance path for heat flow from the isotope heat source to the HSA housing. Results of the study are tabulated in Table 5-7. It is evident from the results that the specification requirement is satisfied.

TABLE 5-7. ACS ANALYSIS SUMMARY

	TEMPERATURES, K (^{O}F)	
	Preliminary Design	Reference Design
Housing	425 (305)	425 (305)
Inner Foil	505 (450)	540 (515)
HSHX	950 (1250)	975 (1295)
Heat Source Surface	1095 (1510)	1050 (1430)
PICS (Iridium Fuel Clad)	1345 (1965)	1325 (1925)

5.5.3 EMERGENCY COOLING SYSTEM (ECS)

The ECS is designed to maintain acceptable heat source temperatures in the event of a failure of flow of the working fluid through the HSHX. The problem is to dissipate the 2260 watts (7713 Btu/Hr) which is normally transferred to the helium-xenon working fluid. The method selected is that of melting/vaporizing/fusing the multifoil insulation blanket until the thermal resistance is sufficiently low to transfer the full 2400 watt (8191) Btu/hr) heat load to space while maintaining safe PICS (iridium fuel clad) temperatures.

The 2D model (Figure 5-14) was utilized to perform the analysis. It must be emphasized that the analytic predictions are ultra conservative in that the effect of self-welding and fusing of the foils is not included in the computer model; the phenomena which was observed in the small scale melt-down tests will considerably alter the temperature response analytically

predicted herein. These analytical results are shown in Figure 5-17 on which 17 representative nodes are plotted. Nine of ten insulation nodes (54 of 60 foil layers) melt and the remaining node reaches a peak temperature of approximately 1530K (2300°F). This insulation node will evaporate in approximately 70 hours. The PICS reaches a peak temperature of approximately 2030K (3200°F) about 40 hours after activation of the ECS and stabilizes at approximately 1615K (2450°F).

Full scale tests should be conducted to verify that these analytic results are indeed overly conservative.

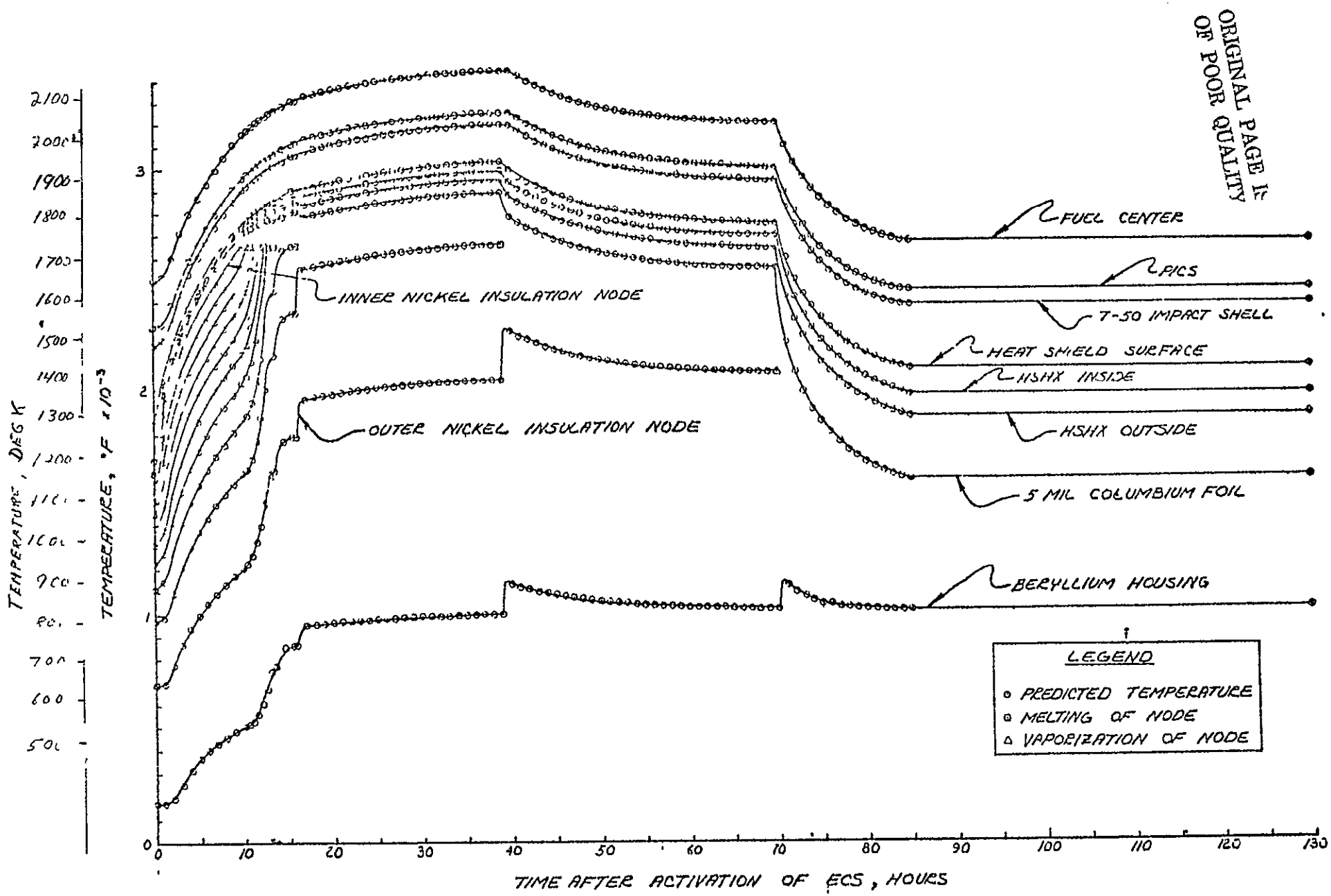

TWO DIMENSIONAL ECS RESPONSE HSA WITH LES 8/9 HEAT SOURCE

FIGURE 5-17

5.5.4.4 TRANSIENT ANALYSIS

A potentially damaging situation during a Brayton system ground demonstration test is failure of the Electric Heat Source. A 3D thermal model analysis examined the transient thermal response of the HSA to a step decrease in power from 2400 watts to zero watts. The shutdown transient was simulated by zeroing the internal generation of the heat source and by stopping the flow of the working fluid, the later being a conservative assumption. The transient temperature response to shutdown is illustrated on Figure 5-18 for the nodes which responded with the largest temperature swings. Since the fluid flow has stopped, all heat is transferred thru the insulation. Consequently, due to the large thermal inertia of the HSA, the response is slow. The maximum temperature ramps are tabulated in Table 5-8. The most critical component is the HSHX and the 85K (150°F) excursion in 15 minutes is judged to be within acceptable limits.

TABLE 5-8. MAXIMUM TEMPERATURE EXCURSION, DUE TO SHUTDOWN TRANSIENT

COMPONENT	MAXIMUM TEMPERATURE EXCURSION K/15 MINUTES (°F/15 MINUTES)
Average Heat Source	70 (125)
Heat Source Surface	10 (15)
HSHX	85 (150)
Columbium Insulation Support Cylinder	80 (140)
Inner Insulation	50 (90)
Outer Insulation	2 (3)
Housing	0.5 (1)

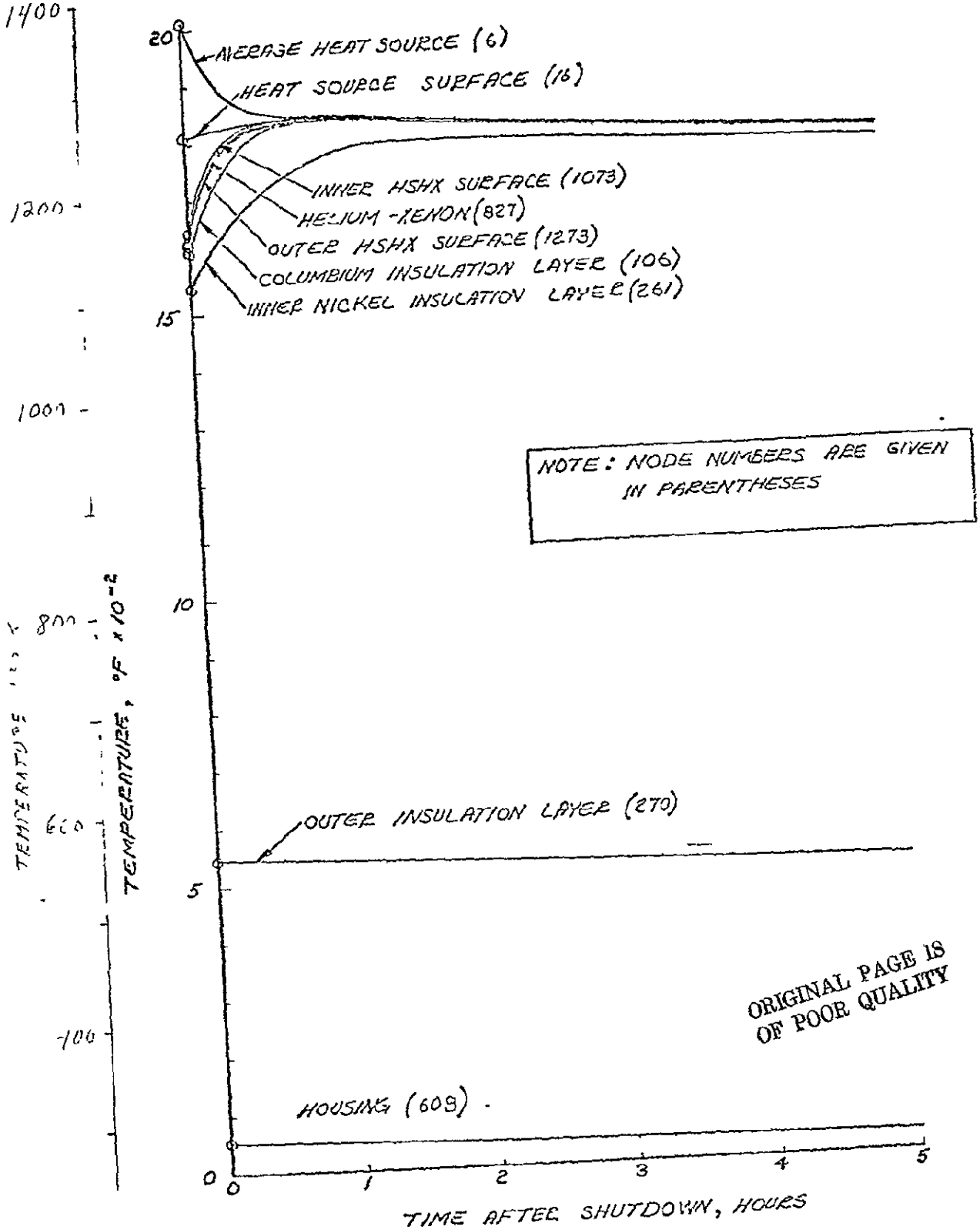

3D HSA Shutdown Transient with Fluid Flow Stopped

FIGURE 5-18

Startup transients are reported in detail in Reference 11. A worst case cold startup analysis indicated that no critical stress conditions are anticipated on any components on the HSA due to these transient conditions.

5.6 SYSTEM INTERFACES

The HSA's are supported off three mounting points on the housing and domes with the inlet and outlet extension ducts welded to the BIPS recuperator, and turbine inlet ducts. The location of the mounting points and the inlet/outlet ducts are the critical mechanical interfaces with the Brayton system. Electrical interfaces are provided by both power and instrumentation connectors. A Gas Management Valve provides the interface with ancillary BIPS support equipment for backfilling and venting the HSA's during auxiliary cooling.

These system interfaces are shown on Figure 5-19 (Dwg. 47E313138).

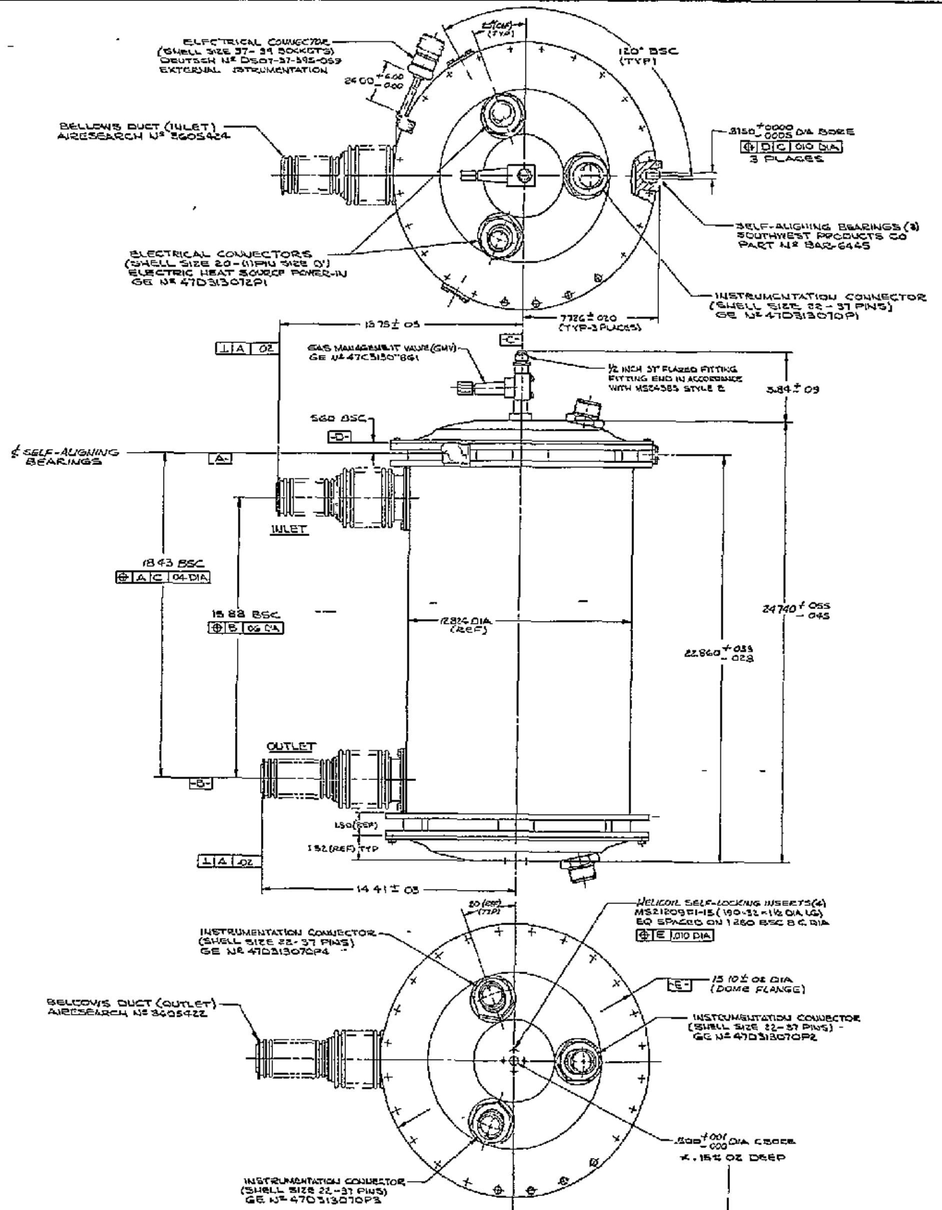

NOTES

1. DRAWING TERMS & TOLERANCES PER GE SPEC 530009
2. FOR COMPLETE HSA DESCRIPTION SEE GE DRAWINGS 47E313000 & 47E313112
3. ALL DIMENSIONS ARE CONTROLLING DIMENSIONS AND SHOULD NOT BE CHANGED WITHOUT PRIOR APPROVAL OF THE CUSTOMER AND THE GENERAL ELECTRIC CO VALLEY FORGE PA
4. ALL DIMENSIONS NOTED ARE AT ROOM TEMPERATURE
5. FOR HSA INSTRUMENTATION SEE GE DRAWINGS 47E313000 & 47D313121

FIGURE 5-19
SYSTEM INTERFACES

REDUCED SIZE PRINT
SCALE 0 1 2
INCHES

GENERAL ELECTRIC
HSA
INTERFACE DWG
E 23991 47E313138

SECTION 6

HARDWARE FABRICATION

6.1 CLEANLINESS REQUIREMENTS

The required seven year operational life of the HSA, and the critical nature of the components in the BIPS fluid loop requires stringent cleanliness criteria to be imposed on the fabrication procedures. Reference 8 specifies in detail these cleanliness requirements. The salient requirement is that all parts that are internal to the Xe-He fluid loop, must be flush cleaned with specified cleaning fluid to assure no residual hydrocarbons and no loose particulates in accordance with the acceptance criteria given below in Table 6-1.

TABLE 6-1

LOOSE PARTICULATE ACCEPTANCE CRITERIA FOR HSHX FLUID LOOP	
Particle Size - Micrometers	Quantity Permitted
150	0
100 - 150	40 particles/ m^2
25 - 100	1000 particles/m^2
0 - 25	unlimited

All HSA parts that are external to the fluid loop are cleaned by immersion or flush cleaning with specified cleaning agents and blown dry with nitrogen or inert gas to remove residual contamination and particulates. Following cleaning, items are packaged in clean Nylon C bags and heat sealed. These are then double protected in a polyethylene outer bag.

6.2 HEAT SOURCE HEAT EXCHANGER (HSHX) FABRICATION

The C-103 HSHX is the major and most critical component of the HSA. The engineering requirements and complete definition of the hardware, including reference to appropriate specifications, are contained in the six GE configuration control drawings listed below which provide the basis for manufacture of deliverable hardware.

Title	Drawing No.
Assembly, Heat Source Heat Exchanger	707E839
Scroll, Inner	101D9580
Scroll, Outer	101D9581
Cylinder, HSHX	101D9586
Bracket	152B4843
Port	152B4585

The assembly drawing indicates the weld assembly of the components, the key interface dimensions which must be controlled in the welding and finish machining operations on ports and mounting brackets, and the necessary post-weld annealing, inspection and test requirements.

A general outline of the process for the manufacture of the HSHX components is indicated in Figure 6-1 and described in greater detail below.

6.2.1 INNER CYLINDER

The inner cylinder is formed from 1.27 cm (0.5 in) thick plate by carefully pressing a forming bar down on the plate which is supported underneath by two parallel forming bars, one on each side of the pressure bar. Except for short lengths at either edge of the plate the plate is formed or "bumped" into a half cylinder using sheet metal templates to guide the "bumping" operations. (See Figure 6-1a).

The formed piece is supported in a milling machine with conventional shop clamping and supporting devices and, in a single set up, the weld preps are machined for both joints.

The cylinder halves are clamped together and installed in the vacuum purged GTA welding chamber. The parts are tack welded together at the weld joint and a single root pass without filler is applied at each weld joint. Subsequent filler wire passes complete these welds; attention was paid to alternating welding direction and to reforming and/or stress relieving the components as required to avoid gross deformation of the part.

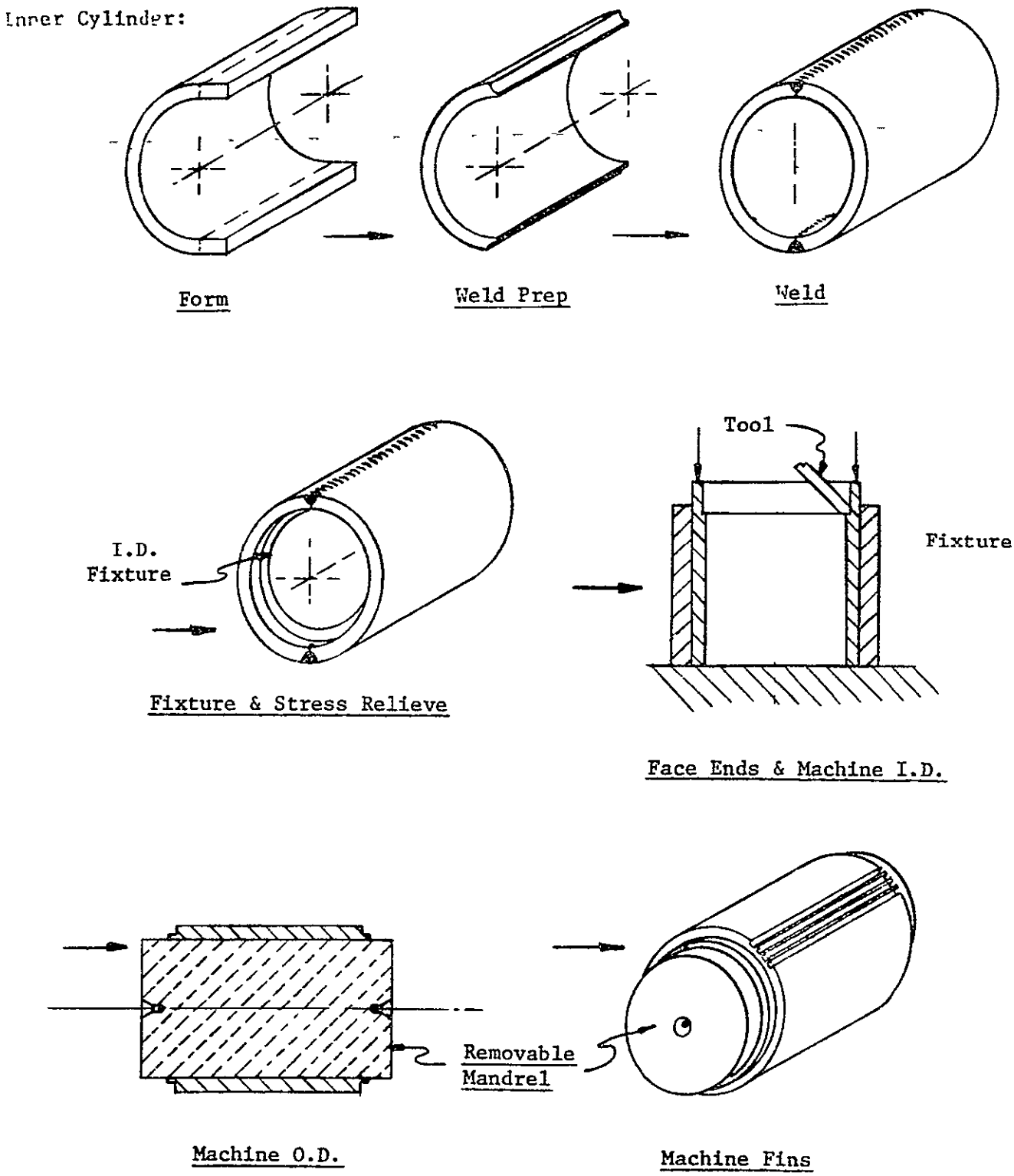

Figure 6-1a. Highlights of HSHX Manufacturing Process Plan

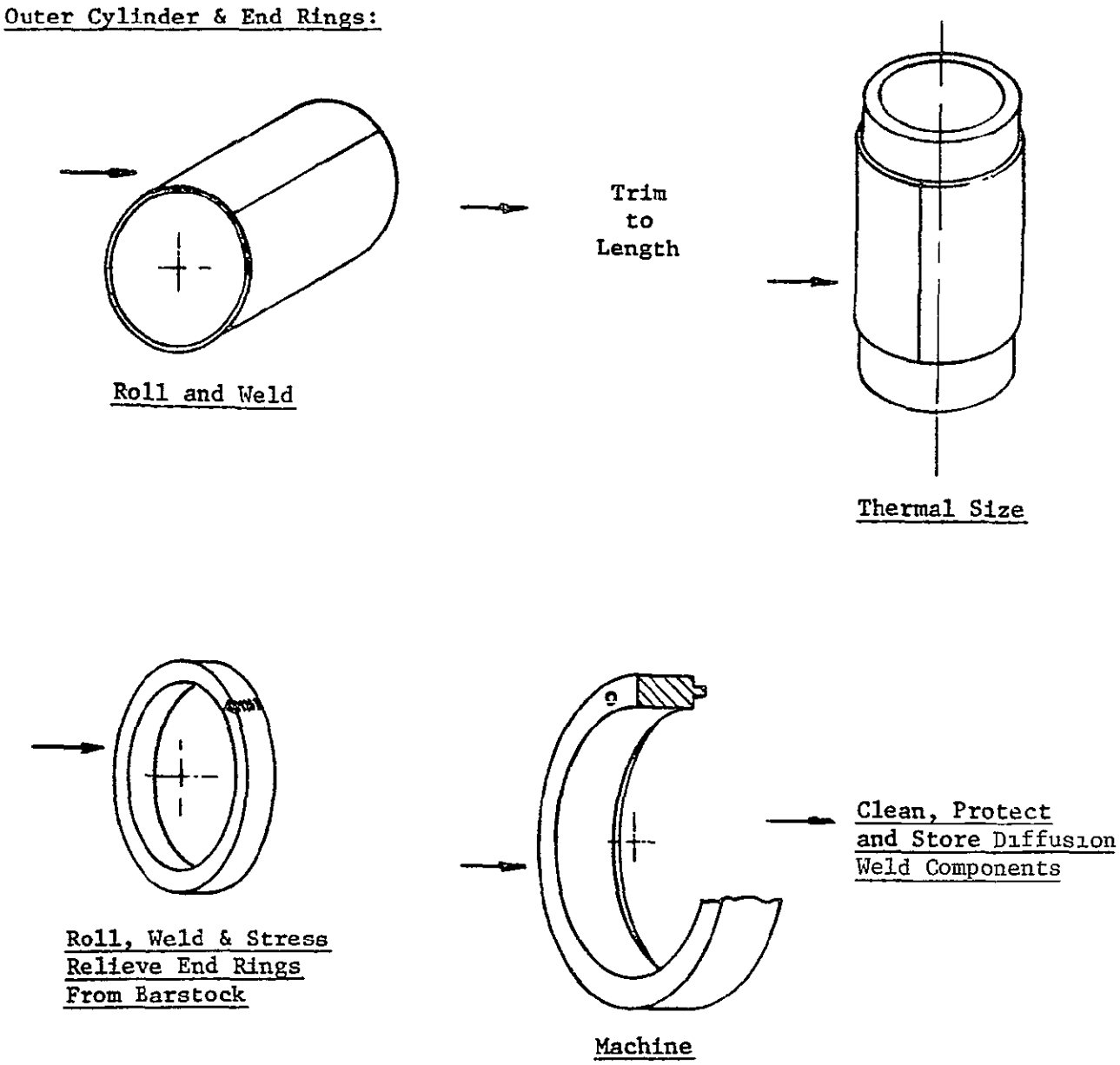

Figure 6-1b. HSHX Manufacturing Plan (continued)

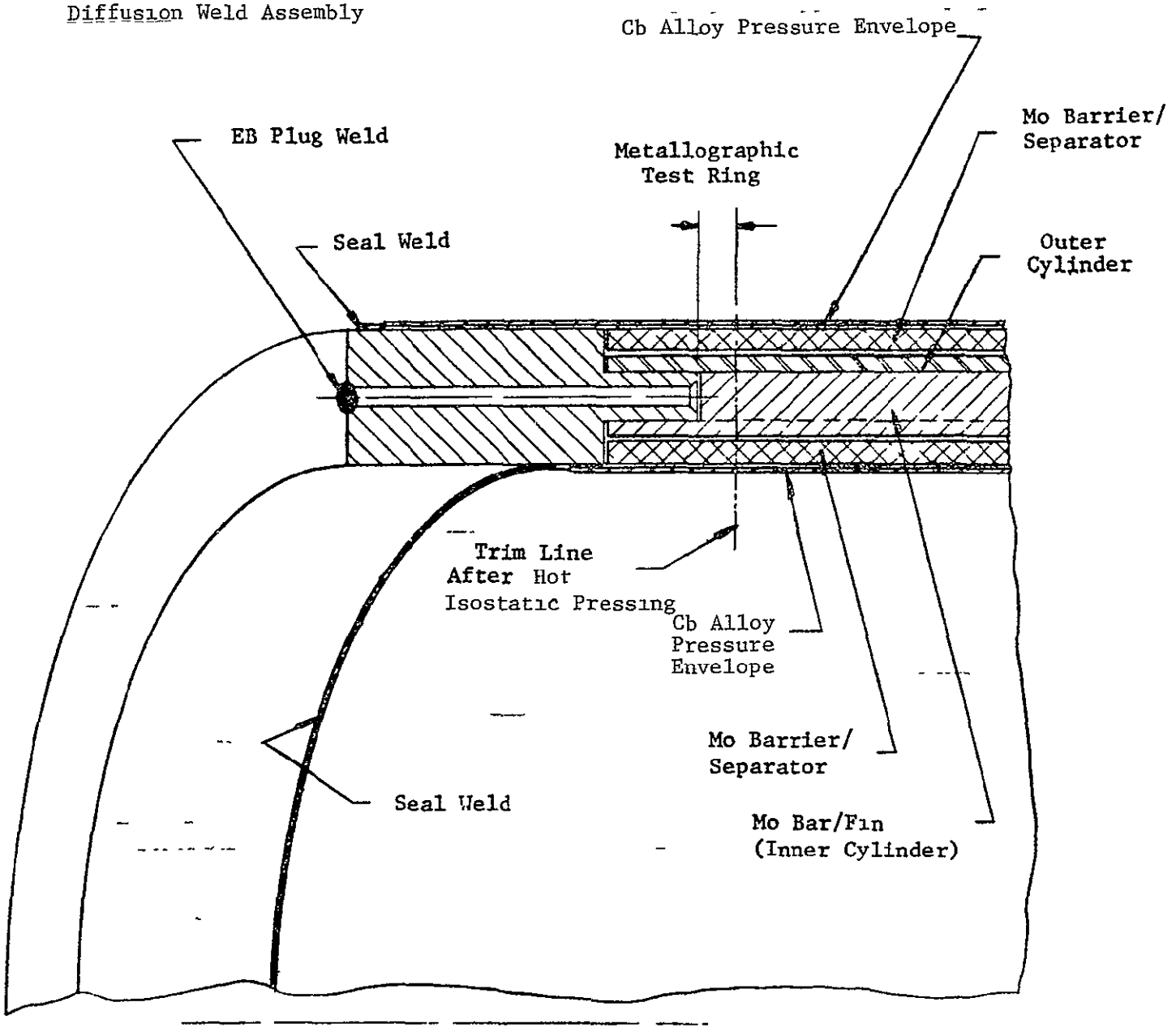

Figure 6-1c. HSHX Manufacturing Plan (continued)

Diffusion Welded Assembly Machining:

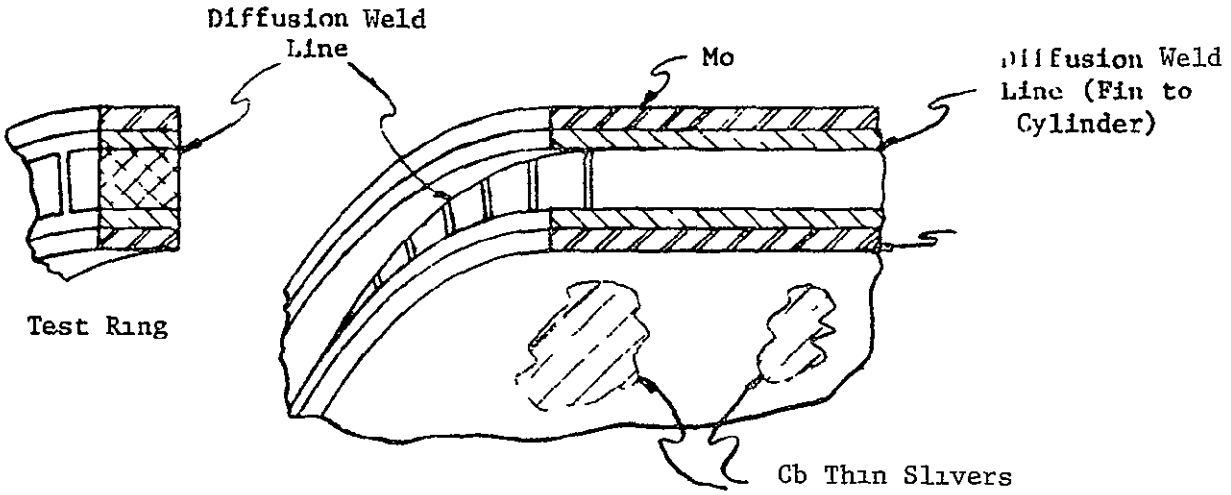

- Operations:
  - Remove Test Sections
  - Finish Trim to Length
  - Turn O.D./I.D. to Remove Cb

Diffusion Welded Assembly Leaching:

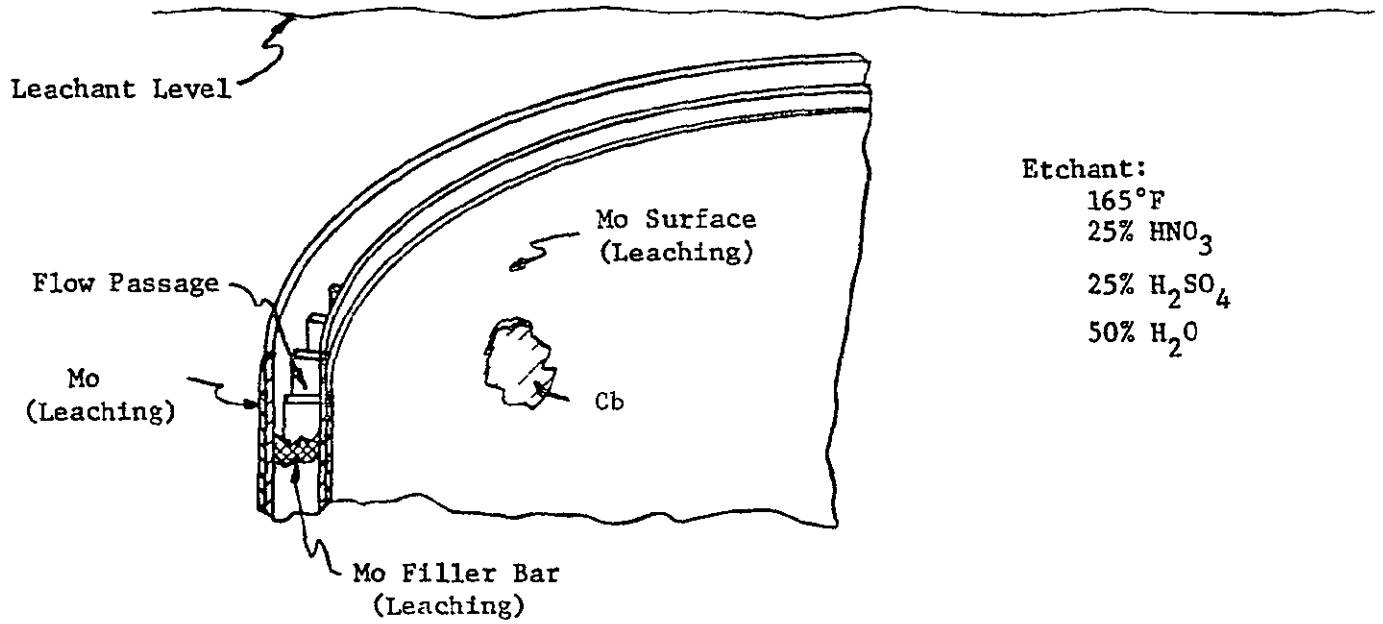

- Operations:
  - Immersion Leach
  - Ultrasonic NDT

Figure 6-1d. HSHX Manufacturing Plan (continued)

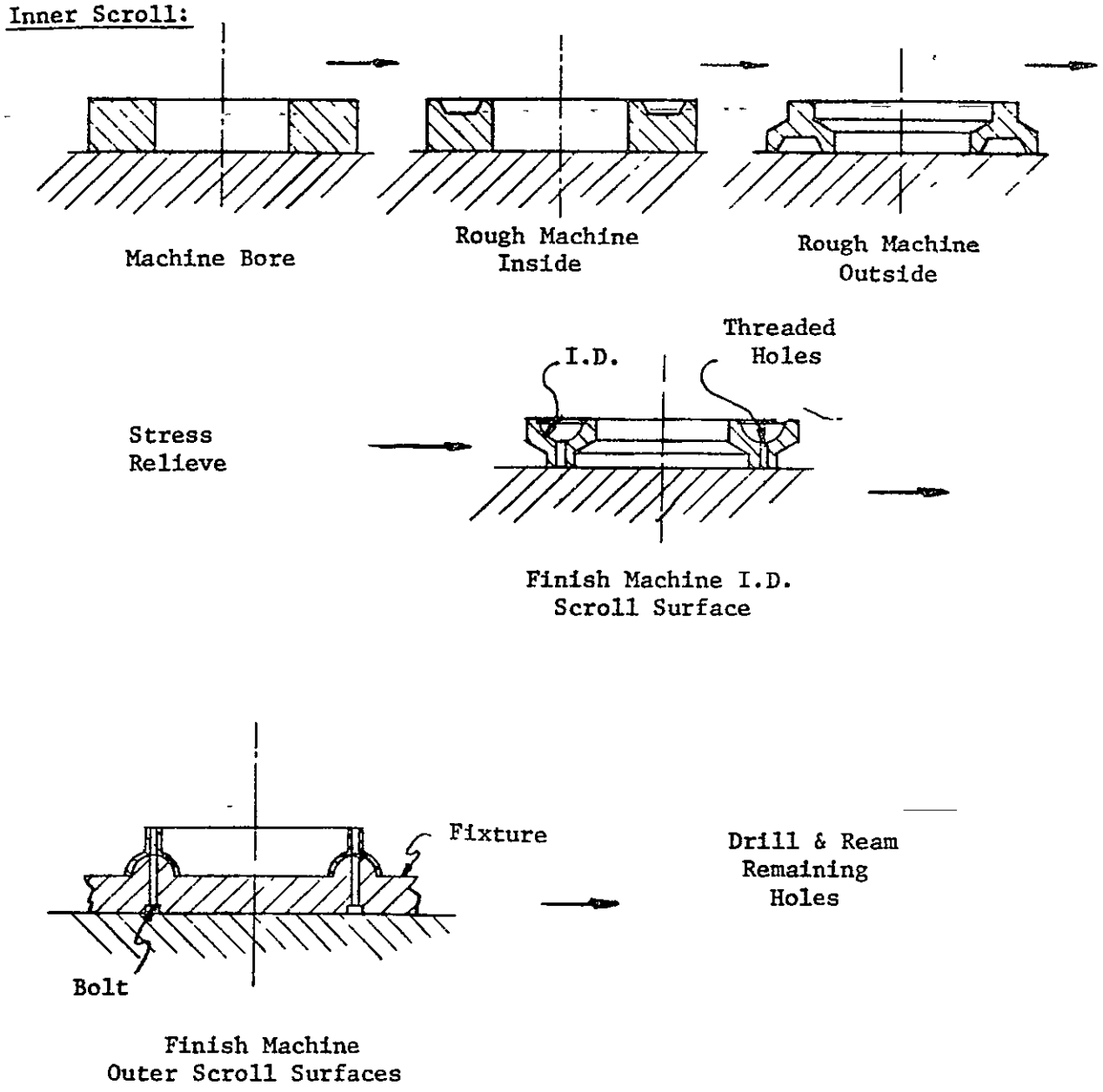

Figure 6-1e. HSHX Manufacturing Plan (continued)

SCROLL FABRICATION:

- Operations
  - Trim Blanks to Size

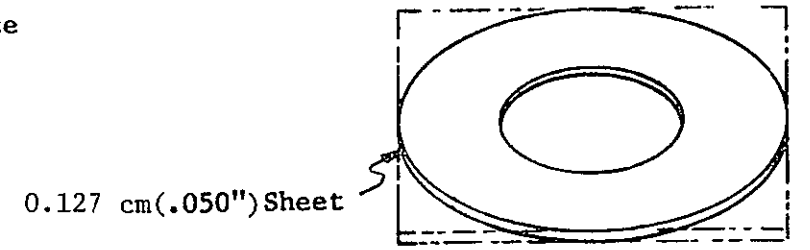

  - Draw Form

  - Stress Relieve

  - Trim Flanges

  - Trapped Rubber Form
    (Same as Draw Form
    but with Rubber
    located in Die Cavity)

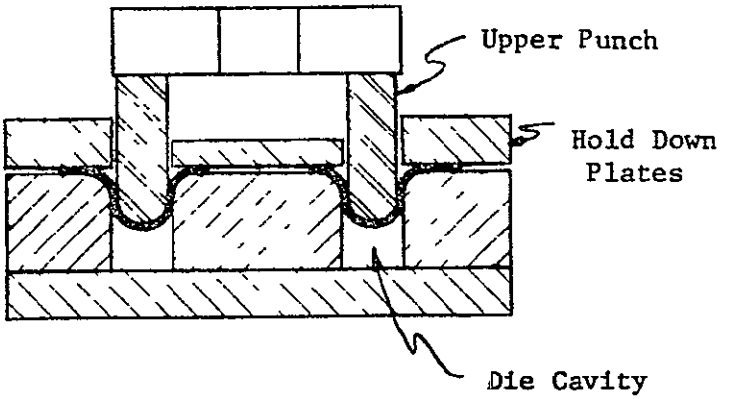

  - Stress Relieve

  - Reform (if necessary)

  - Trim to Size and Weld Prep

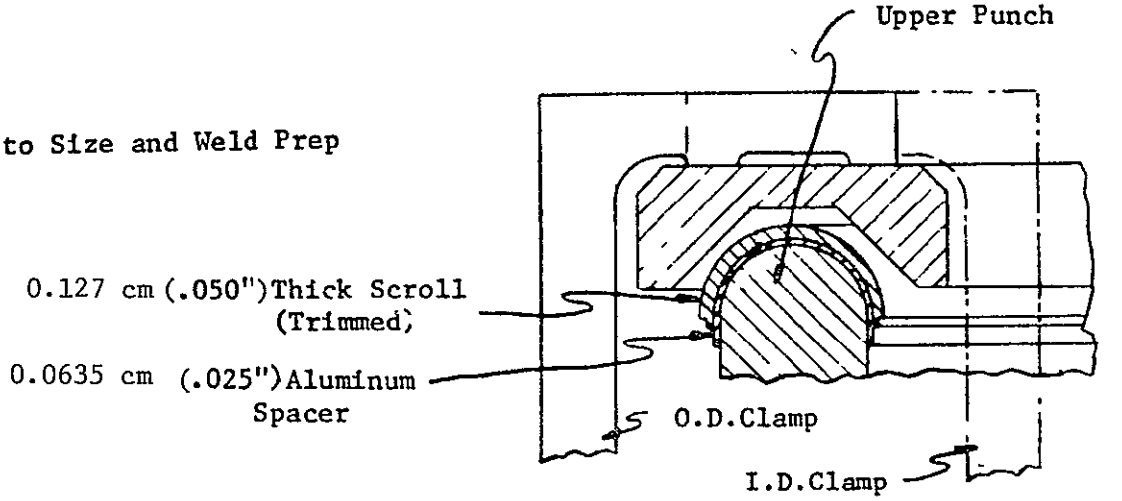

Figure 6-1f. HSHX Manufacturing Plan (continued)

The cylinder is stress relieved at 1700K (2600°F) for one hour. After stress relief, the part is reformed to shape and re-stress relieved, if necessary.

A rough cut is made on the OD of the cylinder to fit it within a support fixture in which the ID surface is turned to final dimension and surface finish. The part is then installed on an expanding mandrel with a precision OD mated to the precision ID of the cylinder. Then the slot machining and machining to length complete this cylinder for diffusion welding assembly. Welds are radiographed and fluorescent penetrant inspected (FPI) and the cylinder is helium leak tested. A photograph of the machined inner cylinder is shown in Figure 6-2 and also in Figure 6-3 along with other components.

6.2.2 OUTER CYLINDER

This component is made from 0.127 cm (0.050 in) thick C-103 sheet by trimming to rough size, rolling into a 360° cylinder and trimming the circumferential length to a dimension which makes allowance for weld shrinkage (Figure 6-1b). The cylinder is fixtured and welded to produce a cylinder very close, but slightly undersize with respect to installation over the inner cylinder. This cylinder is then thermally sized over a stainless steel mandrel by vacuum heating to progressively higher temperatures in the range from 645-1090K (700-1500°F). This sizing operation is specifically tailored for each cylinder to permit a simple, but snug, fitup with the specific cylinder to which it mates.

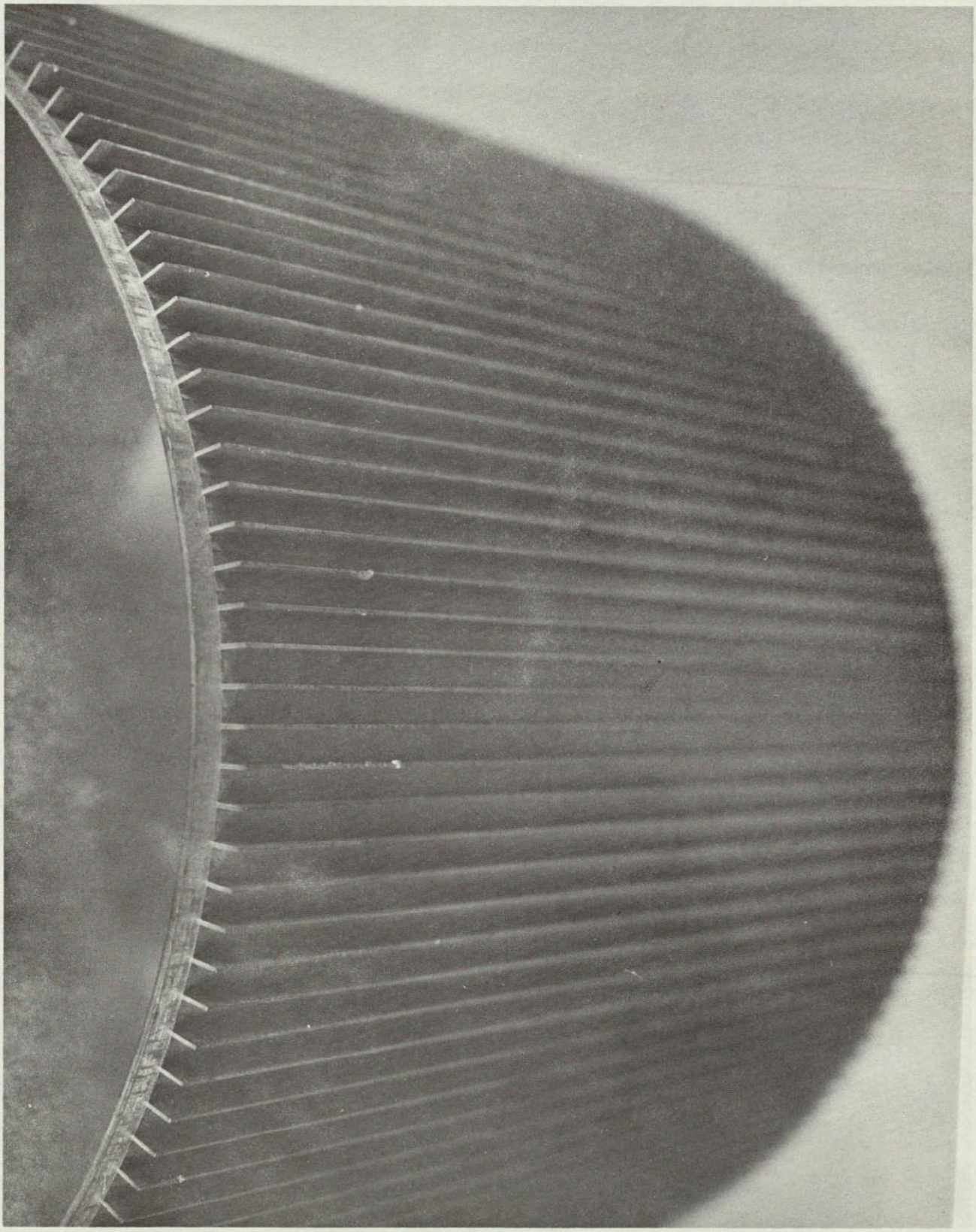

Figure 6-2
Machined Inner Cylinder

Final weld inspection includes radiographic inspection, FPI, and helium leak test. A photograph of the C-103 outer cylinder is shown in Figure 6-3.

6.2.3 DIFFUSION WELDING ASSEMBLY

Several expendable components are required for the diffusion welding assembly. These include the Cb-1Zr inner and outer seal cylinders, the inner and outer molybdenum barrier cylinders, the C-103 end rings, the molybdenum flow passage filler bars and molybdenum and tantalum foil wrapping to protect the assembly from contamination in the high pressure, high temperature autoclaving process.

The Cb-1Zr seal cylinders are formed from rolled and welded sheet. No thermal sizing is required but these cylinders must fit on the inside and outside of the diffusion bonding cylinder assembly with sufficient precision in fit-up to permit weld seal assembly to the end rings. The cylinder welds are radiographic and FPI inspected and the cylinders helium leak tested. A photo is shown in Figure 6-3.

The molybdenum barrier cylinders are rolled in four segments but not welded and fit into place in the diffusion welding assembly between the component and the Cb-1Zr seal envelope. Grinding fixtures are used to trim the circumference to accurate length for precision fit up. A photo showing two segments is given in Figure 6-3.

The end rings are fabricated from rolled and welded bar stock, as shown in Figure 6-1b. Radiographic and FPI inspection are used to verify the welds. The rings are stress relieved, finish machined and the welds in the ring helium leak tested. One of the two required rings have four axially drilled holes located in it for evacuation prior to final sealing of the assembly. A photograph of the rolled bar stock and finished end rings is shown in Figure 6-3.

The diffusion welding assembly is cleaned, assembled, welded, evacuated, baked-out, sealed, diffusion welded, metallographically evaluated, leached and ultrasonically inspected as prescribed in GE Specification P3AYA15.

The assembly is as indicated in Figure 6-1c. The assembly is made in the vertical position on a clean air flow bench using chemically cleaned parts. The inner cylinder is installed over the lower end ring, the molybdenum filler bars are installed, the outer cylinder is dropped in place over the inner cylinder and molybdenum bars, the inner and outer barrier cylinders are installed, the inner and outer seal cylinders are slid into place, and the top end ring is installed.

The diffusion welding assembly is then installed on the rotating ID welding fixture and seal welds are made in the vacuum purged GTA tank between the end rings and the Cb-1Zr seal cylinders.

The assembly is then transferred to the EB welding chamber where it is baked out under vacuum at 335K(140^{o}F) or higher for a minimum of 16 hours. Solid plugs are then placed in the evacuation ports and EB welded in place completing the sealing of the assembly.

FIGURE 6-3
HSHX PRODUCTION PARTS

C-103 OUTER AND INNER CYLINDERS

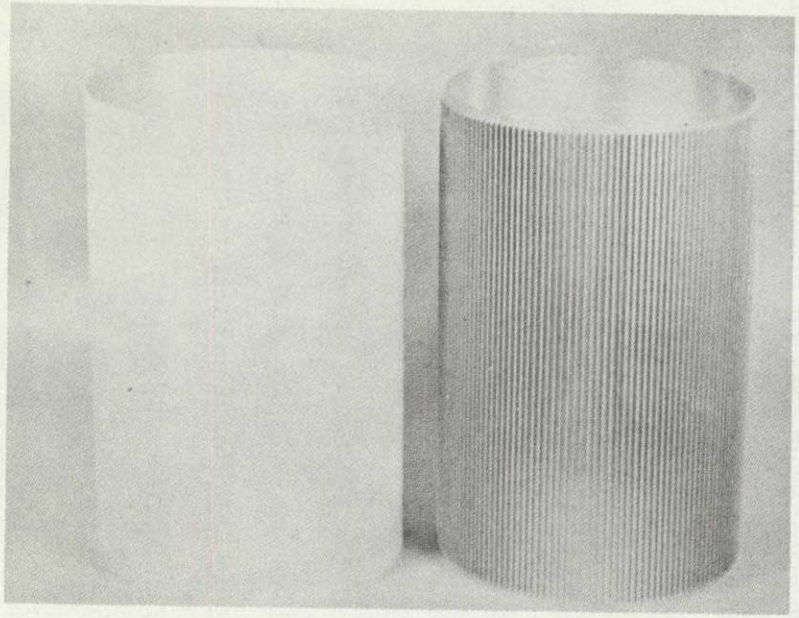

Cb-1Zr SEAL CYLINDERS

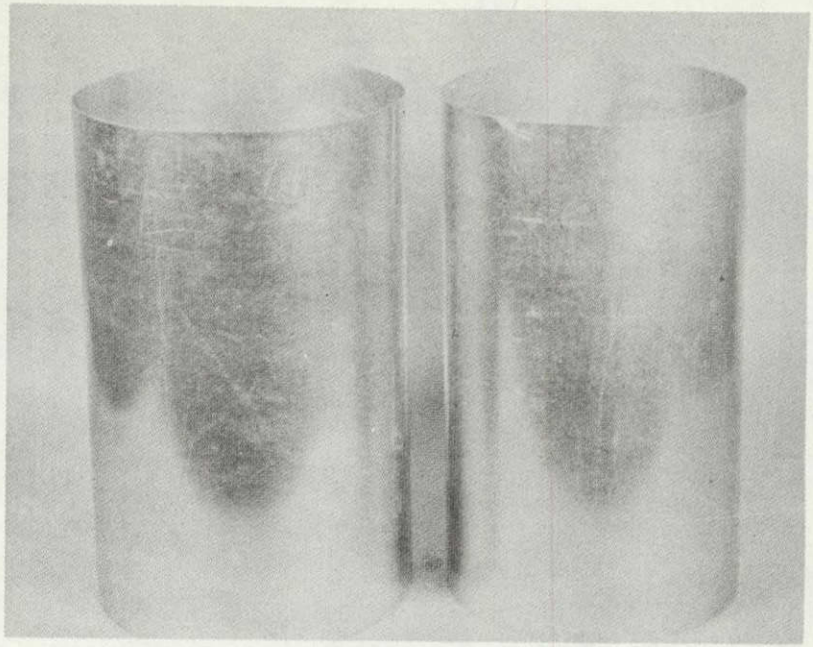

MOLYBDENUM BARRIER CYLINDER SEGMENTS

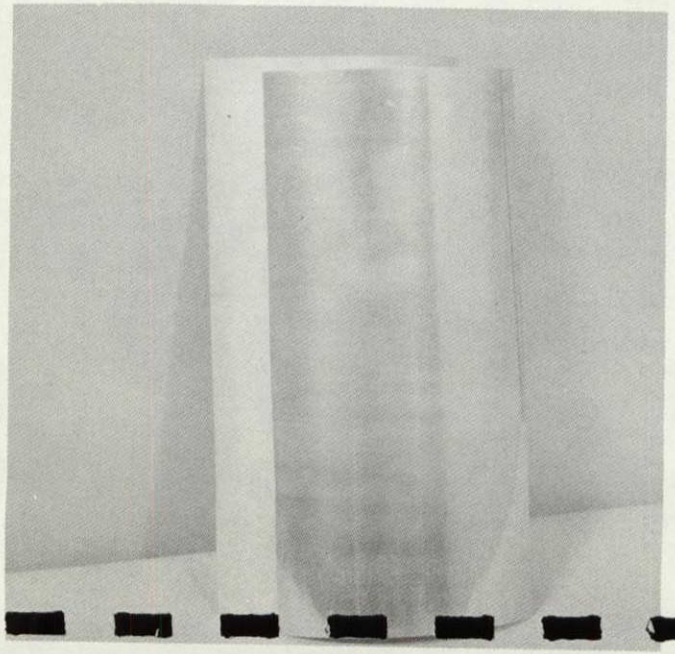

C-103 END RINGS

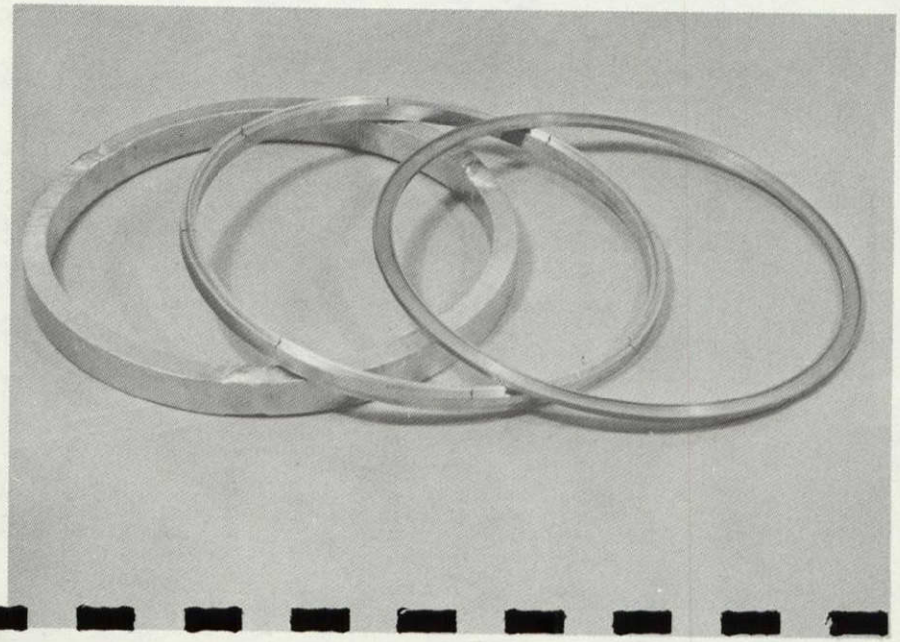

The sealed assembly shown in the photo of Figure 6-4 is then wrapped in layers of tantalum foil and installed in the BCL autoclave. A typical temperature and pressure history applied in the Hot Isostatic Pressing (HIP) process is shown in Figure 6-5. After the temperature equilibrates at 1810K and 68.95 MPa (2800^{o}F and 10000 psi) these conditions are maintained for three hours before the power is turned off and the system is allowed to cool slowly to room temperature.

6.2.4 DIFFUSION WELDED ASSEMBLY CYLINDER MACHINING AND LEACHING

With the diffusion welded assembly fixtured on the holding fixture, metallograhic test rings are machined from each end of the assembly and the ends of the assembly are finish machined to length (Figure 6-1d). The OD and ID of the assembly is carefully machined to partially remove areas of the Cb-1Zr pressure envelope and expose sections of the molybdenum barrier cylinders. A photo of the scalloped assembly is shown in Figure 6-6.

The finished diffusion welded cylinder assembly is recovered by leaching the molybdenum barrier cylinders, removing the Cb-1Zr outer seal cylinders and then continuing to leach the molybdenum filler bars from the flow passages and any remaining areas of the molybdenum barrier cylinders from the OD and ID of the assembly.

Ultrasonic inspection of 100% of all diffusion welds is then performed along with metallography of the test rings. A photograph of the cylinder being ultrasonically inspected is shown in Figure 6-8. The transducer head, which transverses the length of the cylinder as the cylinder is rotated in steps, is out of view on the vertical tube behind the cylinder. A typical "C" scan trace is given in Figure 6-9. The white areas represent the diffusion welded fin to outer cylinder regions. No unwelded areas were observed. Typical metallography from the end test rings is shown in Figure 6-10. Excellent grain growth across the diffusion weld with no evidence of porosity or the location of the original weld interface is apparent. This metallography along with the ultrasonic inspection demonstrate the superior quality of the diffusion welds and give high confidence in the integrity of the heat exchanger.

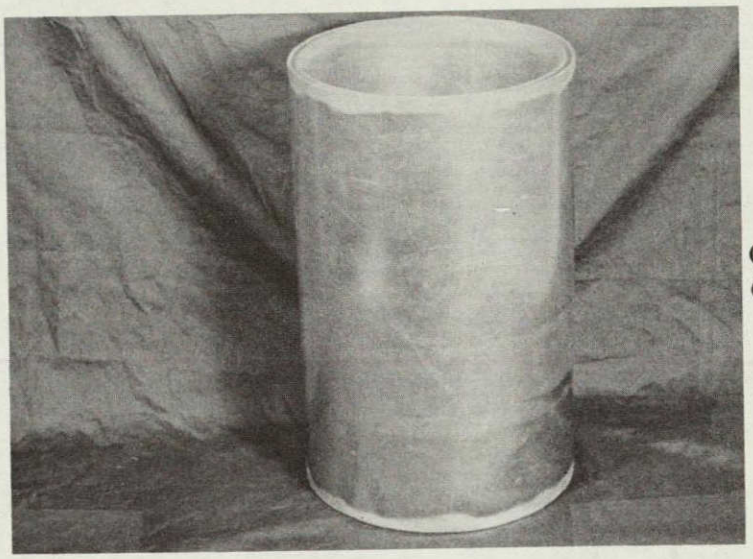

ORIGINAL PAGE IS
OF POOR QUALITY

FIGURE 6-4

SEALED PRODUCTION CYLINDER NO. 1 BEFORE AUTOCLAVING

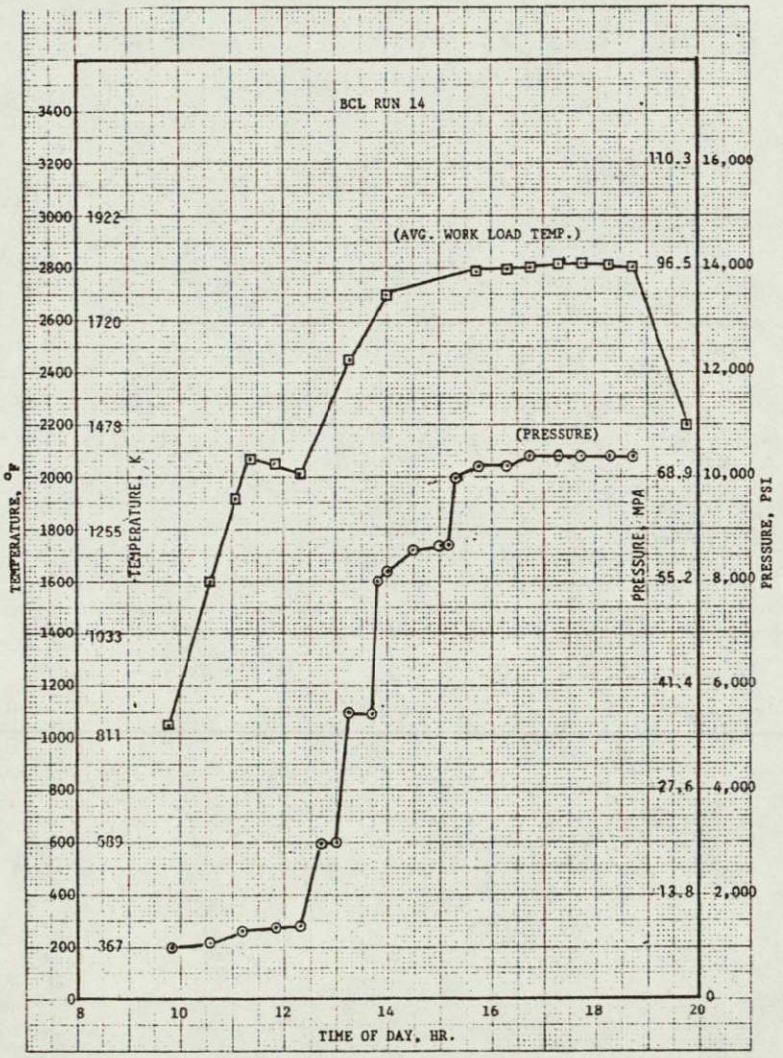

FIGURE 6-5

TYPICAL PRESSURE-TEMPERATURE PROFILE DURING AUTOCLAVING

FIGURE 6-6

MACHINING (SCALLOPING) OF INNER AND OUTER SEAL CYLINDERS OF 1ST AUTOCLAVED PRODUCTION CYLINDER

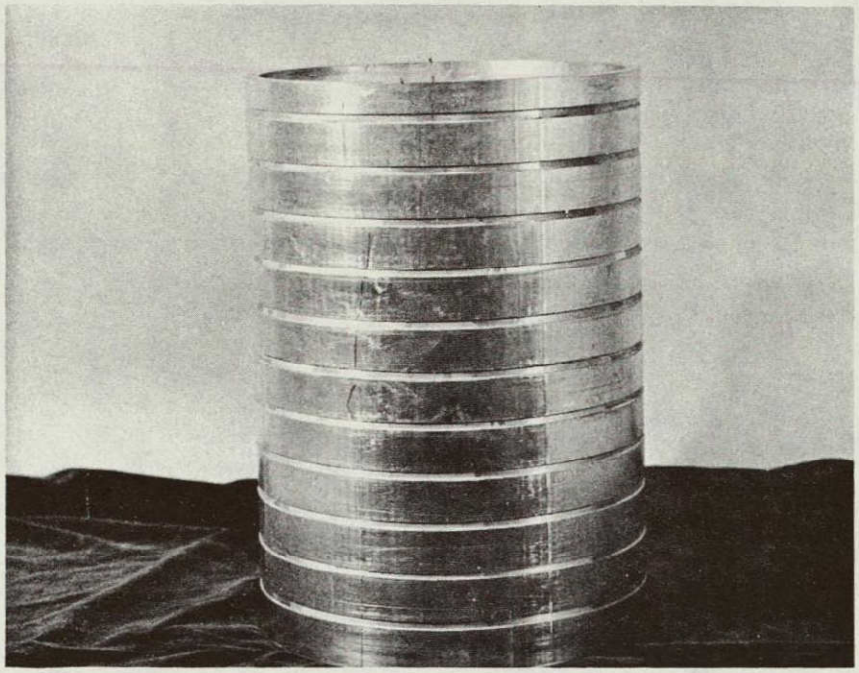

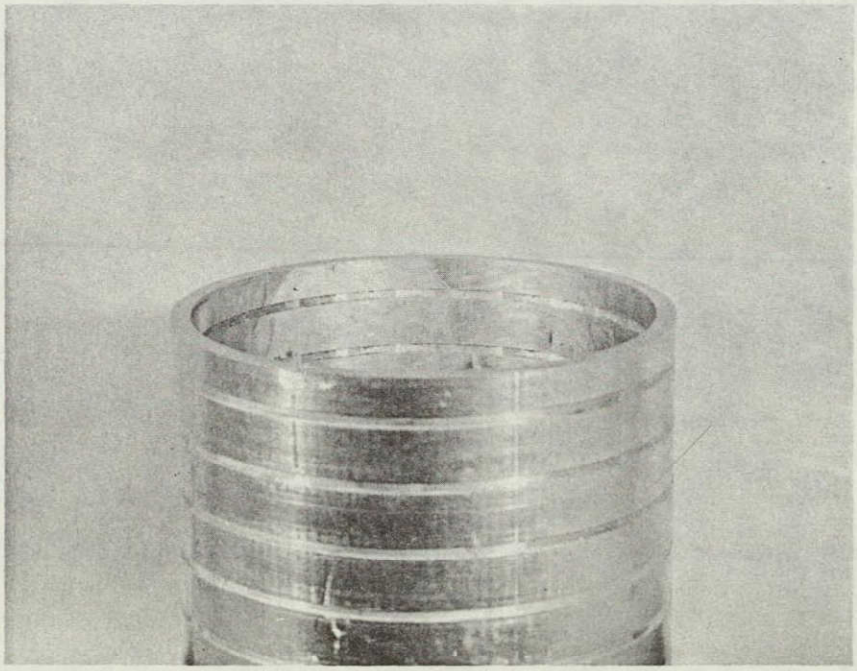

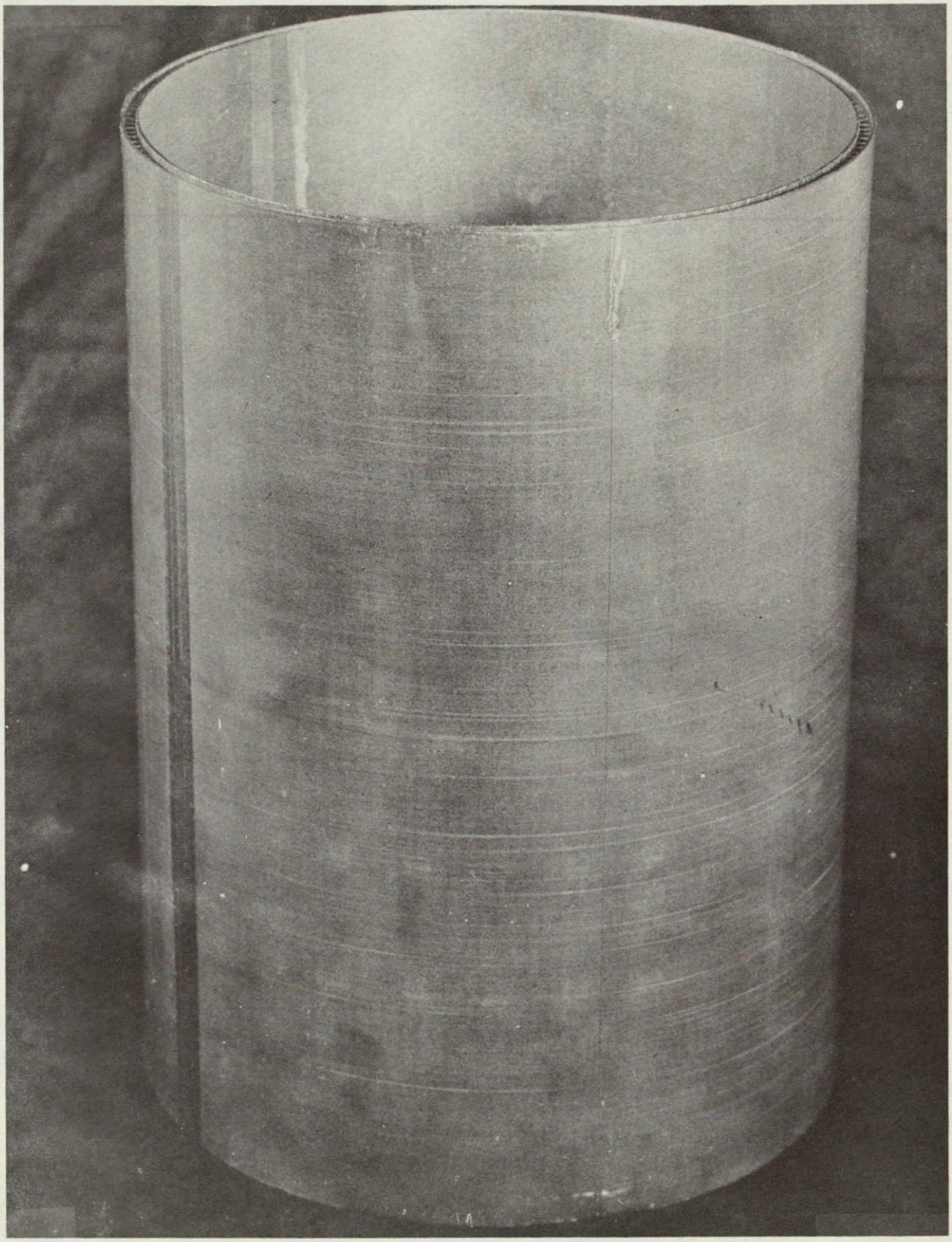

FIGURE 6-7

RECOVERED DIFFUSION WELDED ASSEMBLY AFTER LEACHING

FIGURE 6-8

ULTRASONIC INSPECTION OF PRODUCTION CYLINDER

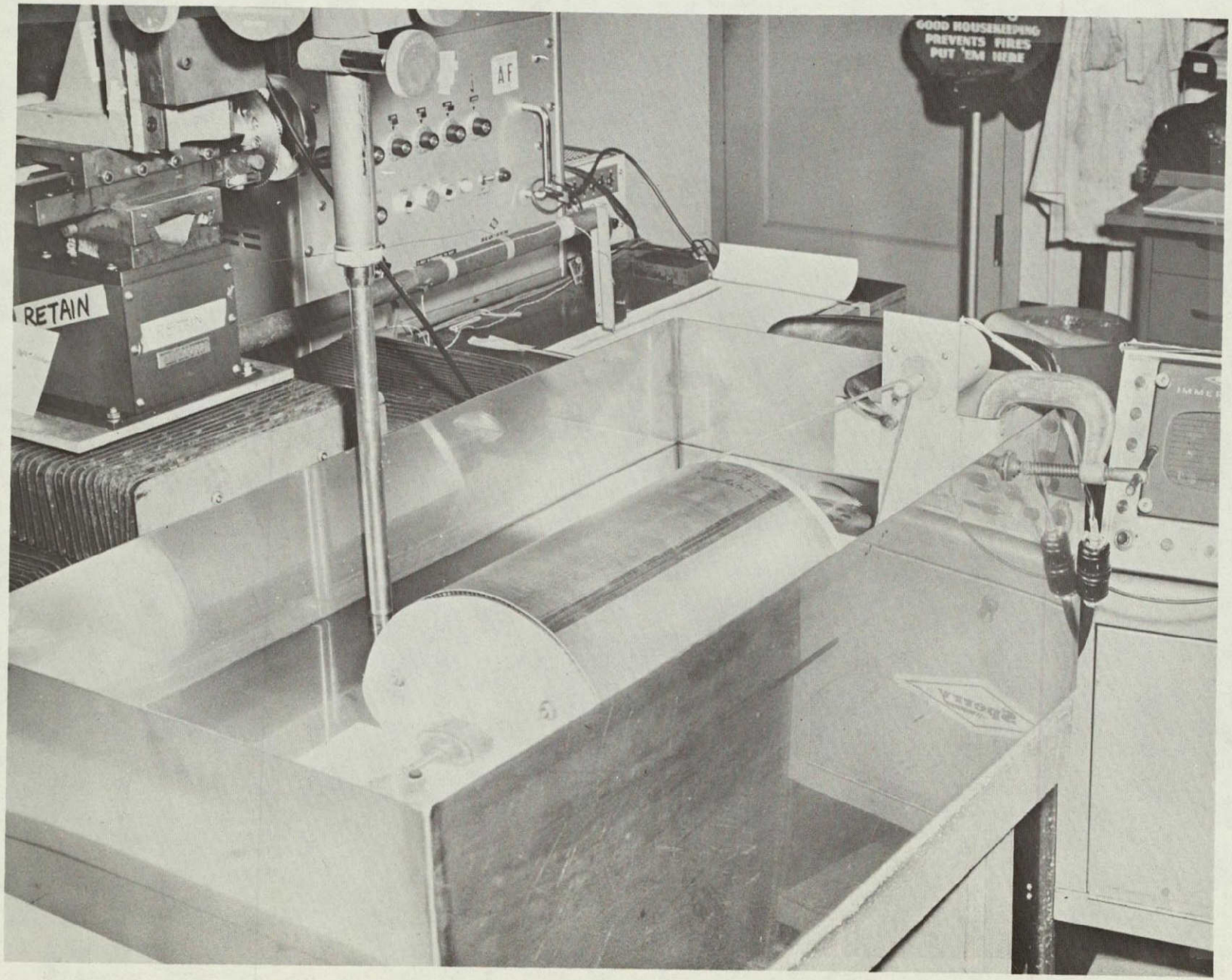

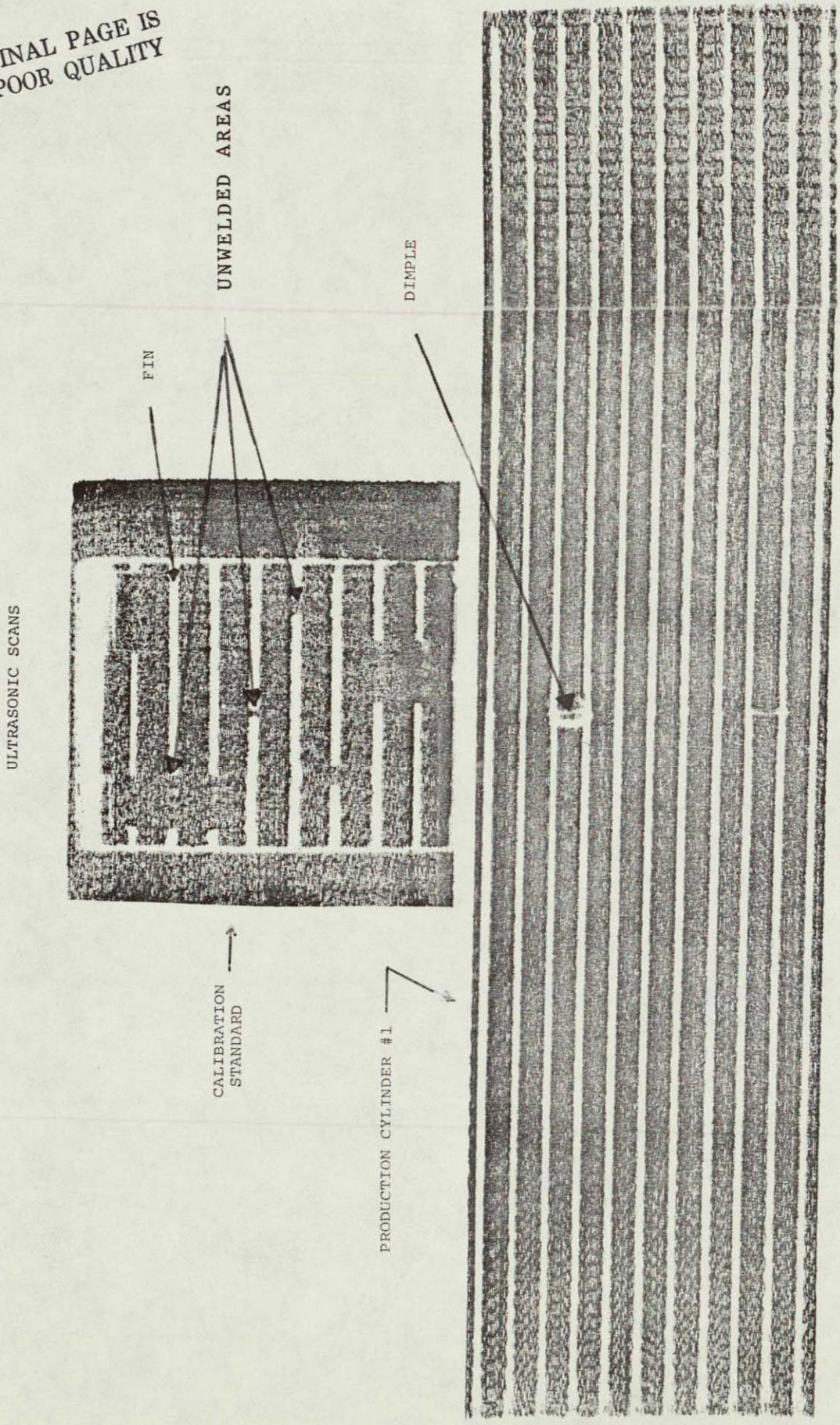

FIGURE 6-9

ULTRASONIC SCAN OF PRODUCTION CYLINDER

FIGURE 6-10

METALLOGRAPHY - 1ST PRODUCTION CYLINDER
MAGNIFICATION 100X

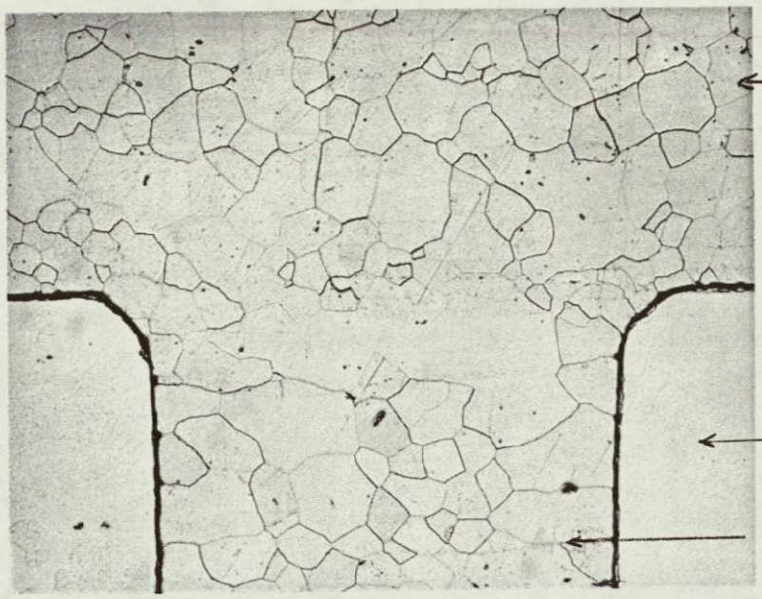

BOTTOM FIN #1

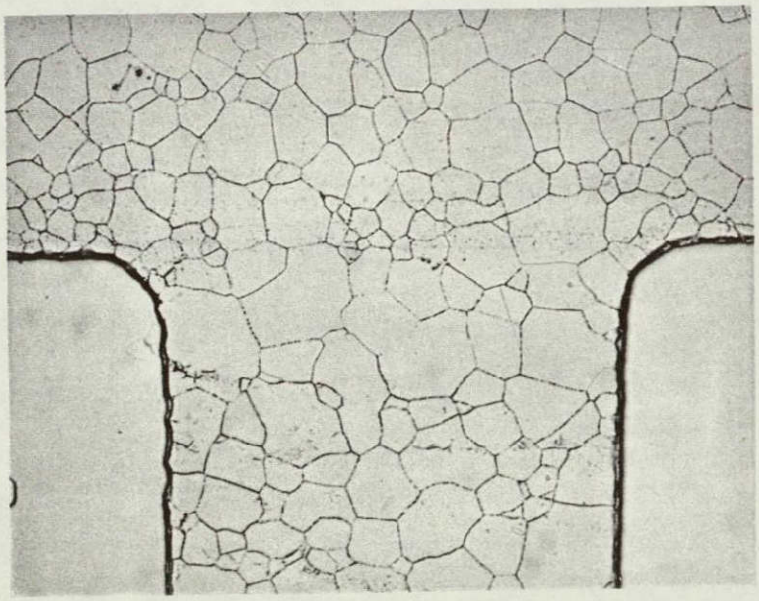

BOTTOM FIN #111

6.2.5 INNER SCROLL MACHINING

The inner scroll is machined from plate stock in several steps as indicated in Figure 6-1e. The bore section of the plate is removed by machining and the concave surface of the scroll is rough machined. The part is reversed and the outer surfaces of the scroll are rough machined. After this, the part is stress relieved at 1700K (2600^{o}F) for one hour. The part is then faced at the cylinder end. After inverting the part, the rabbeted ends of the scroll are machined, the inside surface of the scroll is machined and several of the flow passage holes are drilled and tapped undersize for the next fixturing operation. The part is inverted and installed on a fixture which supports the inside surface of the machined scroll. The part is held on the fixture by means of several undersized drilled and tapped holes located at the eventual location of air flow passage holes. After final contour machining of the outside of the scroll, the locating bolts are removed and the flow passage holes are drilled to final size with the part clamped to the fixture with external clamps. Figure 6-11 shows photographs of the finished part along with a photo of the hole drilling operation.

6.2.6 OUTER SCROLL FORMING

As indicated in Figure 6-1f, the outer scroll forming is accomplished as follows. The 0.127 cm (0.050 in) thick C-103 sheet and aluminum sheet spacers are trimmed to size. The aluminum sheet, which acts to protect the C-103 from galling on the steel die surfaces, is installed on either side of the C-103 forming blank and the assembly is installed

under the hold-down plates of the forming die. After forming, the aluminum spacer materials are removed and the C-103 scroll with integral flanges is chemically cleaned and stress relieved at 1590K (2400°F) for one hour. The flanges are removed and the scroll member formed to final size using trapped rubber forming aided by placement or removal of aluminum spacers to control spring back. The finish formed piece is stress relieved again and a final trimming and weld preparation made.

6.2.7 MISCELLANEOUS PARTS

These include mounting brackets, studs and inlet and outlet ports. The mounting brackets are formed from 0.15 cm (0.06 in) thick C-103 sheet stock with a boss welded on and tapped to receive the stud screws. The inlet and outlet ports are rolled and welded from sheet stock and sized to fit the openings in the scrolls and to provide for full penetration butt welding.

6.2.8 WELD ASSEMBLY

The diffusion welded cylinder and inner scrolls are assembled on a welding fixture which supports the ID surfaces of both parts at the weld joint. The parts are tack welded together at the OD and between the weld fixturing shoes at the ID. The weld fixture is then repositioned with the ID fixturing shoes inboard of and adjacent to the ID welds while the circumferential weld joints are made. After the inner scrolls are assembled, the outer scrolls are held in place by fixturing clamps and the components tack welded and GTA welded on the OD and ID circumferential weld joints. The process in various stages of assembly is shown in Figure 6-12.

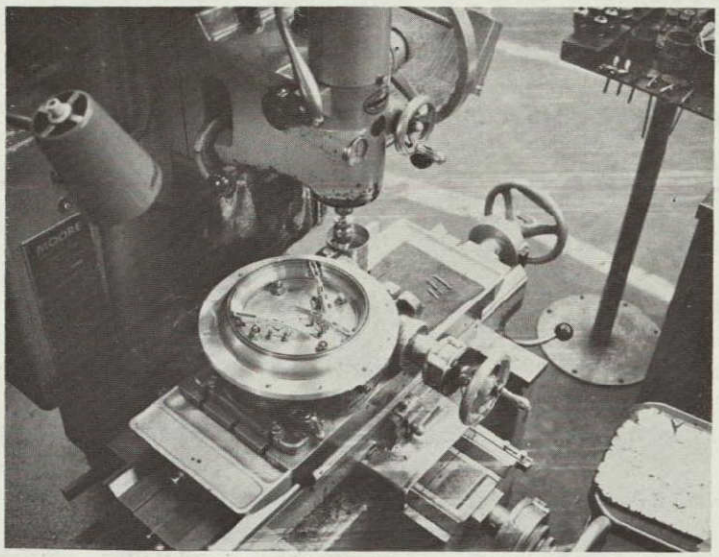

HOLE DRILLING OPERATION

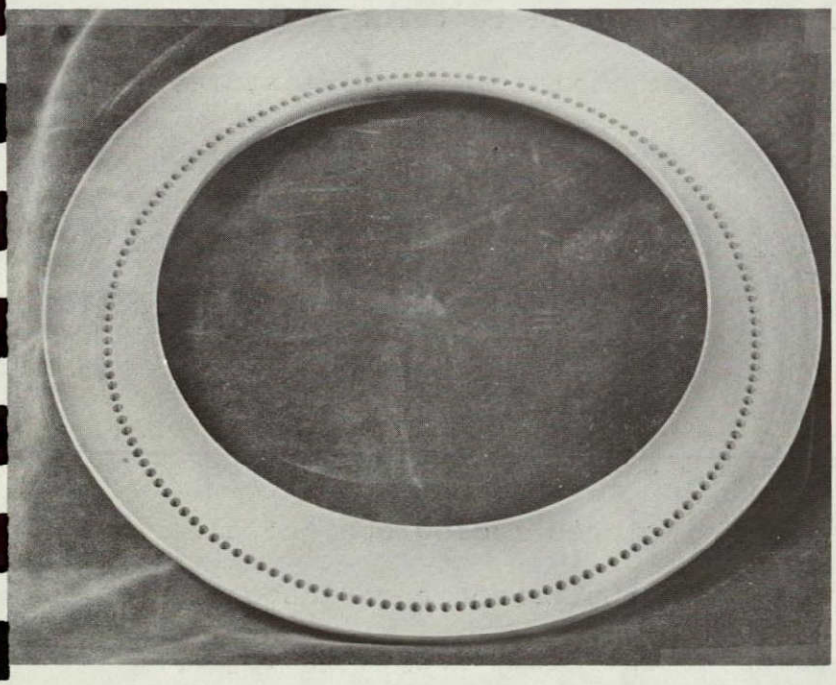

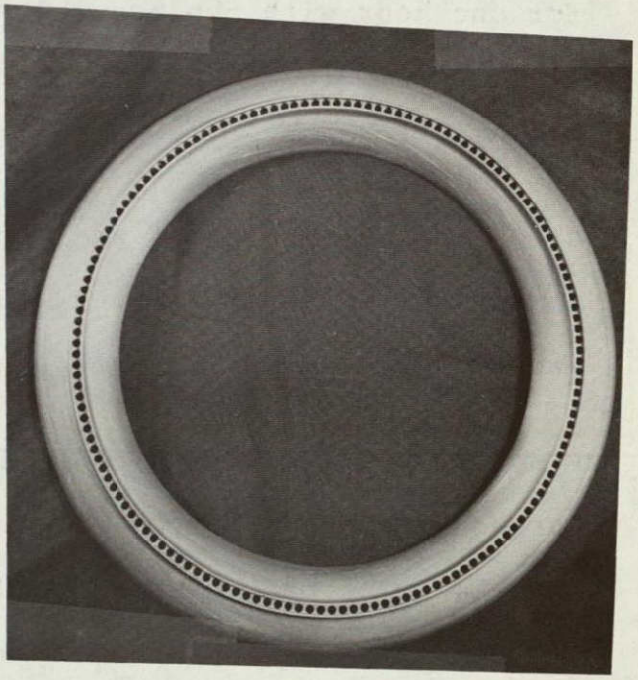

VIEWS OF MACHINED SCROLL

FIGURE 6-11

MACHINED INNER SCROLL

Holes for the forward and aft ports are precisioned machined in the scrolls, to provide for butt weld attachment of the ports. This operation is shown in Figure 6-13. The ports are precisely fixtured to the scrolls and butt welded in place from the outside, and back welded on the inside. Fixturing is required to control distortion during the welding operation. Finished welds are radiographically inspected. After the ports are in place, the forward and aft brackets and studs are welded in position. The brackets are fastened in position on special fixtures which assure accurate location of the tapped holes relative to the final assembly, during the welding operation. This is shown in Figure 6-14.

Final stress relief of the welded assembly is done at 1590K (2400^{o}F) for one hour with the assembly double wrapped in tantalum foil and positioned on a molybdenum wrapped ceramic fixture. Small fixtures are used in each port to control distortion during the heat treat.

After the stress relief the studs are faced off to critical interface dimensions in order to mate with Electric Heat Source supports. This machining operation is shown in Figure 6-15.

Final inspection of the assembly takes place after conformance tests (pressure drop and proof pressure) and includes radiography of all welds (except brackets and stud welds), 100% ultrasonic re-inspection of the diffusion welds and leak tests of the fluid loop. Photographs of a completed HSHX assembly is shown in Figure 6-16.

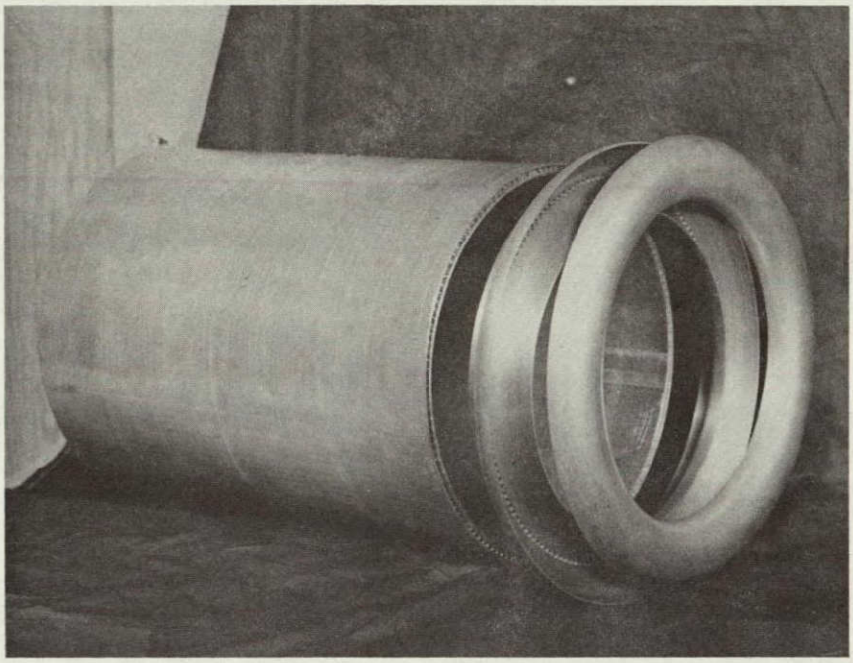

CYLINDER WITH INNER AND OUTER SCROLL PIECES

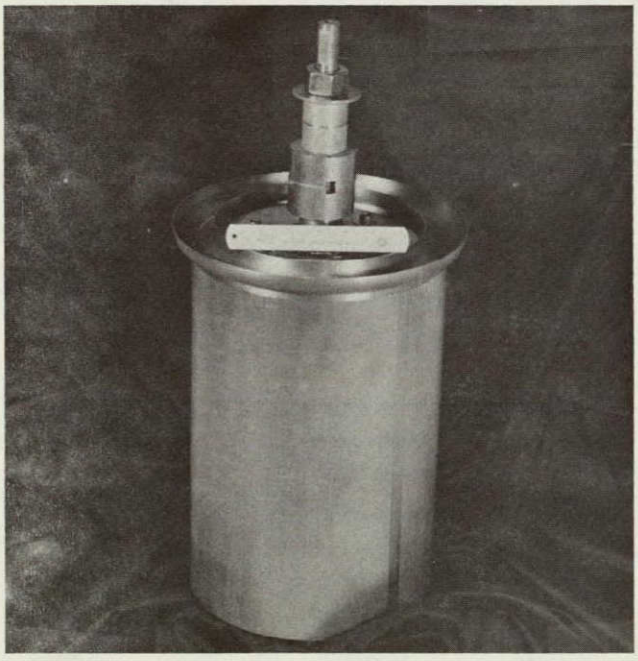

INNER SCROLL WELDED

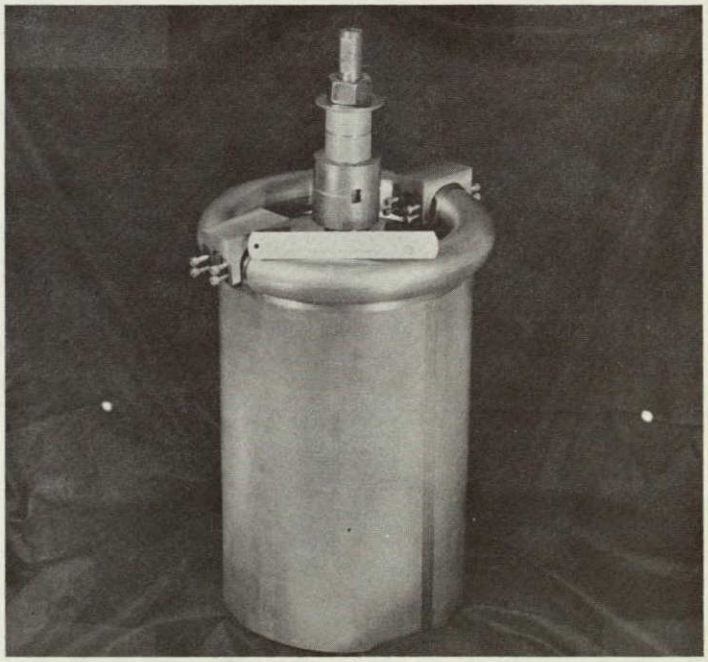

OUTER SCROLL FIXTURED

FIGURE 6-12

HSHX WELD ASSEMBLY IN VARIOUS STAGES OF COMPLETION

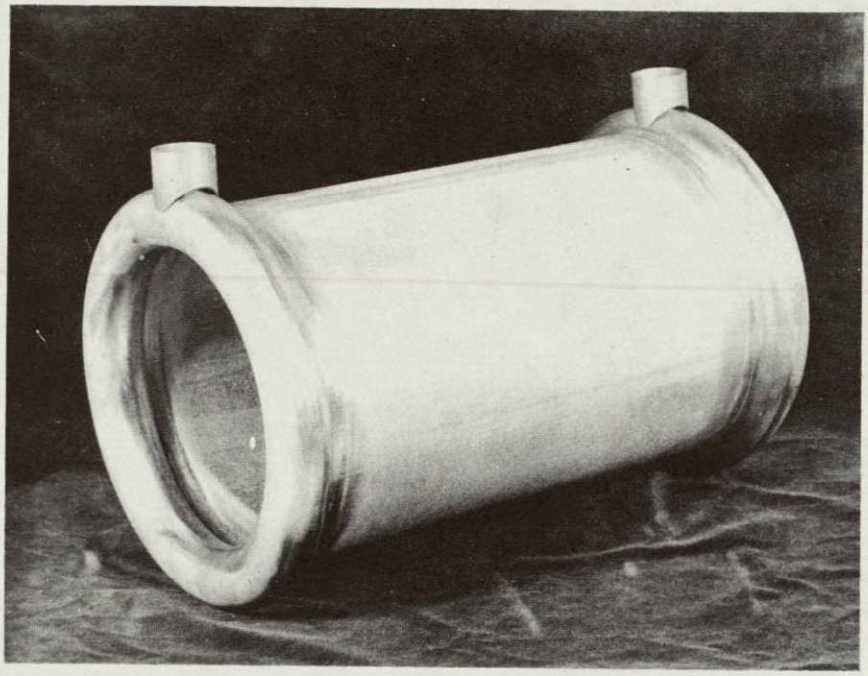

HSHX NO. 1 WITH SCROLLS WELD ASSEMBLED
AND PORTS TEMPORARILY POSITIONED.

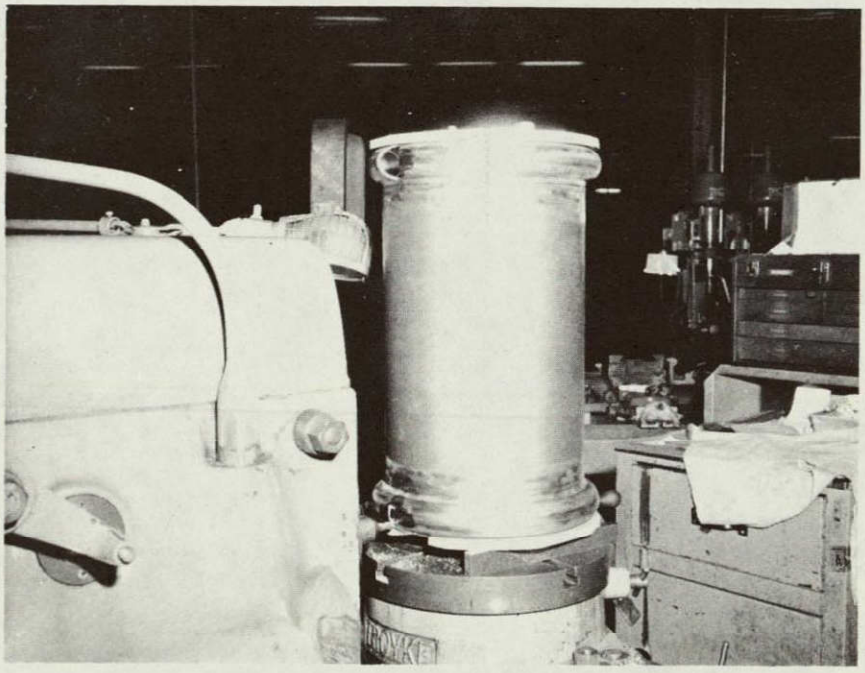

HSHX NO. 1 DURING MACHINING OF INLET
AND OUTLET PORTS.

FIGURE 6-13

PORT HOLE MACHINING

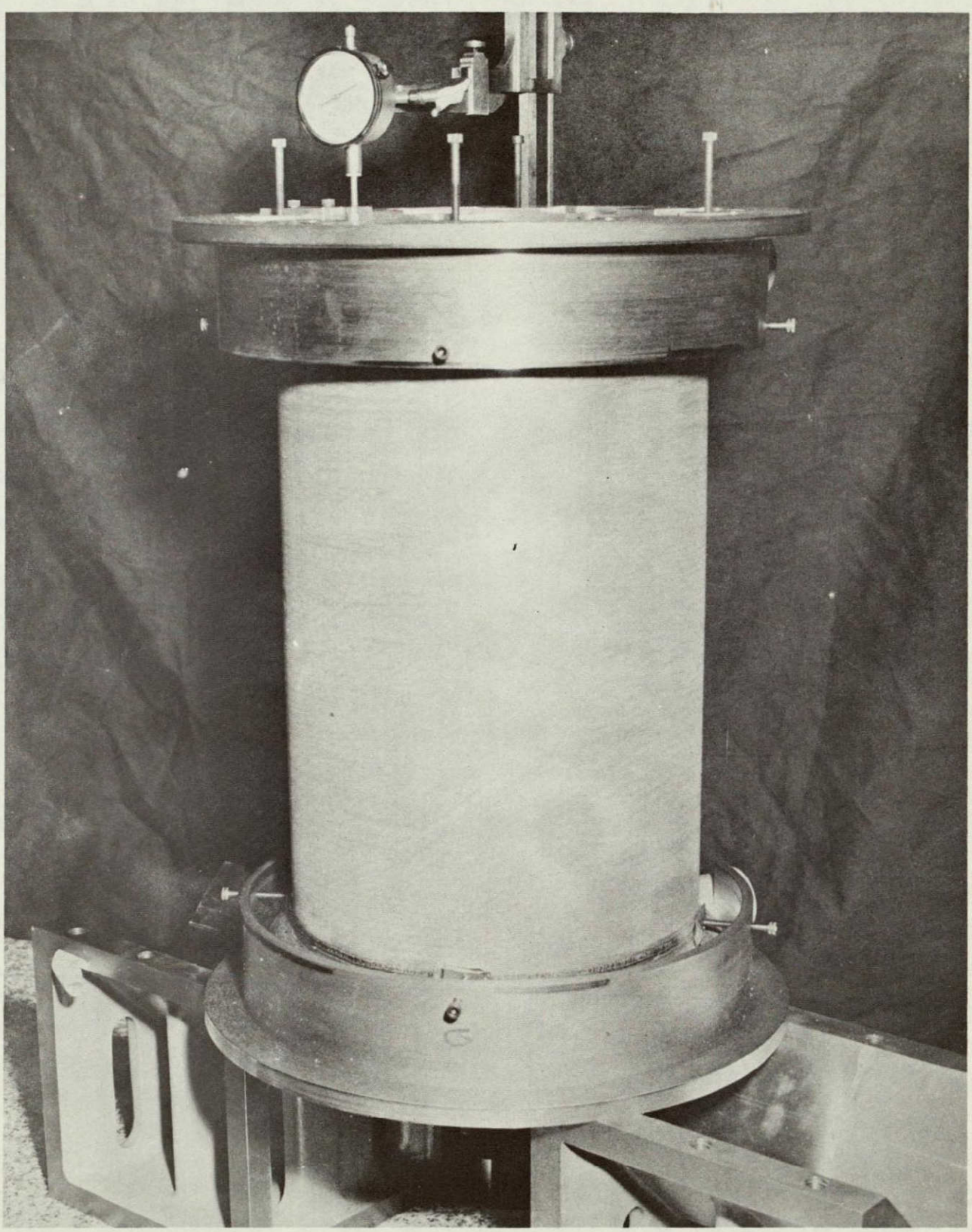

FIGURE 6-14
BRACKET FIXTURING

FIGURE 6-15

FINAL STUD MACHINING TO INTERFACE DIMENSIONS

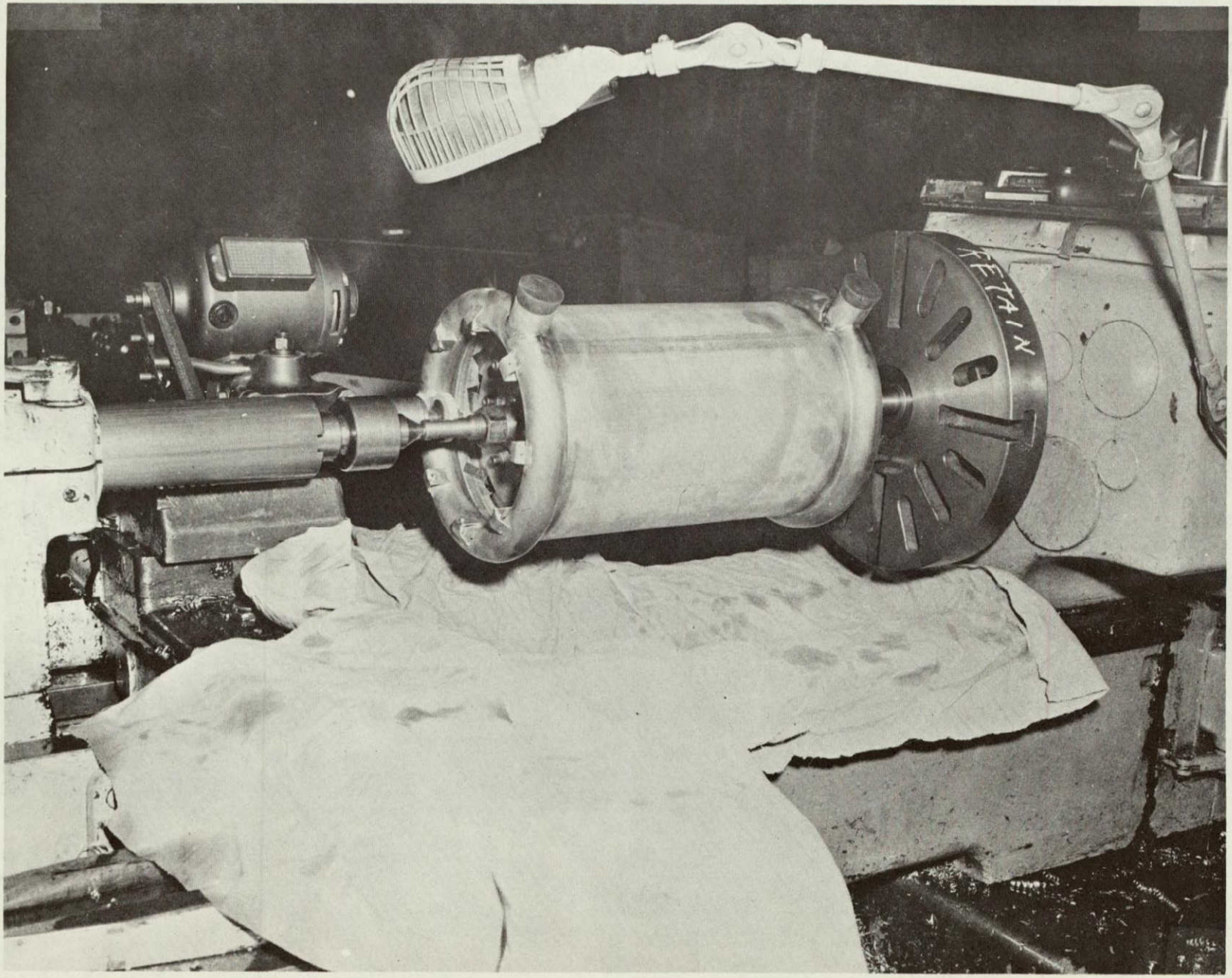

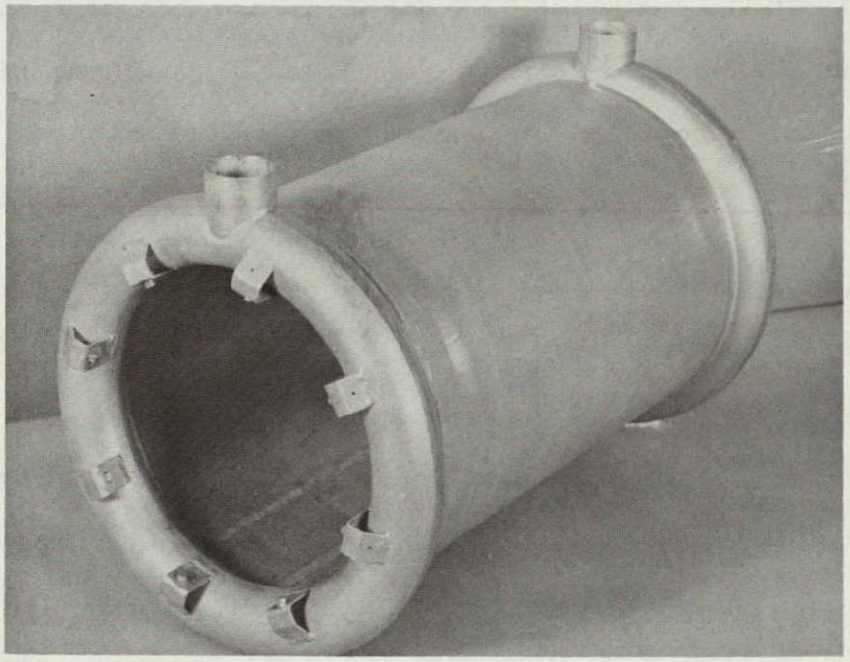

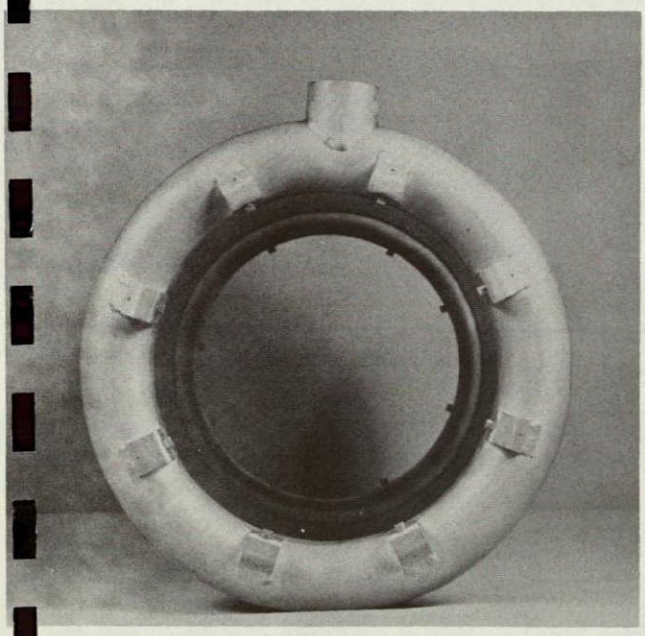

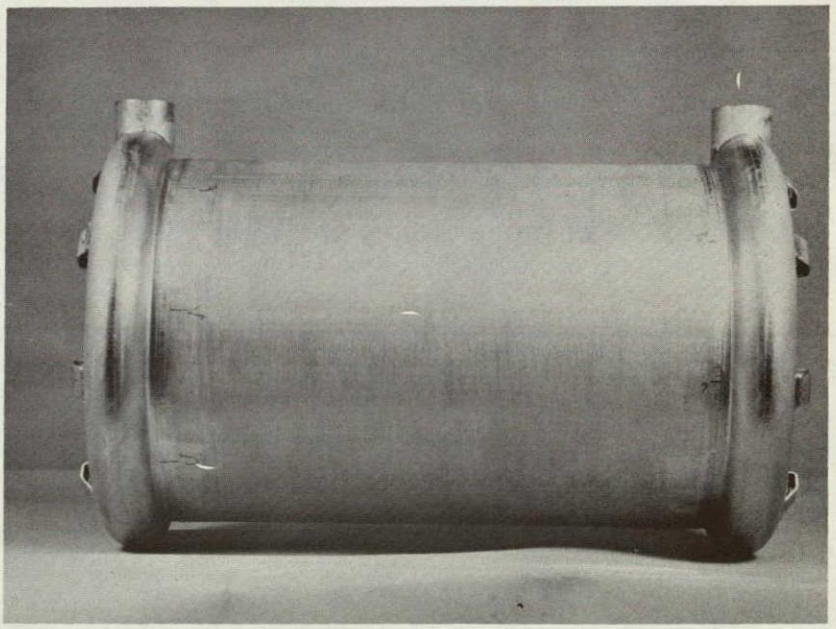

FIGURE 6-16

COMPLETED HEAT SOURCE HEAT EXCHANGER (HSHX)

6.3 SUPPORT AND MISCELLANEOUS HARDWARE

A majority of the HSA hardware components - other than the HSHX were fabricated by vendors and subcontractors. A brief description of these are given below.

6.3.1 HOUSING AND DOMES

The housing and two end domes constitute the outer envelope of the HSA and provide the mechanical support interface with the BIPS support structure. The housings and domes are machined from stainless steel (CRES 304L) and plasma sprayed with a high emissivity Radifrax coating. In a flight system these components would be fabricated from beryllium to minimize weight. Photographs of the housing and domes are shown in Figures 6-17 and 6-18.

6.3.2 END ENCLOSURE AND PRELOAD SCREW

The end enclosures are machined from a titanium alloy (6-2-4-2) and plasma sprayed with the Radifrax coating. These interface with the housing and the heat source and provide the support and load path for the electric heat source. By means of the preload screw, a prescribed preload is applied to this system. Photographs of the preload screw and enclosure are shown in Figures 6-19 and 6-20.

FIGURE 6-17

STAINLESS STEEL HOUSING

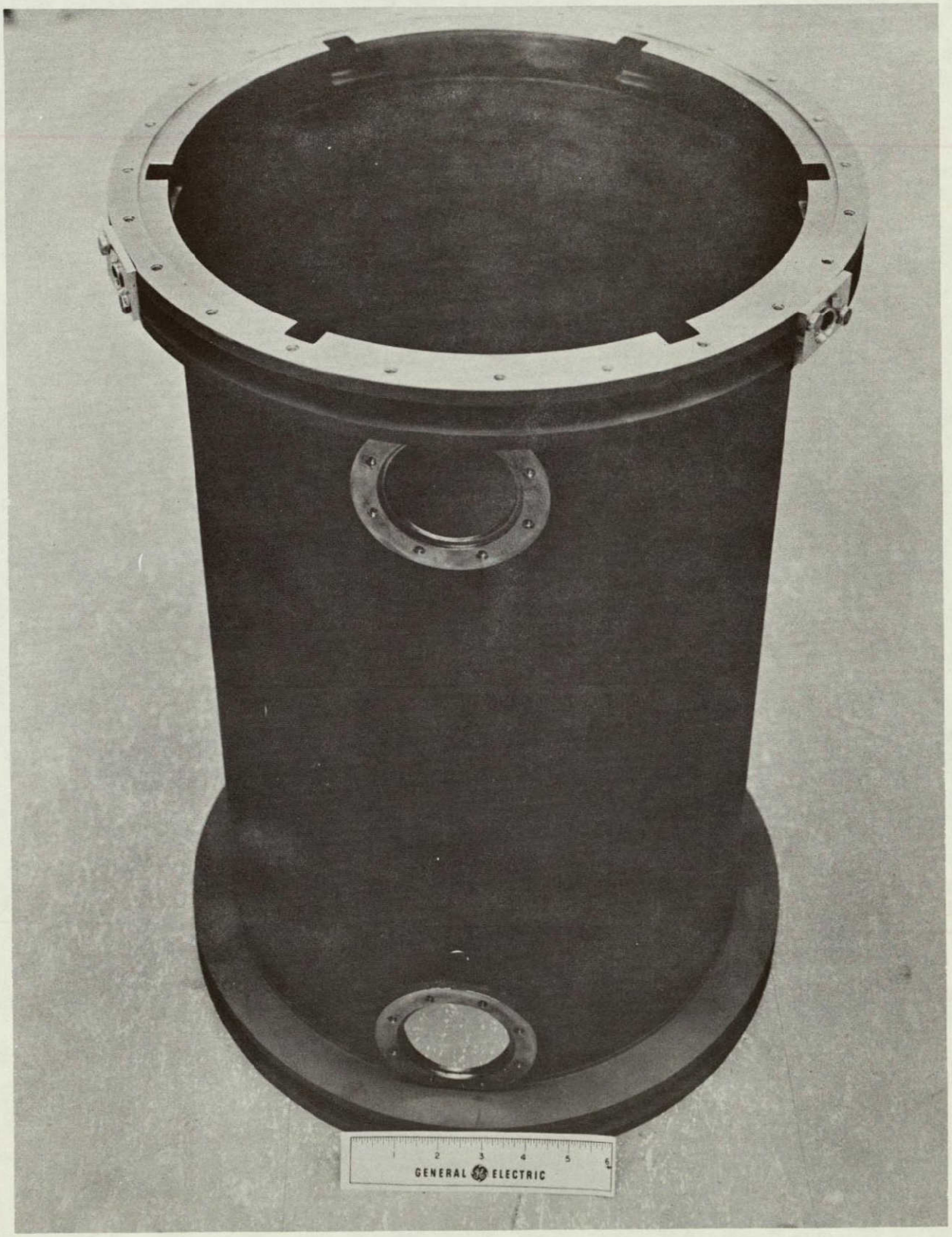

FIGURE 6-18

STAINLESS STEEL DOME WITH GAS MANAGEMENT ASSEMBLY

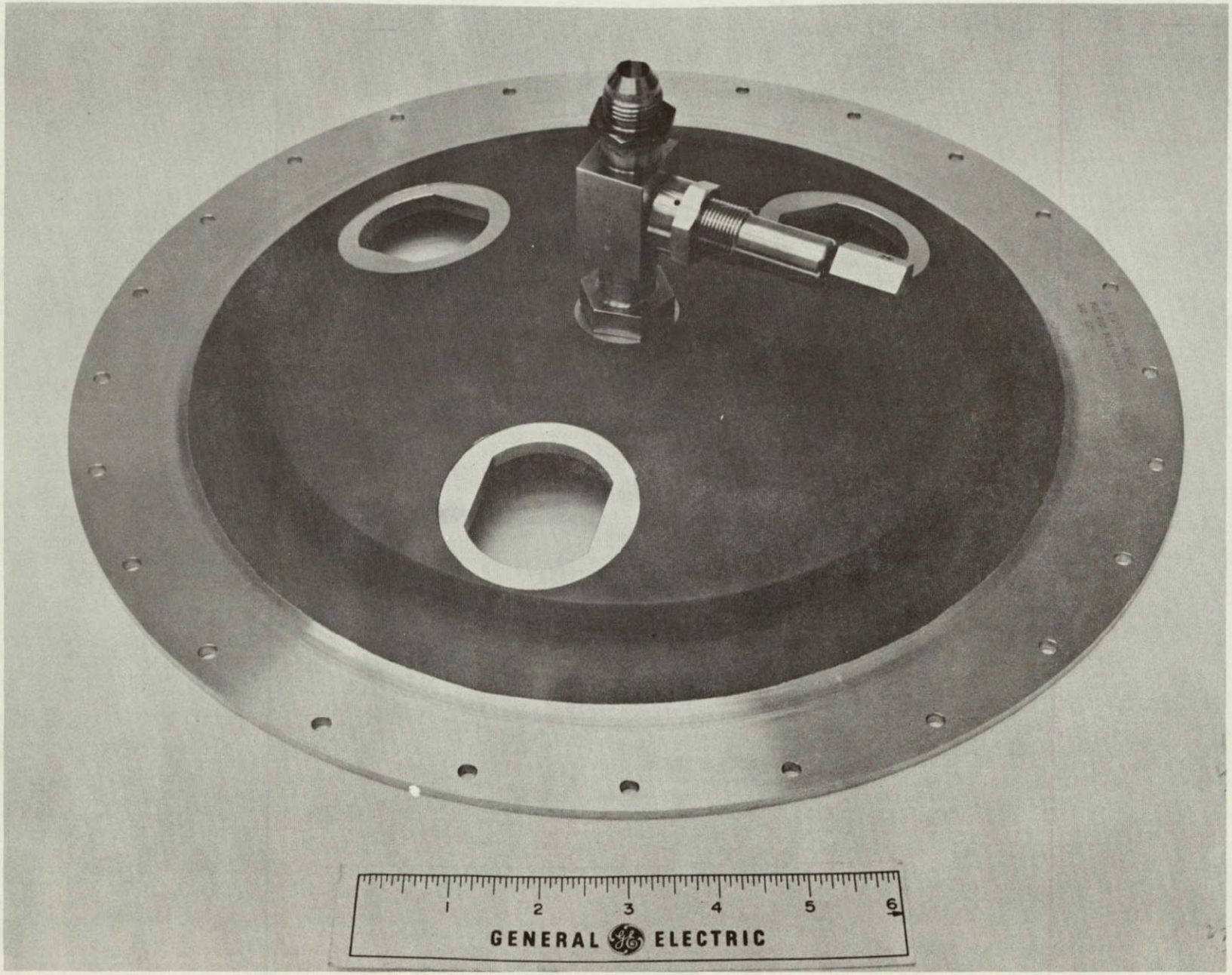

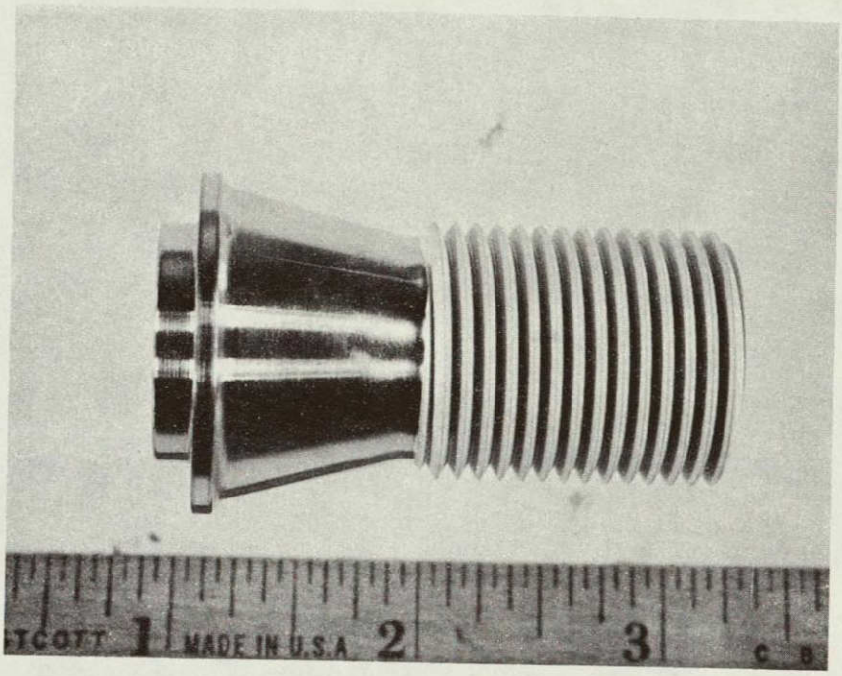

FIGURE 6-19

PRELOAD SCREW

FIGURE 6-20

TITANIUM END ENCLOSURE

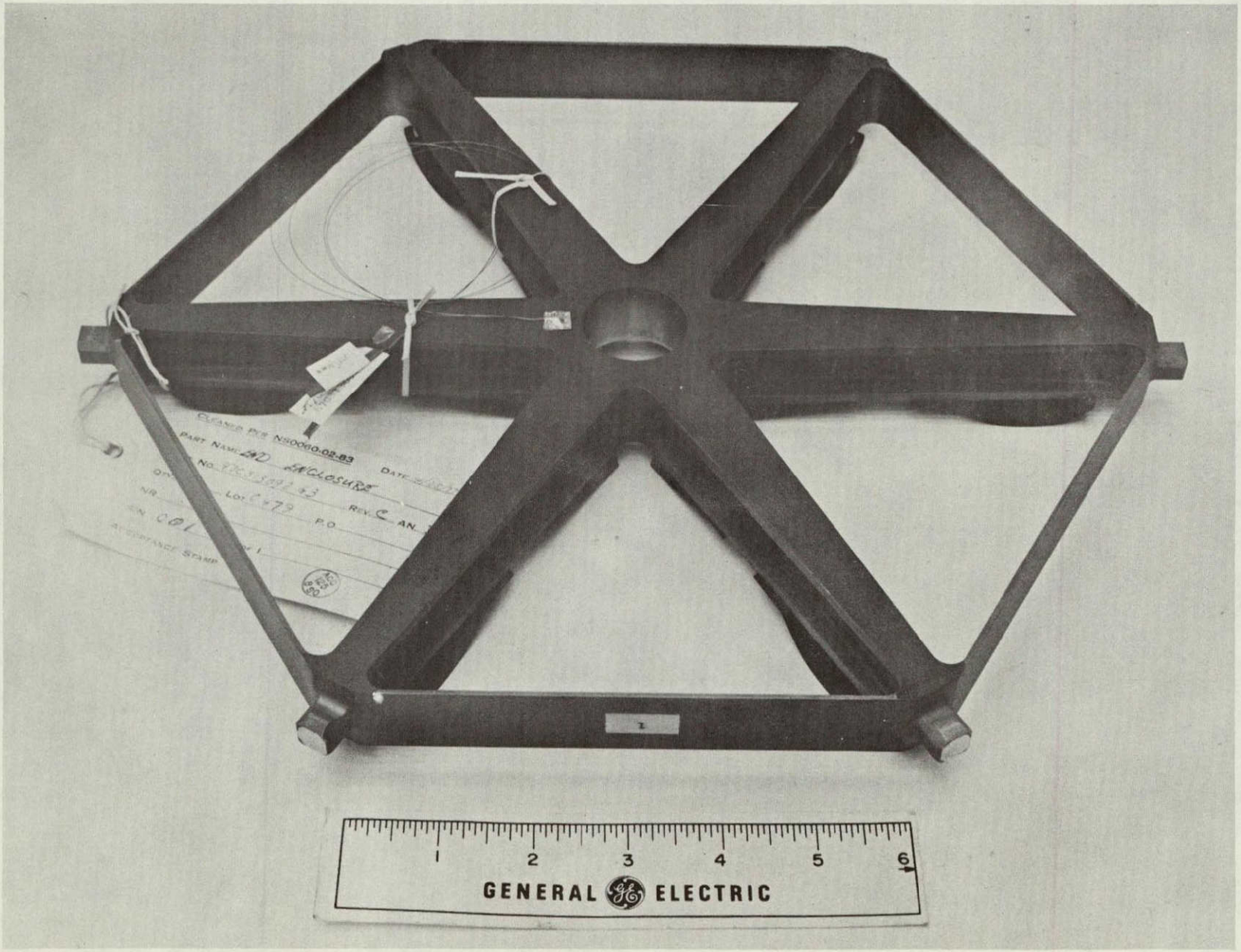

6.3.3 GAS MANAGEMENT ASSEMBLY

The gas management assembly (GMA) provides the valving for both back-filling the HSA with inert gas for auxiliary cooling modes of operation and venting the inert gas for vacuum operation. A photograph of the GMA is shown in Figure 6-21.

6.3.4 CONNECTORS

Four connectors for thermocouple instrumentation and two electric heat source power connectors are located in the end domes. A photograph of these two types of connectors is shown in Figure 6-22.

6.3.5 BELLOWS

A C-103 bellows provides the "seal" between the stainless steel housing and the inlet and outlet ducts for the auxiliary cooling mode of operation. The bellows with a "C" seal is bolted to the housing on one end and welded to the inlet/outlet duct on the opposite end. The bellows allow for lateral growth of the heat exchanger during heat up from room temperature. A photograph of the bellows is shown in Figure 6-23.

FIGURE 6-21

GAS MANAGEMENT ASSEMBLY

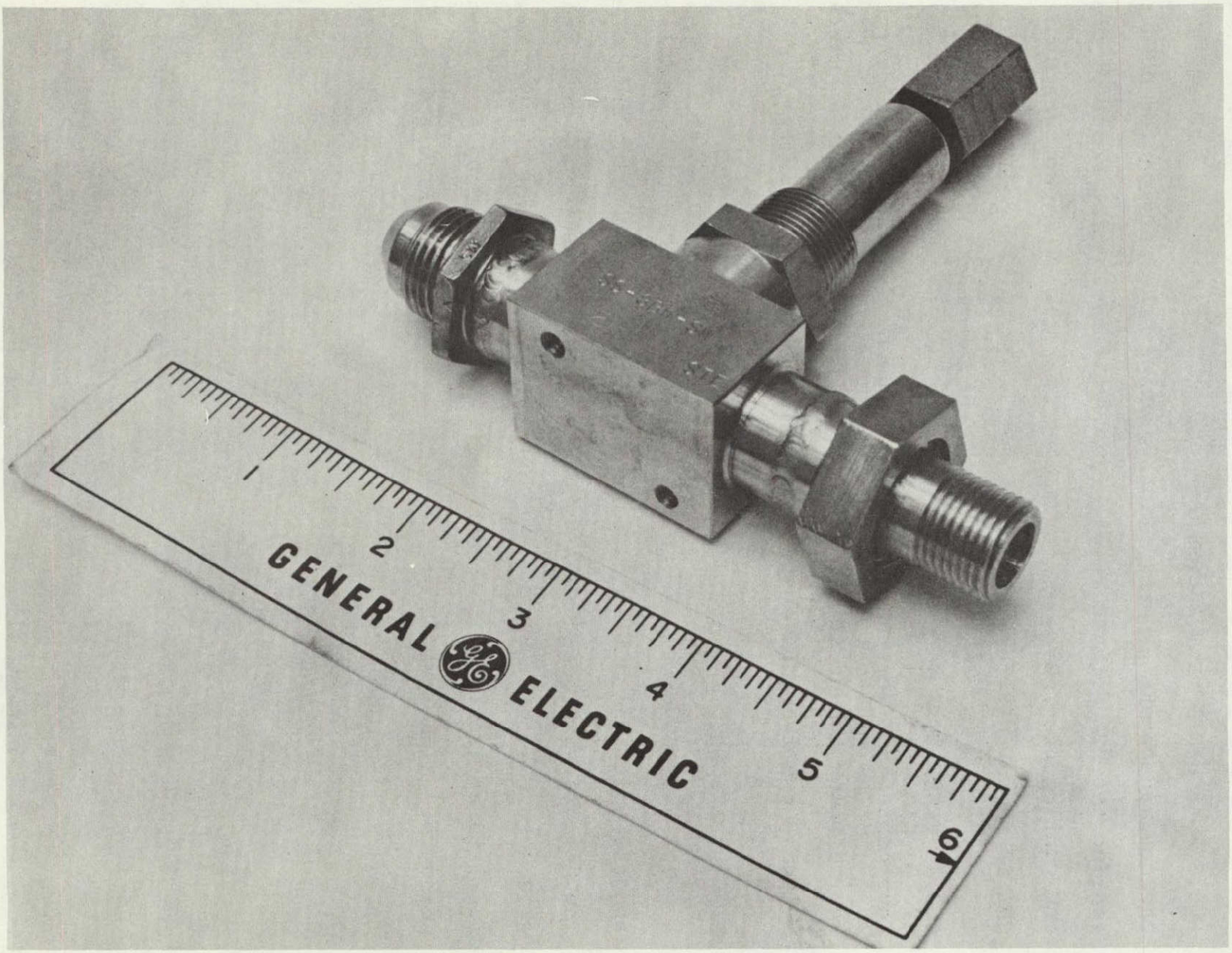

FIGURE 6-22

CONNECTORS

POWER CONNECTOR

INSTRUMENTATION CONNECTOR

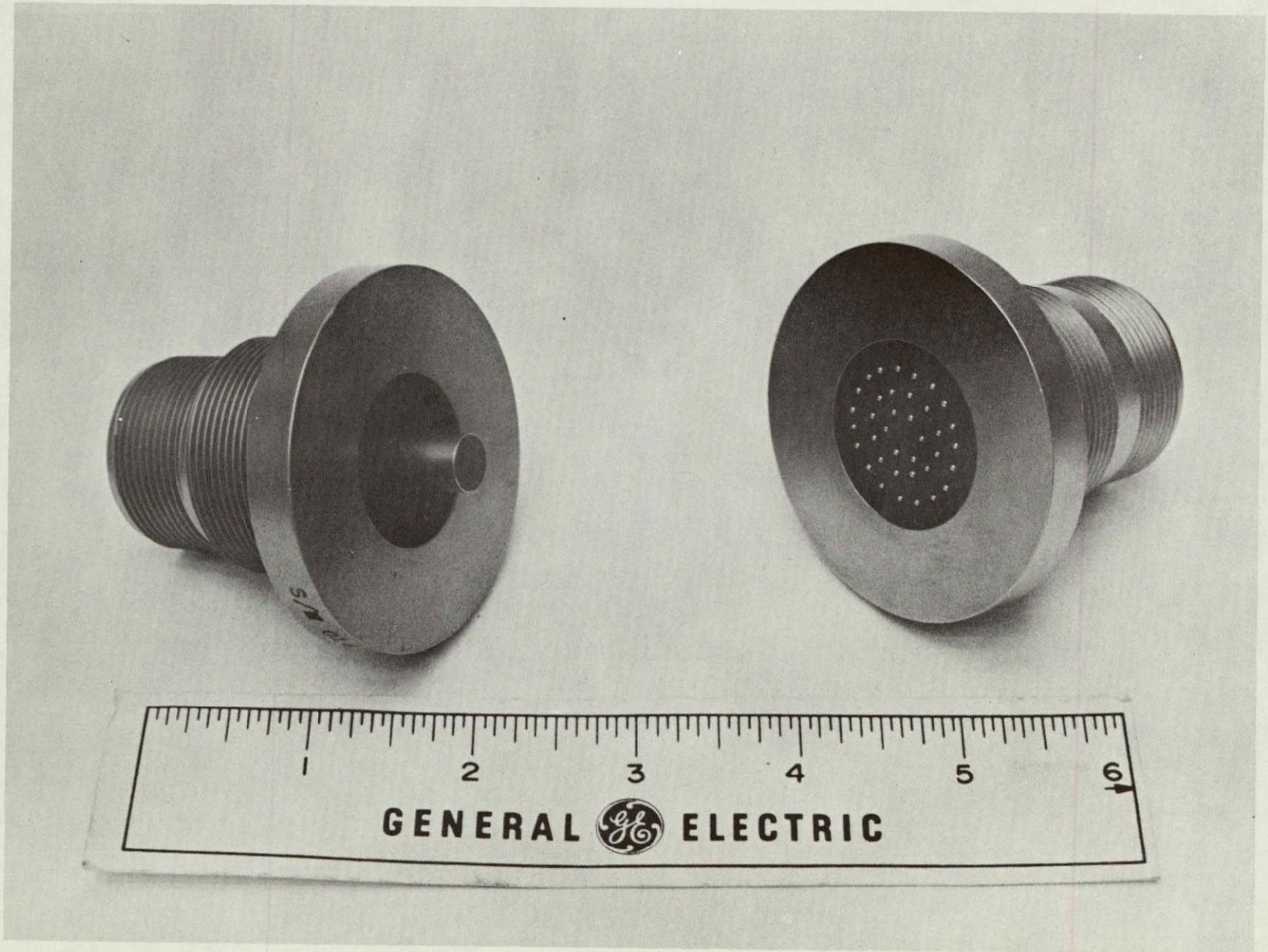

FIGURE 6-23

HSA BELLOWS

6.4 INSULATION

The multifoil insulation system consists of a large cylindrical blanket and two end caps which form a cylindrical enclosure surrounding the HSHX and two short cylindrical blankets which insulate the inlet and outlet ports. The large cylindrical blanket consists of 39 inboard layers of 0.00127 cm (0.0005 in) molybdenum foils followed by 20 layers of 0.00127 cm (0.0005 in) nickel foils. These foils are supported by a 0.076 cm (.030 in) C-103 tube inboard of the blanket. A 0.0076 cm (0.003 in) stainless steel outboard cylindrical sheet surrounds the blanket to aid in handling. The end caps and short port cylindrical blankets consist of 60 layers of 0.00127 cm (0.0005 in) molybdenum foils. The foil on the end caps are sandwiched between two sheets of 0.038 cm (0.015 in) C-103 alloy. All of the foils are sparcely coated on the inboard surface with zirconia. Five to six percent of the surface area is coated with zirconia with a coating density of about 0.030 to 0.090 mg/cm^2. Photographs of the instrumented large cylindrical blanket and end cap are shown in Figures 6-24 and 6-25 respectively.

6.5 WEIGHT

Table 6-2 presents calculated and actual measured weights. Additionally an estimate of a flight configuration is given. The latter assumes a beryllium housing and domes as well as a weight optimized insulation support configuration.

FIGURE 6-24

INSULATION CYLINDER

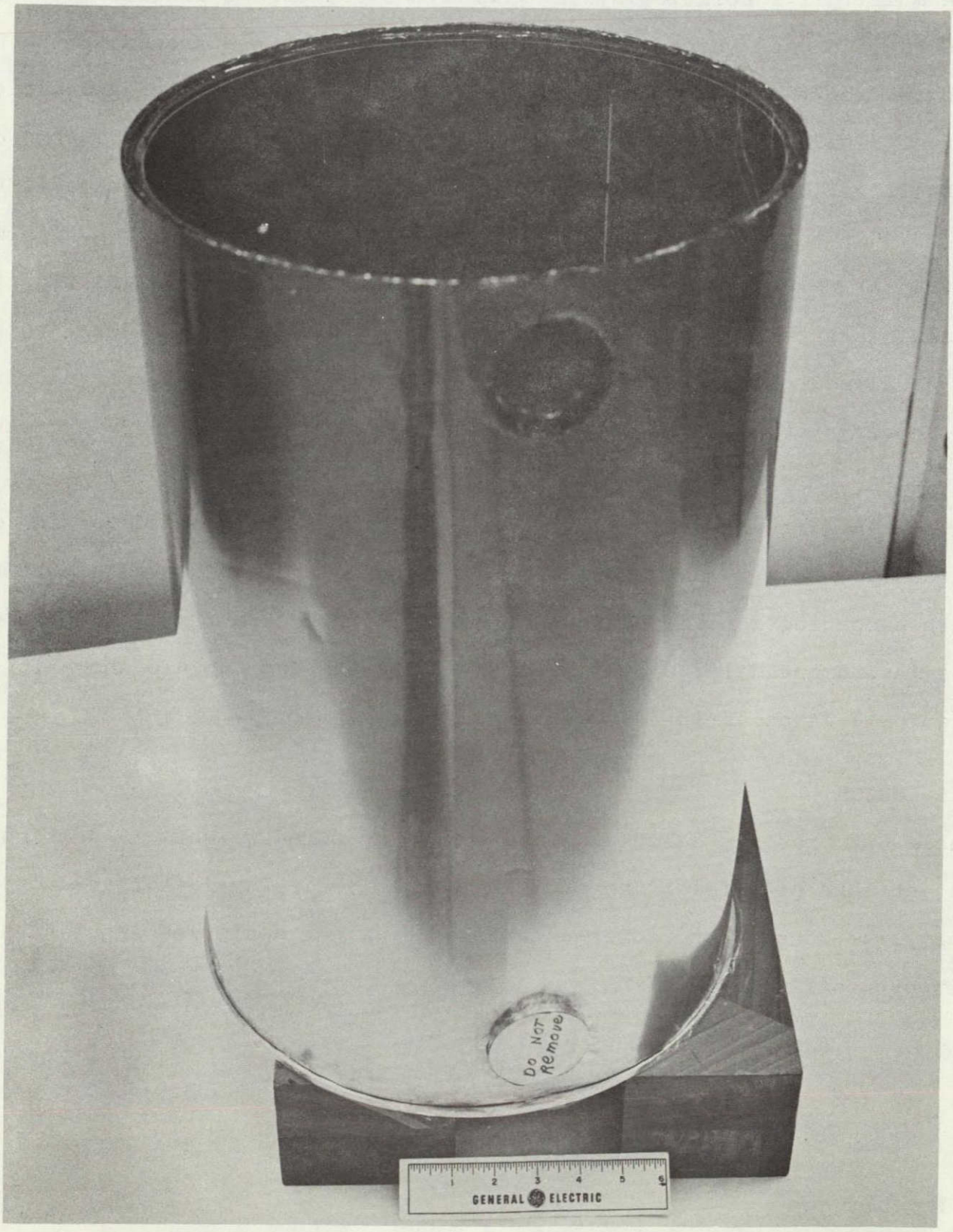

FIGURE 6-25

INSULATION END CAP

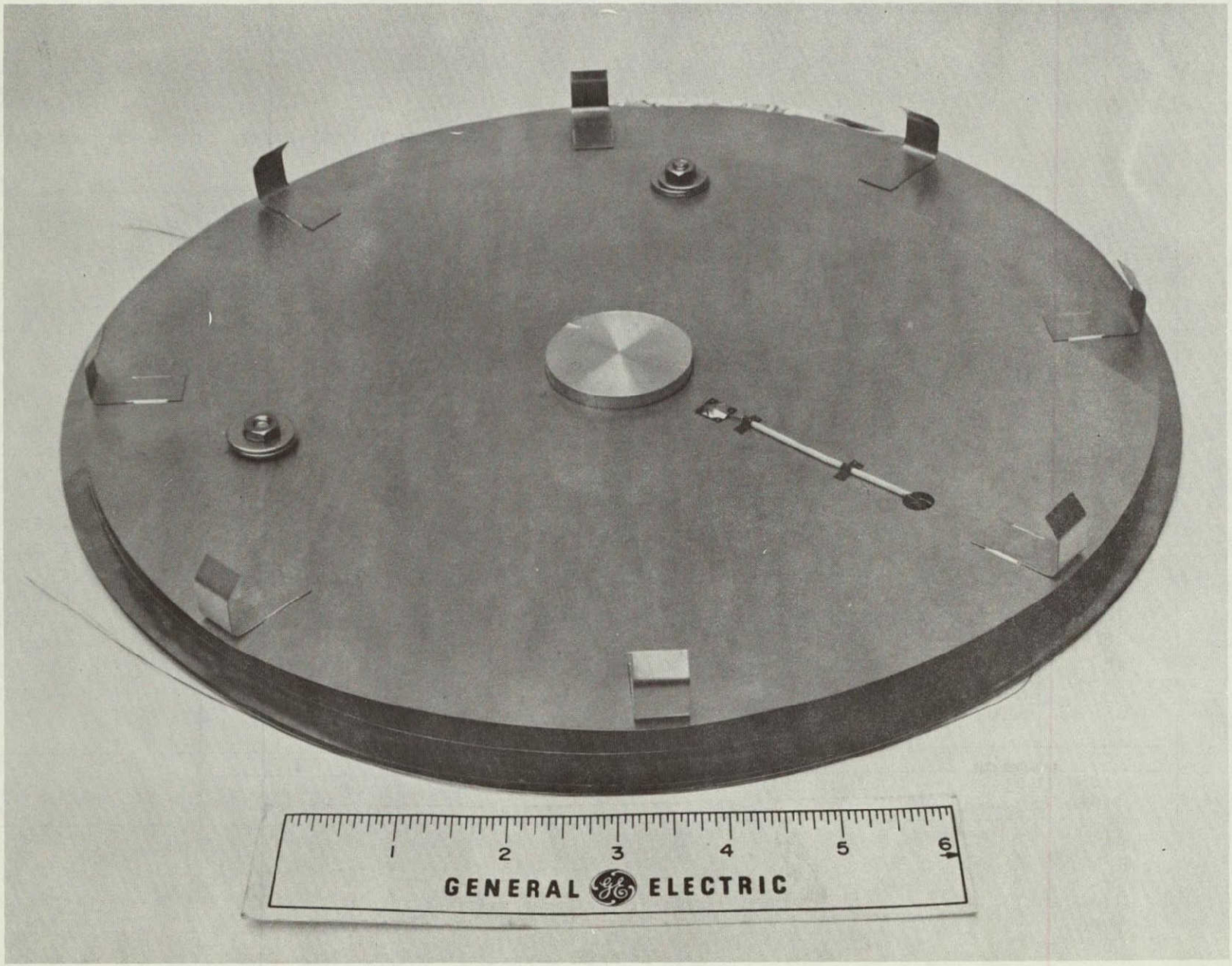

TABLE 6-2

HSA WEIGHT SUMMARY

Item	Qty.	GDS Total Wt. (Calculated)			GDS Total Wt. (Measured)			Projected Flight Wt.		
		Kg	Lb		Kg	Lb		Kg	Lb	
HSHX	1	8.886	19.59		9.299	20.50		9.299	20.50	
Housing Assy.	1	14.370	31.68		14.288	31.50		3.225	7.11	(Beryllium)
Insulation Cyl.	1	6.709	14.79		7.516	16.57		3.606	7.95	
Insulation End	2	1.964	4.33		2.141	4.72		0.930	2.05	
End Enclosure	2	1.950	4.30	103.65	2.304	5.08	103.71	1.814	4.00	
Preload Screw	2	0.218	0.48	Lb.	0.295	0.65	LB	0.295	0.65	
Dome	2	10.414	22.96		9.095	20.05		1.207	2.66	
Connector-Power	2	0.835	1.84		0.703	1.55			-	
Connector-Instru.	4	1.669	3.68		1.402	3.09			-	
Bellows	2				0.830	1.83		0.830	1.83	
Gas Mgt. Assy.	1				0.476	1.05		0.476	1.05	
Misc. Hardware (Seals, Screws, Insul., etc.)		3.969	8.75*		2.663	5.87				
Subtotal		51.006	112.45					23.932	52.76	
EHS		21.546	47.5						-	
IHS			-					18.824	41.50	
Total Weight		72.552	159.95					42.756	94.26	

*Including Bellows and Gas Mgt. Assembly

e. Successful completion of a room temperature air flow test of the first HSHX unit fabricated to verify pressure drop. The tests should be conducted at design pressure with the air flow adjusted to match Reynolds numbers expected with the design working fluid. A helium leak test of this unit shall be conducted as the last test prior to delivery.

7.2 TEST FLOW PLAN

The sequential plan to accomplish the acceptance tests is depicted in the flow plan given in Figure 7-1. It provides for acceptance testing of the HSHX's prior to assembly in the HSA's. Since the final HSA assembly was not required, those tests indicated in the figure for "HSA Assembly" were not performed .

7.3 HSHX PROOF PRESSURE TEST

7.3.1 TEST CONDITIONS

The HSHX was tested at room temperature under a gauge pressure of 2.5 MPa $\pm$ 0.07 MPa (360 psi $\pm$ 10 psi) for a period of not less than 10 minutes. This pressure requirement is based upon a 1.5 safety factor over the design operating pressure and takes into consideration the increased yield strength of C-103 alloy at room temperature as compared to its yield strength at operating temperature as indicated in the equation:

$$P_T = k \times \frac{\sigma RT}{\sigma ET} \times P_D$$

where:

P_T = Room temperature proof test pressure - 2.5 MPa (360 psig)

k = Safety factor (1.5)

σ_{RT} = Room temperature 0.2% yield strength - 275 MPa (40 ksi)

σ_{ET} = Elevated temperature 0.2% yield strength - 127 MPa at 1227K (18.5 ksi at 1750°F)

P_D = Design pressure - 0.8 MPa at 1227K (115 psia at 1750°F)

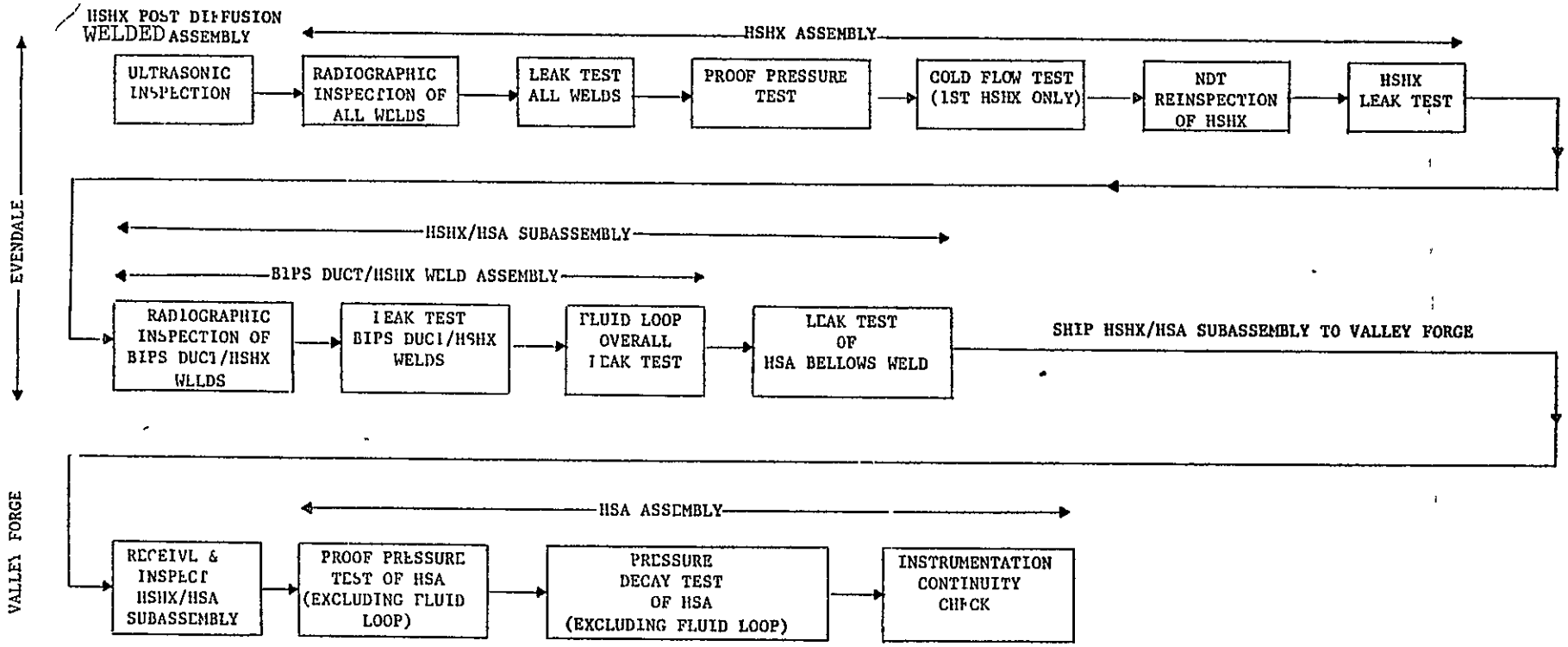

MINI-BRAYTON HSA ACCEPTANCE TEST FLOW PLAN

FIGURE 7-1

7.3.2 TEST EQUIPMENT

Hydraulically pumped distilled water was used as the pressurizing medium. The high pressure water supply was connected by means of high pressure tubing to the HSHX through a control valve, particle filter and a calibrated pressure gauge; connections at the HSHX was made using expandable neoprene rubber plugs. The HSHX was filled with water in such a manner as to minimize the possibility of entrapment of air pockets with the test system. Figure 7-2 shows a schematic of the test set up.

7.3.3 PRESSURE TEST PROCEDURE

The pressure was increased slowly in five approximately equal pressure increments holding for a minimum of 10 seconds at each of the four pressure increments and for a minimum of 10 minutes at the 2.5 MPa $\pm$ 0.07 MPa (360 psig $\pm$ 10 psig) maximum pressure. After completion of the test the pressure was slowly released in five successive approximately equal increments holding for a minimum of 10 seconds at each of the four pressure increments.

7.3.4 TEST RESULTS

All three HSHX units successfully passed the proof pressure tests without any visible effects and without any indication of leaks or degradation of welds as indicated by subsequent leak tests, and radiographic and ultrasonic inspection.

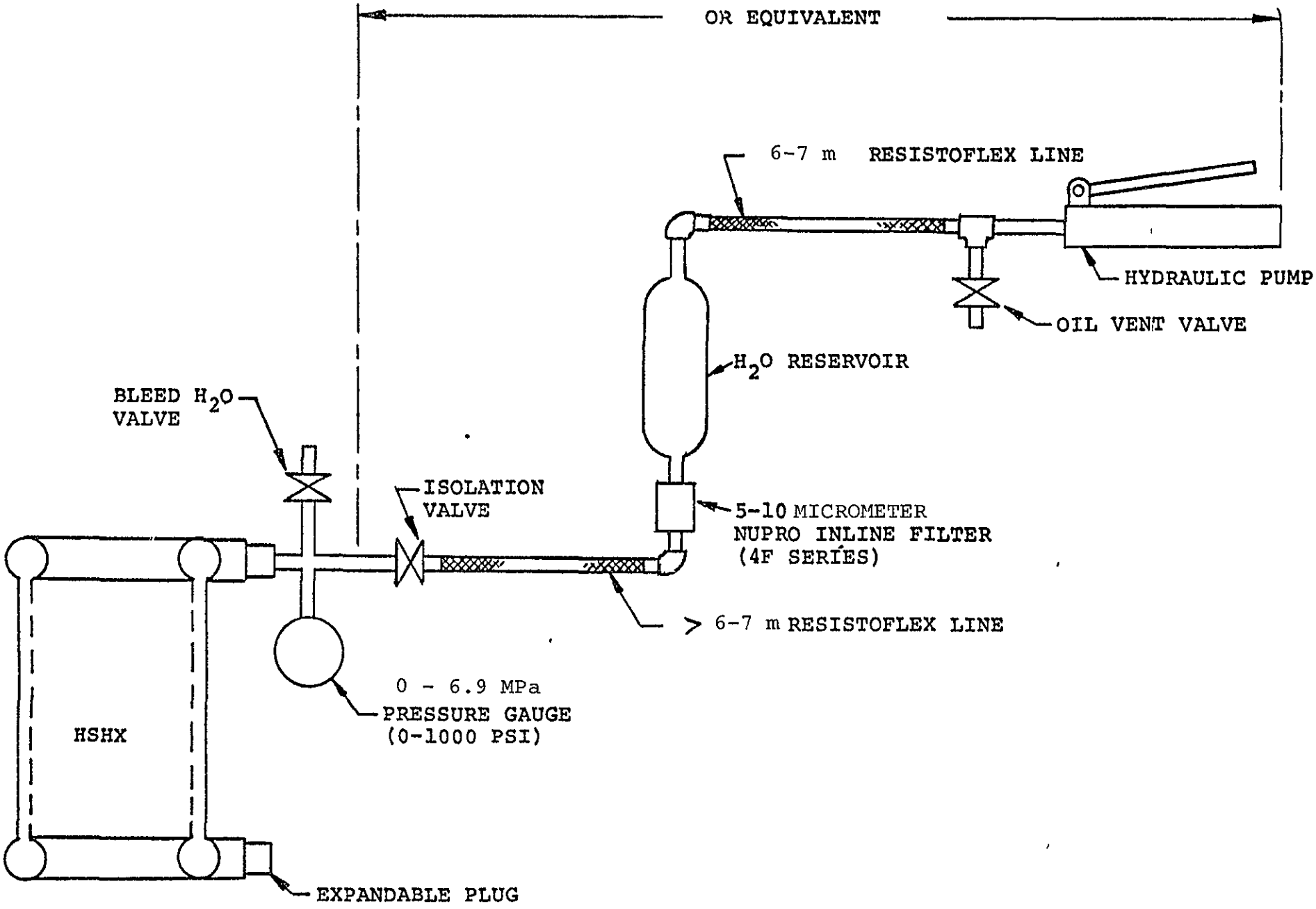

FIGURE 7-2 HSHX PROOF PRESSURE TEST SET-UP

7.4 HSHX PRESSURE DROP TEST

7.4.1 TEST CONDITIONS

HSHX flow conditions required by design parameters are as follows:

Temperature	1061K (1450°F) (mean)
Pressure	0.243 MPa (35.3 psia)
Maximum Pressure Drop	0.0015 MPa (0.22 psia)
Flow Rate	0.057 Kg/sec (0.126 lb/sec)
Fluid	83.8 Molecular Weight (He/Xe)

In order to retain equivalent Reynolds number flow conditions using air in a flow test at room temperature, the following conditions were utilized:

Temperature	R.T. - 300K (80°F)
Pressure	0.243 MPa (35.3 psia) or (20.6 psig)
Maximum Pressure Drop	92.4 Pa (0.0134 psia) or 0.37 inch H_2O
Flow Rate	0.0158 Kg/sec (0.0348 lb/sec) or 2.09 lb/min)
Fluid	Air

7.4.2 TEST EQUIPMENT

The HSHX was connected to a pressurized air supply through a pressure regulator, flow control valve, pressure gauge and air flowmeter as shown in Figure 7-3; a throttling valve was installed down-stream of the HSHX exit port to maintain system pressure at the HSHX inlet and a water manometer was installed to read the pressure differential between the HSHX inlet and outlet. For flow stability purposes a ten diameter length of 3.81 cm (1-1/2 inch) ID tubing was connected to the inlet and outlet ports. Pressure gauge and water manometer connections were made in these test duct

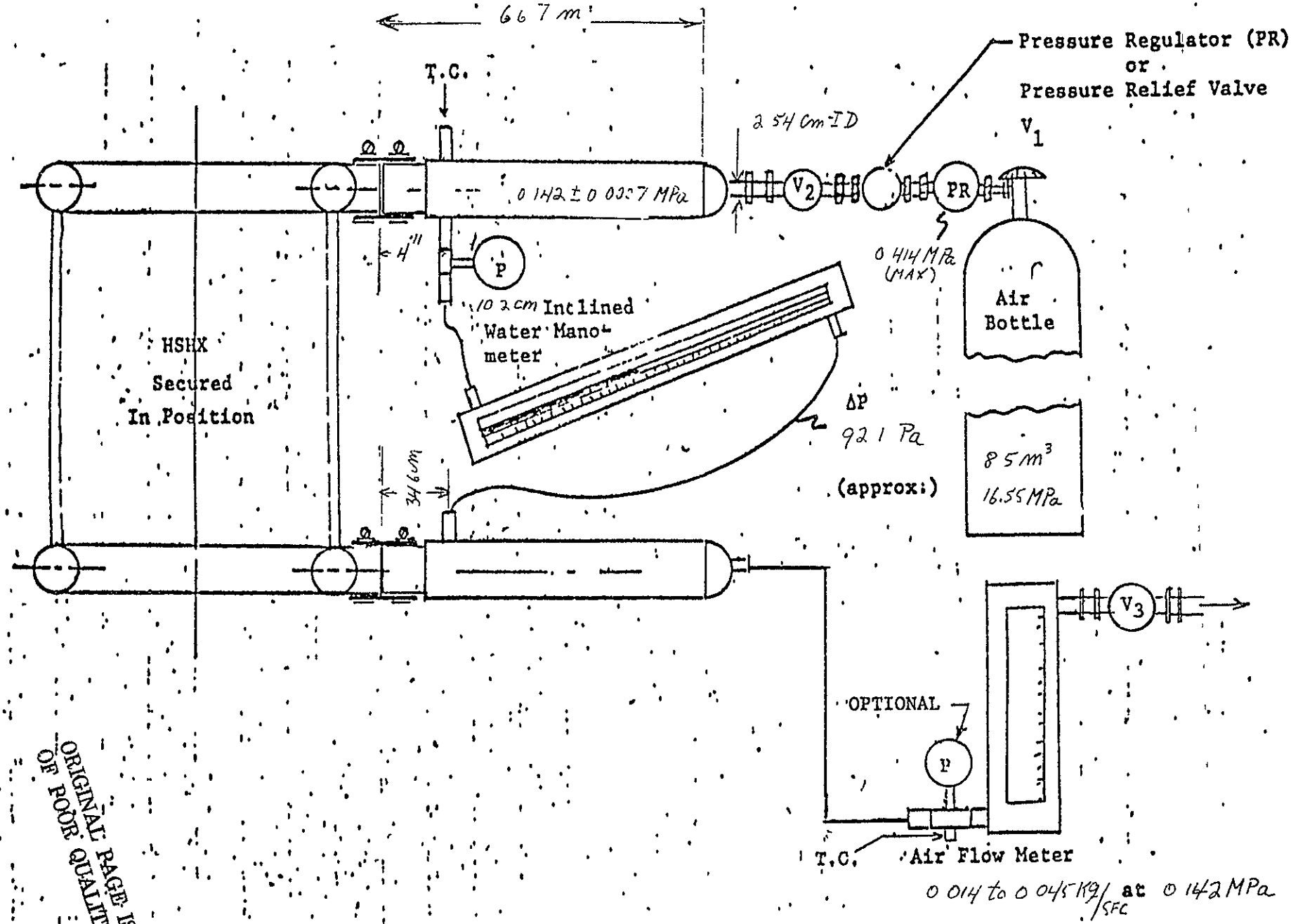

FIGURE 7-3 HSHX PRESSURE DROP FLOW TEST SET-UP

extensions as near as practical to the inlet and outlet ports of the HSHX. Temporary butt joints were made between these test ducts and the HSHX inlet and outlet ports by means of hose clamped rubber sleeves over the butt joints.

7.4.3 TEST PROCEDURE

At least six air flow tests were performed at 0.243 MPa (35.3 psia or 20.6 psig + 0.1 psig) at flow rates from below 0.0158 Kg/sec (0.0348 lb/sec) to approximately 0.0454 Kg/sec (0.1 lb/sec). Flow rate and pressure were conducted by regulating the inlet and outlet air control valves and the water manometer was read when required test conditions were established.

7.4.4 TEST RESULTS

Although pressure drop tests were required only on one HSHX, tests were conducted on all three HSHX's. Test results are shown in Figure 7-4 along with the results scaled to the pressure level 0.445 MPa (64.6 psia) and flow 0.05 Kg/sec (0.11 lb/sec) at operating temperature required for the 1.3 KW BIPS. The results indicate that HSHX No. 1, No. 2 and No. 3 exceed the required pressure drop by 21%, 24% and 10% respectively. The BIPS system requirements however differ from the HSA contract requirements. The flow and allowable pressure drop for the two HSA (1.3 KW) and three HSA (2 KW) system configuration are shown in Table 7-1 below.

TABLE 7-1

BIPS SYSTEM FLOW REQUIREMENTS

	2 HSA System	3 HSA System
Flow, Kg/sec (lb/sec) each HSA	0.05028 (0.11085)	0.05062 (0.1116)
Pressure, MPa (psi)	0.445 (64.6)	0.6877 (99.74)
$\Delta P/P$	0.003	0.002
ΔP, MPa (psi)	0.001336 (0.1938)	0.001376 (0.1995)

Scaling the test data to the two and three HSA conditions results on the following pressure drops for the two assemblies tested.

TABLE 7-2

HSA SCALED PRESSURE DROP TEST DATA

	BIPS 2 HSA System	BIPS 3 HSA System
HSA #1 ΔP, KPa (psi)	0.7963 (0.1155)	0.5240 (0.076)
HSA #2 ΔP, KPa (psi)	0.8156 (0.1183)	0.5350 (0.0776)
HSA #3 ΔP, KPA (psi)	0.7239 (0.1050)	0.4744 (0.0688)

Comparing these values of ΔP to those in the preceding table indicates that the scaled test pressure drop is only 60% of the maximum allowable pressure drop for the worst case (2 HSA System).

It is, therefore, concluded that HSA's No. 1, No. 2, and No. 3 more than meet the pressure drop requirements for the BIPS 1.3 KW and higher power configurations.

FIGURE 7-4

HSHX PRESSURE DROP FLOW TEST RESULTS

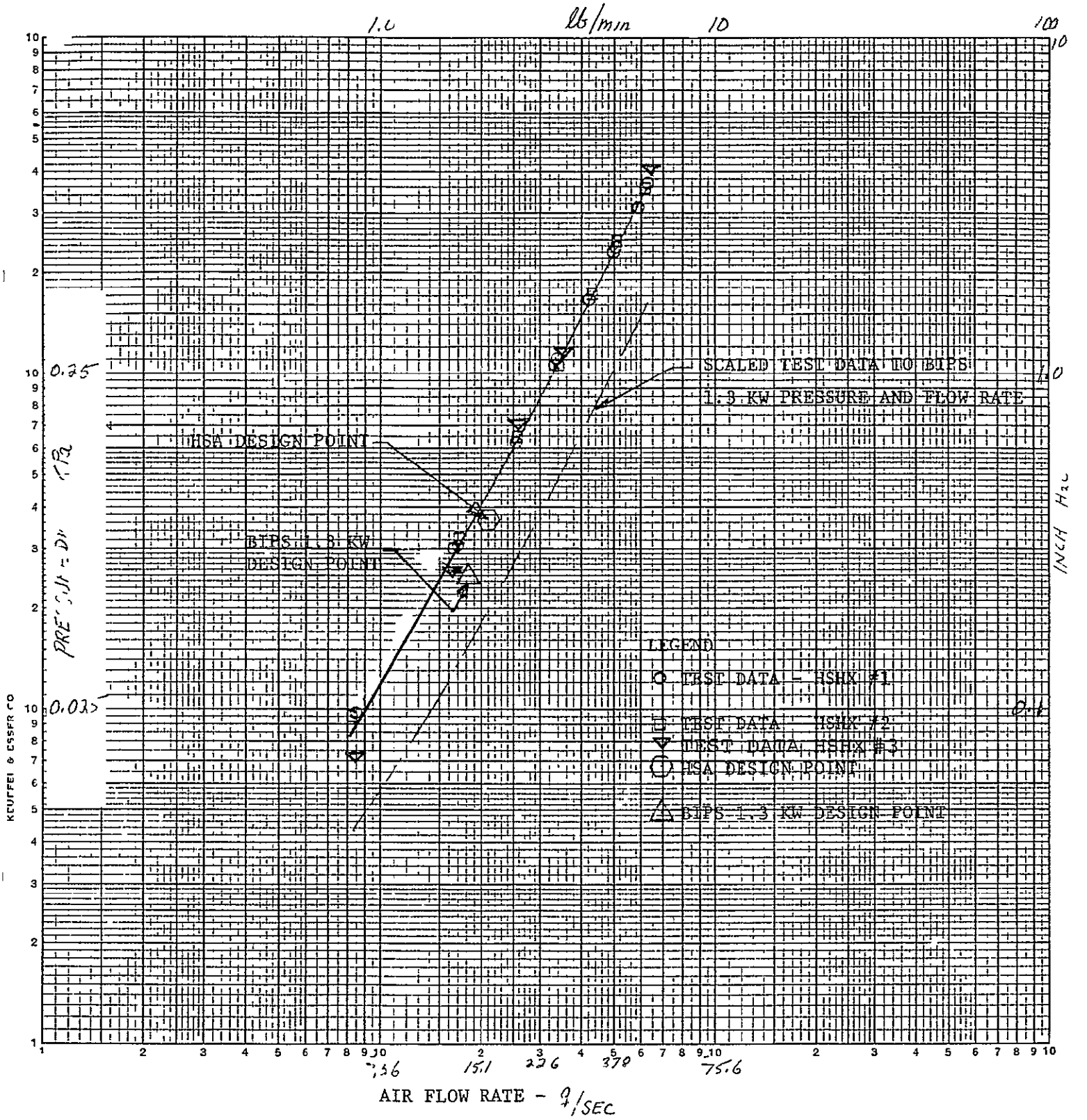

7.5 HSHX LEAK TESTS

Leak tests were conducted on the completed HSHX's using a helium mass spectrometer leak detector to verify that the overall leak rate did not exceed specification limits. Tests were conducted both before and after proof pressure tests with the leak test being the last test in the acceptance test sequence. The results of the final leak tests indicated no detectable leaks within the sensitivity of the leak detector. For the three leak tests this sensitivity (minimum detectable leak of the leak detector) ranged from 1.27×10^{-8} to 0.91×10^{-9} std cc Helium per second.

7.6 HSA PROOF PRESSURE TEST

This test would be conducted on a complete HSA assembly (excluding the HSHX fluid loop). The HSA would be proofed at room temperature at 0.28 MPa (40 psia) internal pressure for ten (10) minutes.

7.7 HSA PRESSURE DECAY TEST

This test would be conducted on a complete HSA assembly. The HSA unit (excluding the HSHX fluid loop) would be pressurized to 0.17 ± 0.003 MPa (25 ± 0.5 psia) of argon and a minimum of five pressure readings taken over a 48 hour period. The requirement for acceptance will be a HSA leak rate of less than 0.0125 MPa (1.81 psia) over the 48 hour period at ambient conditions.

SECTION 8

CONCLUSIONS AND RECOMMENDATIONS

The development of a light weight diffusion welded refractory alloy (C-103) heat exchanger for space power applications represents an advancement in the state of the art. The Battelle Columbus Laboratory autoclave which was modified for this program to provide the capability of hot isostatic pressing (HIP) at 1810K (2800°F) and 69. MPa (10,000 psi) is currently the largest known autoclave in the world with this temperature and pressure capability. The superior diffusion welds resultant from this HIP process, exhibited excellent grain growth across the original weld joint interface. Metallographically, there was no evidence of the original joint interface, suggesting that the mechanical properties will be characteristic of the parent C-103 alloy material. The use of C-103 for the heat source heat exchanger permits high working fluid temperatures for the Brayton Isotope Power System (BIPS). This temperature capability provides growth potential beyond the current design specifications for flight systems with high cycle efficiency.

The use of a melting/fusing foil insulation to effect emergency cooling is a simple, passive and reliable system. It does however require verification by full scale tests. Such a test program is strongly recommended. Additionally assembly of the two HSA's should be accomplished as soon as feasible. A ground demonstration system test employing the refractory alloy HSA's along with the other suitable components of the BIPS should be a goal in the further development of this versatile power system for future space missions.

SECTION 9

REFERENCES

1. "Standard Method of Test for Thermal Conductivity of Materials by Means of the Guarded Hot Plate", ASTM-C177-63 (reapproved 1968), American Society for Testing Materials, Philadelphia, Pa.

2. J. Crank, Mathematics of Diffusion, Oxford University Press, London (1967) p. 34-5.

3. I. I. Kornilov and E. N. Pylaeva, Izv. Akad. Nauk SSSR, Metally 1966(5) 132-6(Russ).

4. I. J. Duerden and W. Hume-Rothery, J. Less-Common Met. 11, 381-7 (1966).

5. A. S. Bulatov et al, Chem. Abstracts 71, 15458v (1969) and Zh. metal. metalloved., 23, No. 2, 380, 381 (1967) UDC.669.24:548.7.

6. L. S. Birks and R. E. Seebold, J. Nuclear Mat. 3, 249-59 (1961).

7. R. P. Agarwala and Ken-ichi Hirano, Trans. J. I. M. 13, 425-7 (1972).

8. GE Report TIS No. R66FPD171, "Snap - Improved Computer Program for the analysis of shells of revolution with Axisymmetric loading", L. Beitch.

9. NASA CR-121223, VOL I, Final Report Mini-Brayton Heat Source Assembly Design Study, Dec. 1973

10. Heyda, J. F. and Fulton, C. D., Discussion of "Inlet and Exit Header Shapes for Uniform Flow thru a Resistance Parallel to the Main Stream", by Morris Perlmutter (ASME Paper No. 60-WA-160).

11. GE Document: PIR-5983, "Transient Temperature and Stress Analysis of Heat Source Assembly", C. E. Kelly, G. R. Ambrose, 7/19/77.

APPENDIX A

ACRONYMS

ACS	Auxiliary Cooling System
BIPS	Brayton Isotope Power System
BMI	Battelle Memorial Institute
bcc	body centered cubic
BCL	Battelle Columbus Laboratories
BRU	Brayton Rotating Unit
DOE	Department of Energy
EB	Electron Beam (welding)
ECS	Emergency Cooling System
EHS	Electric Heat Source
ERDA	Energy Research Development Agency
FPI	Fluorescent Penetrant Inspection
GFE	Government Furnished Equipment
GTA	Gas Tungsten Arc (welding)
HIP	Hot Isostatic Pressing
HS	Heat Source (identical to "Isotope Heat Source")
HSA	Heat Source Assembly
HSHX	Heat Source Heat Exchanger
HSIS	Heat Source Insulation System
IHS	Isotope Heat Source (identical to "Heat Source")
IPM	Inches Per Minute
LES	Lincoln Experiment Satellite
MHW	Multi-Hundred Watt
MINI-BRU	Mini-Brayton Rotating Unit (identical to "Brayton Rotating Unit")

NDT	Non Destruction Test
PICS	Post Impact Containment Sphere (Iridium fuel clad)
RTG	Radioisotope Thermoelectric Generator
SFM	Standard Feet Per Minute (machine cutter speed)
T/C	Thermocouple
TECO	Thermo-Electron Corporation
W_e	Watts, electrical
W_t	Watts, thermal

DISTRIBUTION LIST FOR CONTRACTOR REPORT ON
MINI-BRAYTON HEAT SOURCE ASSEMBLY DEVELOPMENT

NASA-Lewis Research Center
Attn R. H. Titran, M.S. 105-1 (10)
W. D. Klopp, M.S. 105-1 (1)
C. P. Blankenship, M.S. 105-1 (1)
J C. Freche, M.S. 49-1 (1)
R. W. Hall, M.S. 49-1 (1)
G. K. Watson, M.S. 105-1 (1)
J. E. Bolander, M.S. 500-312 (1)
S. J. Grisaffe, M.S. 49-3 (1)
N. T Musial, M.S. 500-311 (1)
T. J. Moore, M.S. 105-1 (1)
H B Probst, M.S. 49-3 (1)
R. E. English, M.S. 3-15 (1)
P. T Kerwin, M.S. 500-210 (1)
S. H. Gorland, M.S. 501-7 (1)
L I. Shure, M.S. 500-202 (1)
R. P. Migra, M.S. 500-202 (1)
TU Office, M.S. 7-3 (1)
Library, M.S. 60-3 (2)
AAMRDL Office, M.S. 77-5 (1)
Reports Control Office, M.S. 5-5 (1)
21000 Brookpark Road
Cleveland, OH 44135

NASA Headquarters
Attn: RWM-3/J. Gangler (1)
RP-6/J. Lazar (1)
RP-6/J. Mullin (1)
RP-6/L. Holcomb (1)
600 Independence Avenue, S.W.
Washington, DC 20546

NASA-Scientific and Technical
Information Facility (10)
Attn: Accessioning Department
P. O. Box 8757
Baltimore/Washington International
Airport
Maryland 21240

U.S. Army Research Office (1)
Attn George Mayer
Metallurgy & Materials Science Division
Durham, NC 27706

Battelle Memorial Institute (1)
Attn: E. S. Bartlett
Metals & Ceramics Information Center
505 King Avenue
Columbus, OH 43201

Battelle Columbus Laboratory
Attn Dr. C Alexander (1)
D Woessner (1)
505 King Avenue
Columbus, OH 43201

TRW, Inc
Attn: J. A. Alexander (1)
H. E. Collins (1)
Materials Technology
23555 Euclid Avenue
Cleveland, OH 44117

Westinghouse Electric Corporation
Attn· D. C. Goldberg (1)
R. W. Buckman (1)
P. O. Box 10864
Pittsburgh, PA 15236

Department of Energy
Attn: Dyer Kenney (1)
J. Lombardo (1)
J. Griffo (1)
C Tarr (1)
Division of Nuclear Research and Appli-
cations
Washington, DC 20545

( ) indicates number of copies

Oak Ridge National Laboratory
Attn: A. Schaffhauser (1)
H. Inouye (1)
Post Office Box X
Bldg. 4508
Oak Ridge, TN 37830

Fairchild Space and Electronics Co.
Attn: A. Schock (1)
H. Kling (1)
M. Eck (1)
Germantown, MD 20767

Thermal Electron Engineering Corporation
Attn: F. Huffman (1)
85 First Avenue
Waltham, MA 02154

AiResearch Manufacturing Company
Attn: J. McCormick (1)
H. Longee (1)
L. G. Miller (1)
J Hadley (1)
F Dobler (1)
T. Ashe (1)
J. Teets (1)
402 South 36th Street
Phoenix, AZ 85010

AiResearch Manufacturing Company
Attn: J Killacky (1)
9851-9951 Sepulveda Blvd.
Los Angeles, CA 90045

Wayne State University
Attn. Dr. C. L. Corey (1)
Department of Materials Science
Detroit, MI 48202

Wah Chang Corporation
Attn. R. Marsh (1)
Albany, OR 97321

GENERAL ELECTRIC

Space Division

Headquarters Valley Forge, Pennsylvania ☐ Daytona Beach, Fla ☐ Evendale, Ohio

☐ Huntsville, Ala ☐ Bay St Louis, Miss ☐ Houston, Texas ☐ Sunnyvale, Calif

☐ Beltsville, Md ☐ Tacoma, Wash ☐ Palmdale, Calif ☐ Bedford, Mass

☐ Washington, D C Area